

NASA MEMO 3-31-59L

~~UNCLASSIFIED~~**NASA**~~NASA T-07445 78-71~~**MEMORANDUM**

INVESTIGATION OF DRAG AND STATIC LONGITUDINAL AND LATERAL
STABILITY AND CONTROL CHARACTERISTICS OF A MODEL
OF A 45° SWEPT WING AIRPLANE AT MACH NUMBERS
OF 1.57, 1.87, 2.16, AND 2.53

PHASE II MODEL

By Melvin M. Carmel and Kenneth L. Turner

Langley Research Center
Langley Field, Va.

Declassified by authority of [redacted]
Classification Change Notices No. 214
Dated 9-30-71

**NATIONAL AERONAUTICS AND
SPACE ADMINISTRATION**

'N71-74022

(ACCESSION NUMBER)

163

(PAGES)

(IHRU)

None

(CODE)

DECLASSIFIED

NATIONAL AERONAUTICS AND SPACE ADMINISTRATION

MEMORANDUM 3-31-59L

INVESTIGATION OF DRAG AND STATIC LONGITUDINAL AND LATERAL
STABILITY AND CONTROL CHARACTERISTICS OF A MODEL
OF A 45° SWEPT WING AIRPLANE AT MACH NUMBERS
OF 1.57, 1.87, 2.16, AND 2.53* **

PHASE II MODEL

By Melvin M. Carmel and Kenneth L. Turner

SUMMARY

Tests were performed in the Langley Unitary Plan wind tunnel to determine the drag and static longitudinal and lateral stability and control characteristics of a model of a 45° swept wing airplane at Mach numbers of 1.57, 1.87, 2.16, and 2.53. This is the second phase in a series of tests performed on this model. The Reynolds numbers for these tests, based on the mean aerodynamic chord of the wing, are 1.406×10^6 , 1.269×10^6 , 1.116×10^6 , and 0.714×10^6 at Mach numbers of 1.57, 1.87, 2.16, and 2.53, respectively. The model had a 12° wing tip dihedral, a larger vertical tail, and a modified duct.

INTRODUCTION

An investigation of the aerodynamic characteristics of a model of a 45° swept wing airplane at supersonic speeds has been undertaken by the National Aeronautics and Space Administration. This is the second phase in a series of tests being conducted on this model at the Langley

*The information presented herein was previously given limited distribution in NACA Research Memorandum SL57A14.

Unitary Plan wind tunnel. Results of the first phase of tests on this model may be found in reference 1. These results indicated that the airplane directional stability would be marginal and the roll characteristics undesirable; therefore, the model was modified to include 12° of wing tip dihedral and a larger vertical fin and rudder. The current model also had a double-compression ramp (5° to 8°) in place of a single-compression 9° ramp. The exterior contour of the duct was also modified; these modifications are shown in figure 1.

This paper contains results obtained at Mach numbers of 1.57, 1.87, 2.16, and 2.53, for angles of attack from -2° to 32° , and for angles of sideslip from -10° to 16° .

COEFFICIENTS AND SYMBOLS

The results of these tests are presented as coefficients of forces and moments referred to the stability-axes system. All aerodynamic moments were taken about the center of gravity which is longitudinally located at 33 percent of the mean aerodynamic chord of the wing and at a station 0.976 inch above the root chord of the wing. Symbols used in this paper are as follows:

b	wing span, in.
\bar{c}	mean aerodynamic chord of wing, in.
\bar{c}_t	mean aerodynamic chord of stabilator, in.
M_a	moment area of aileron, cu ft
M_{a_r}	moment area of rudder, cu ft
S	wing area (theoretical total), sq ft
S_h	stabilator area, sq ft
A_b	base axial force, lb
A_c	chamber axial force, lb
D'_i	internal-duct force along X-axis, lb
F'_D	force along X stability axis, lb

~~DECLASSIFIED~~

3

L	lift, lb
m	pitching moment, in-lb
l	rolling moment, in-lb
n	yawing moment, in-lb
Y	lateral force, lb
N _t	normal force on stabilator, lb
h _L	left aileron hinge moment, ft-lb
h _R	right aileron hinge moment, ft-lb
h _r	rudder hinge moment, ft-lb
h _t	stabilator hinge moment, in-lb
C' _{D_b}	base-drag coefficient, $-\frac{A_b \cos \alpha}{qS}$
C' _{D_c}	chamber-drag coefficient, $-\frac{A_c \cos \alpha}{qS}$
C' _D	drag coefficient, $\frac{F'}{qS}$
C' _{D_i}	internal-duct drag coefficient, $\frac{D'_i}{qS}$
ΔC _D	change in drag coefficient due to fixing transition
C _{D_e}	net external drag coefficient
C _L	lift coefficient, L/qS
C _m	pitching-moment coefficient, m/qSc
C _l	rolling-moment coefficient, l/qSb
C _{nb}	yawing-moment coefficient, n/qSb

T-52

4

C_Y	lateral-force coefficient, Y/qS
C_{N_t}	stabilator normal-force coefficient, $\frac{N_t}{qS}$
C_{n_B}	slope of yawing-moment curve
C_{h_L}	left-aileron hinge-moment coefficient, $\frac{h_L}{2qM_a}$
C_{h_R}	right-aileron hinge-moment coefficient, $\frac{h_R}{2qM_a}$
C_{h_r}	rudder hinge-moment coefficient, $\frac{h_r}{2M_{a_r} q}$
C_{h_t}	stabilator hinge-moment coefficient, $\frac{h_t}{q\bar{c}_t S_h}$
C_l_B	slope of rolling-moment curve
P	free-stream static pressure, lb/sq ft
M	free-stream Mach number
q	free-stream dynamic pressure, lb/sq ft = $0.7PM^2$
α	angle of attack of wing chord, deg
β	angle of sideslip of fuselage center line, deg
i_t	incidence of stabilator, deg
δ_{a_L}	left-aileron deflection angle (positive deflection, trailing edge down), deg
δ_{a_R}	right-aileron deflection angle (positive deflection, trailing edge down), deg
δ_F	flap-deflection angle, deg
δ_r	rudder-deflection angle, deg
δ_z	spoiler-deflection angle (left wing only), deg

DECLASSIFIED

5

m_E	mass flow at duct exit
m_1	free-stream mass flow based on inlet area
F.S.	fuselage station
B.L.	body line
L 5 2 4	W.L. water line
	H.L. hinge line

APPARATUS AND METHODS

The tests were conducted in the low Mach number test section of the Langley Unitary Plan wind tunnel. This tunnel is a variable-pressure, continuous, return-flow type. The test section is 4 feet square and approximately 7 feet long. The nozzle leading to the test section is of the asymmetric sliding-block type. Mach numbers may be continuously varied through the range of approximately 1.57 to 2.80 without tunnel shutdown.

Model and Support System

A three-view drawing of the model is presented in figure 2. Missiles were attached to the model for all test configurations except those in which the center-line store was used, for which configurations they were considered to be fired. The missiles were tested in a retracted position unless otherwise noted. The right aileron was deflected in conjunction with the left spoiler in all cases in which the spoiler-aileron combination was used. Geometric characteristics of the model are presented in table I. Photographs of the configurations tested are presented in figure 3.

The model was attached to the forward end of an enclosed six component electrical strain-gage balance. This balance was connected to the central-support system of the tunnel by means of a sting. The central-support components consisted of a remotely operated adjustable coupling, a variable-offset coupling, and a 5° bent coupling or a 20° bent coupling. The variable-offset coupling and the 20° bent coupling were means of offsetting the model from the tunnel center line in order to obtain increased angle of attack. The 5° coupling was used to offset the model from the center line in order to obtain increased angle of sideslip. The adjustable coupling was used to change the angle of the model in the vertical plane.

Measurements and Accuracy

Pitch tests were made throughout an angle-of-attack range of approximately -2° to 22° . Sideslip tests were made throughout an angle range of approximately -10° to 16° at angles of attack of approximately 0° , 7° , 13° , and 17° , at Mach numbers of 1.57, 1.87, 2.16, and 2.53. In addition, at a Mach number of 1.87, sideslip tests were also made at angles of attack of approximately 21° , 27° , and 32° . All basic model tests were performed with a stabilator incidence of 0° . The angles of attack and sideslip are corrected for deflection of the sting and balance under load, and the angles are estimated to be accurate within $\pm 0.1^\circ$. The maximum deviation of local Mach number in the portion of the tunnel occupied by the model is ± 0.015 from the average values given.

The dewpoint, measured at stagnation pressure, was maintained below -30° F and the stagnation temperature was maintained at approximately 125° F.

The stagnation pressure was maintained at approximately 6.5 pounds per square inch absolute except for the sideslip tests at angles of attack of 21° , 27° , and 32° , when it was held at approximately 5.0 pounds per square inch absolute.

The tunnel has not been completely calibrated and any angularity of flow that might exist in the tunnel has not been determined. The pressure gradients in the region of the model have been determined and are sufficiently small so as not to induce any buoyancy effect on the model.

The accuracy of the force and moment coefficients, based on balance calibration and repeatability of data, is estimated to be within the following limits:

REF ID: A65724
RECLASSIFIED

7

The drag data have been adjusted to correspond to zero-balance chamber-drag coefficient ($C_{Dc}^t = 0$). An example of the variation of measured balance chamber-drag coefficients with angle of attack for all test Mach numbers are presented in figure 4 in order to show the magnitude of these coefficients.

Internal-duct drag and choke base-pressure drag were obtained only for one pitch run at each Mach number. The internal drag was obtained from an average total-pressure measurement from four tubes placed 1/8 inch ahead of the choke location which was at the duct exit. Base-pressure drag of the duct was obtained from measurements of the average static pressure on the duct base. The variation of internal-duct drag and duct base-pressure drag coefficients with angle of attack for all test Mach numbers are also presented in figure 4.

In an attempt to assure turbulent flow over the model, a transition strip was fixed around the model nose one inch rearward of the tip and also on the 10-percent chord of the wing (top and bottom, full span). The transition strips were 1/4 inch wide and consisted of no. 60 carborundum grains imbedded in shellac with approximately 15 grains per 1/4 square inch. The results of these tests are presented in figure 5. In order to obtain net external drag, the drag coefficients shown on the characteristic plots must first be increased by the incremental difference in drag coefficient shown in figure 5 at the same model attitude. This resultant drag must then be reduced by the amount of the internal drag and the choke base drag at the same model attitude ($C_{De} = C_D^t + \Delta C_D - C_{D_i}^t - C_{D_b}^t$).

Figure 6 presents variation of mass flow ratio with angle of attack at the test Mach numbers.

Schlieren photographs were taken of many of the model configurations and attitudes. Typical examples of the schlieren photographs are presented in figure 7. A study of the force results and tunnel geometry in conjunction with the schlieren photographs indicates wall-reflected shock waves striking the model at $\alpha = -2^\circ$ and 22° and at $\beta = 16^\circ$ at a Mach number of 1.56.

PRESENTATION OF RESULTS

The results of the data obtained are plotted in figures 8 to 22.

031912201030

Figure

Effect of horizontal tail on aerodynamic characteristics in pitch	8
Variation of stabilator hinge-moment and normal-force coefficient with lift coefficient	9
Effect of ailerons and spoilers on aerodynamic characteristics in pitch	10
Effect of aileron deflection on aileron hinge-moment coef- ficient in pitch	11
Effect of missiles extended on aerodynamic characteristics in pitch	12
Effect of external stores on aerodynamic characteristics in pitch	13
Effect of speed brakes on aerodynamic characteristics in pitch	14
Effect of vertical tail on aerodynamic characteristics in sideslip	15
Effect of aileron and spoiler deflections on aerodynamic characteristics in sideslip	16
Effect of aileron deflections on aileron hinge-moment coefficient in sideslip	17
Effect of missiles extended on aerodynamic characteristics in sideslip	18
Effect of external stores on aerodynamic characteristics in sideslip	19
Effect of rudder deflection on aerodynamic characteristics in sideslip	20
Effect of rudder deflection on rudder hinge-moment coefficient in sideslip	21
Comparison of directional stability derivatives between results of phase I and phase II tests	22

REF ID: A6572
DECLASSIFIED

SUMMARY OF RESULTS

The basic results are presented with minimum analysis, and some general observations relative to the data are as follows:

- L
5
2
4
1. The minimum drag coefficients for the complete model with a tail incidence of 0° are 0.040, 0.039, 0.037, and 0.037 at Mach numbers of 1.57, 1.87, 2.16, and 2.53, respectively. These values of drag coefficient are for net external drag with a turbulent boundary layer and are somewhat greater than those obtained for the phase I model.
 2. The results indicate positive static directional stability for complete model configuration in the Mach number and angle-of-attack range tested except at a Mach number of 1.87 for angles of attack of 26.5° and 31.7° where the model becomes directionally unstable. The directional stability, as expected, decreases with Mach number; for a Mach number of 2.53, the directional stability becomes marginal at the highest angles of attack.
 3. A comparison of the rolling-moment derivatives for the current model tests with those for the phase I model tests indicates that incorporating a larger vertical tail and a 12° dihedral in the wing tips produced a more negative C_{lB} . The effective dihedral for the current model, however, is essentially neutral for angles of attack up to 6° in the test Mach number range.

Langley Research Center,
National Aeronautics and Space Administration,
Langley Field, Va., December 18, 1956.

REFERENCE

1. Carmel, Melvin M., and Gregory, Donald T.: Preliminary Investigation of the Static Longitudinal and Lateral Stability Characteristics of a Model of a 45° Swept Wing Airplane at Mach Numbers of 1.59, 1.89, and 2.09. NASA MEMO 3-30-59L, 1959.

031312201030 8

TABLE I.- GEOMETRIC CHARACTERISTICS OF A MODEL OF A 45° SWEPT WING AIRPLANE (PHASE II)

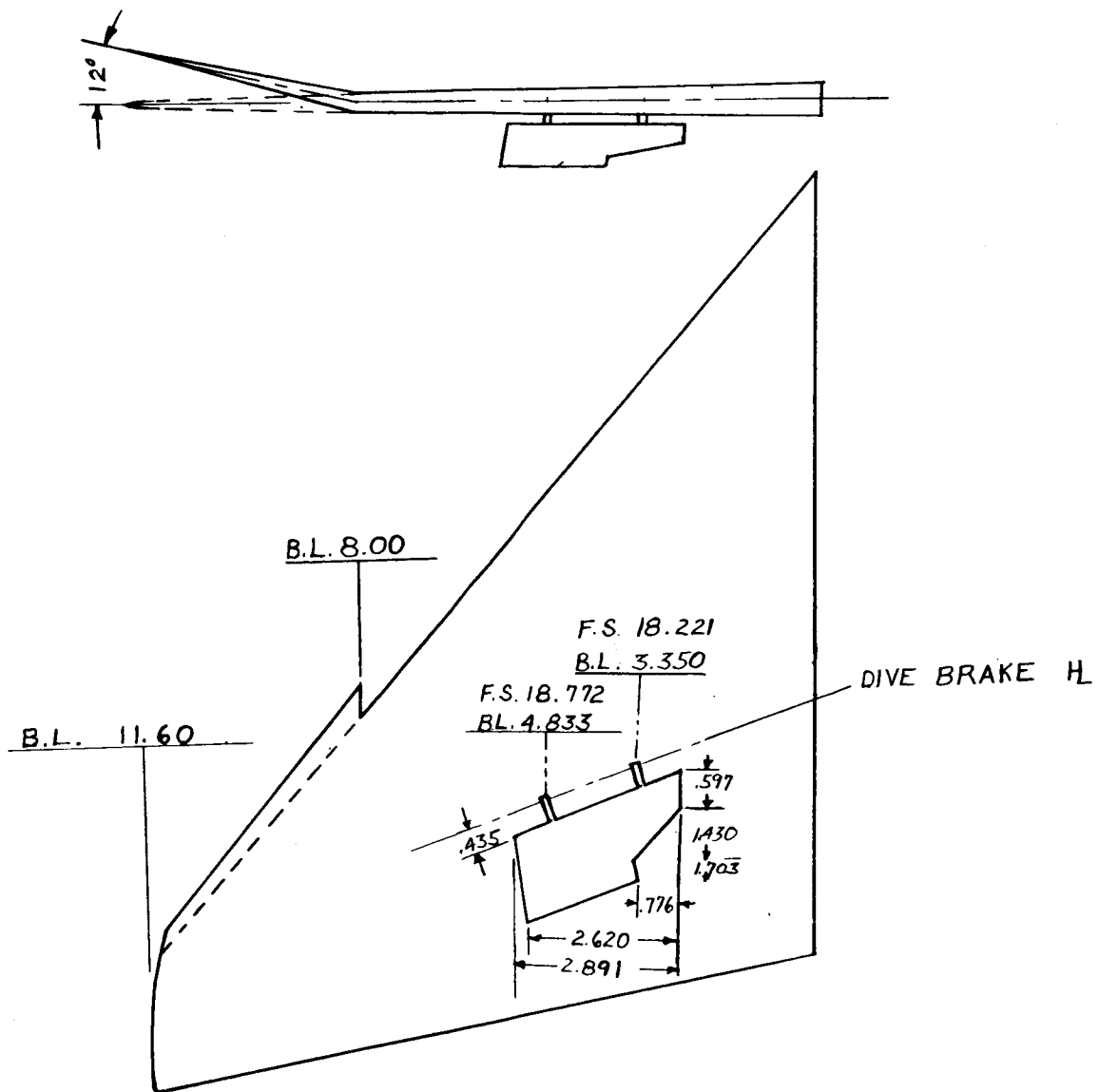
[Fuselage station 0.00 is 0.42 inch rearward of nose]

Model scale, percent	5
Center-of-gravity location, percent of mean aerodynamic chord	33
Wing:	
Loading (combat), lb/sq ft	65
Area, sq ft:	
Exposed	0.886
Theoretical	1.325
Span, in.	23.2
Aspect ratio	2.821
Taper ratio	0.167
Sweep angle of quarter-chord line, deg	45
Dihedral, deg	0 inboard, 12 at tip
Incidence, deg	1
Geometric twist, deg	0
Airfoil:	
Root	NACA 0006.4-65 (modified)
Body line 8.0	NACA 0004.0-64 (modified)
Tip	NACA 0003.0-64 (modified)
Root chord, in.	14.10
Tip chord, in.	2.35
Root-chord location:	
Longitudinal (leading edge)	Fuselage station 7.518
Vertical	Water line 0.574
Mean aerodynamic chord, in.	9.63
Mean-aerodynamic-chord location:	
Longitudinal (leading edge)	Fuselage station 13.054
Lateral	Body line 4.42
Fuselage:	
Length, in.	33.60
Width (maximum), in.	3.375
Depth (maximum), in.	3.730
Overall fineness ratio	8.40
Base area	None
Horizontal tail:	
Area (theoretical), sq ft	0.237
Span, in.	10.626
Aspect ratio	3.310
Taper ratio	0.200
Root chord, in.	5.35
Tip chord, in.	1.07
Mean aerodynamic chord, in.	3.686
Mean-aerodynamic-chord location:	
Longitudinal (leading edge)	Fuselage station 29.16
Lateral	Body line 2.065
Tail length (distance from quarter-chord point of mean aerodynamic chord of wing to quarter-chord point of mean aerodynamic chord of horizontal tail), in.	14.619
Sweep angle of quarter-chord line, deg	35.5
Dihedral, deg	-15
Geometric twist, deg	0
Airfoil:	
Root	NACA 0003.7-64 (modified)
Tip	NACA 0003.0-64 (modified)
Vertical tail:	
Area (theoretical), sq ft	0.197
Span, in.	3.825
Aspect ratio	0.5976
Root-chord length, in.	10.35
Tip-chord length, in.	2.355
Mean aerodynamic chord, in.	7.192
Mean-aerodynamic-chord location:	
Longitudinal (leading edge)	Fuselage station 26.11
Vertical (leading edge)	Water line 4.836
Tail length (distance from quarter-chord point of mean aerodynamic chord of wing to quarter-chord point of mean aerodynamic chord of vertical tail), in.	11.507
Airfoil:	
Root	NACA 0003.2-64 (modified)
Tip	NACA 0002.5-64 (modified)
Duct with double compression ramp (5° to 8°):	
Capture area, sq ft/side	0.011944
Exit, sq ft/side	0.007906

I-524

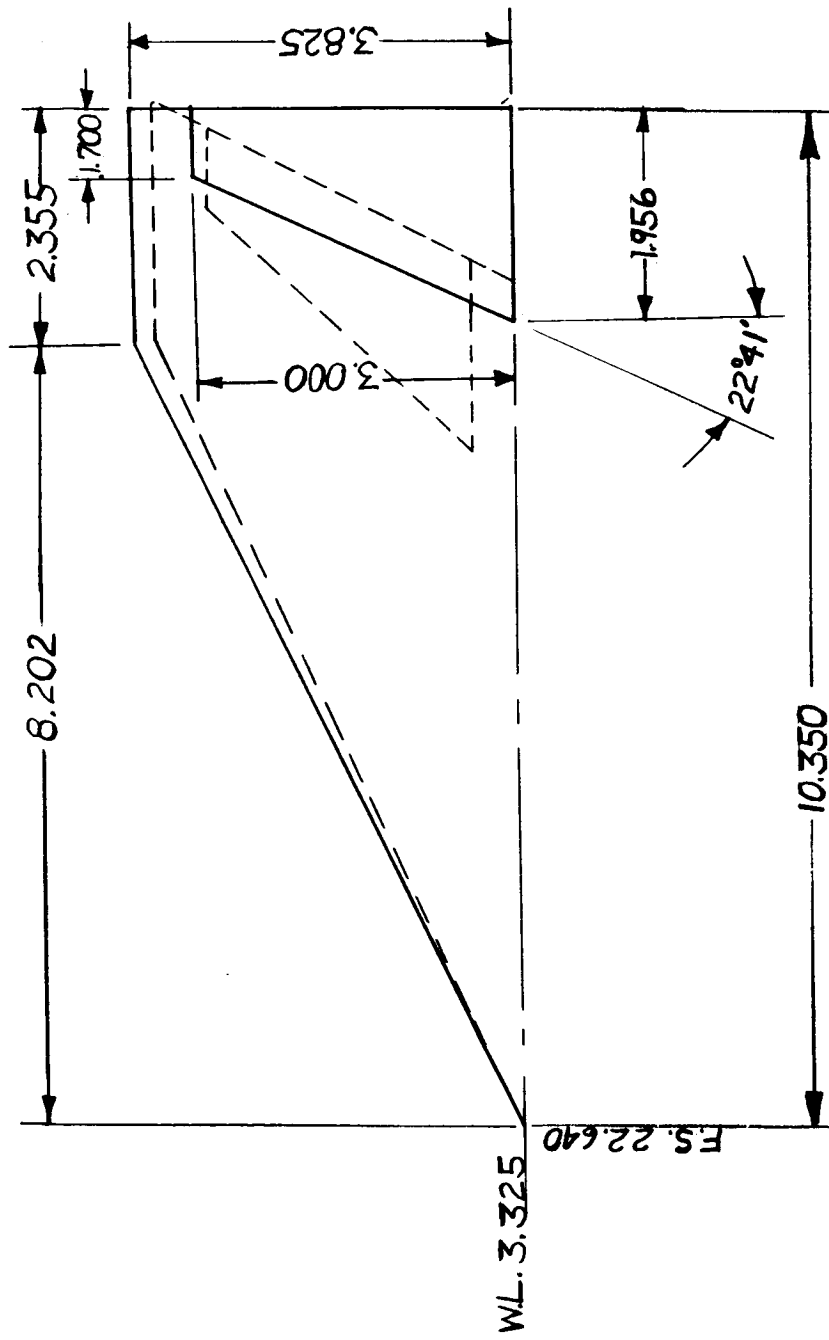
DECLASSIFIED

11



(a) Wing.

Figure 1.- Modifications to model after phase I tests. (Dotted lines indicate phase I model.)

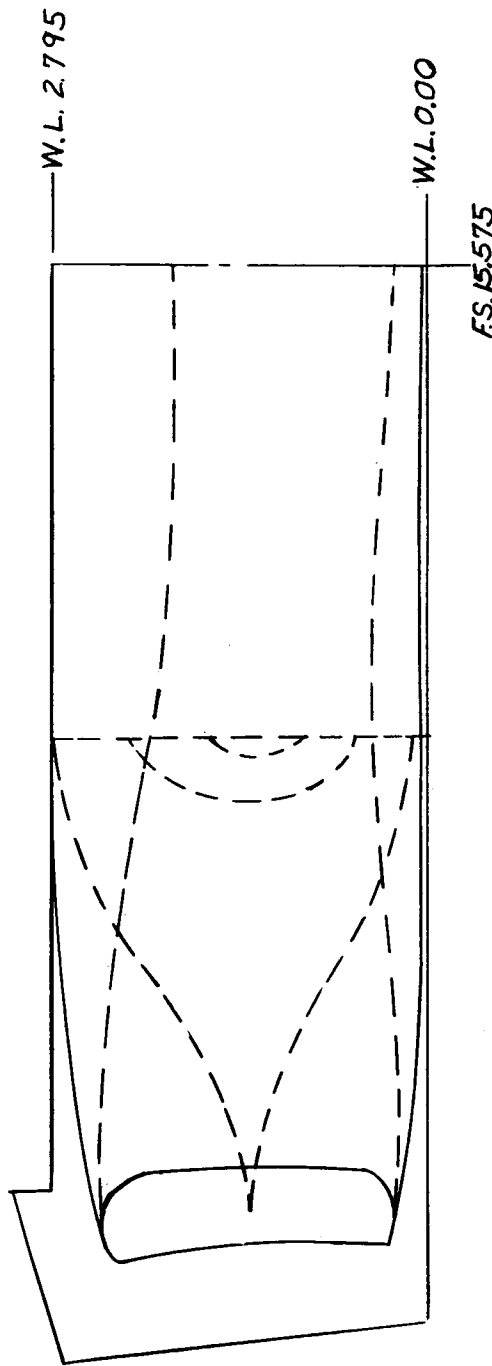
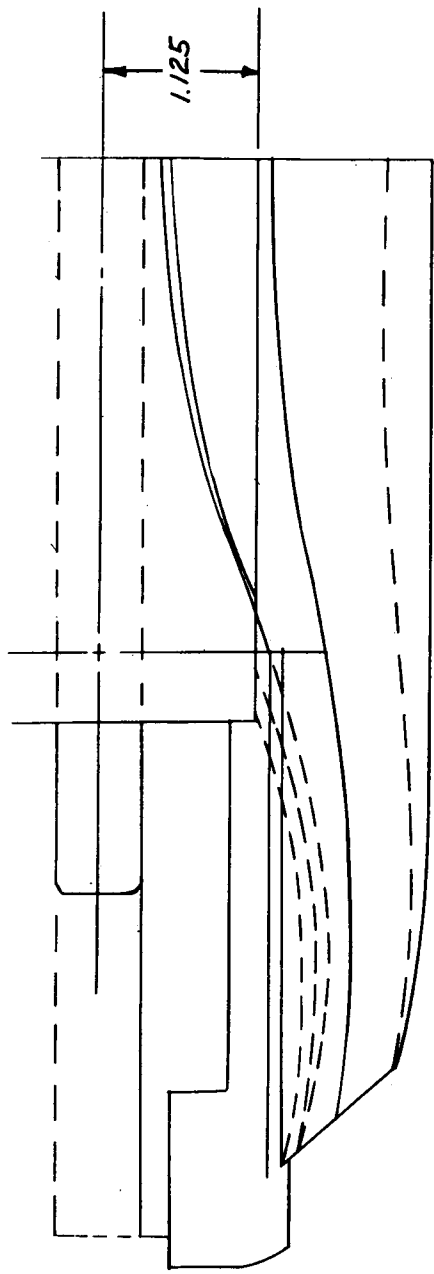


(b) Vertical tail.

Figure 1.- Continued.

DECLASSIFIED

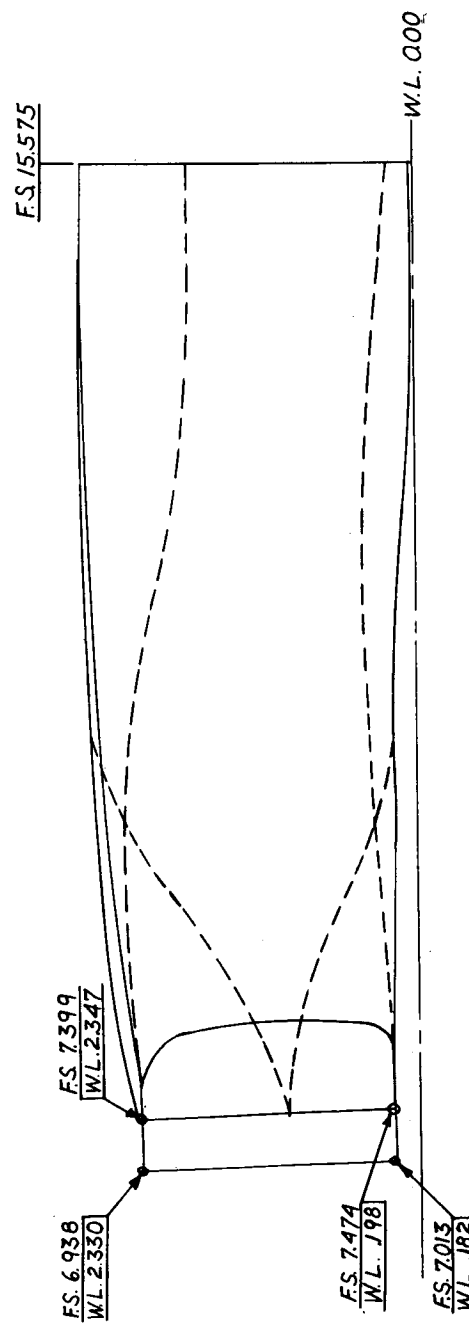
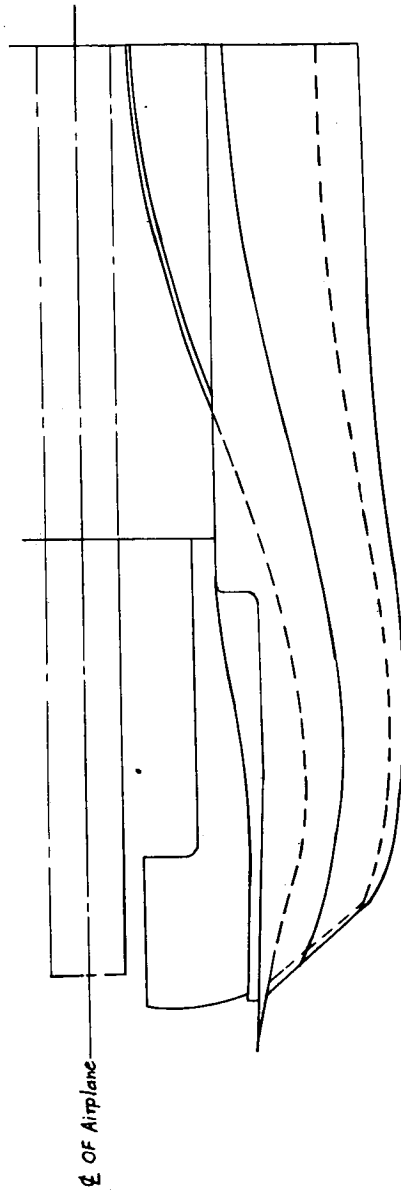
13



(c) Duct for phase I tests.

Figure 1.- Continued.

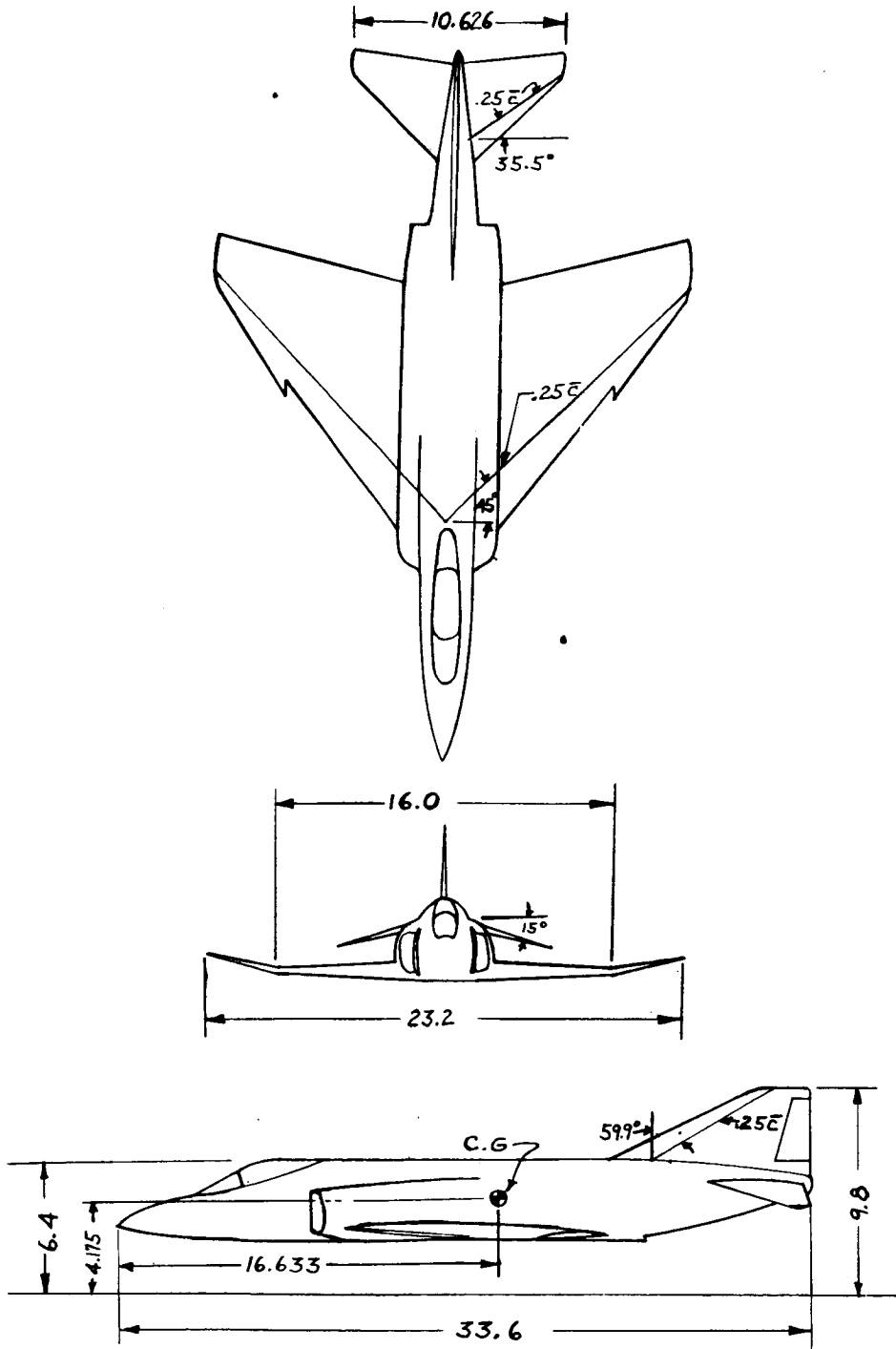
031312201030



(d) Duct for phase II tests.

Figure 1.- Concluded.

DECLASSIFIED

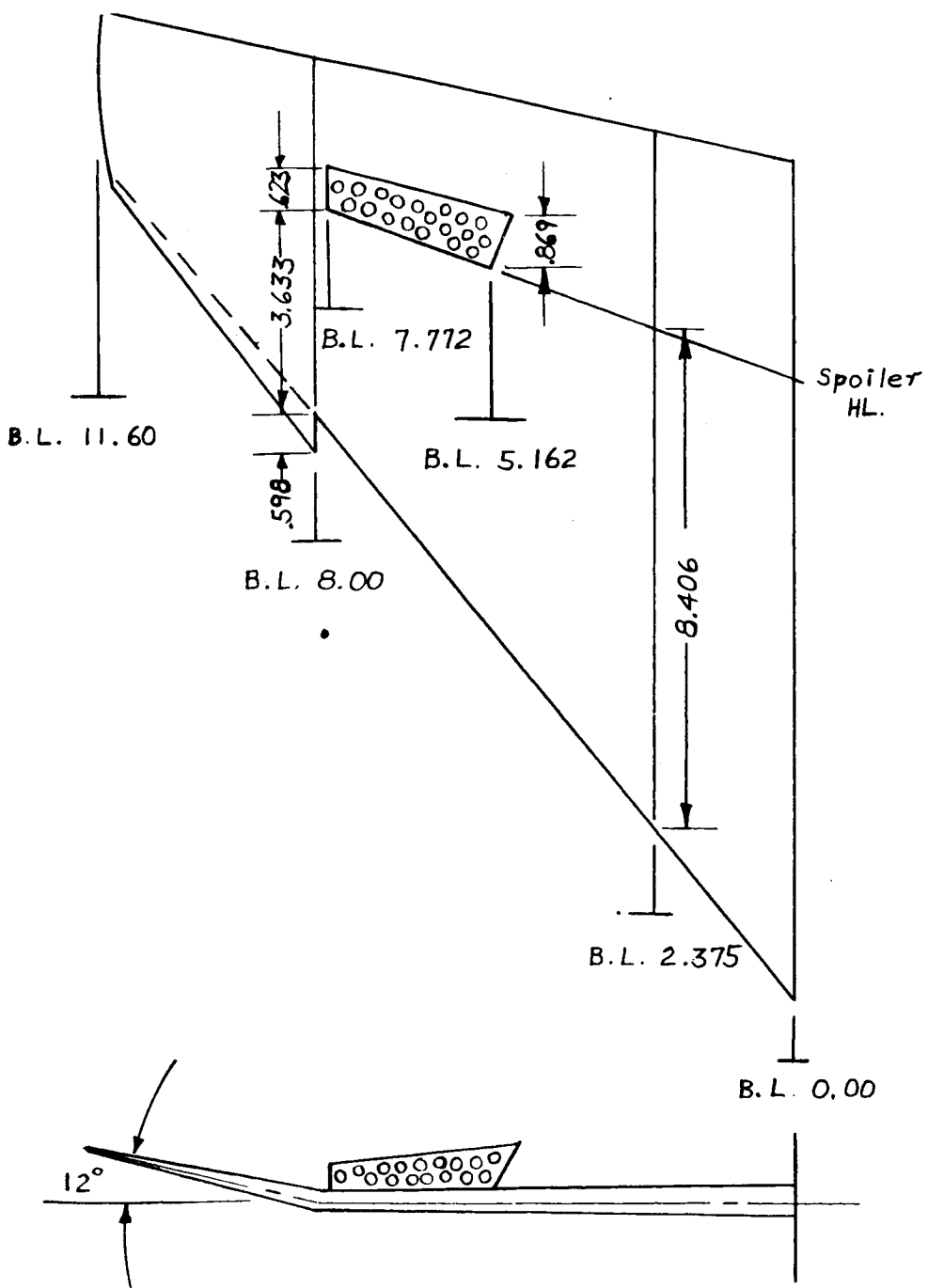


(a) Three-view drawing.

Figure 2.- Model of a 45° swept wing airplane. All dimensions are in inches.

0010000000000000

00



(b) Detail of spoiler (20-percent porosity).

Figure 2.- Concluded.

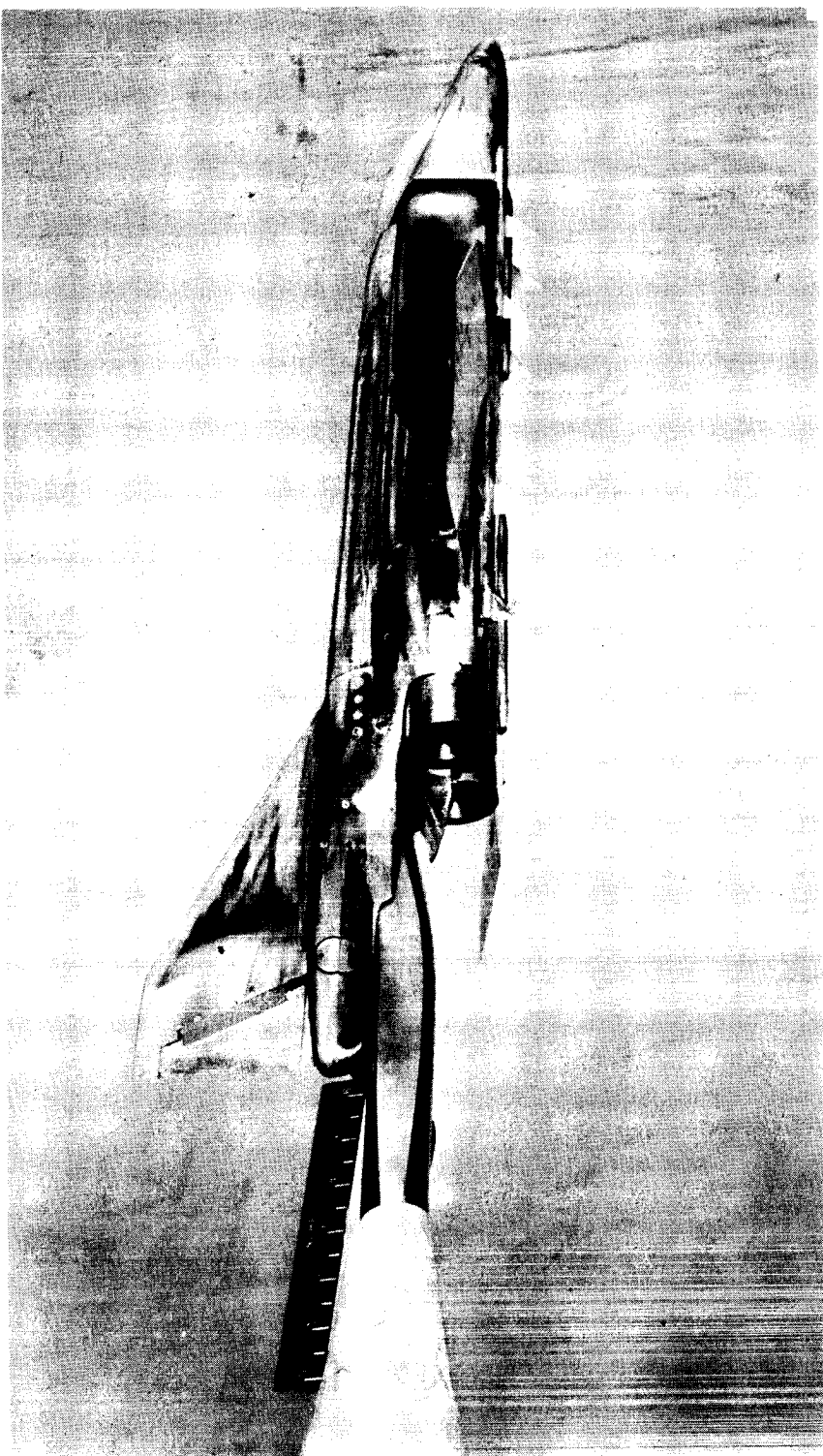
3C

L-524



L-94907
(a) Top view.

Figure 3.- Photographs of a model of a 45° swept wing airplane.

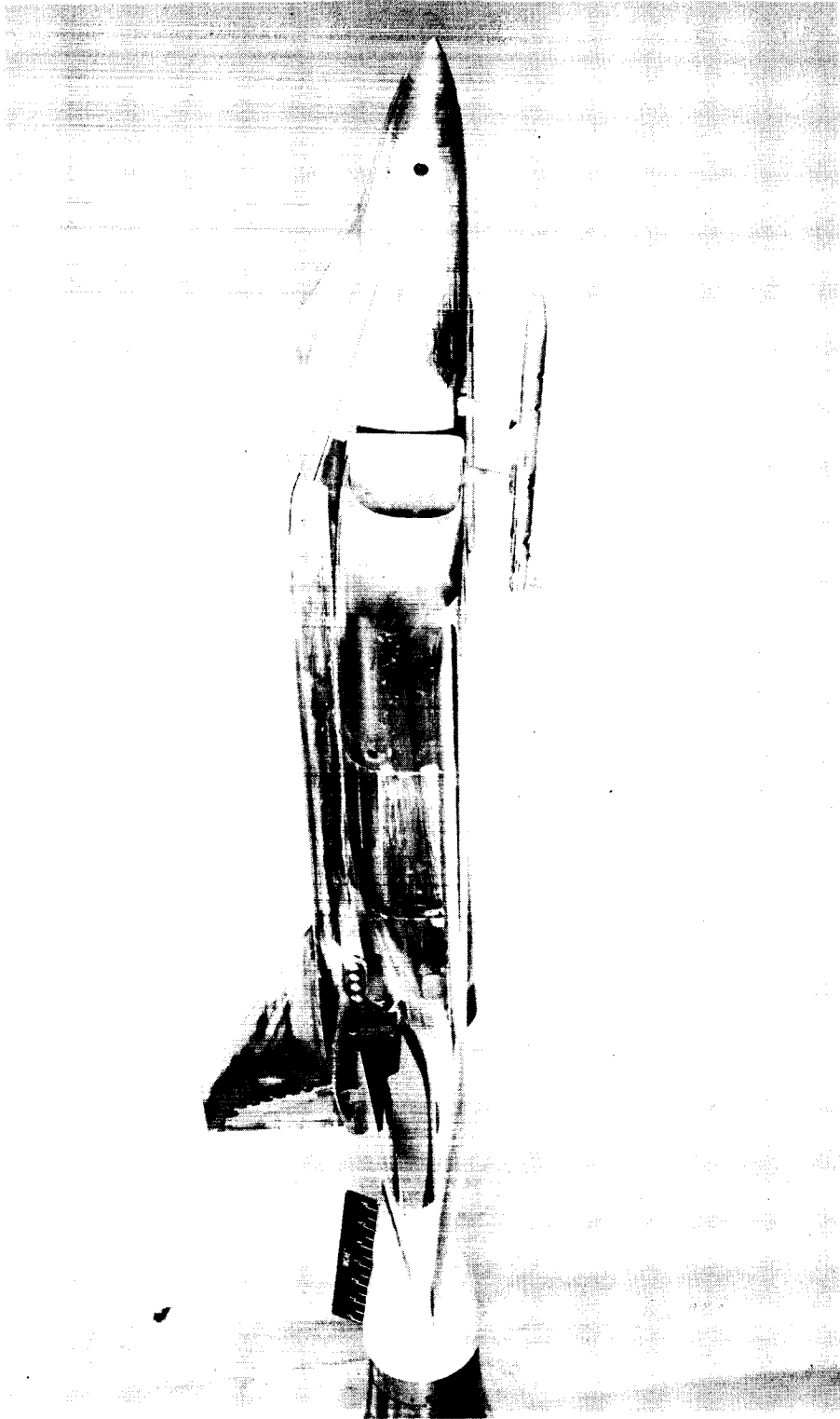


L-94899
(b) Three-quarter rear view.

Figure 3.- Continued.

REF ID: A69122
DECLASSIFIED

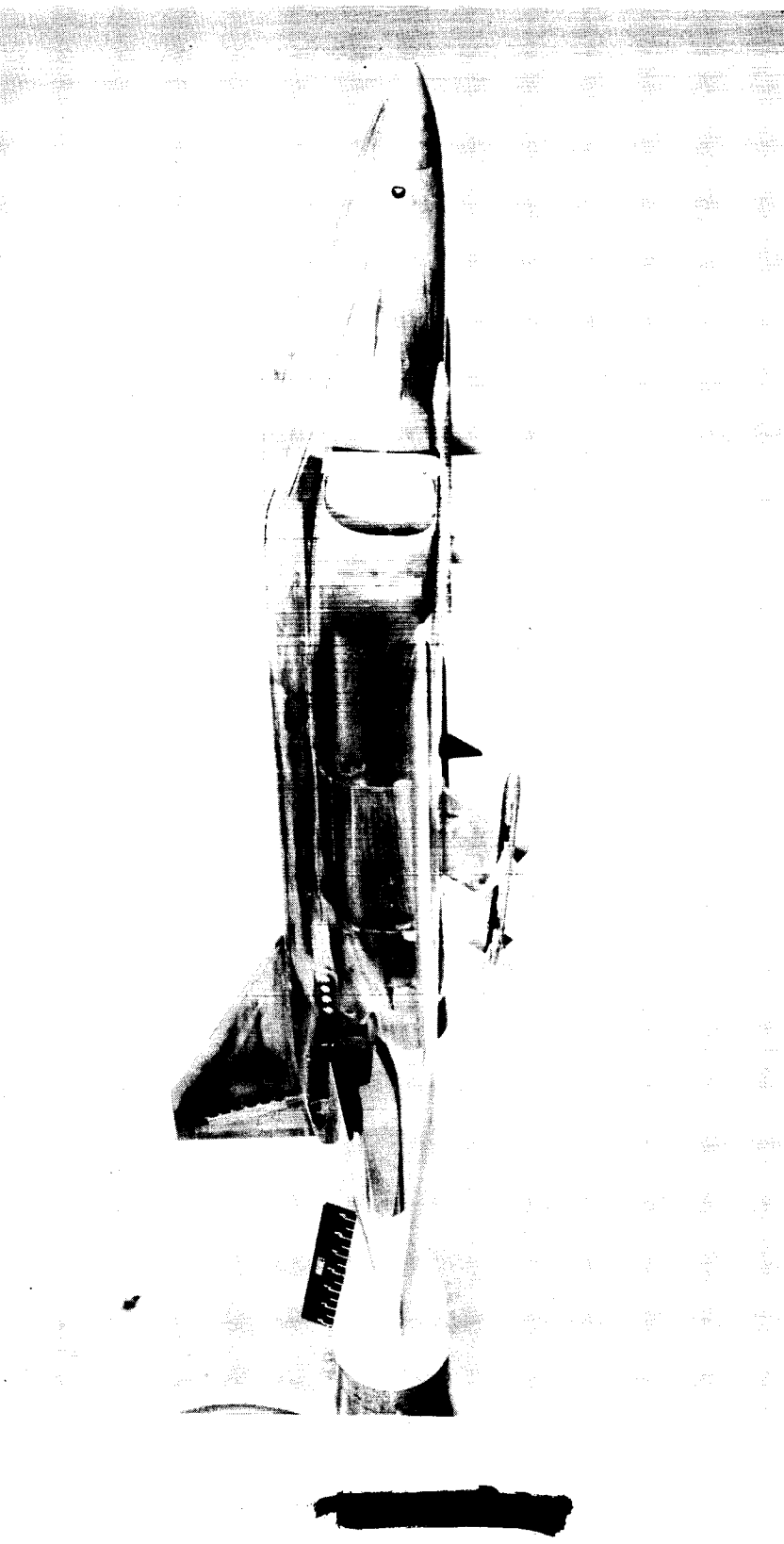
19



L-94905
(c) Three-quarter front view with forward missile extended.

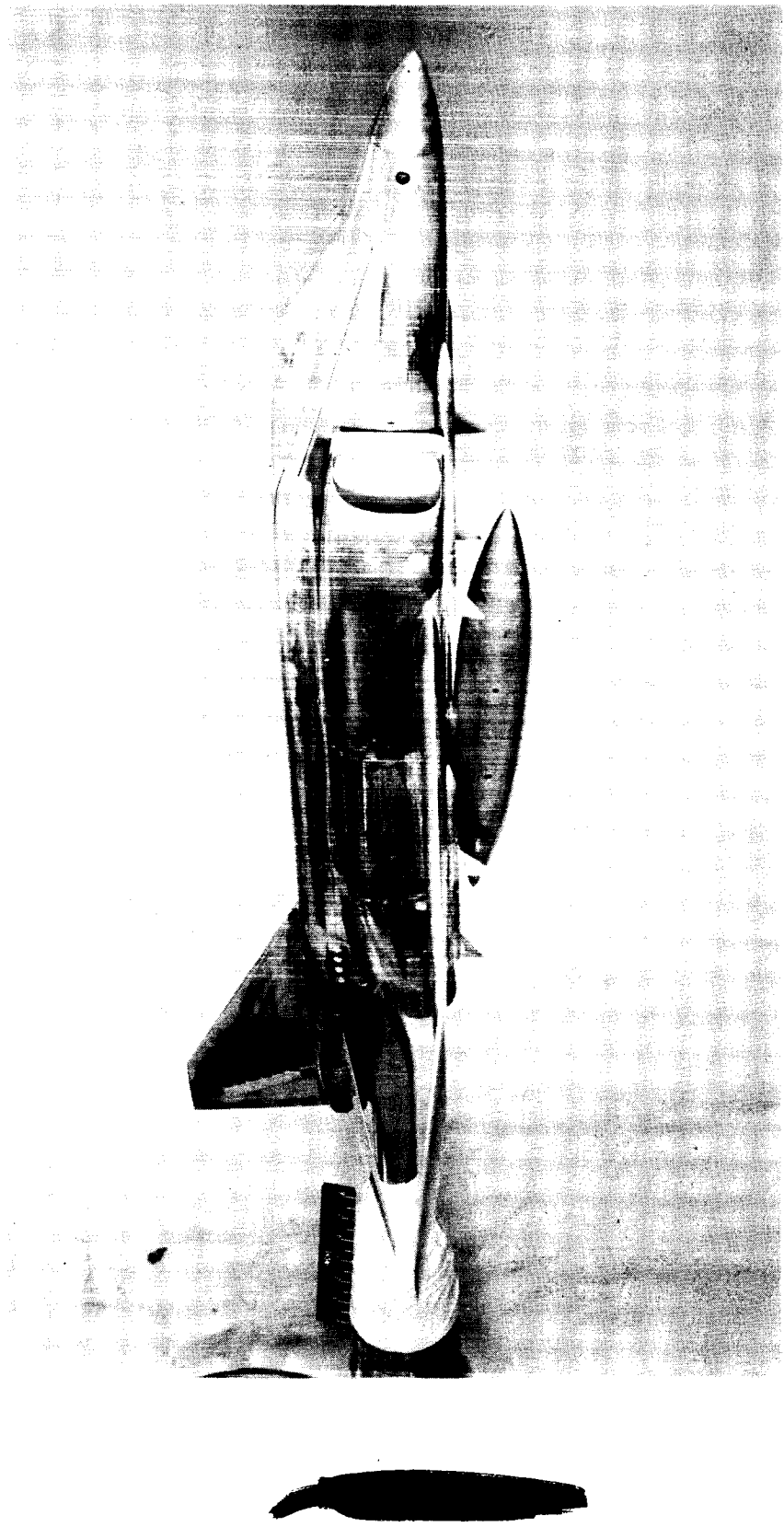
Figure 3.- Continued.

L-524



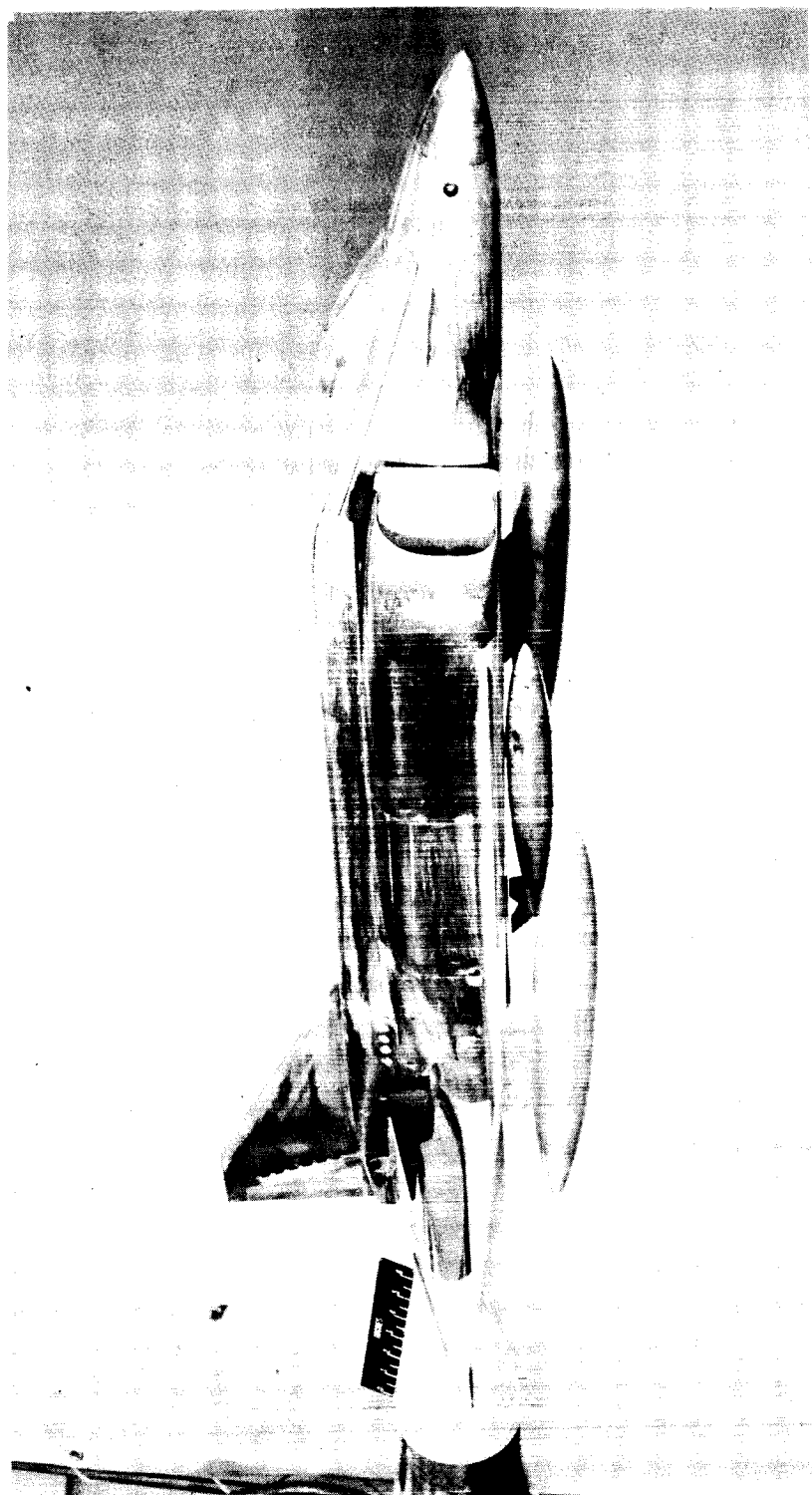
(d) Three-quarter front view with rear missile extended. L-94901

Figure 3.- Continued.



(e) Three-quarter front view with center-line tank. L-94902

Figure 3.- Continued.

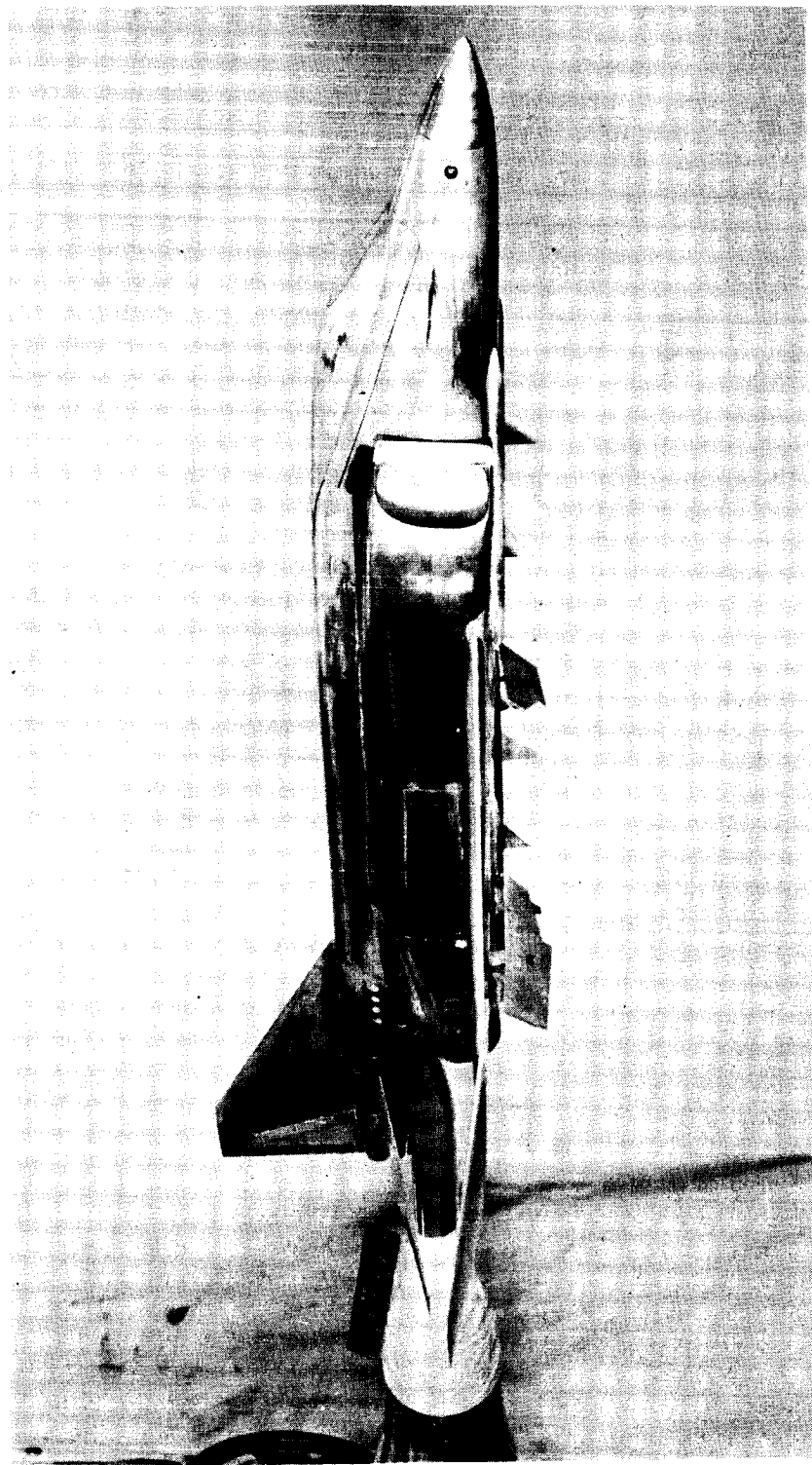


L-94906

(f) Three-quarter front view with wing tanks and center-line store.

Figure 3.- Continued.

REF ID: A65121



(g) Three-quarter front view with flaps deflected. L-94900

Figure 3.- Concluded.

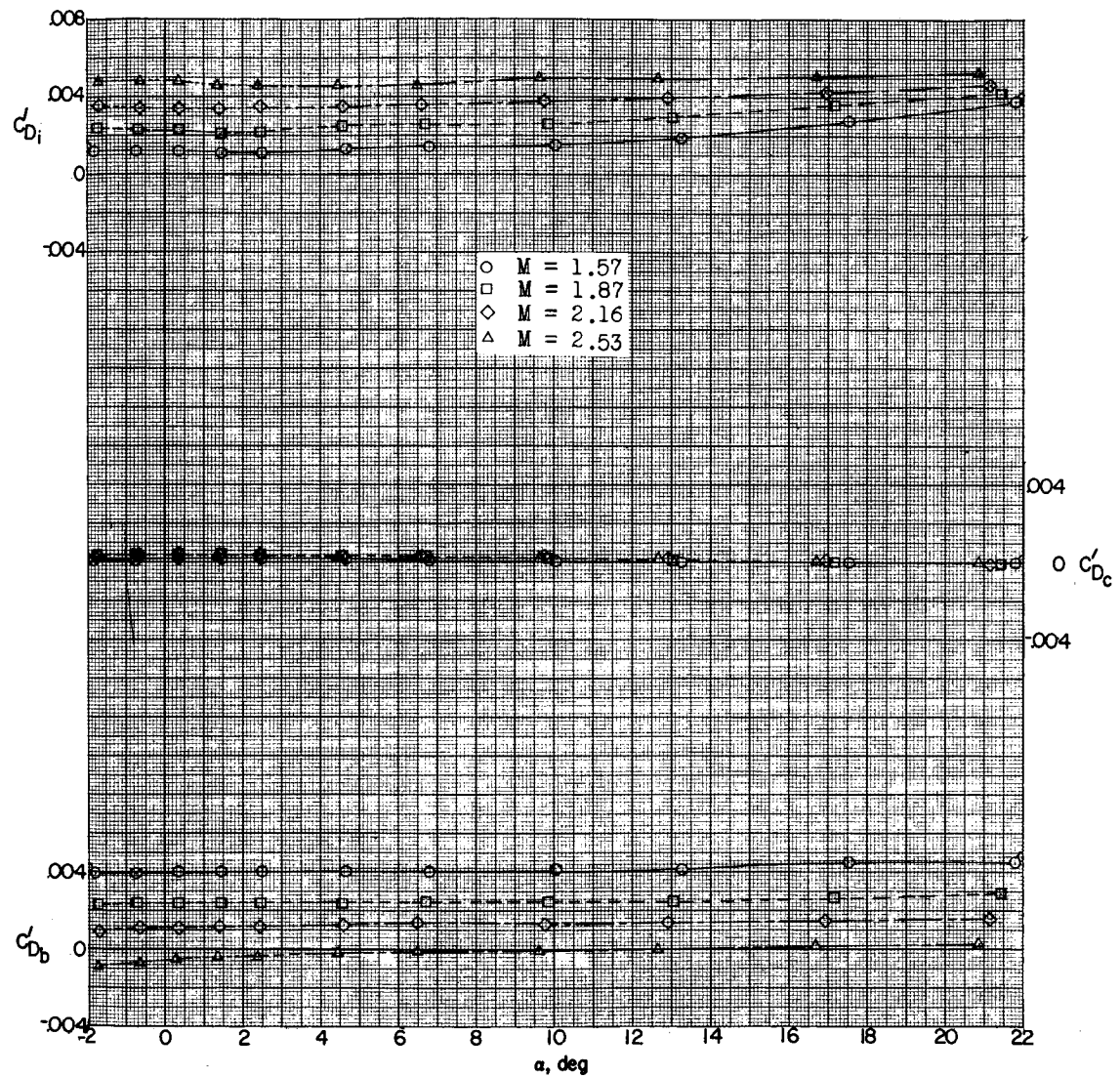


Figure 4.- Variation of internal-, chamber-, and base-drag coefficients with angle of attack. (Flagged symbols denote wall-reflected shock waves striking the tail.)

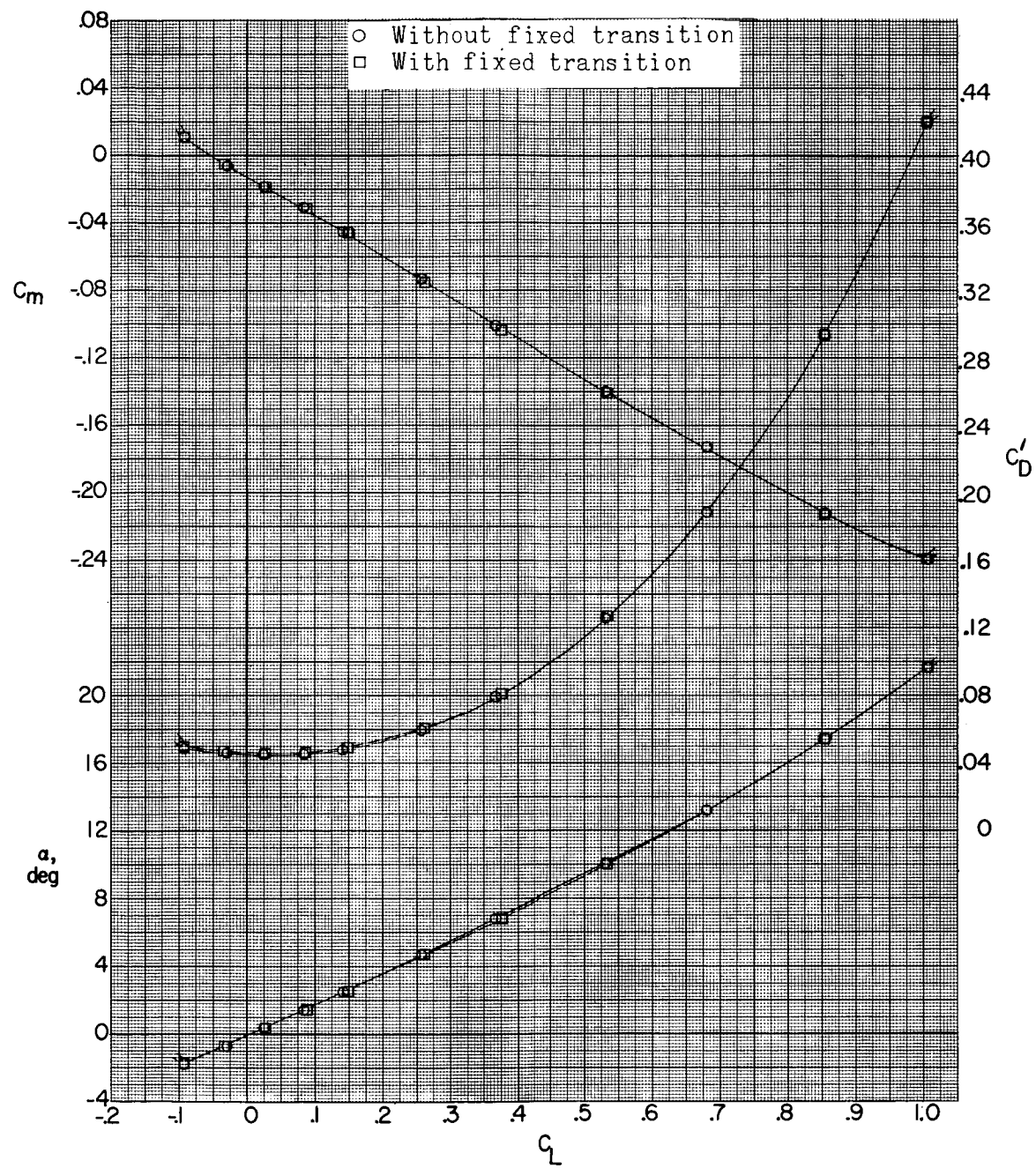
(a) $M = 1.57$.

Figure 5.- Effect of fixed transition on aerodynamic characteristics in pitch. (Flagged symbols denote wall-reflected shock waves striking the tail.)

0317122A1030

8

26

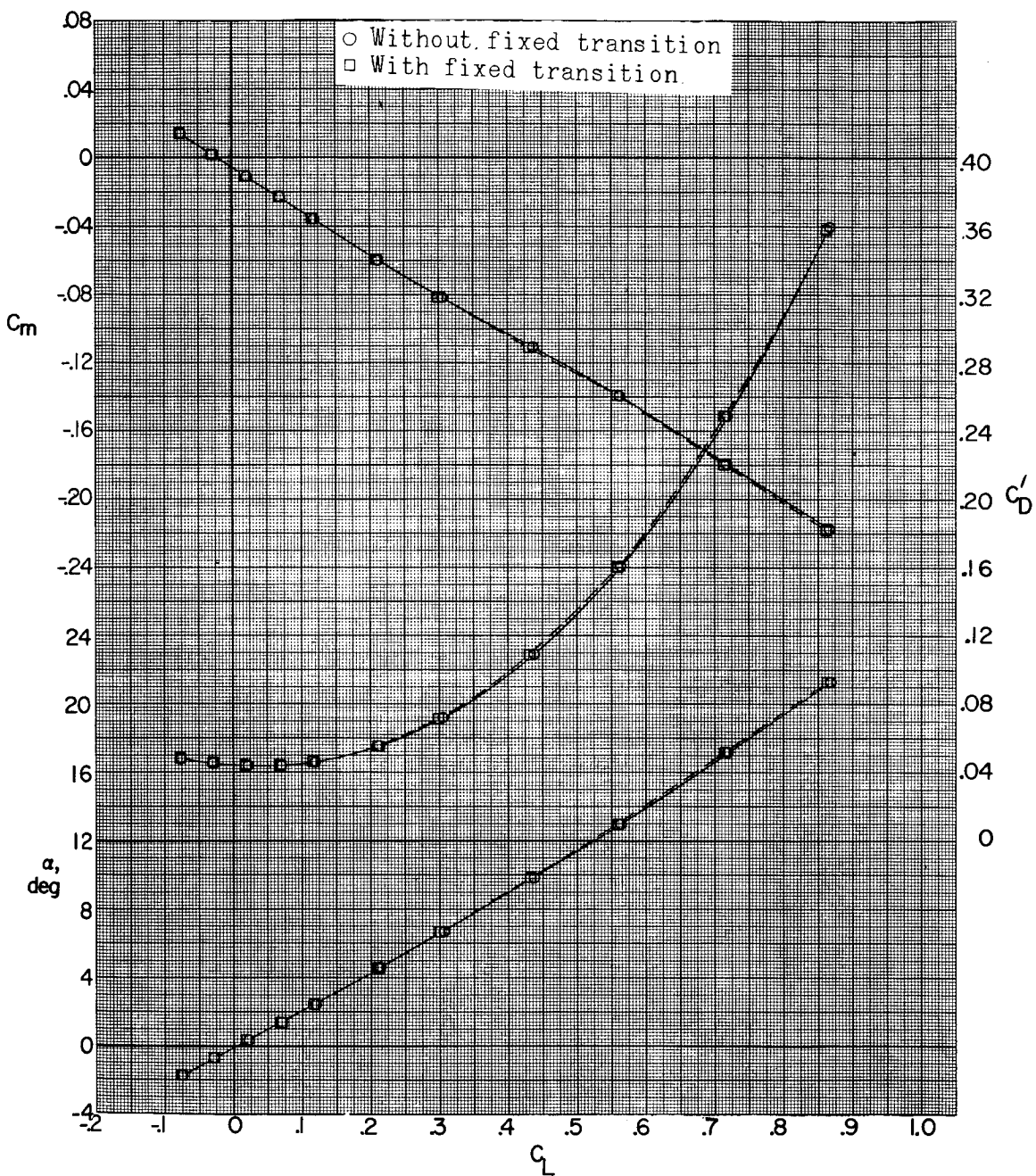
(b) $M = 1.87$.

Figure 5.- Continued.

REF ID: A6572

REF ID: A6572 CIFIED

27

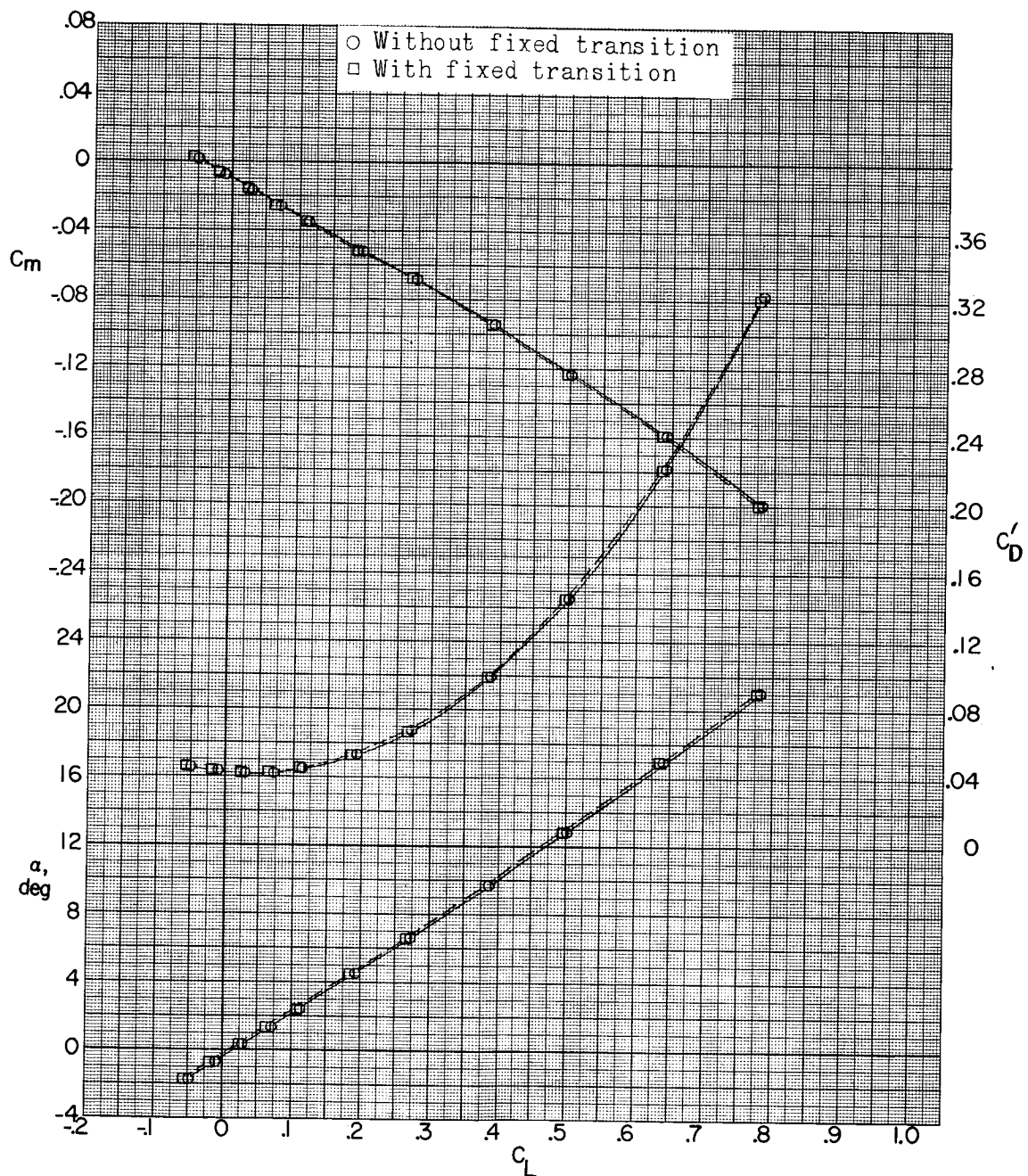
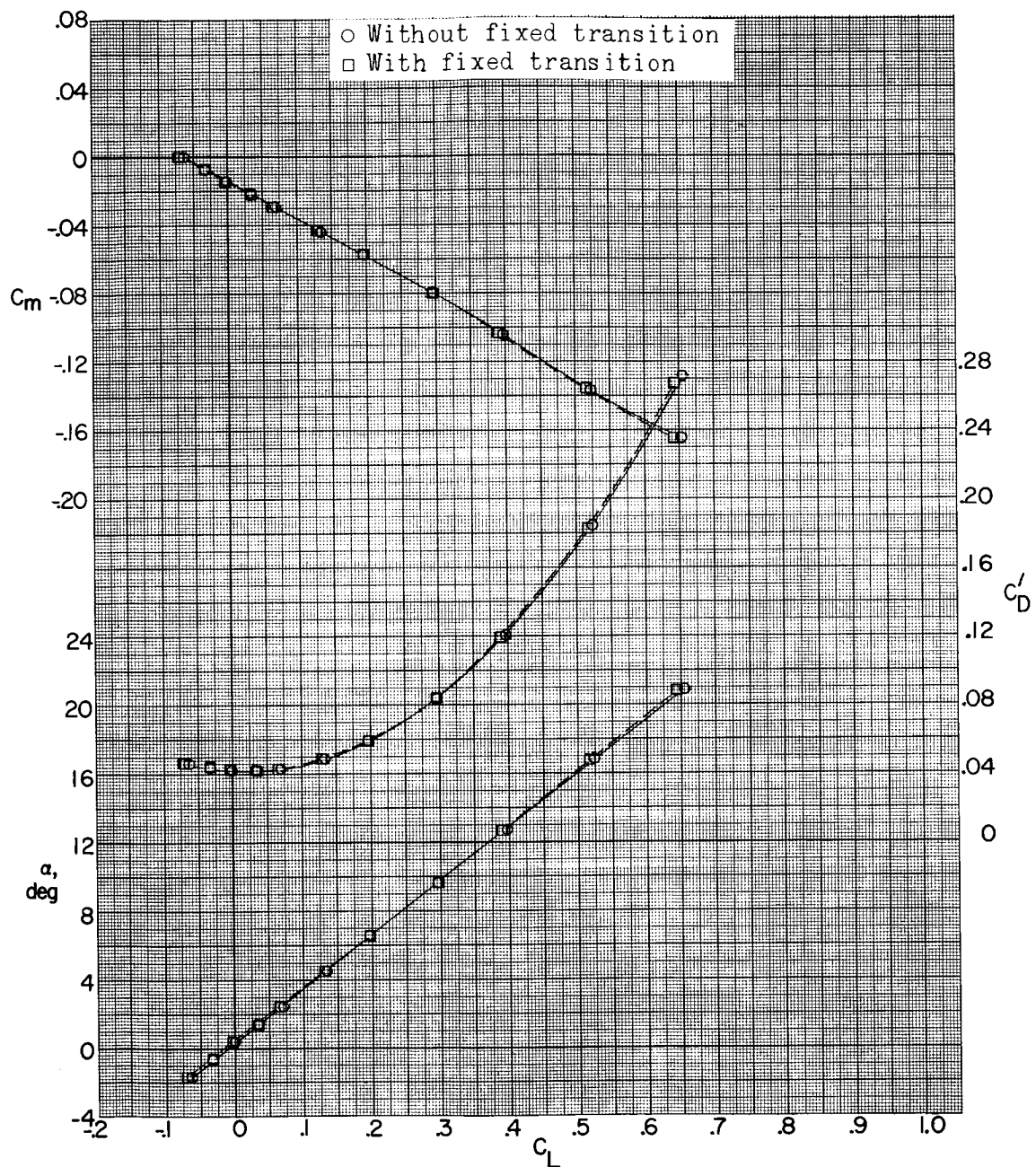
(c) $M = 2.16.$

Figure 5.- Continued.

0313102A1030

28



(d) $M = 2.53$.

Figure 5.- Concluded.

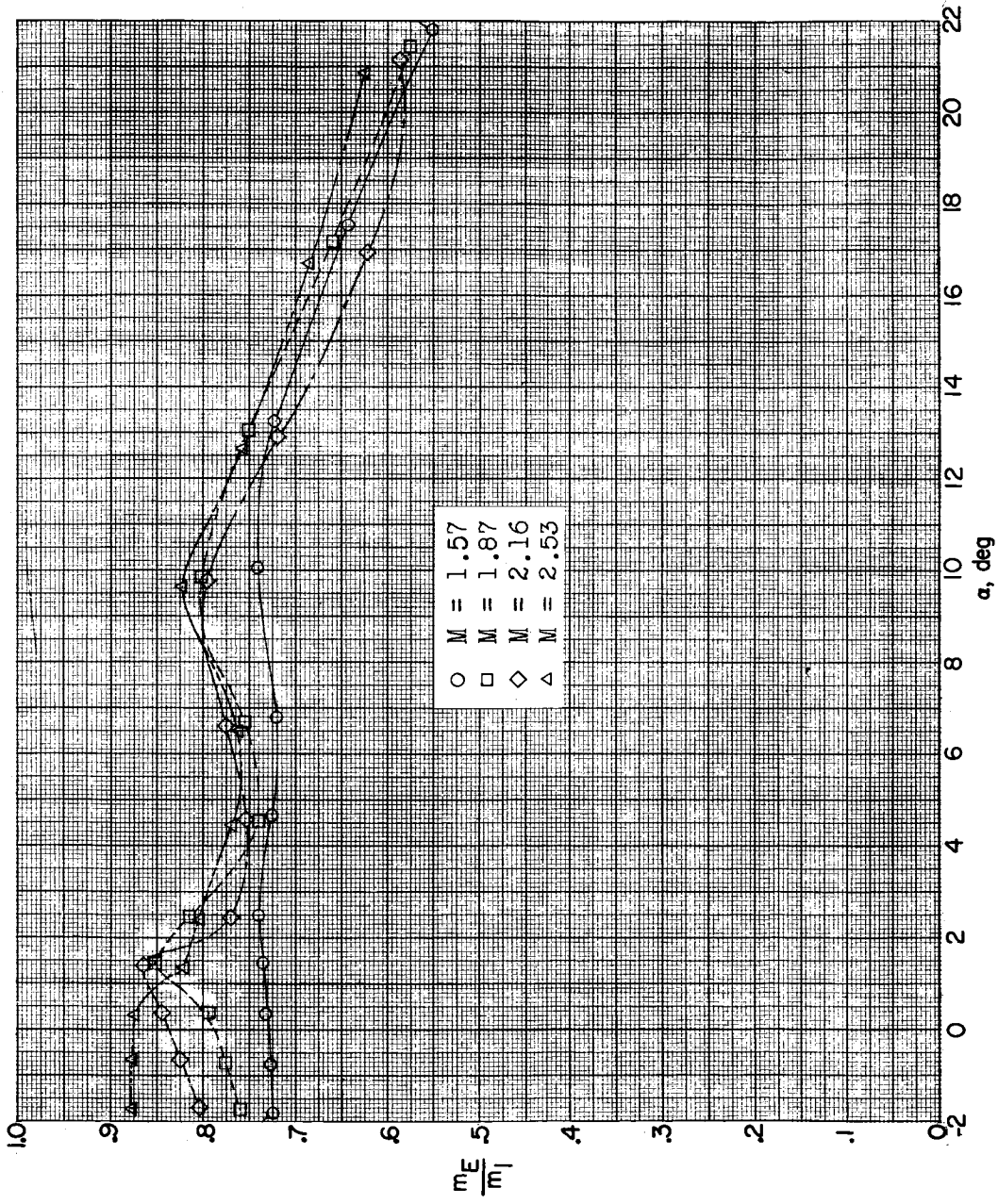
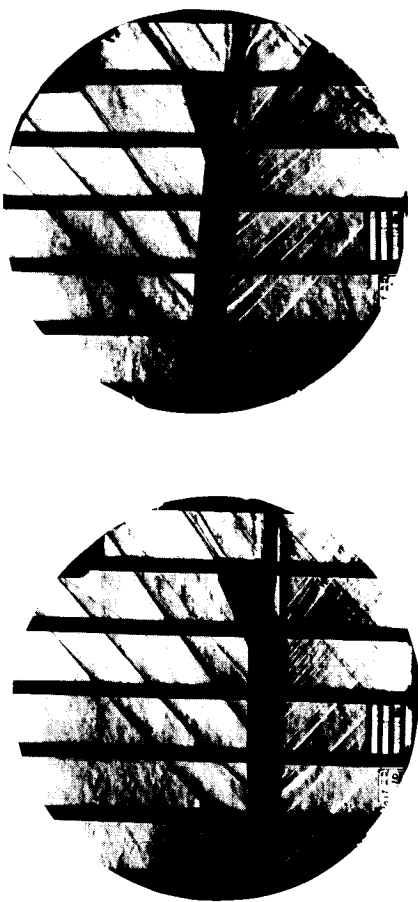


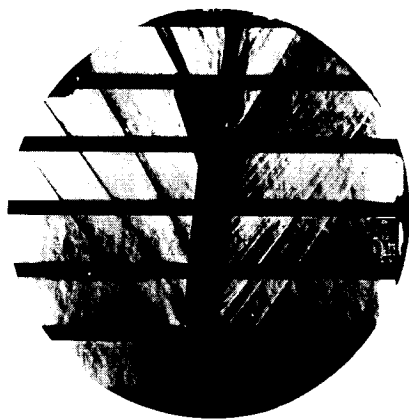
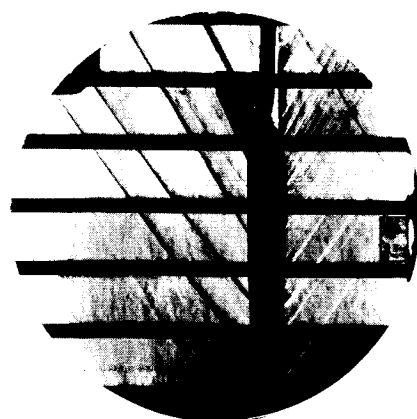
Figure 6.- Variation of mass-flow ratio with angle of attack. (Flagged symbols denote wall-reflected shock waves striking the tail.)

03/31/2010 30

 $\alpha = 4^\circ, \beta = 0^\circ$  $\alpha = 13.2^\circ, \beta = 0^\circ$  $\alpha = 17.4^\circ, \beta = 0^\circ$  $\alpha = 21.7^\circ, \beta = 0^\circ$ (a) Basic model; $M = 1.57$.

L-57-108

Figure 7.- Typical schlieren photographs of a model of a 45° swept wing airplane.
Phase II.

REF ID: A6274
CLASSIFIED $\alpha = 17.1^\circ, \beta = 0^\circ$  $\alpha = 31.7^\circ, \beta = 0^\circ$  $\alpha = 6.6^\circ, \beta = 0^\circ$  $\alpha = 25.5^\circ, \beta = 0^\circ$  $\alpha = 4^\circ, \beta = 0^\circ$  $\alpha = 21.3^\circ, \beta = 0^\circ$

L-57-109

(b) Basic model; M = 1.87.

Figure 7.- Continued.

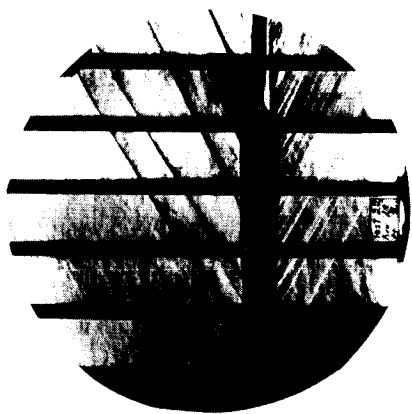
031310201030



$\alpha = 6.5^\circ, \beta = 0^\circ$



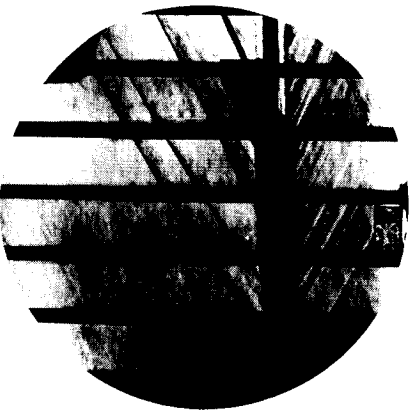
$\alpha = 21.14^\circ, \beta = 0^\circ$



$\alpha = 3^\circ, \beta = 0^\circ$



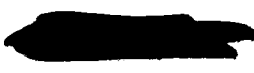
$\alpha = 16.9^\circ, \beta = 0^\circ$



$\alpha = -1.71^\circ, \beta = 0^\circ$



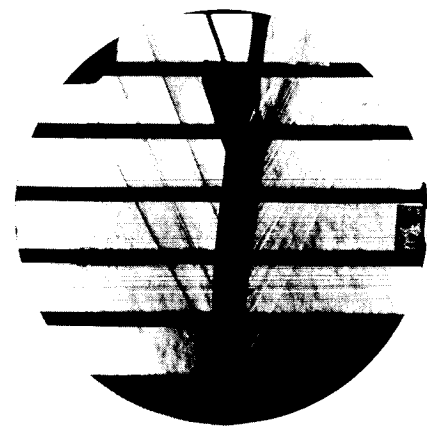
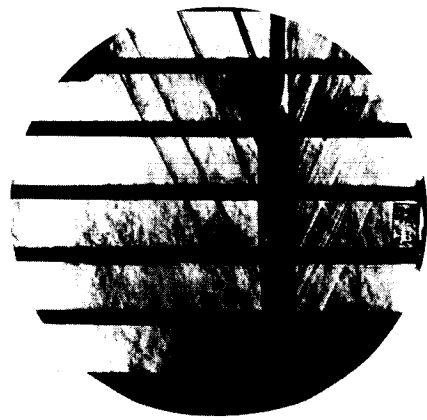
$\alpha = 12.7^\circ, \beta = 0^\circ$



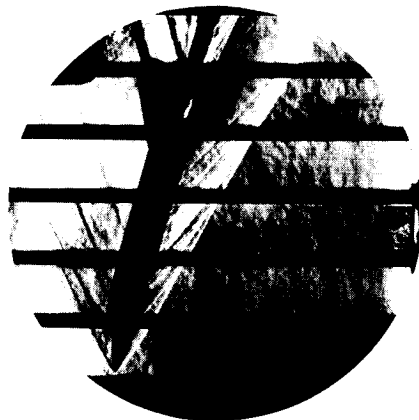
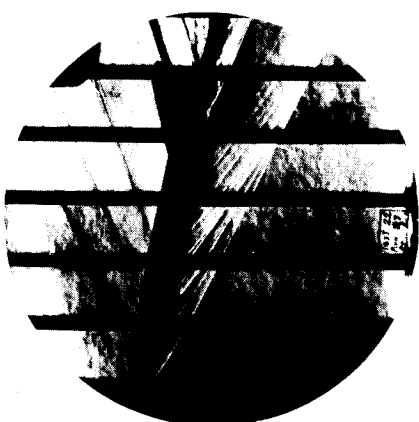
(c) Basic model; $M = 2.16$.

L-57-110

Figure 7.- Continued.


 $\alpha = 6.4^\circ, \beta = 0^\circ$

 $\alpha = 3^\circ, \beta = 0^\circ$

 $\alpha = -1.7^\circ, \beta = 0^\circ$

 $\alpha = 20.86^\circ, \beta = 0^\circ$

 $\alpha = 16.7^\circ, \beta = 0^\circ$

 $\alpha = 12.0^\circ, \beta = 0^\circ$

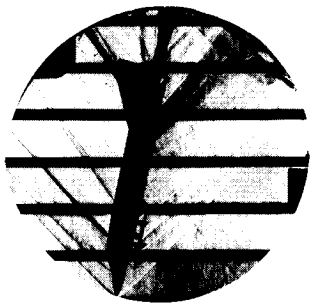
L-57-111

(d) Basic model; M = 2.53.

Figure 7.- Continued.

0313122AJ030

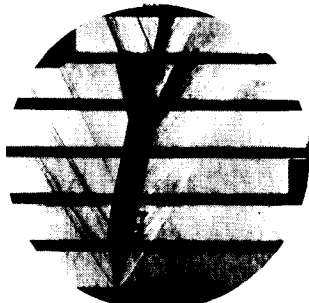
34



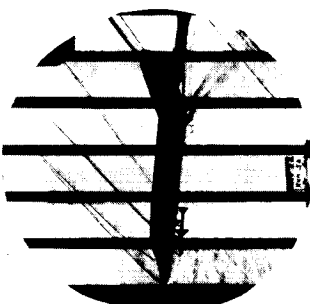
$\alpha = 3^\circ, \beta = 0^\circ$



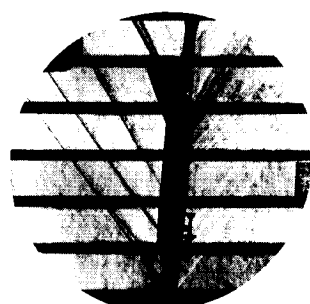
$\alpha = 13.32^\circ, \beta = 0^\circ$



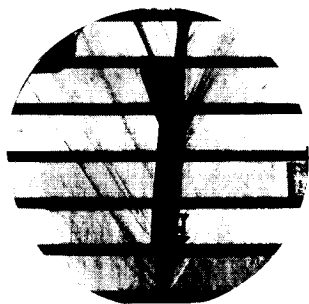
$\alpha = 13^\circ, \beta = 0^\circ$



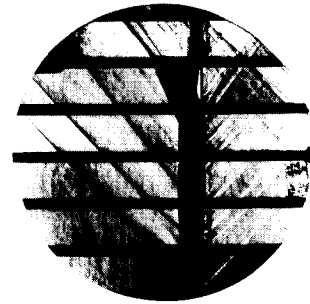
$\alpha = 6.7^\circ, \beta = 0^\circ$



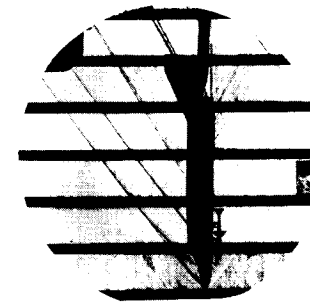
$\alpha = 6.7^\circ, \beta = 3^\circ$



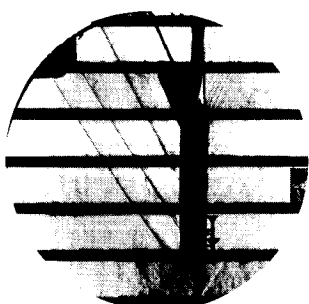
$\alpha = 12.8^\circ, \beta = 0^\circ$



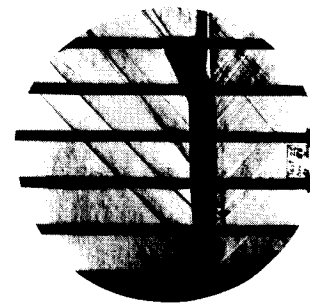
$\alpha = 2.54^\circ, \beta = 0^\circ$



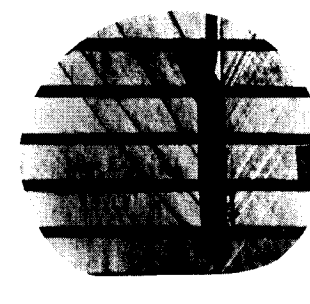
$\alpha = 2.4^\circ, \beta = 0^\circ$



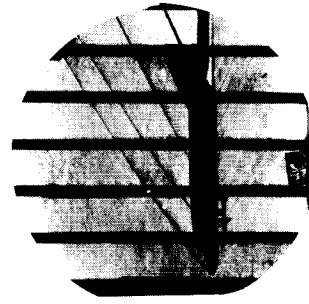
$\alpha = 6.55^\circ, \beta = 0^\circ$



$\alpha = 3^\circ, \beta = 0^\circ$



$\alpha = 3^\circ, \beta = 0^\circ$



$\alpha = 3^\circ, \beta = 0^\circ$

(e) Forward missile extended.

Figure 7.4 Concluded.

8

UNCLASSIFIED

35

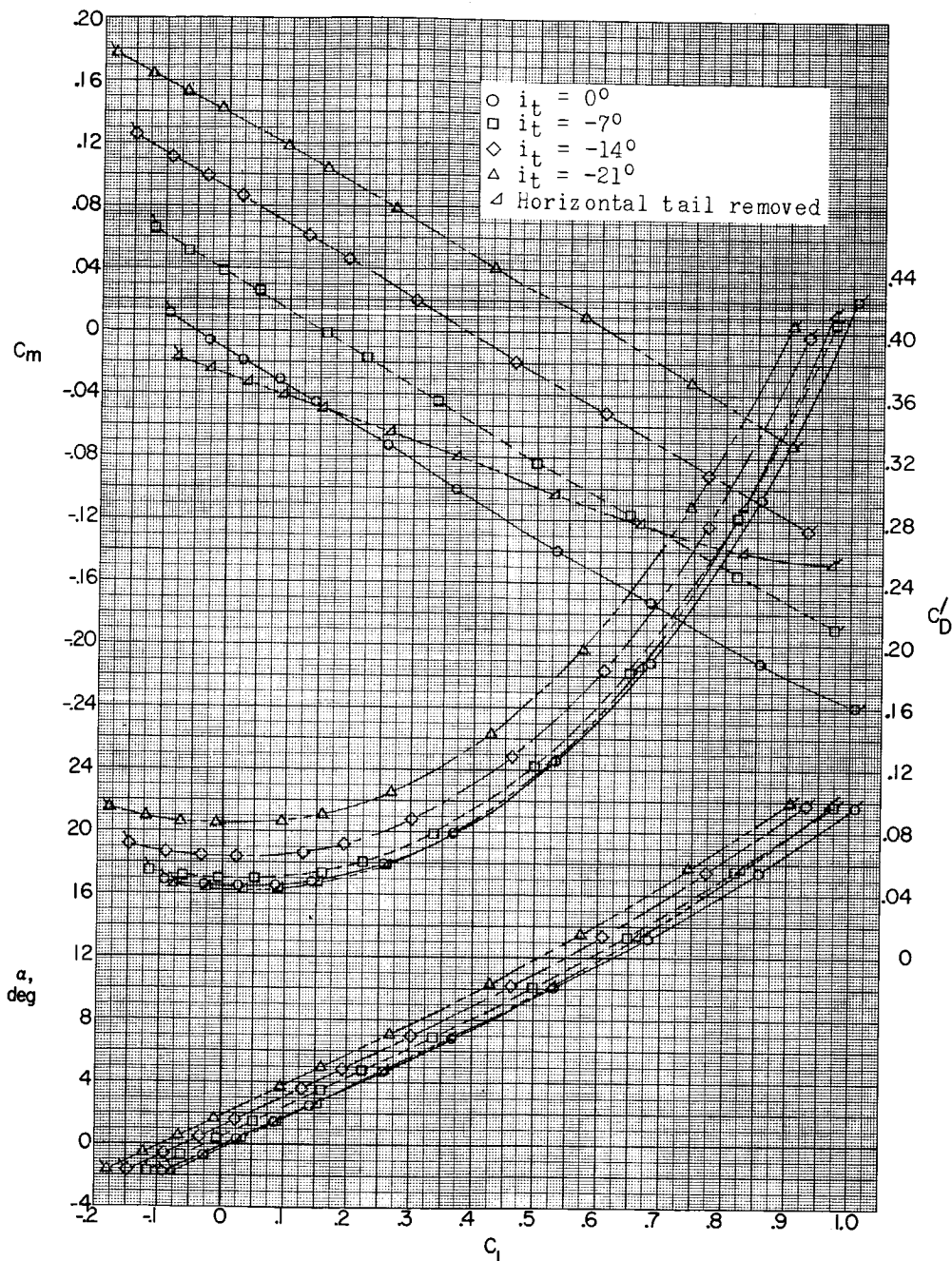
(a) $M = 1.57$.

Figure 8.- Effect of horizontal tail on aerodynamic characteristics in pitch. (Flagged symbols denote wall-reflected shock waves striking the tail.)

0317122A1030

36

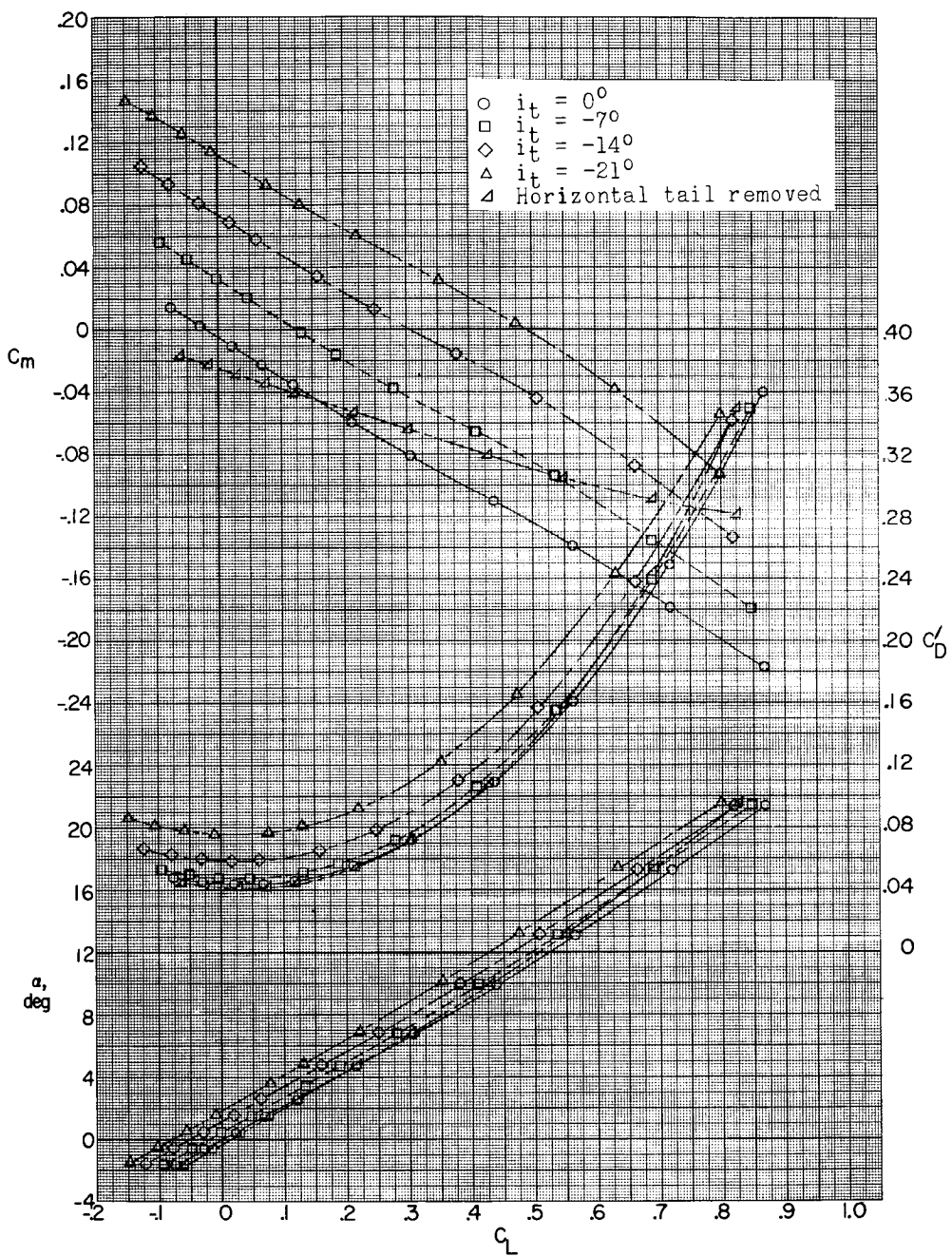
(b) $M = 1.87$.

Figure 8.- Continued.

8

REF ID: A6251

37

L-524

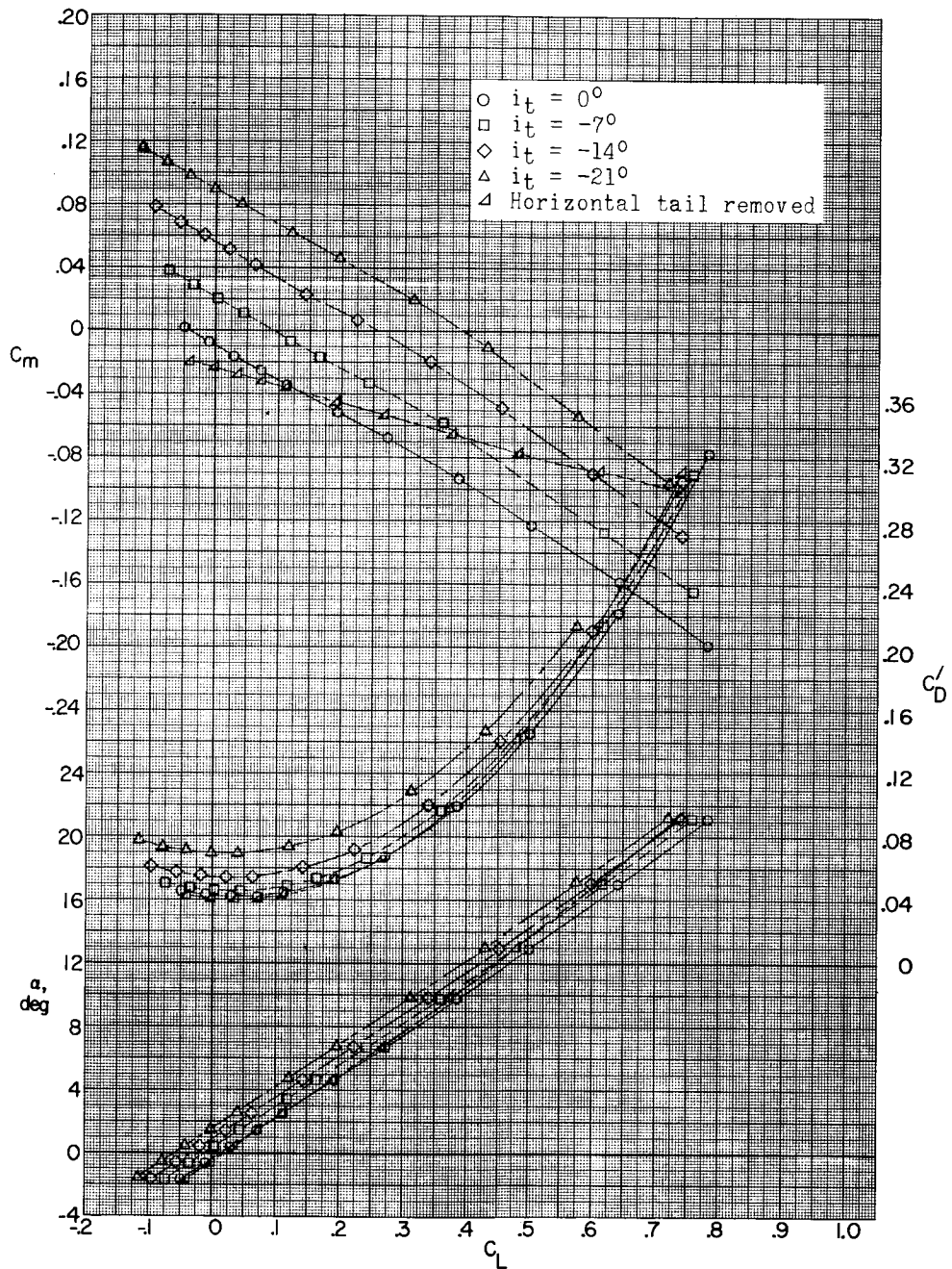
(c) $M = 2.16.$

Figure 8.- Concluded.

031718201030

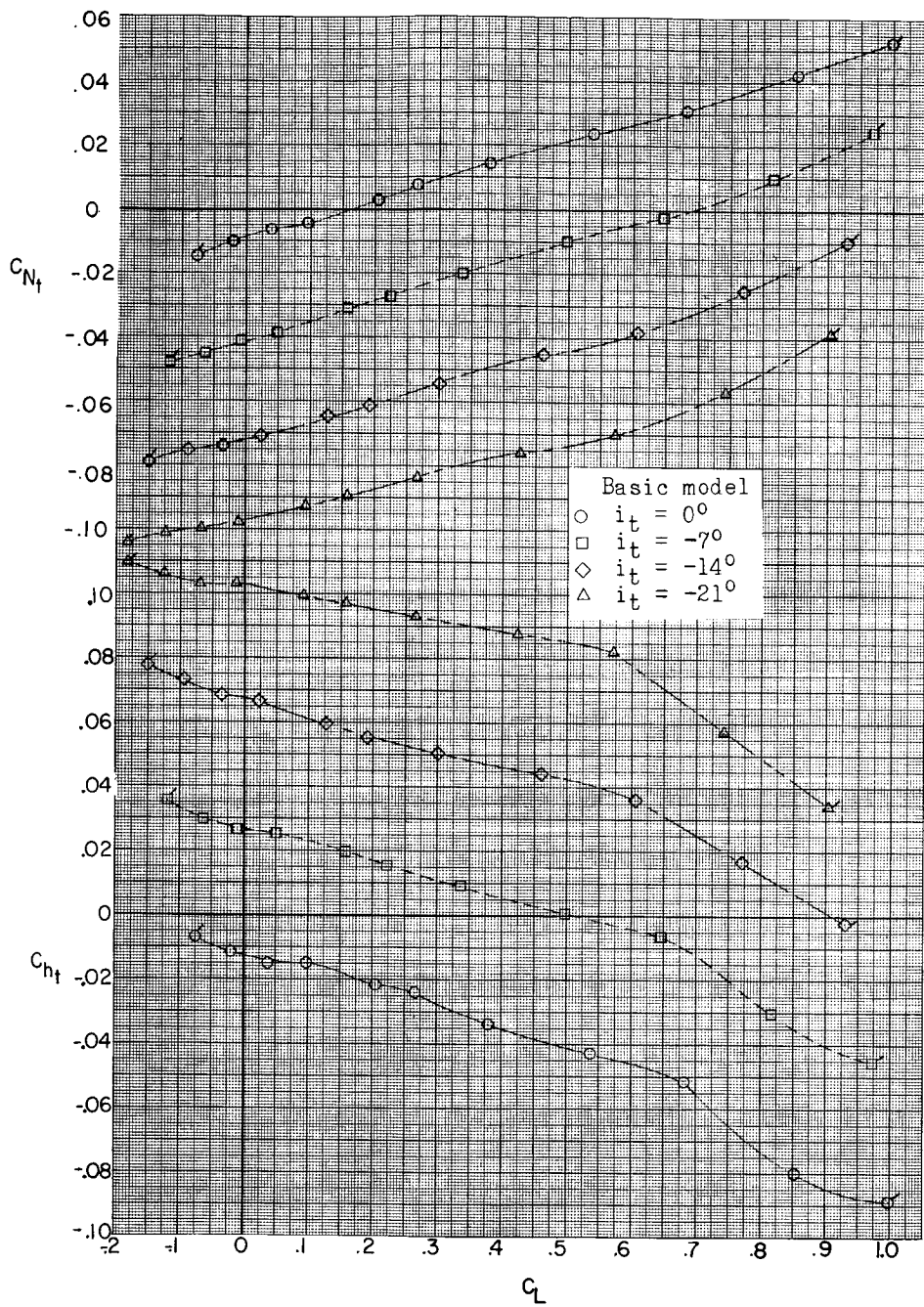
(a) $M = 1.57$.

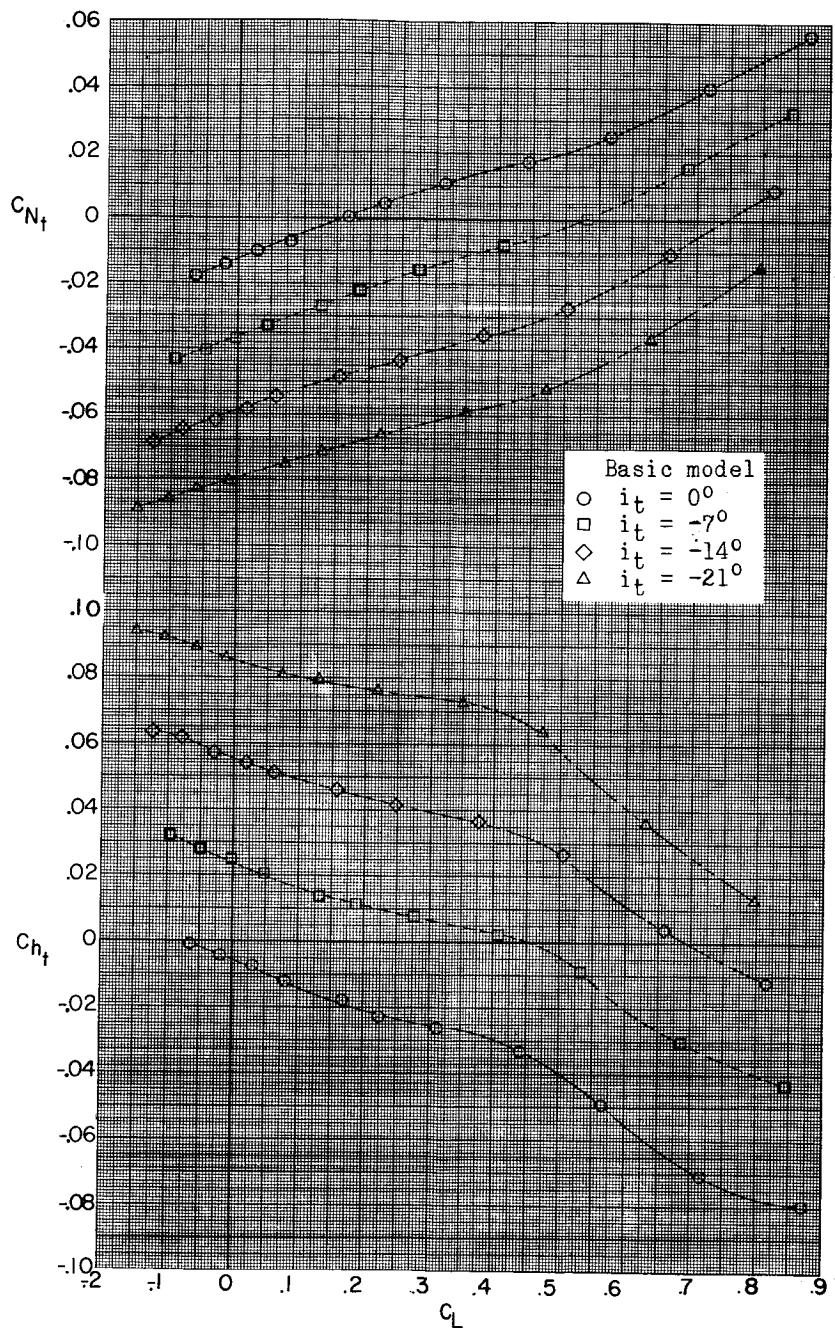
Figure 9.- Variation of stabilator hinge-moment and normal-force coefficient with lift coefficient. (Flagged symbols denote wall-reflected shock waves striking the tail.)



SECRET CLASSIFIED

39

L-524

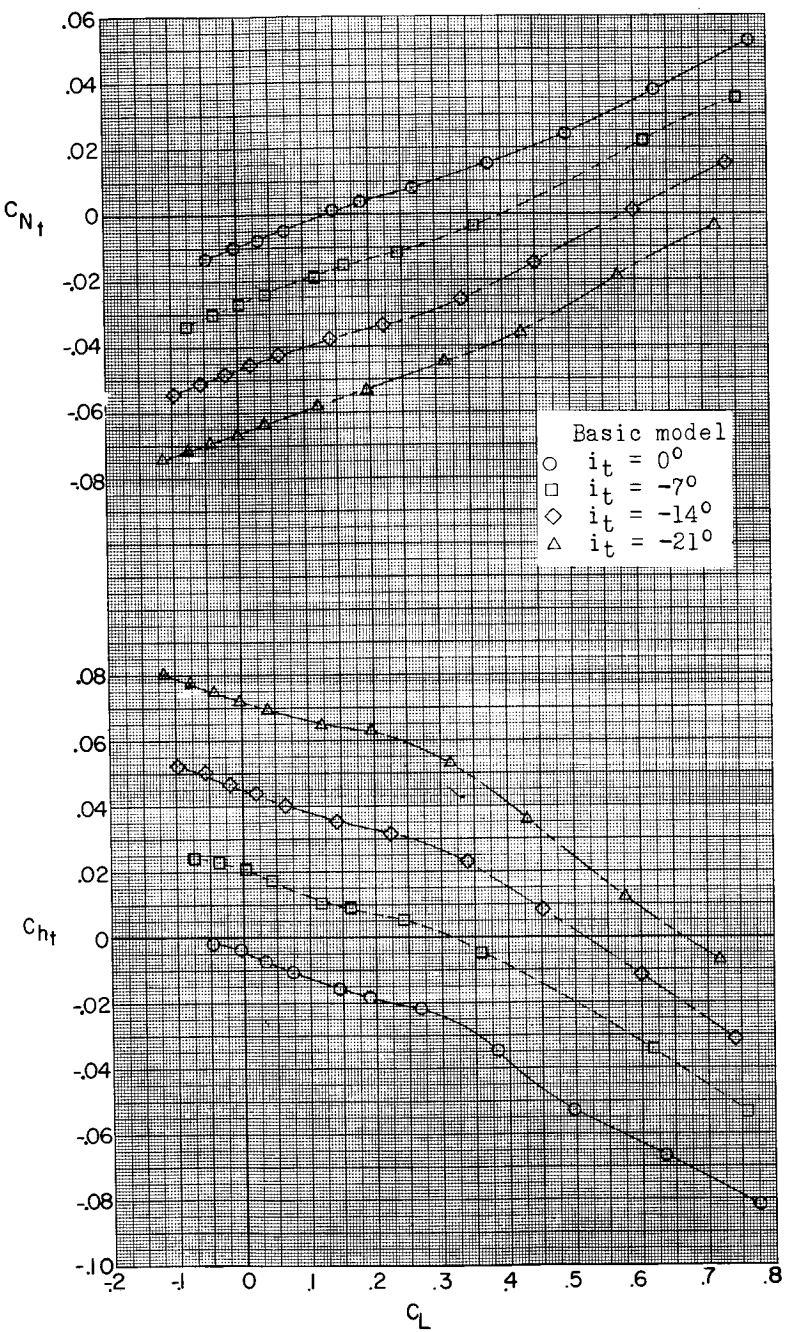


(b) $M = 1.87$.

Figure 9.- Continued.

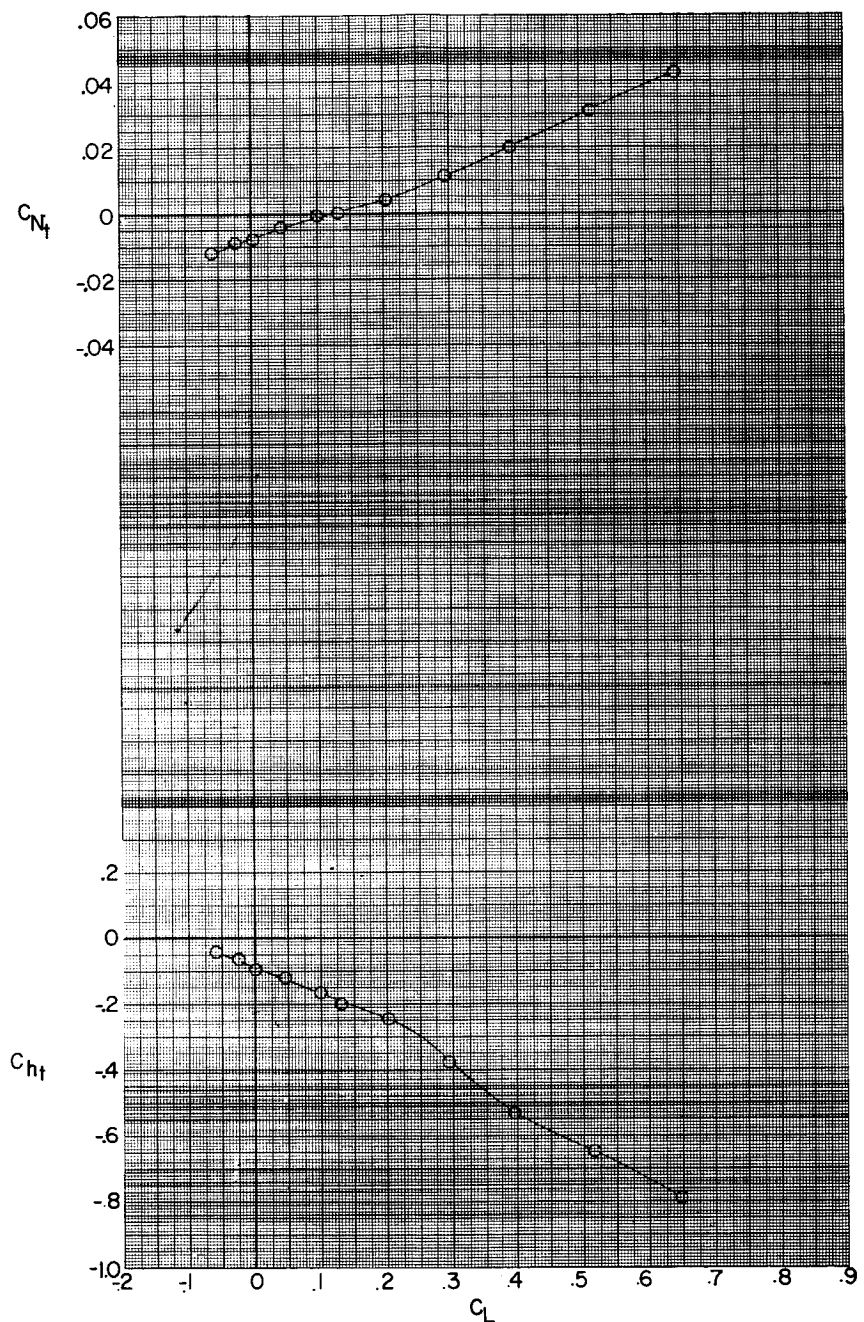
031312201030

40



(c) $M = 2.16.$

Figure 9.- Continued.



(d) $M = 2.53; i_t = 0^\circ$.

Figure 9.- Concluded.

031713200110

42

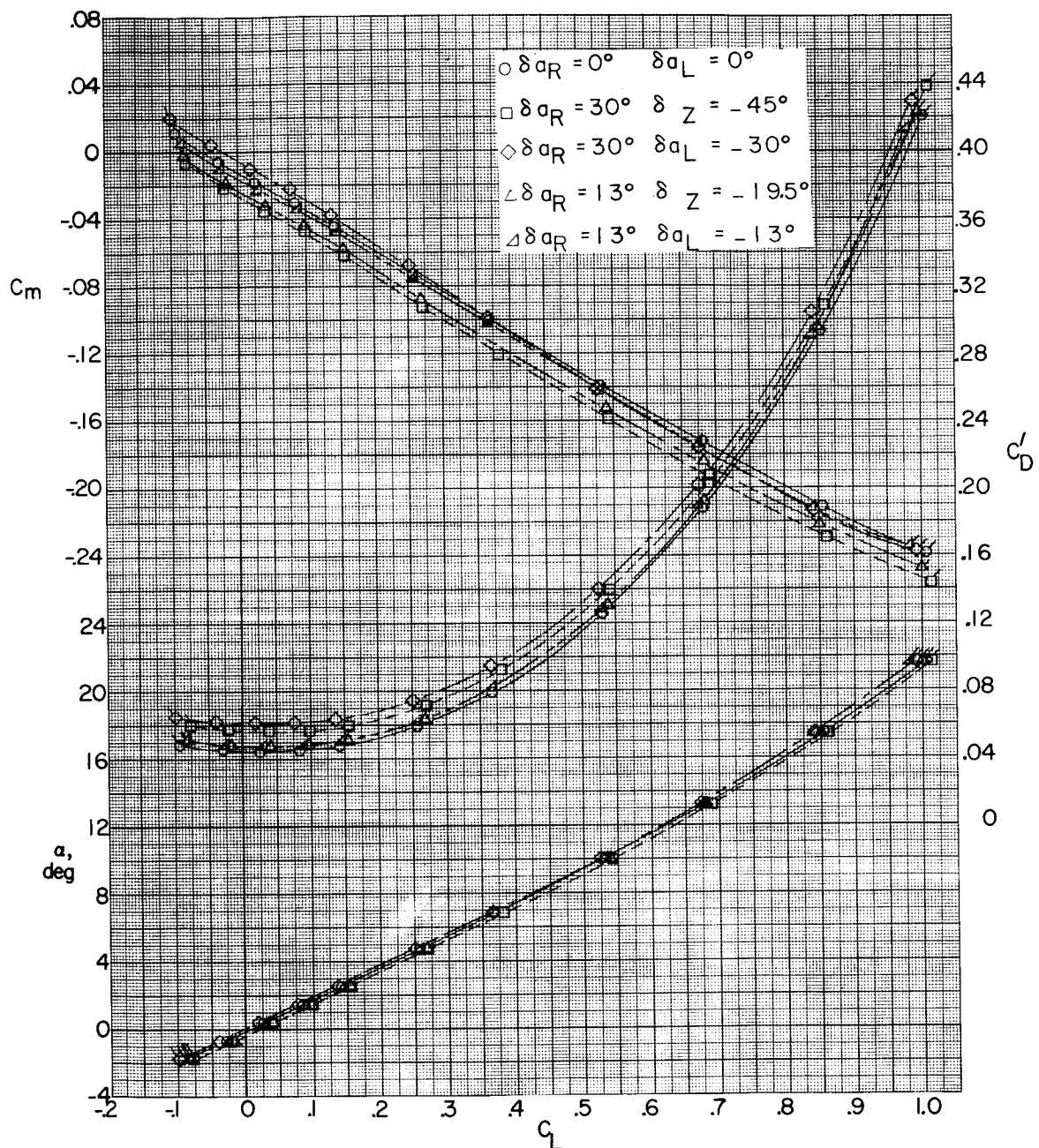
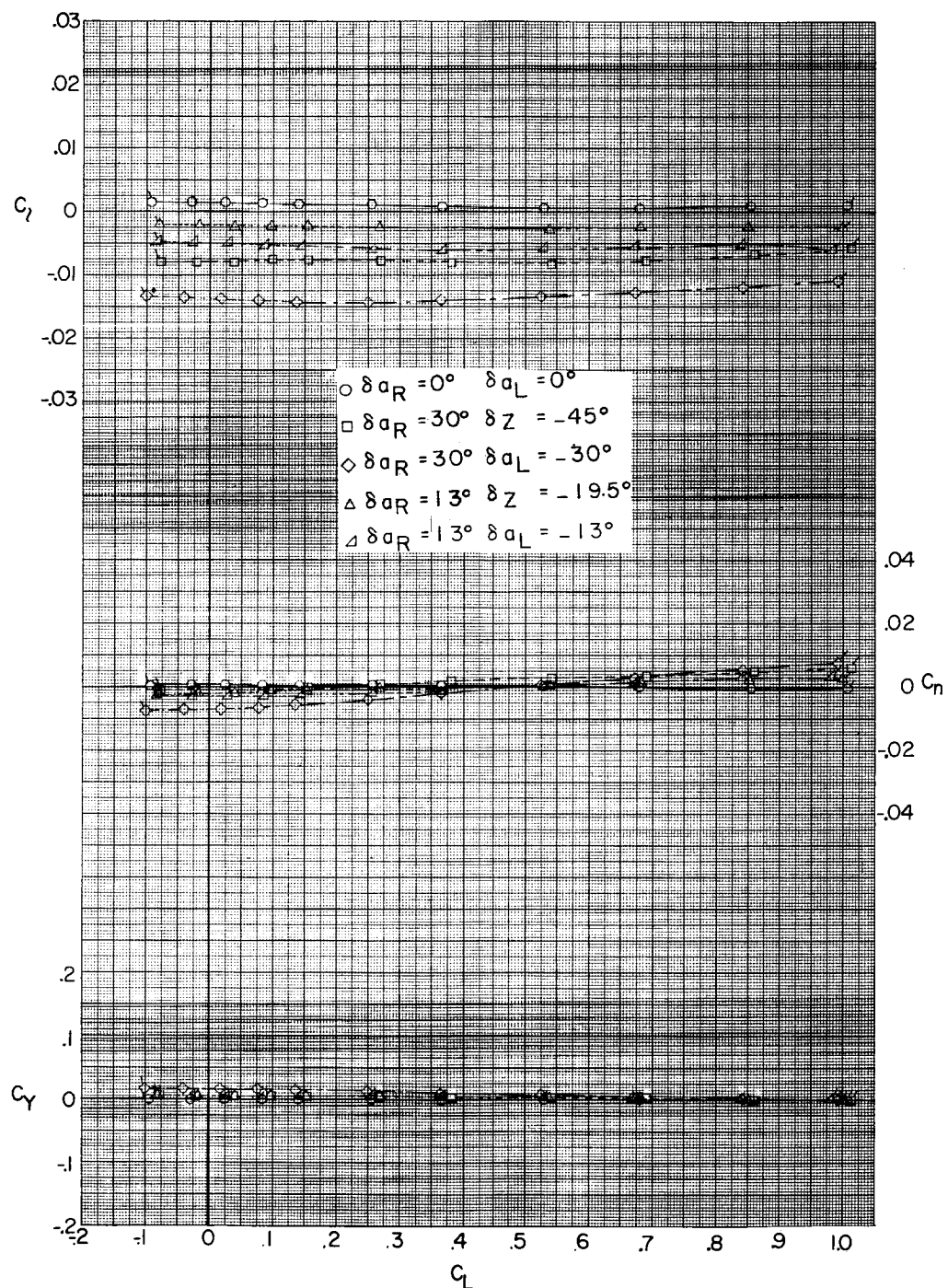
(a) $M = 1.57$.

Figure 10.- Effect of ailerons and spoilers on aerodynamic characteristics in pitch. (Flagged symbols denote wall-reflected shock waves striking the tail.)



(a) Concluded.

Figure 10.- Continued.

031313 28 JUN 90

44

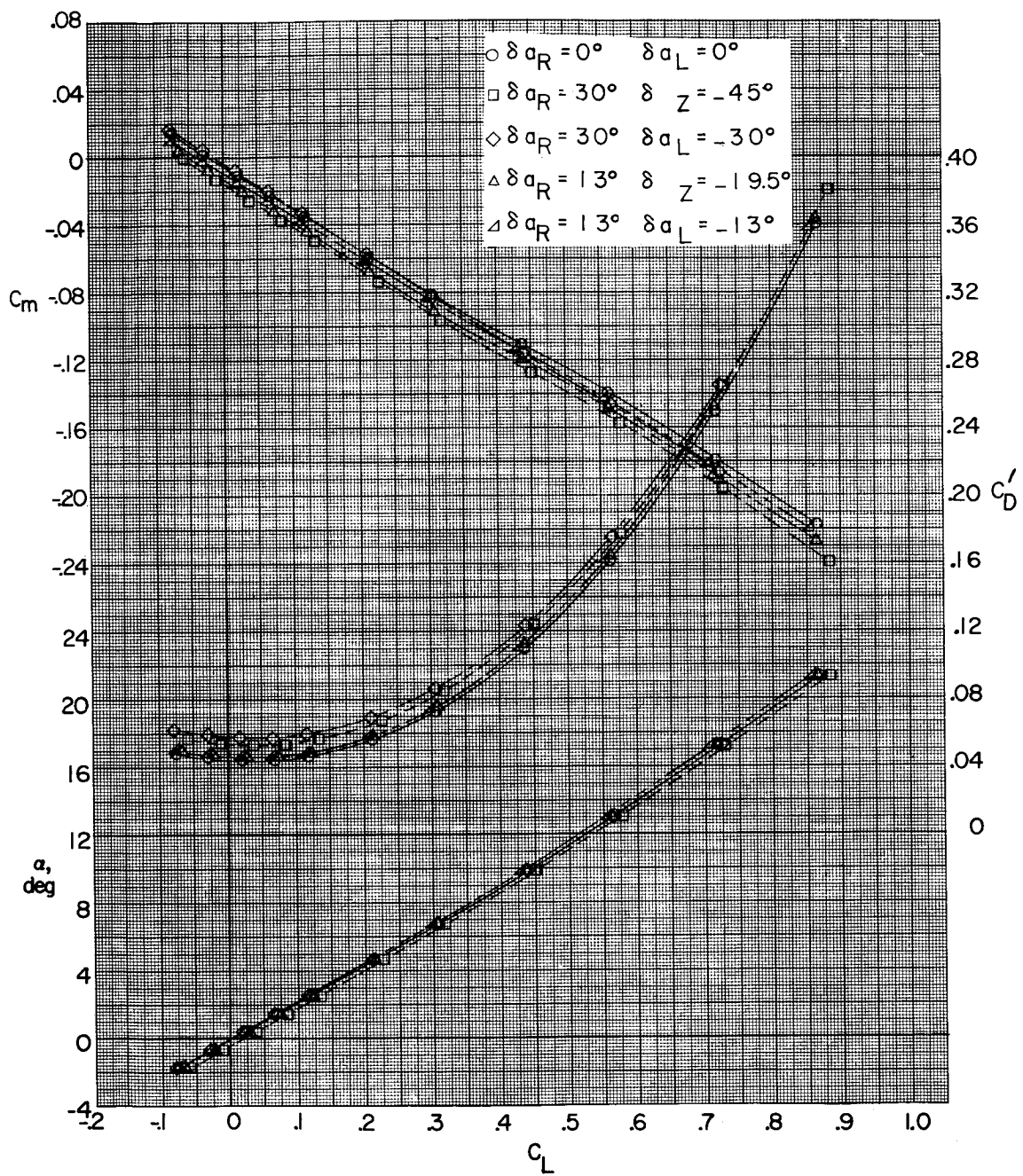
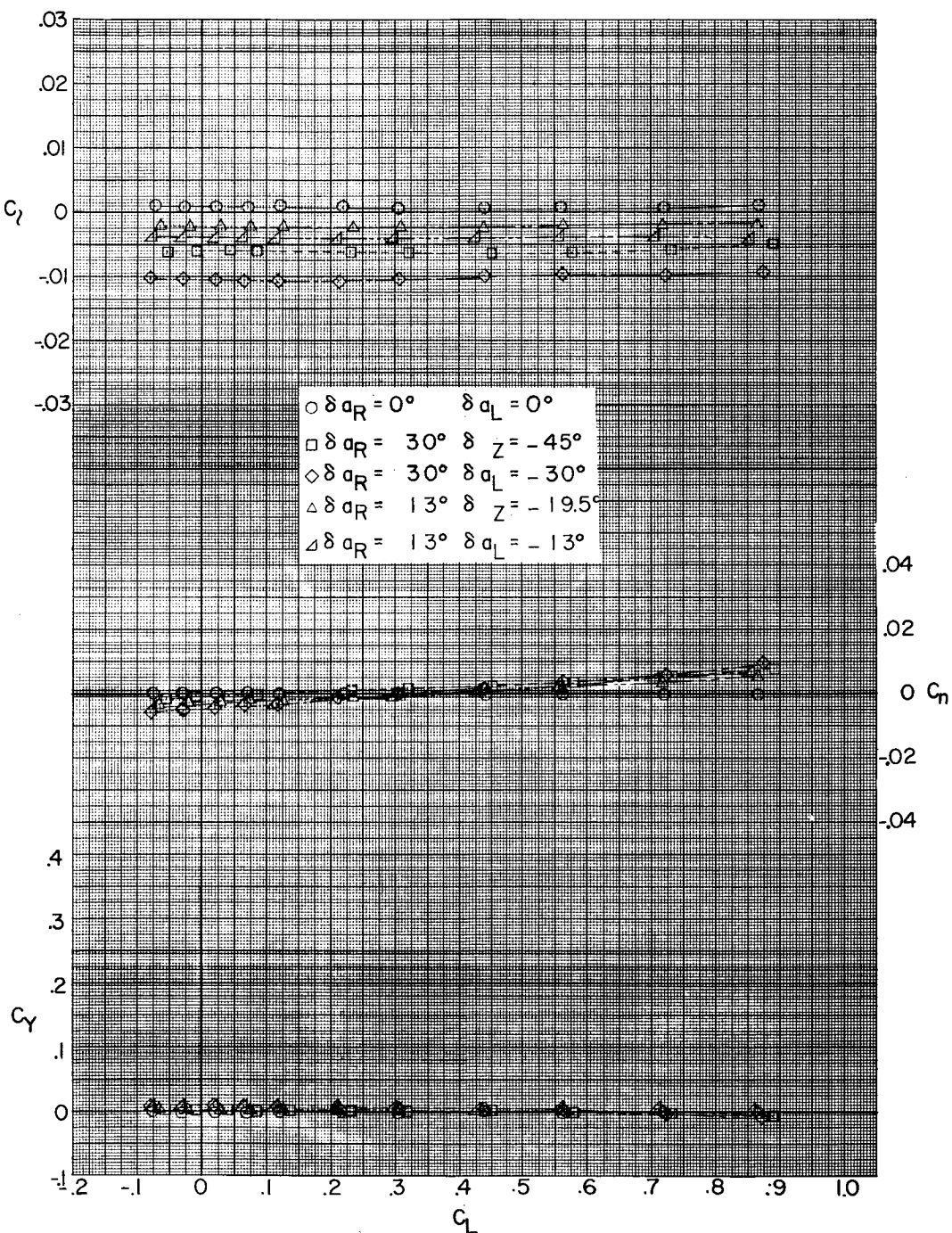
(b) $M = 1.87$.

Figure 10.- Continued.

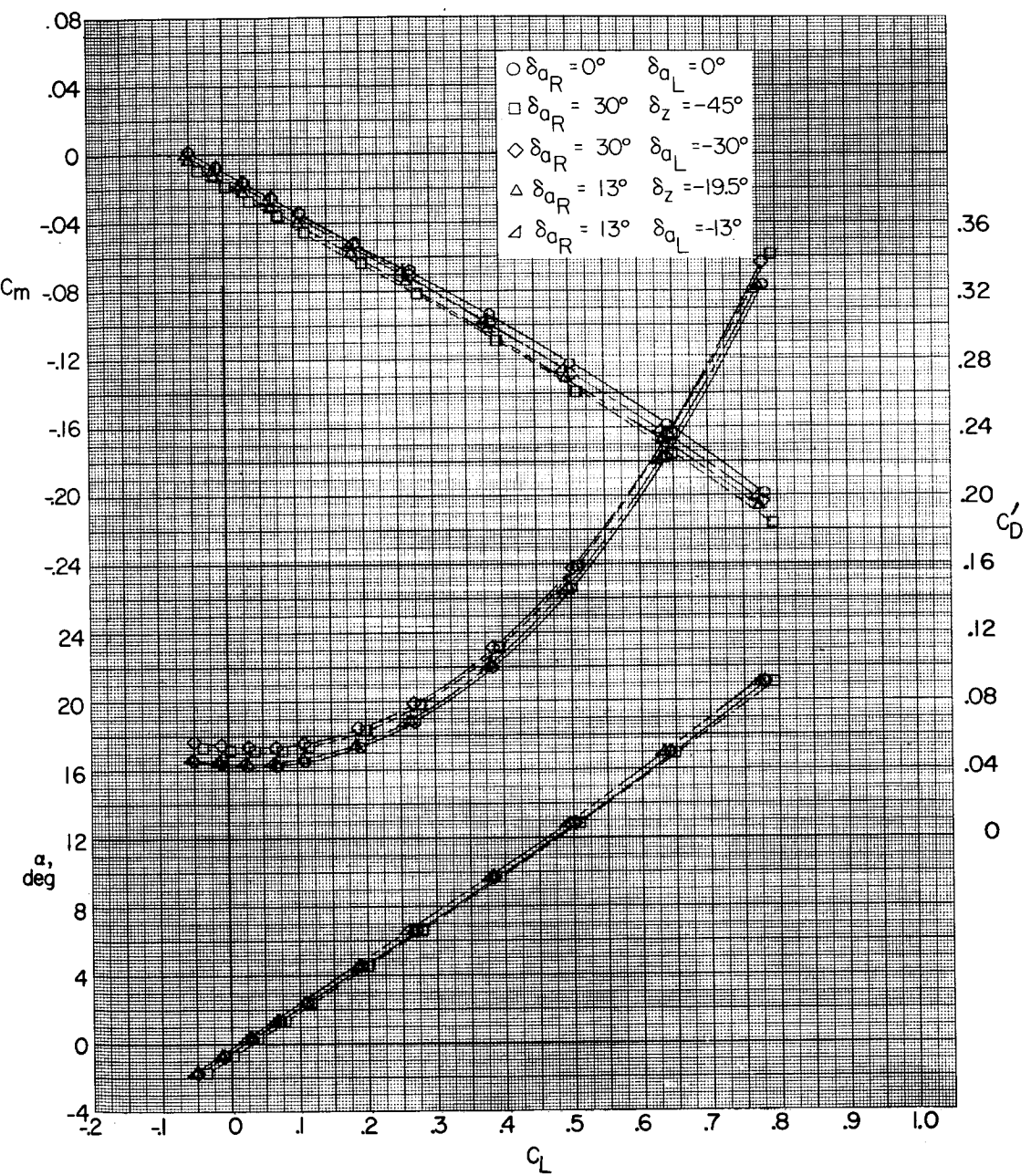
REF ID: A6524
CLASSIFIED

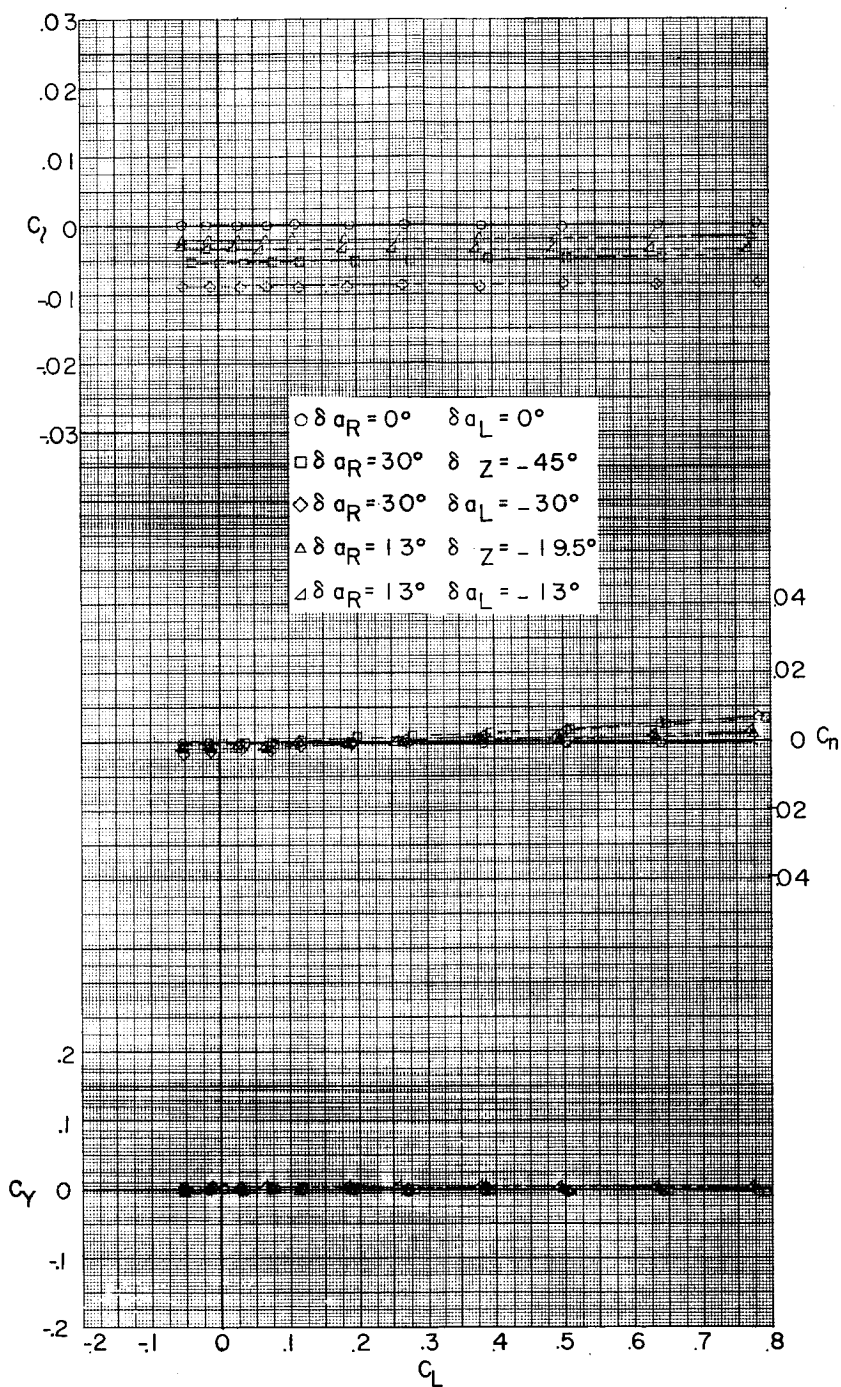
45



(b) Concluded.

Figure 10.- Continued.





(c) Concluded.

Figure 10.- Concluded.

0019123610340

L-524

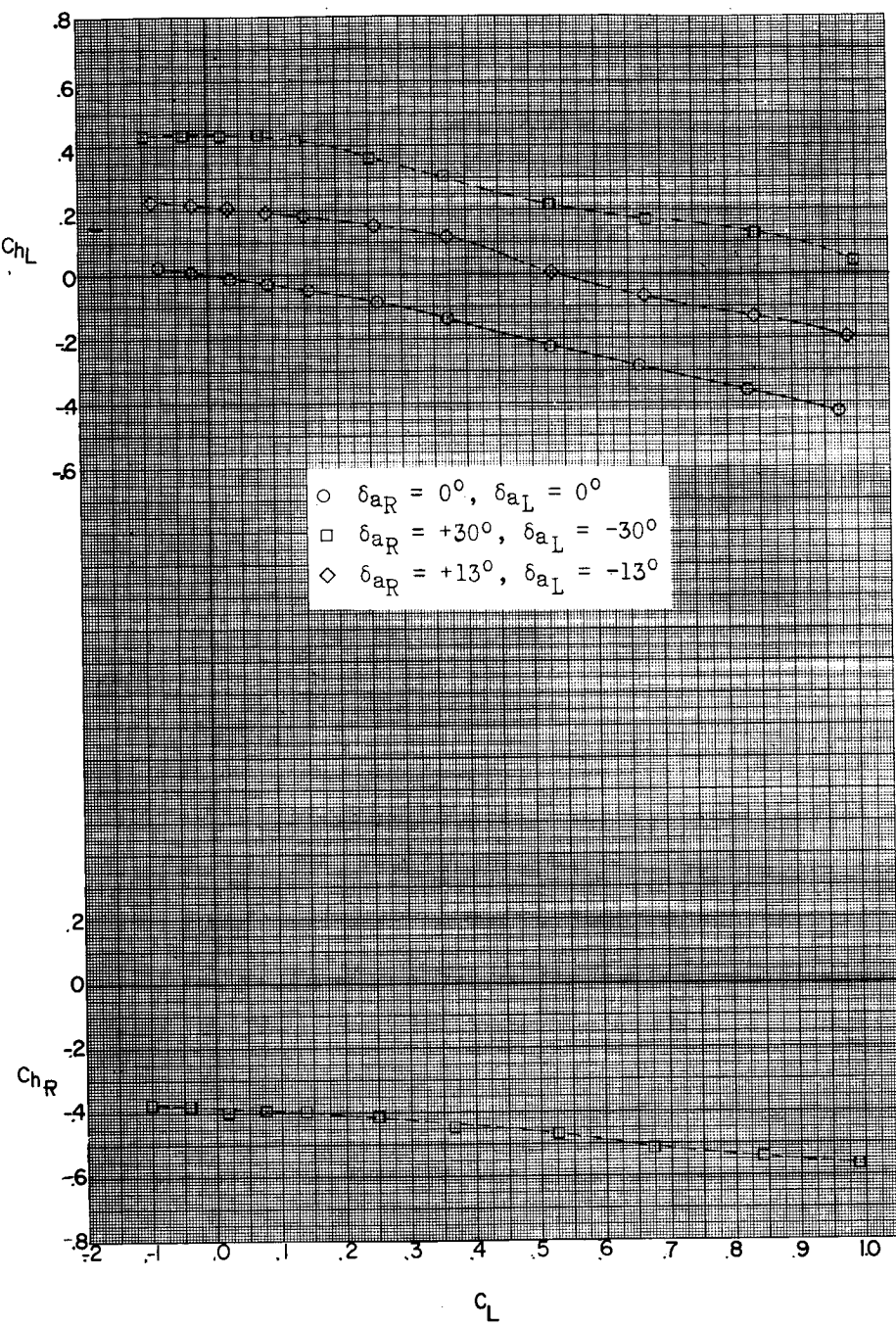
(a) $M = 1.57$.

Figure 11.- Effect of aileron deflection on aileron hinge-moment coefficient in pitch.

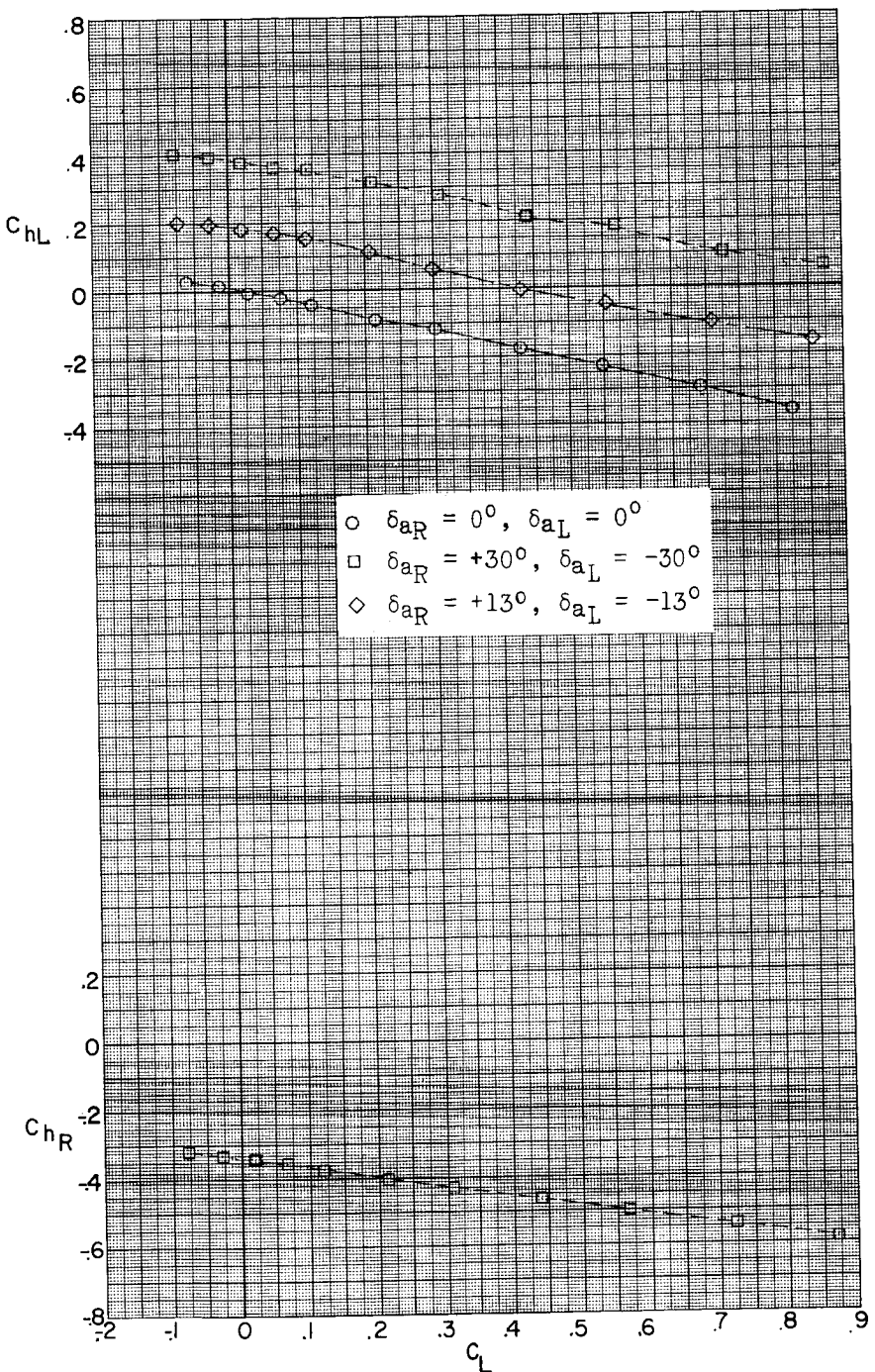
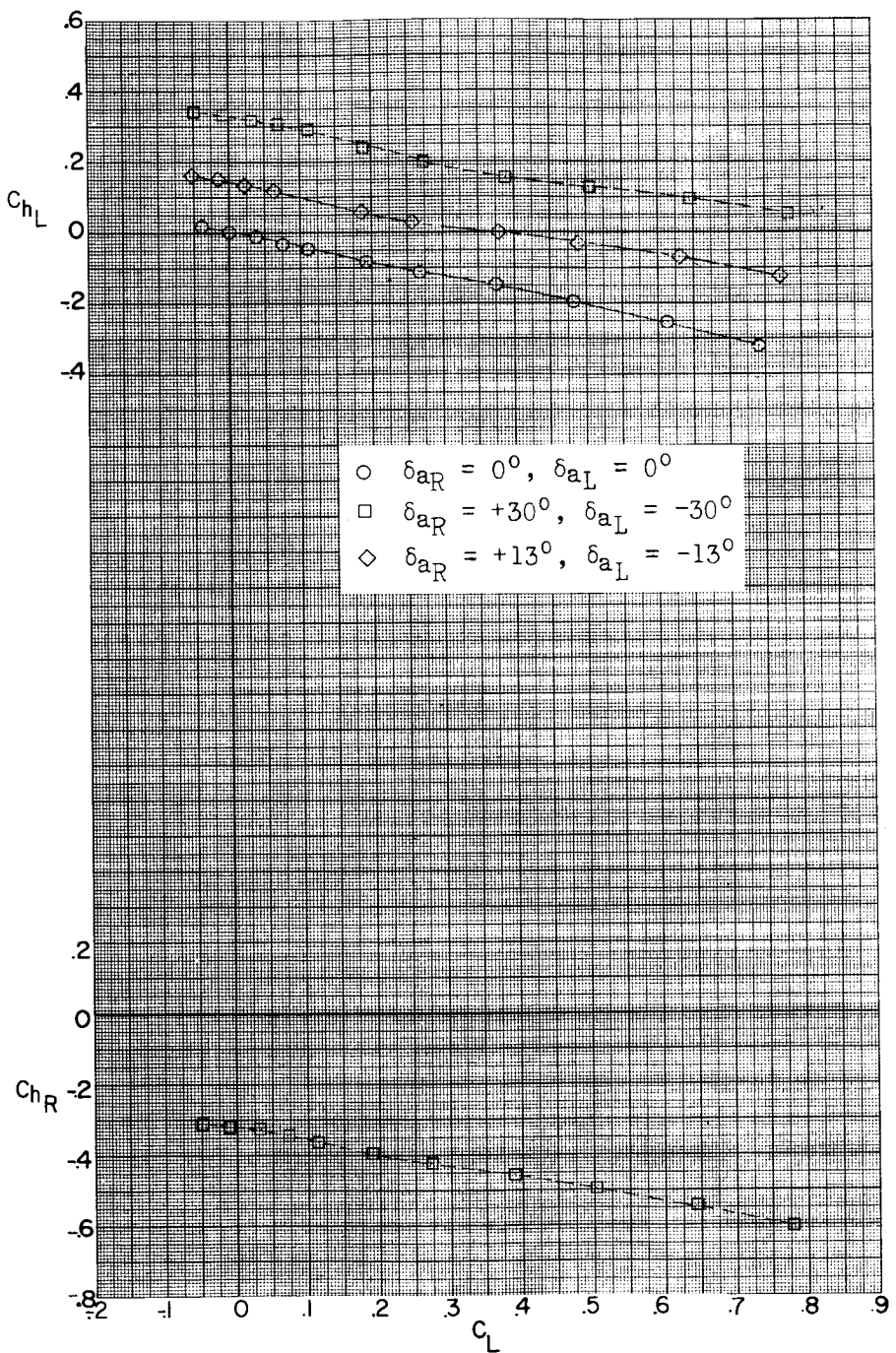
(b) $M = 1.87$.

Figure 11.- Continued.



(c) $M = 2.16$.

Figure 11.- Concluded.

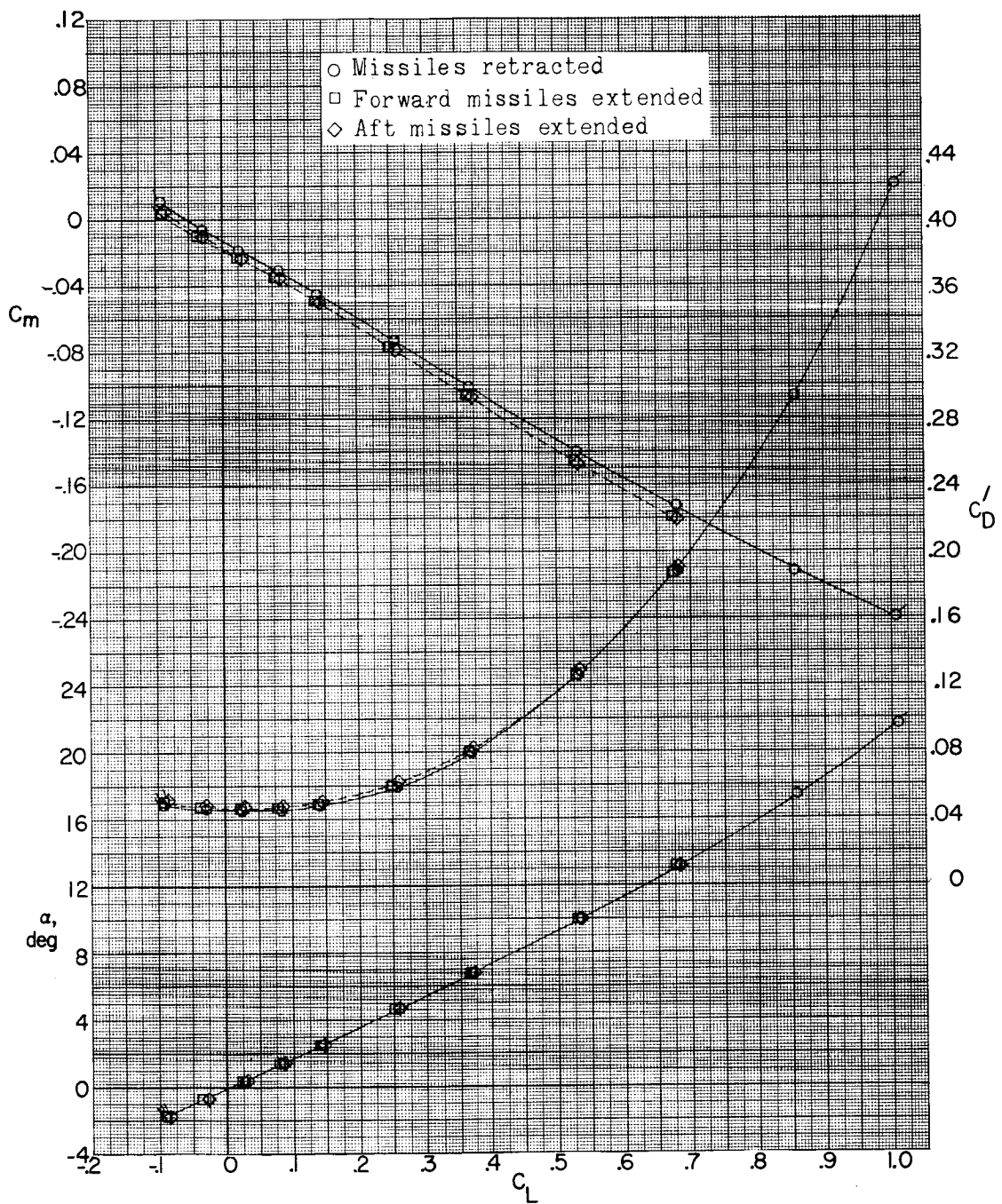
(a) $M = 1.57$.

Figure 12.- Effect of missiles extended on aerodynamic characteristics in pitch. (Flagged symbols denote wall-reflected shock waves striking the tail.)

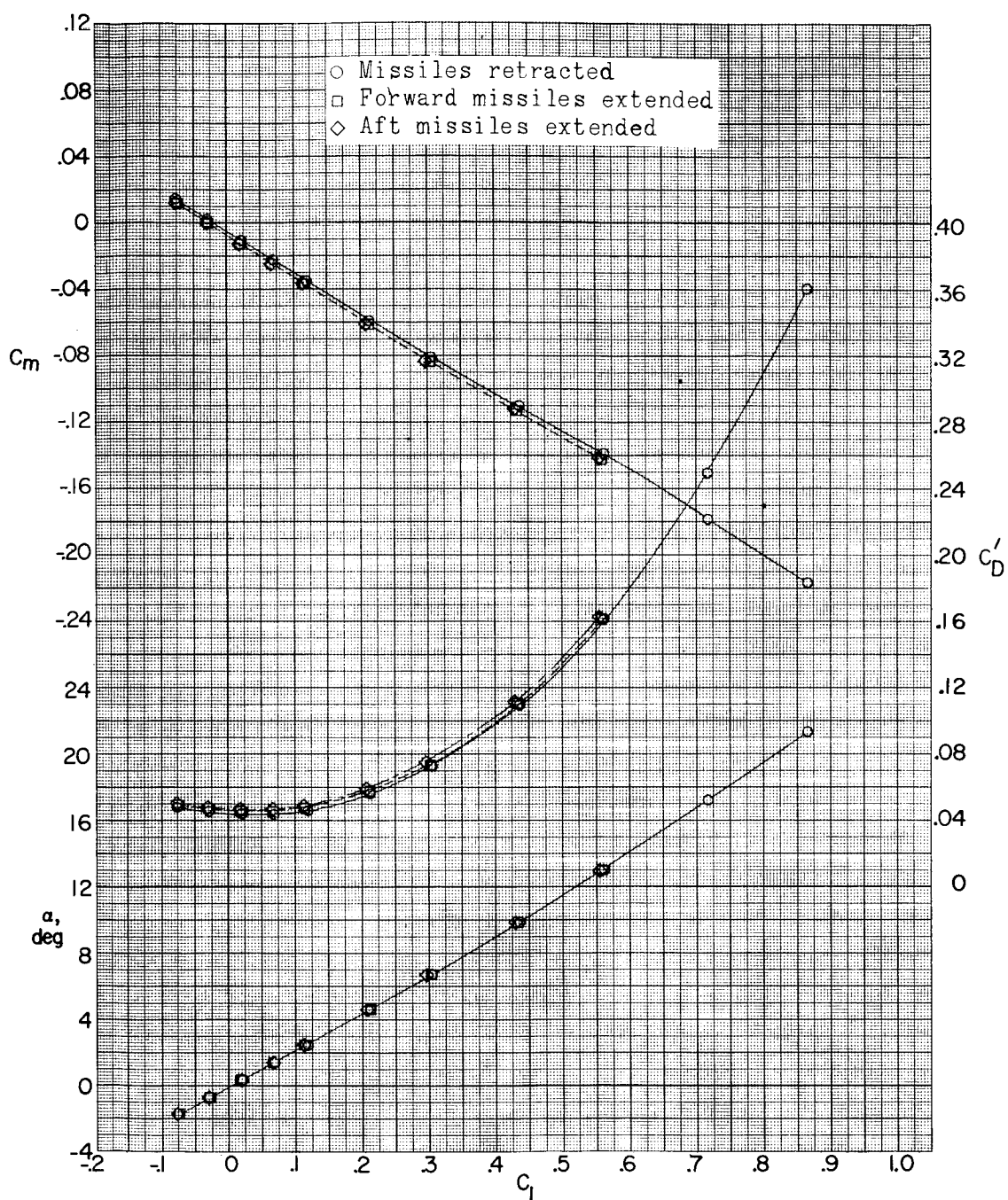
(b) $M = 1.87$.

Figure 12.- Continued.

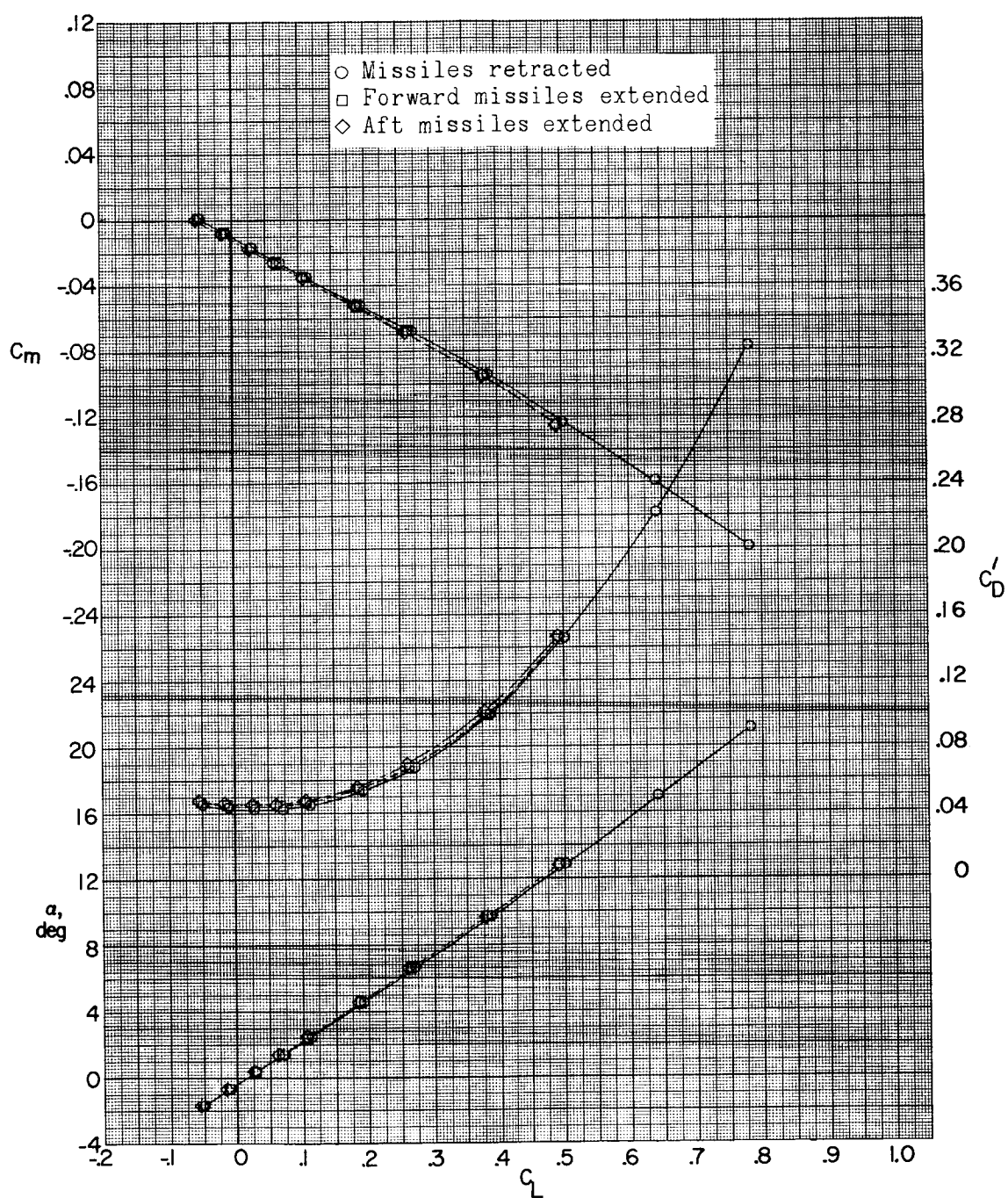
(c) $M = 2.16$.

Figure 12.- Concluded.

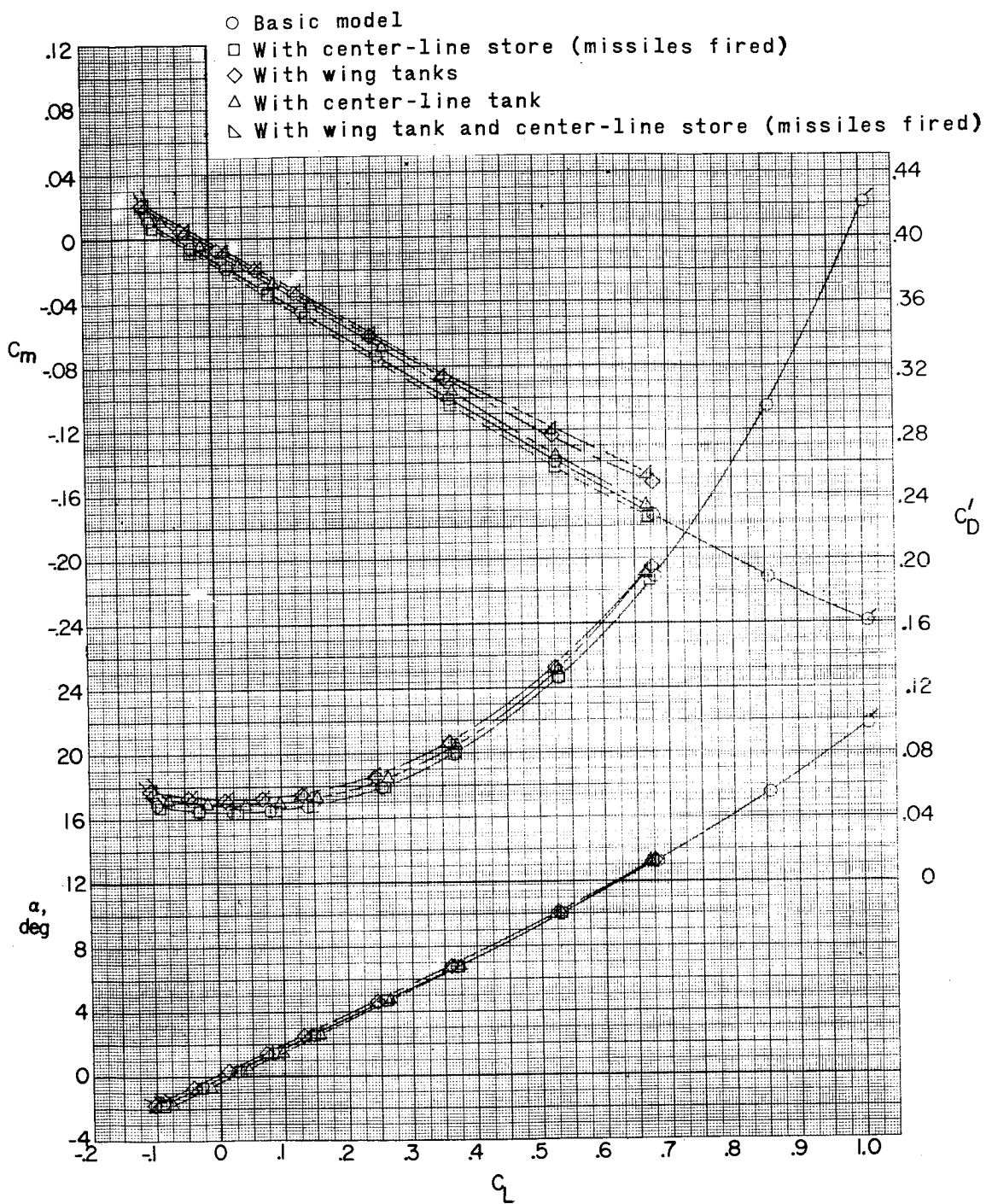
(a) $M = 1.57$.

Figure 13.- Effect of external stores on aerodynamic characteristics in pitch. (Flagged symbols denote wall-reflected shock waves striking the tail.)

REF ID: A6524

REF ID: A6524
CLASSIFIED

55

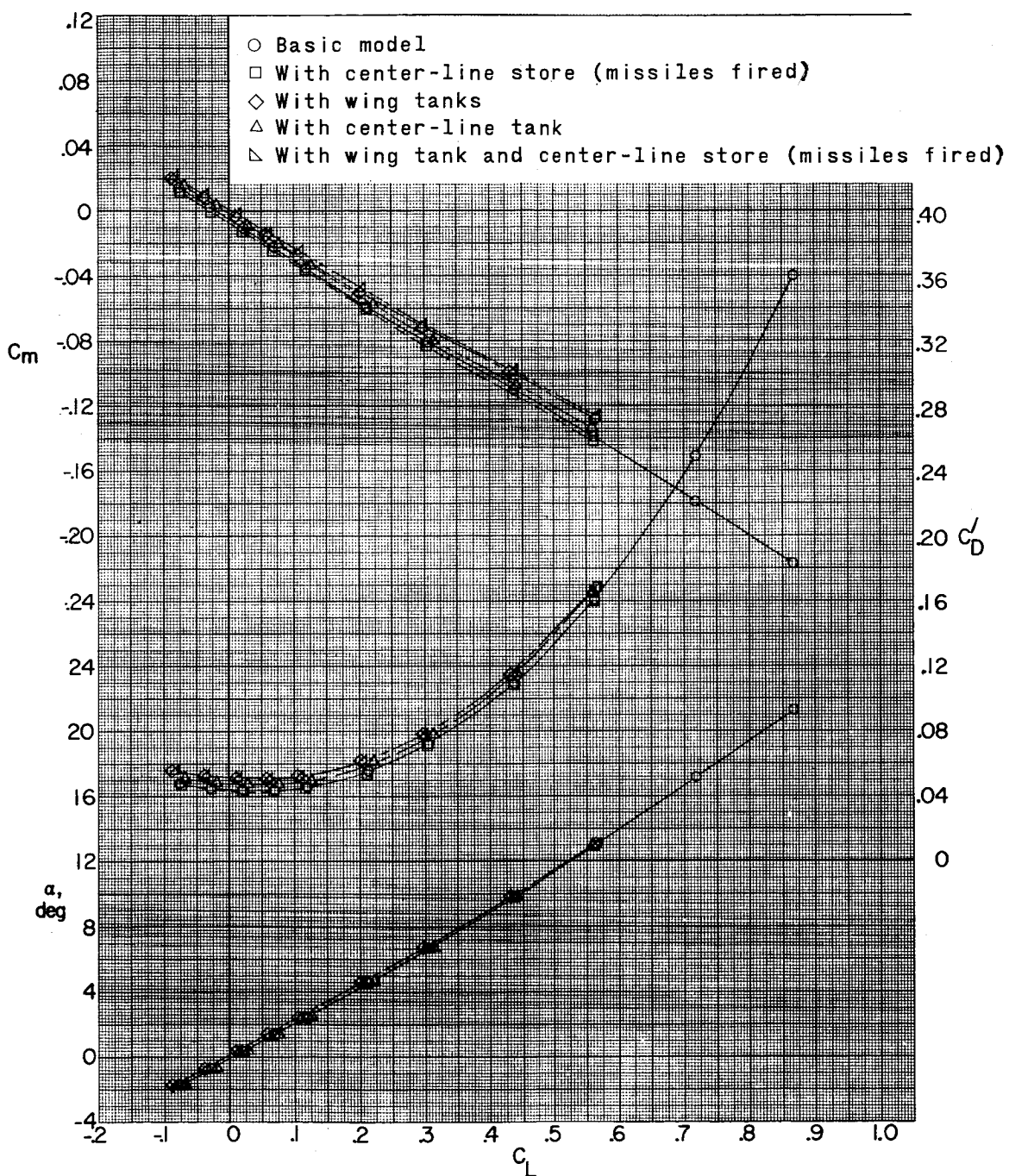
(b) $M = 1.87$.

Figure 13.- Continued.

0319132A1030

00

56

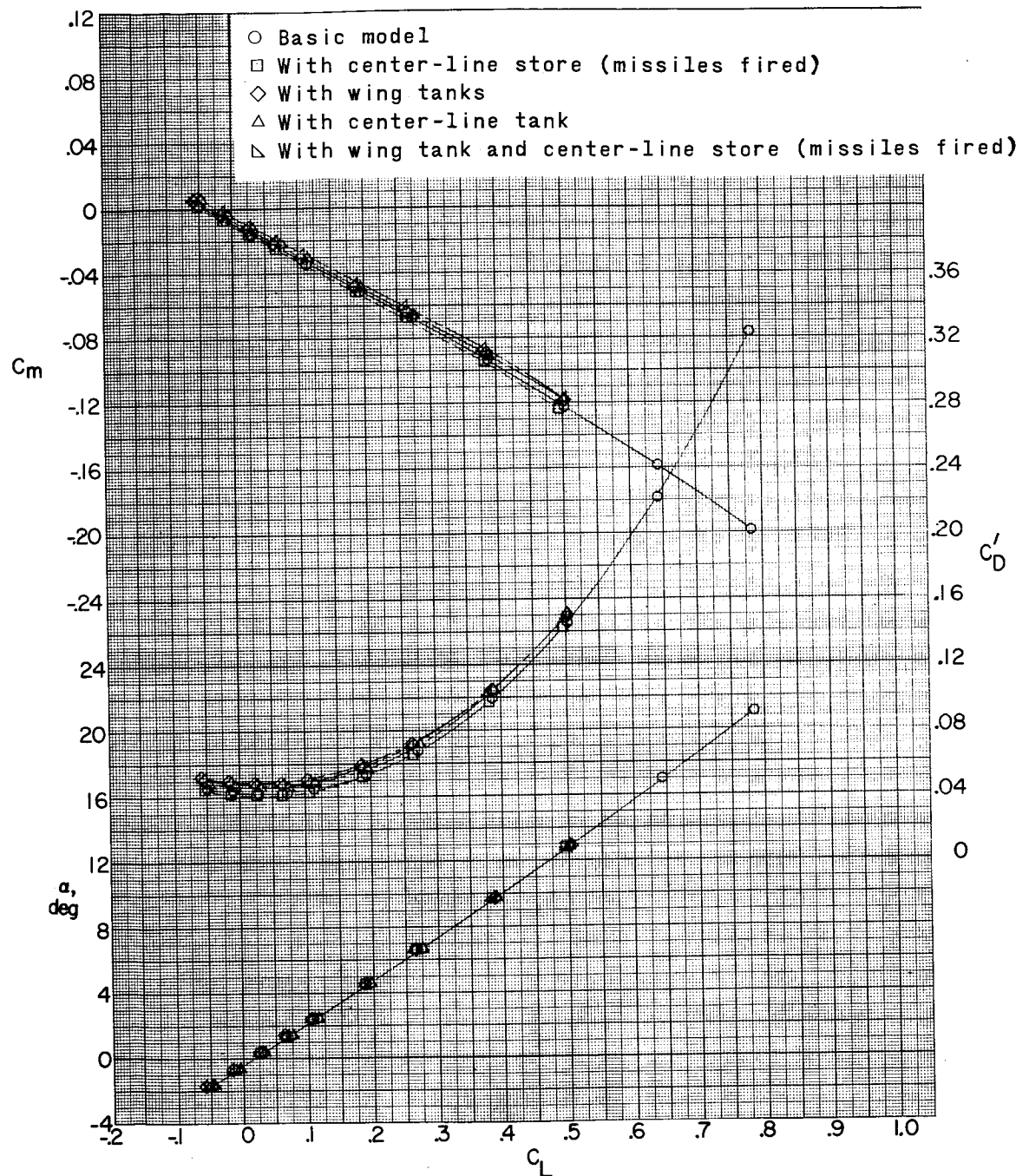
(c) $M = 2.16.$

Figure 13.- Concluded.

8C

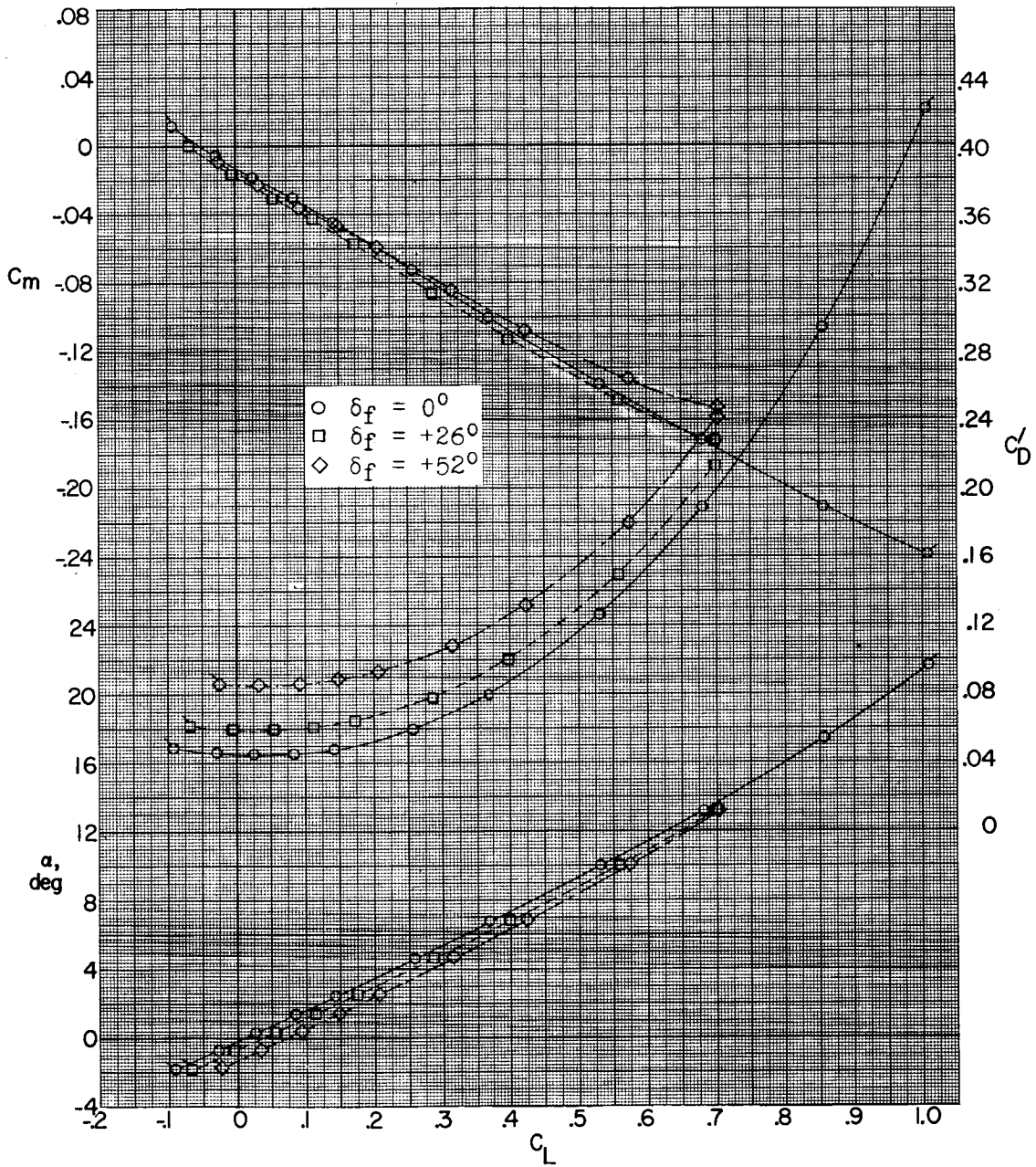
A 3x4 grid of 12 black dots arranged in three rows and four columns.

REF ID: A6512

UNCLASSIFIED

57

I-524



(a) $M = 1.57$.

Figure 14.- Effect of speed brakes on aerodynamic characteristics in pitch. (Flagged symbols denote wall-reflected shock waves striking the tail.)

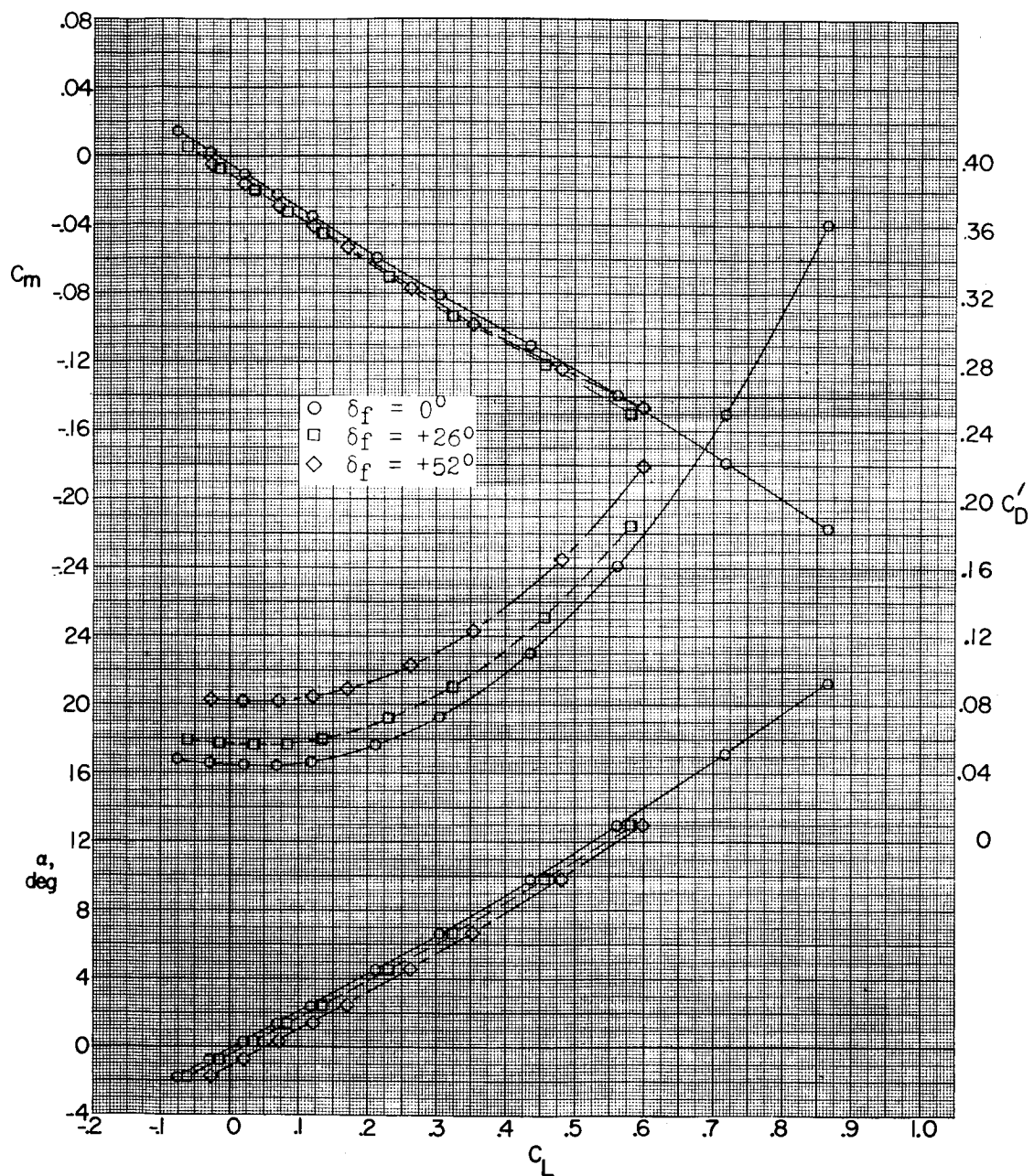
(b) $M = 1.87$.

Figure 14.- Continued.

REF ID: A6579

DECLASSIFIED

59

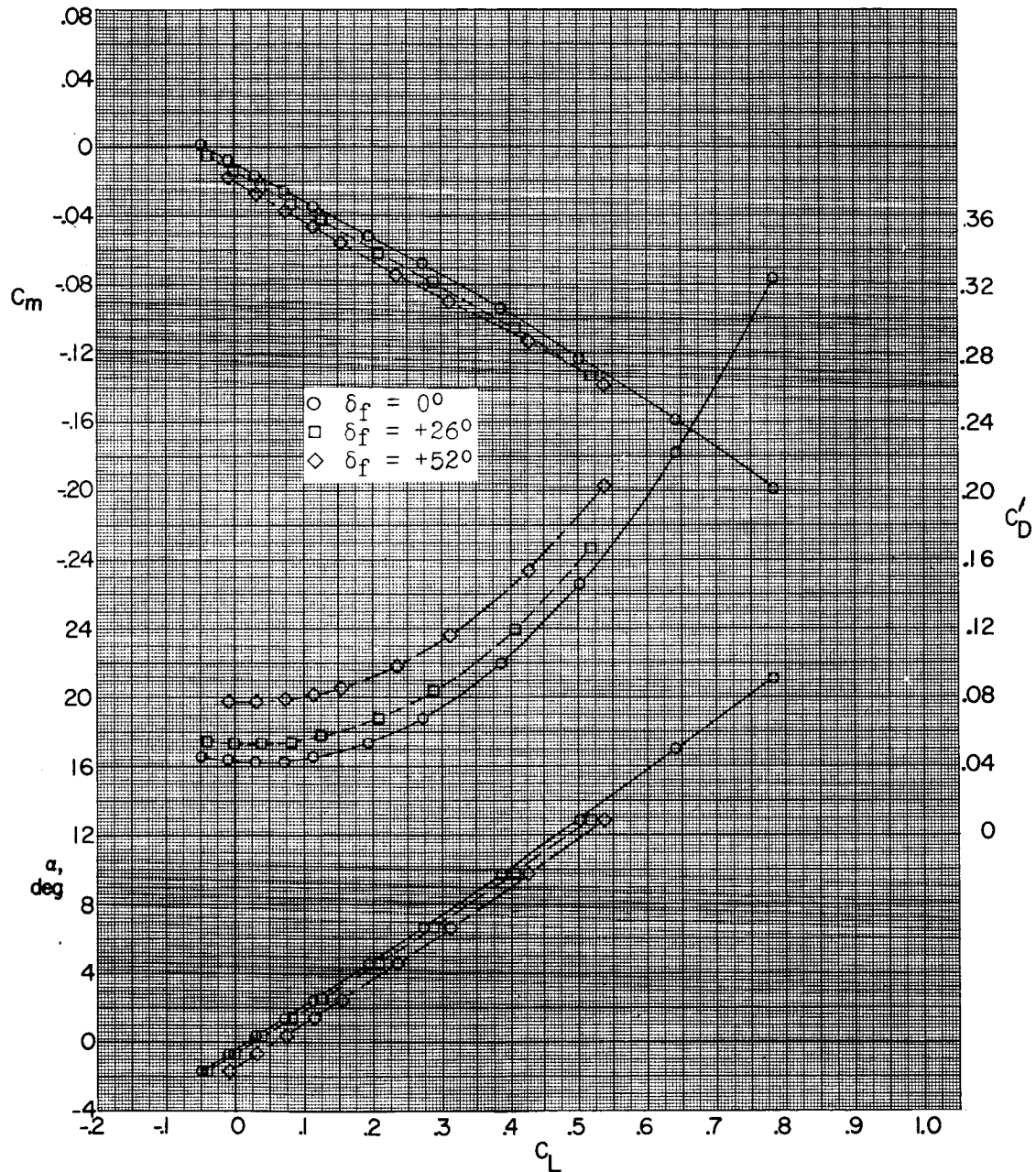
(c) $M = 2.16$.

Figure 14.- Concluded.

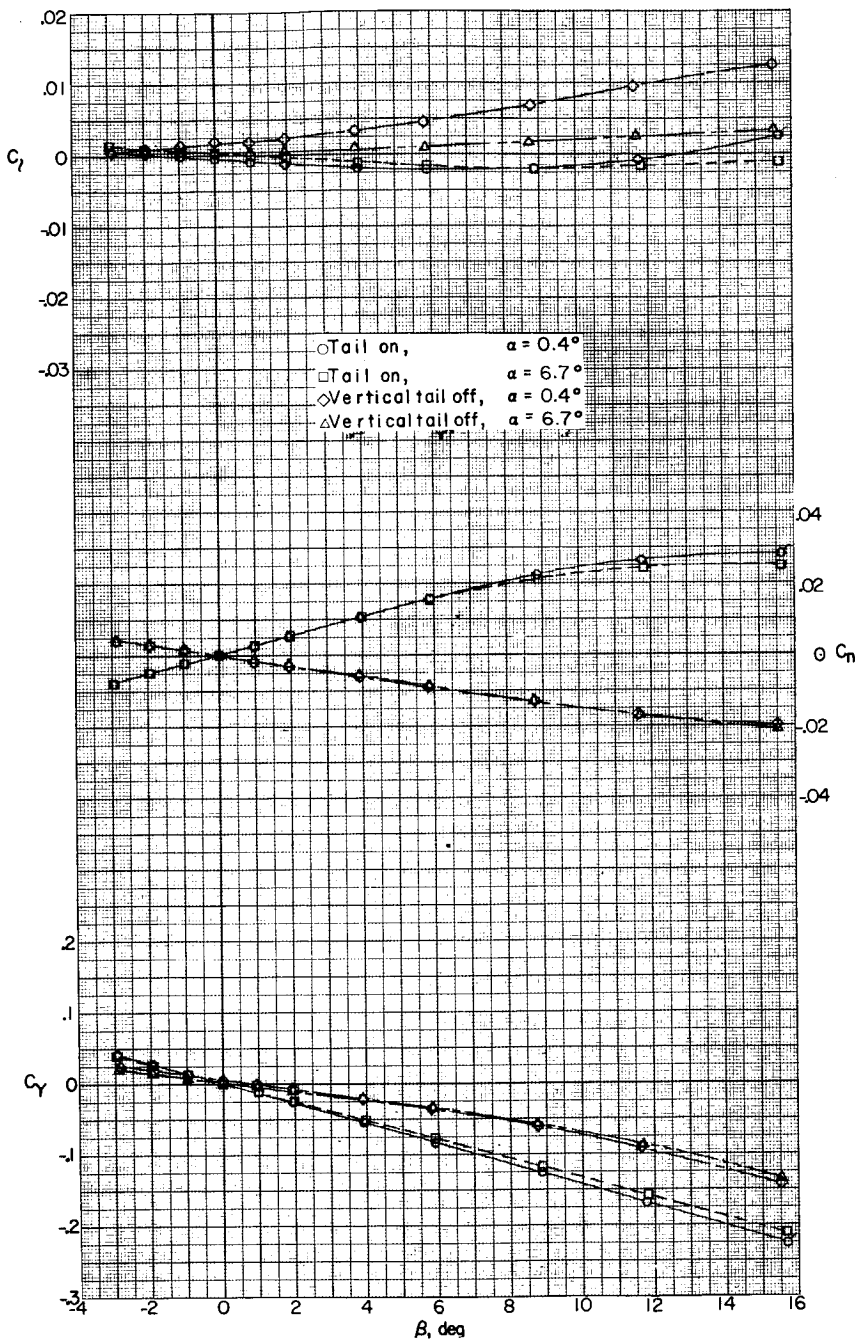
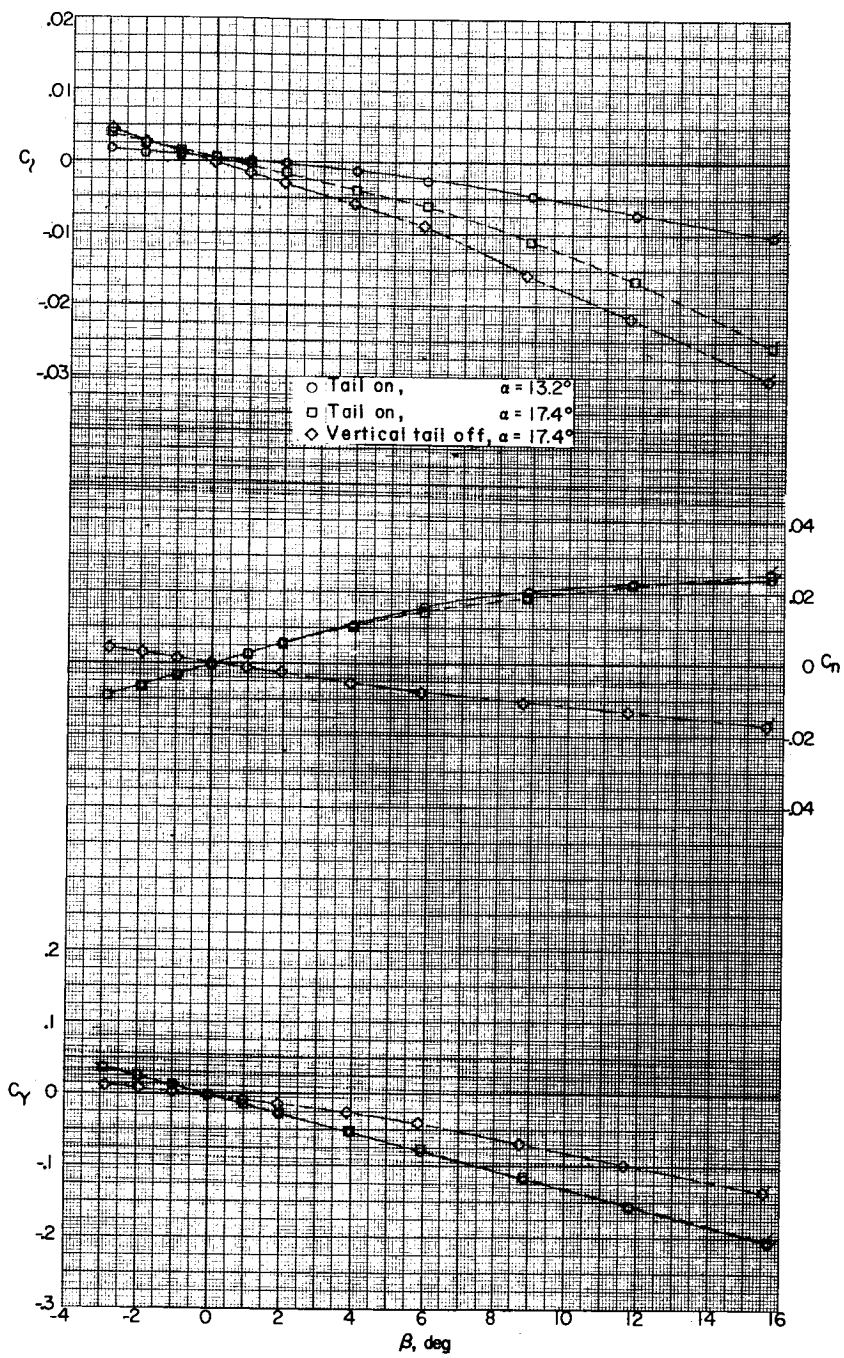
(a) $M = 1.57$.

Figure 15.- Effect of vertical tail on aerodynamic characteristics in sideslip. (Flagged symbols denote wall-reflected shock waves striking the tail.)

L-524



(a) Concluded.

Figure 15.- Continued.

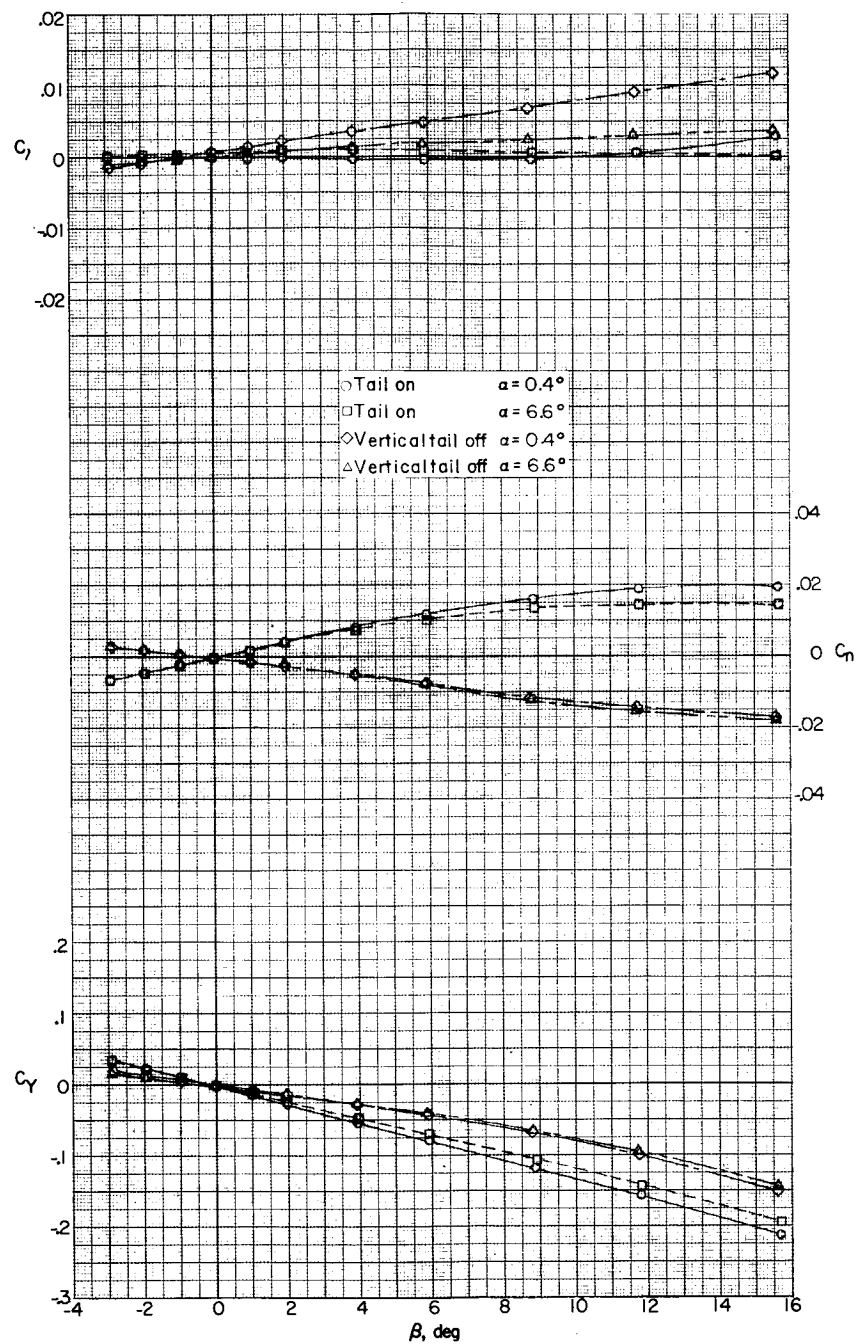
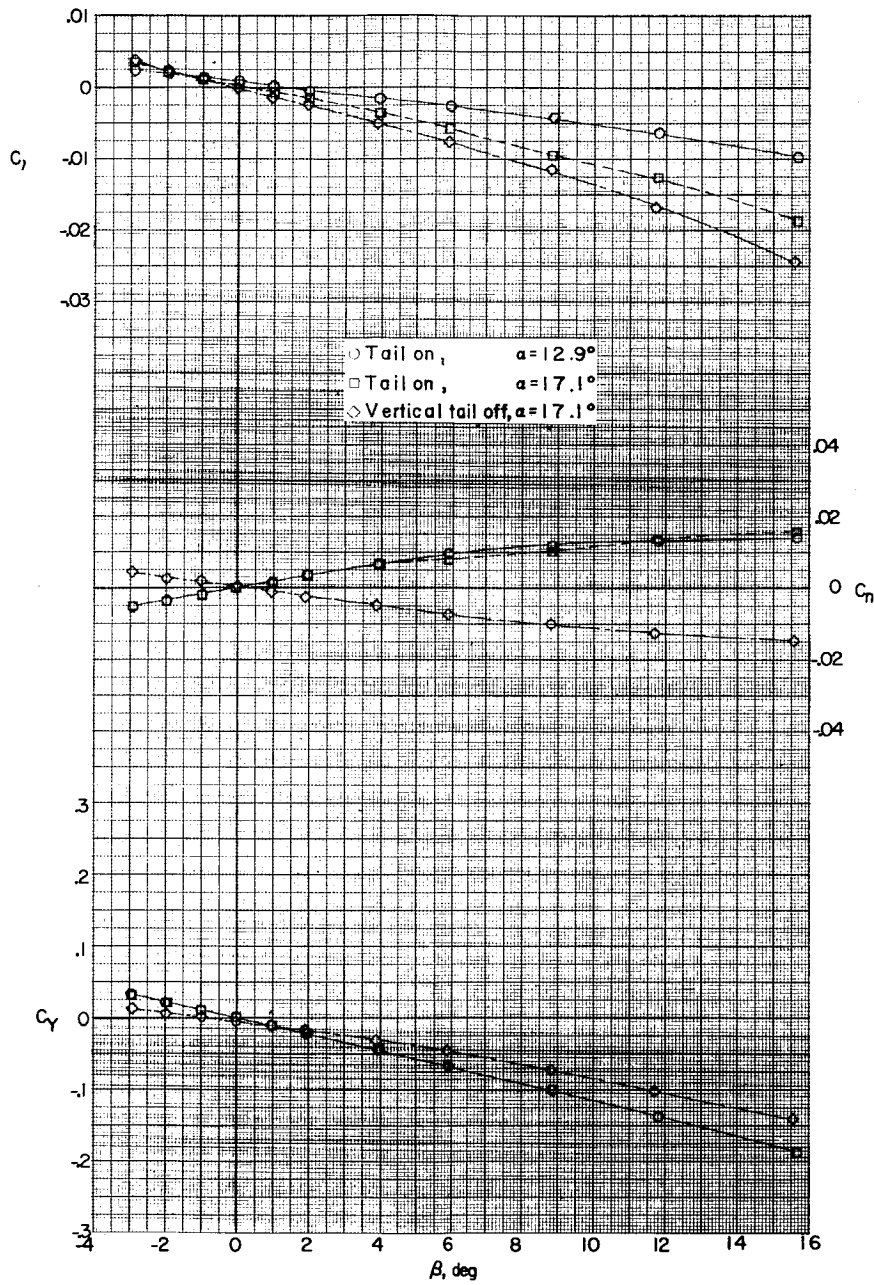
(b) $M = 1.87$.

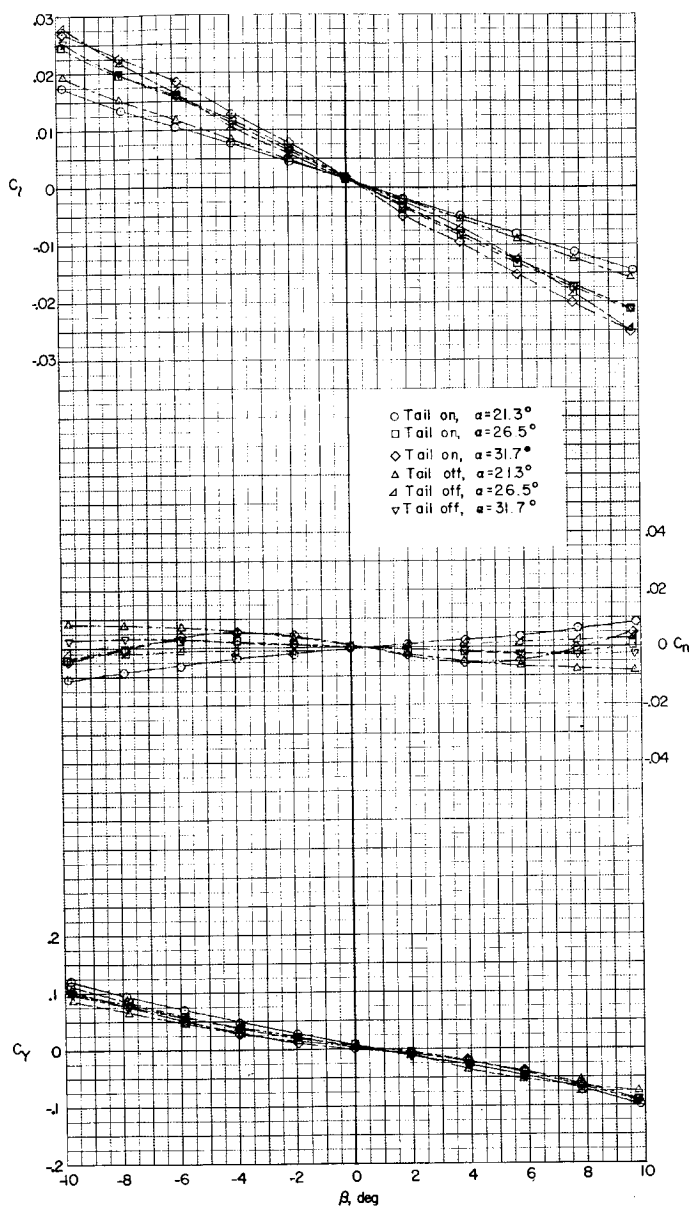
Figure 15.- Continued.

~~SECURITY CLASSIFIED~~

(b) Continued.

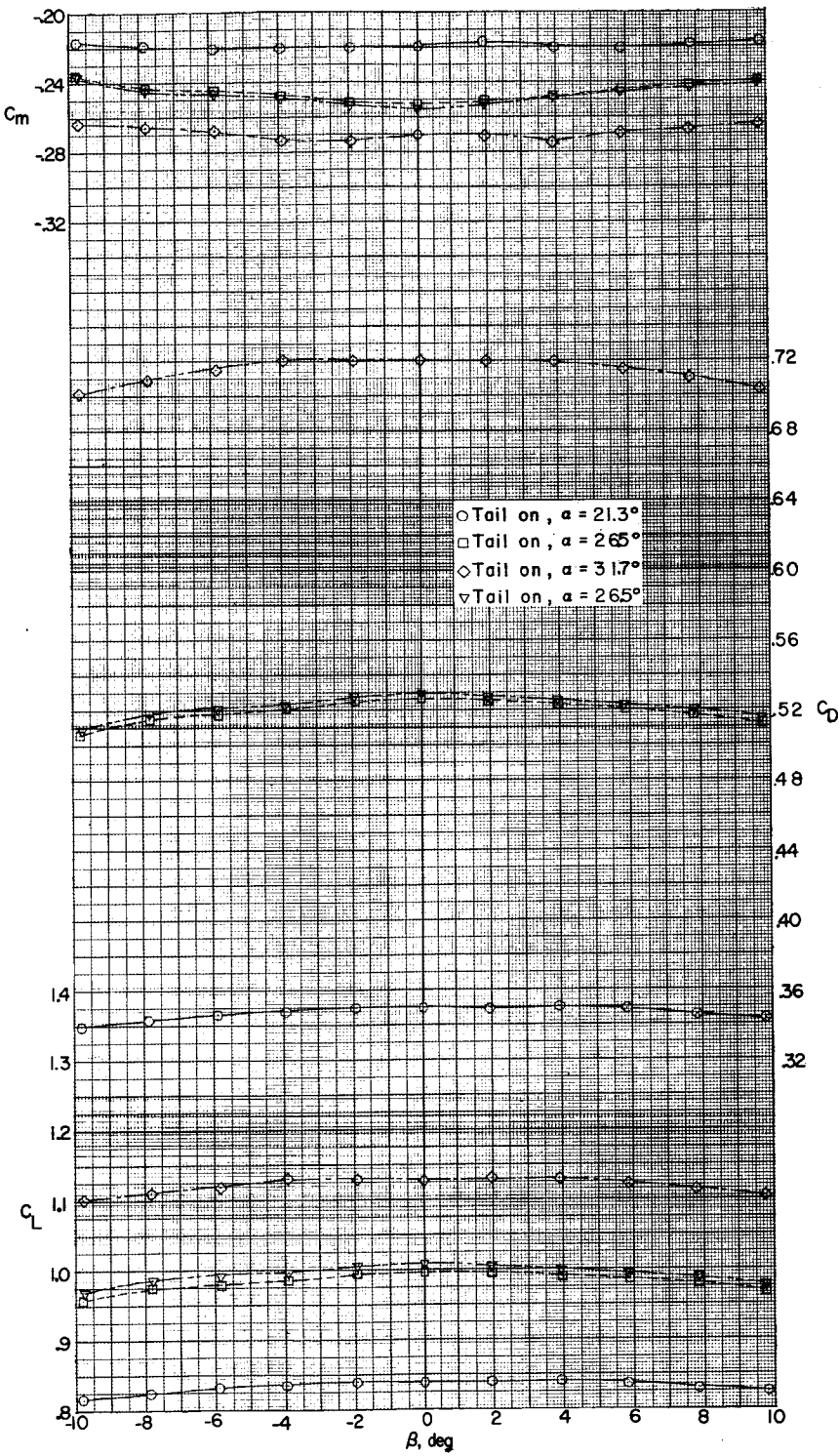
Figure 15.- Continued.

~~SECURITY CLASSIFIED~~



(b) Continued.

Figure 15.- Continued.



(b) Concluded.

Figure 15.- Continued.

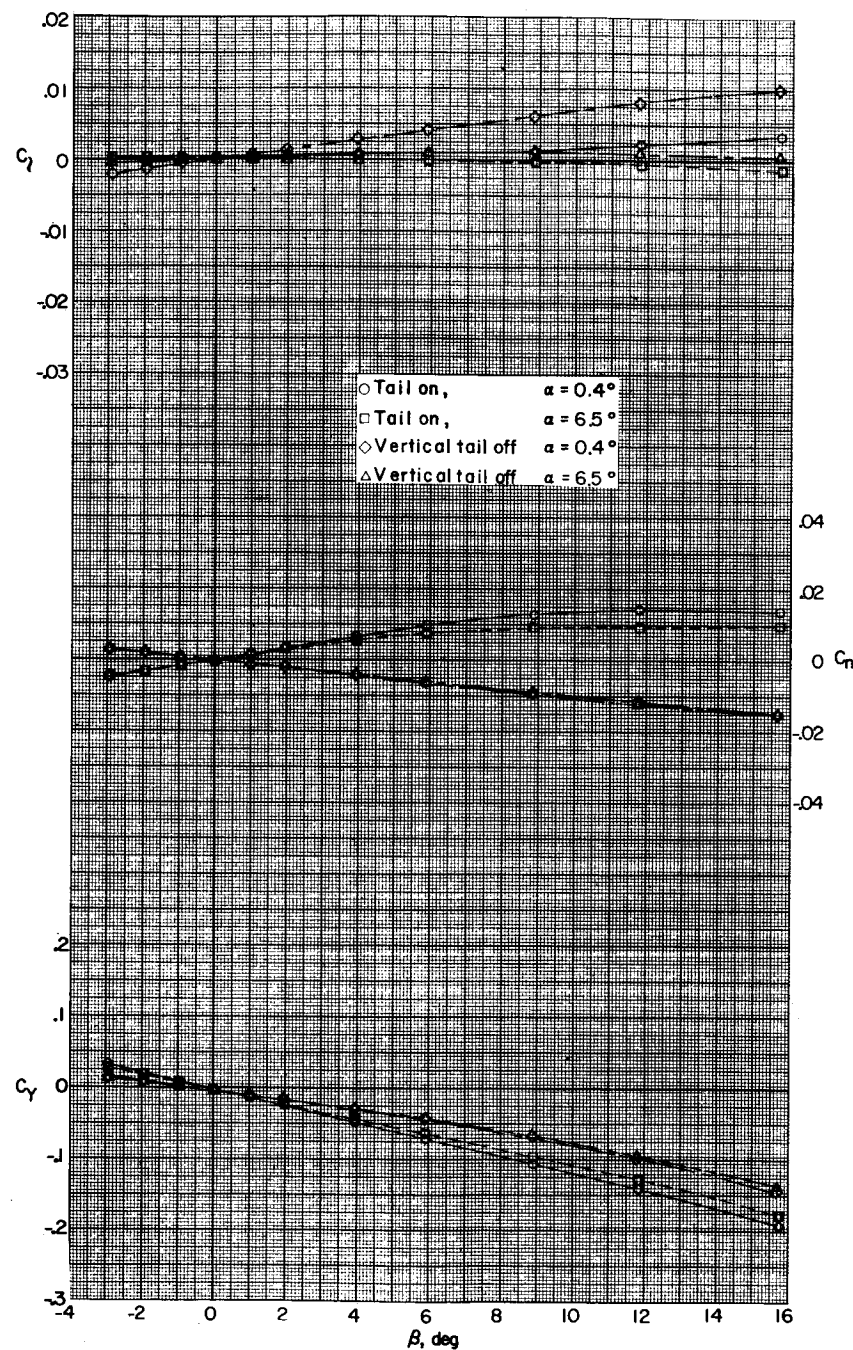
(c) $M = 2.16$.

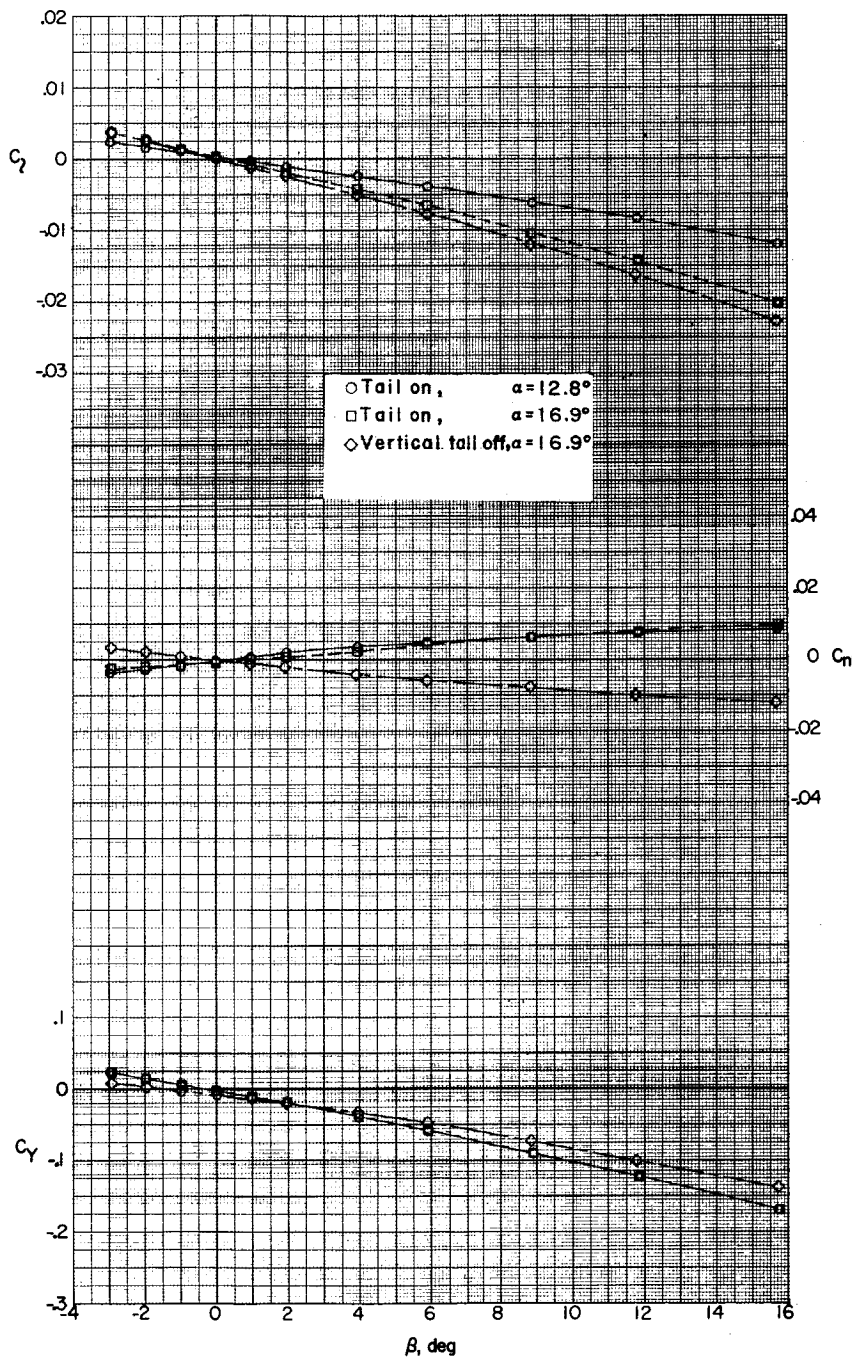
Figure 15.- Continued.

REF ID: A6542

REF ID: A6542
CLASSIFIED

67

I-524



(c) Concluded.

Figure 15.- Continued.

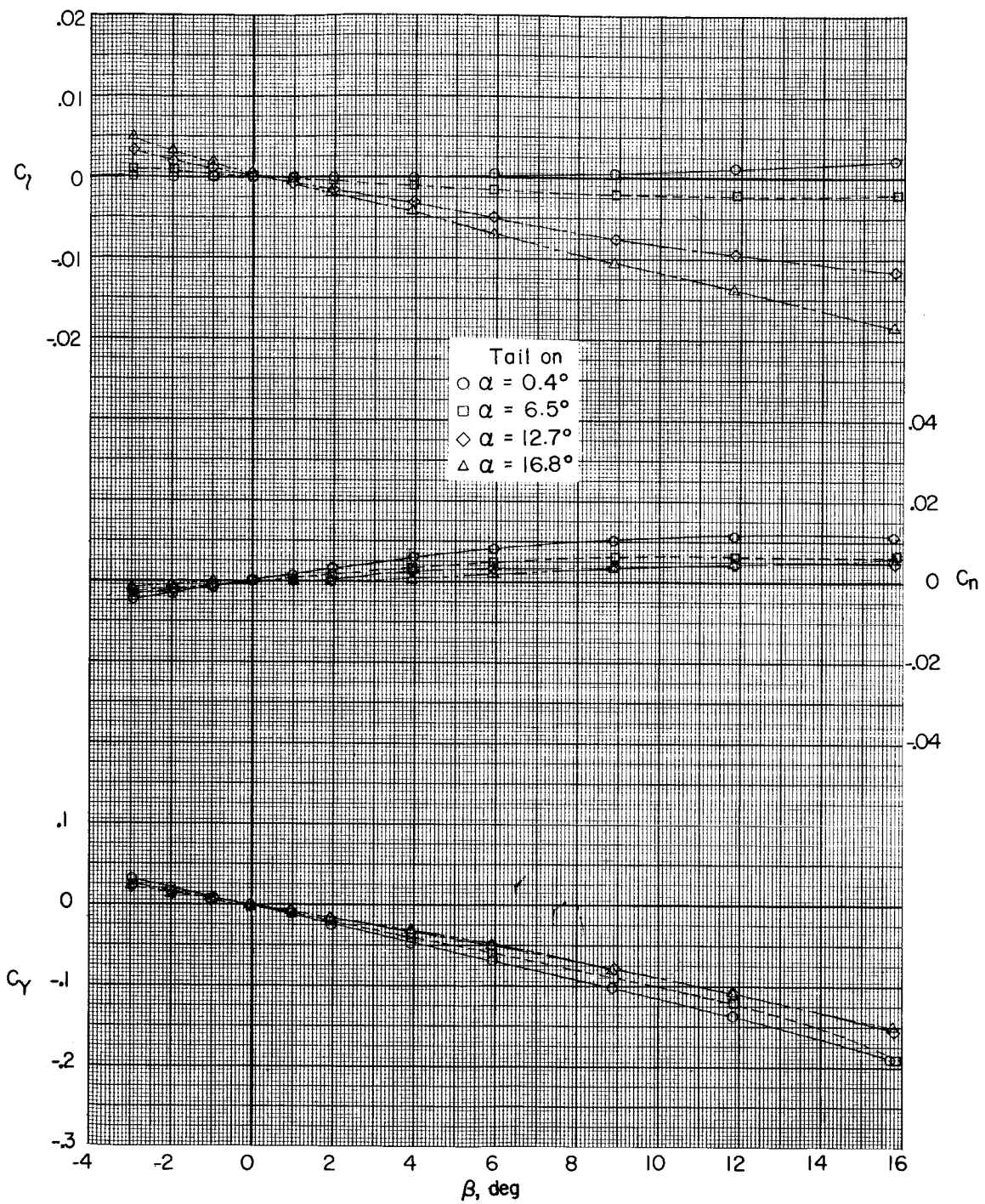
(d) $M = 2.53$.

Figure 15.- Concluded.

REF ID: A65124

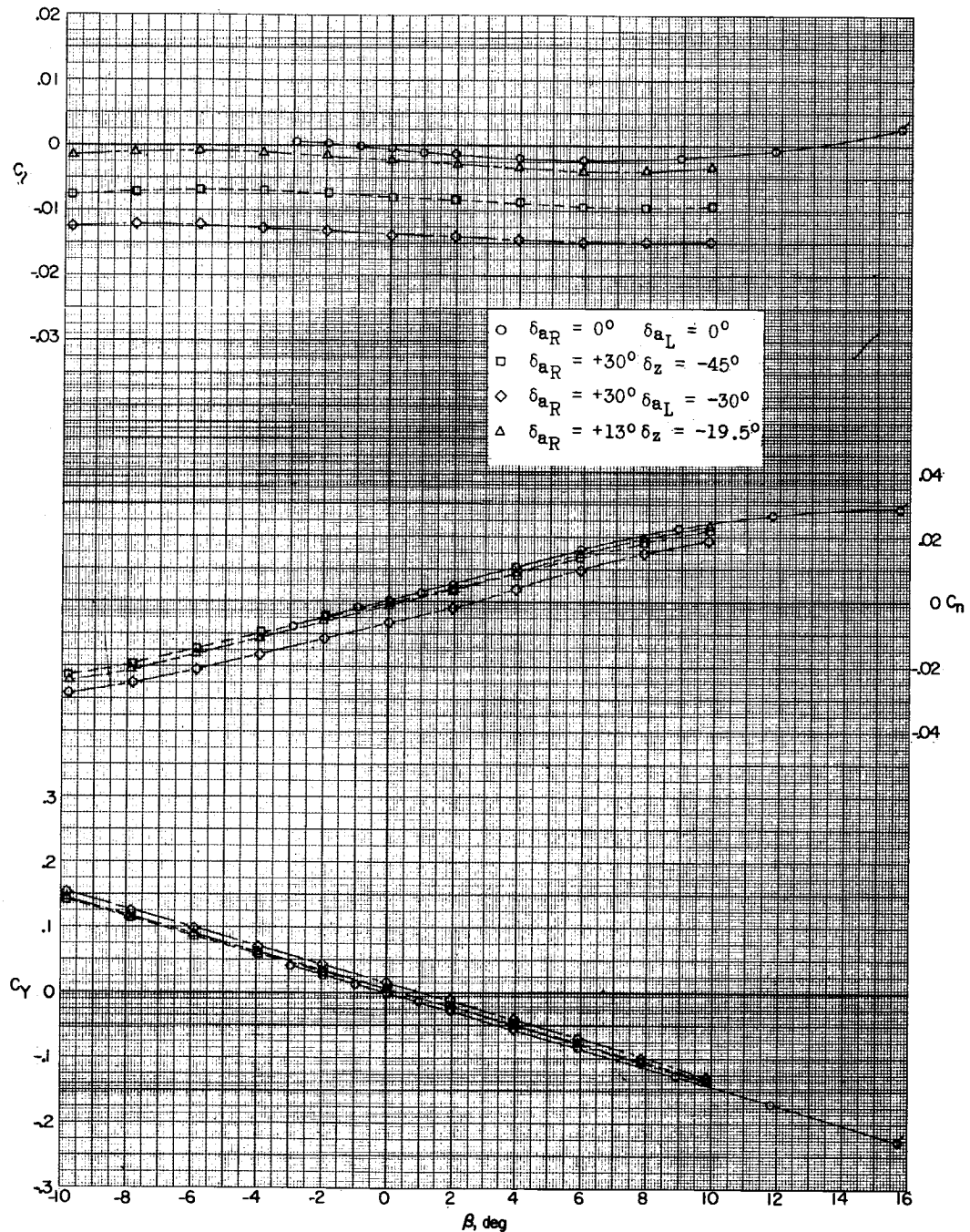
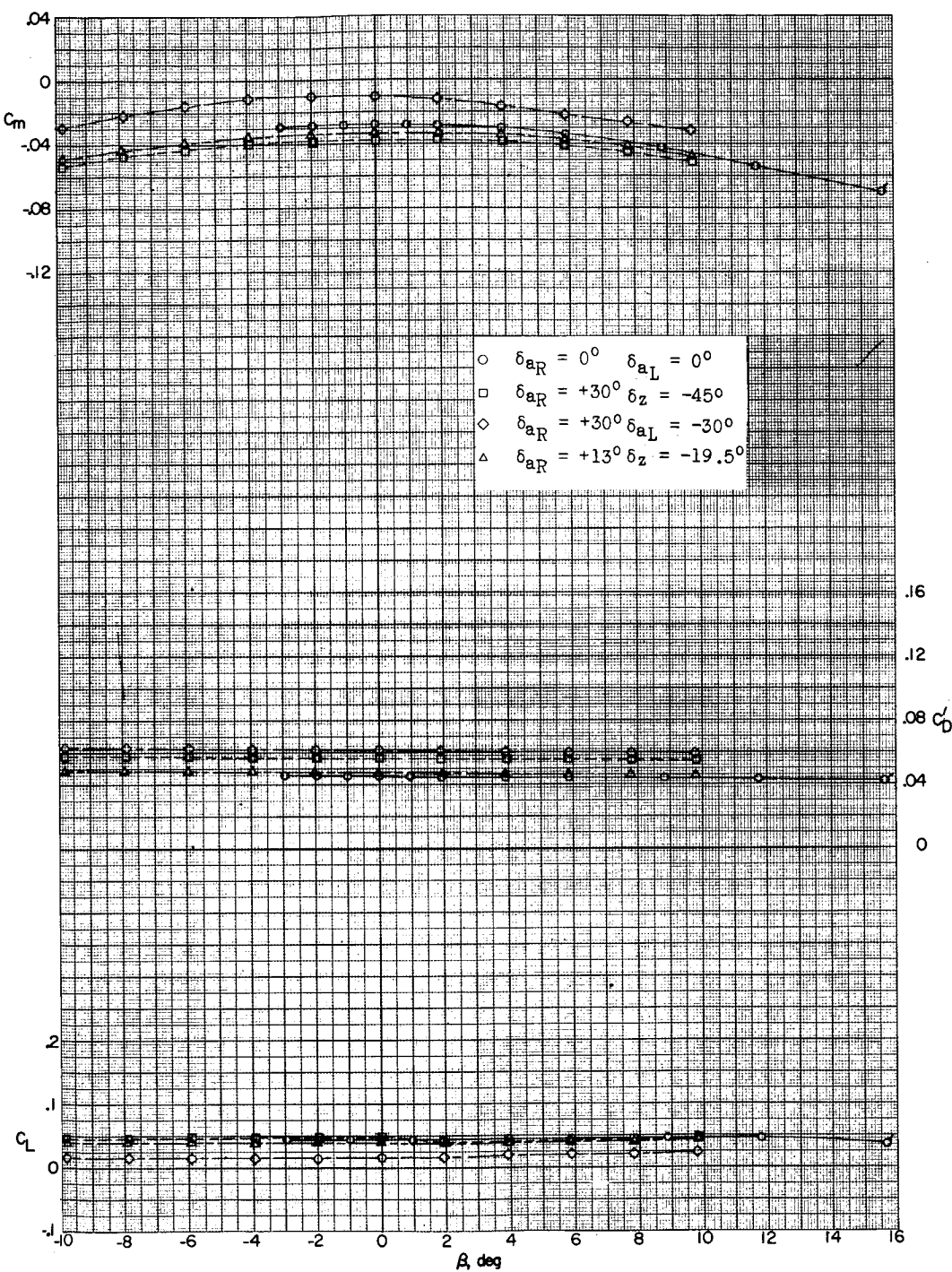
REF ID: A65124
CLASSIFIED(a) $M = 1.57; \alpha = 0.4^\circ$.

Figure 16.- Effect of aileron and spoiler deflection on aerodynamic characteristics in sideslip. (Flagged symbols denote wall-reflected shock waves striking the tail.)



(a) Concluded.

Figure 16.- Continued.

U

REF ID: A65422
CLASSIFIED

71

L-524

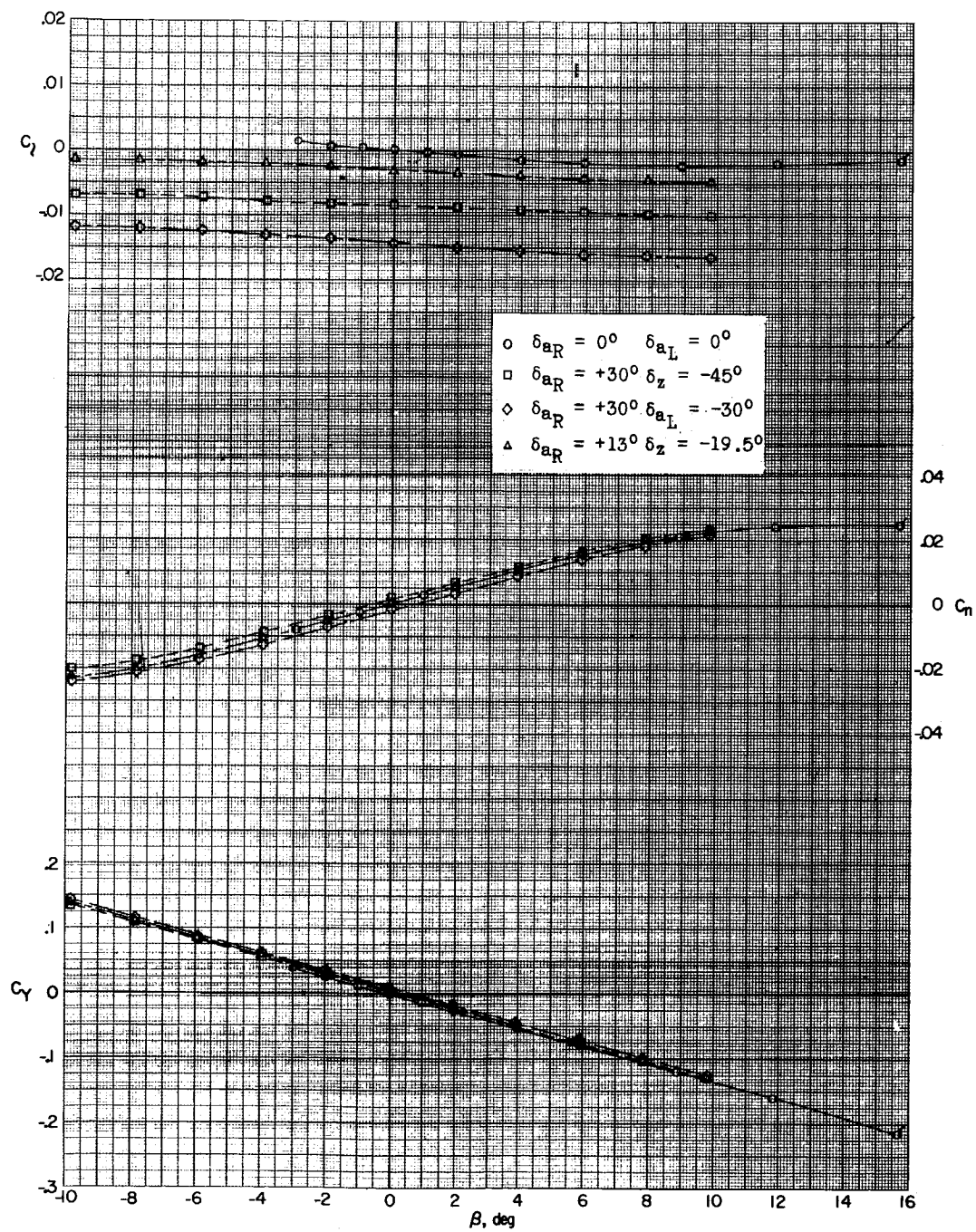
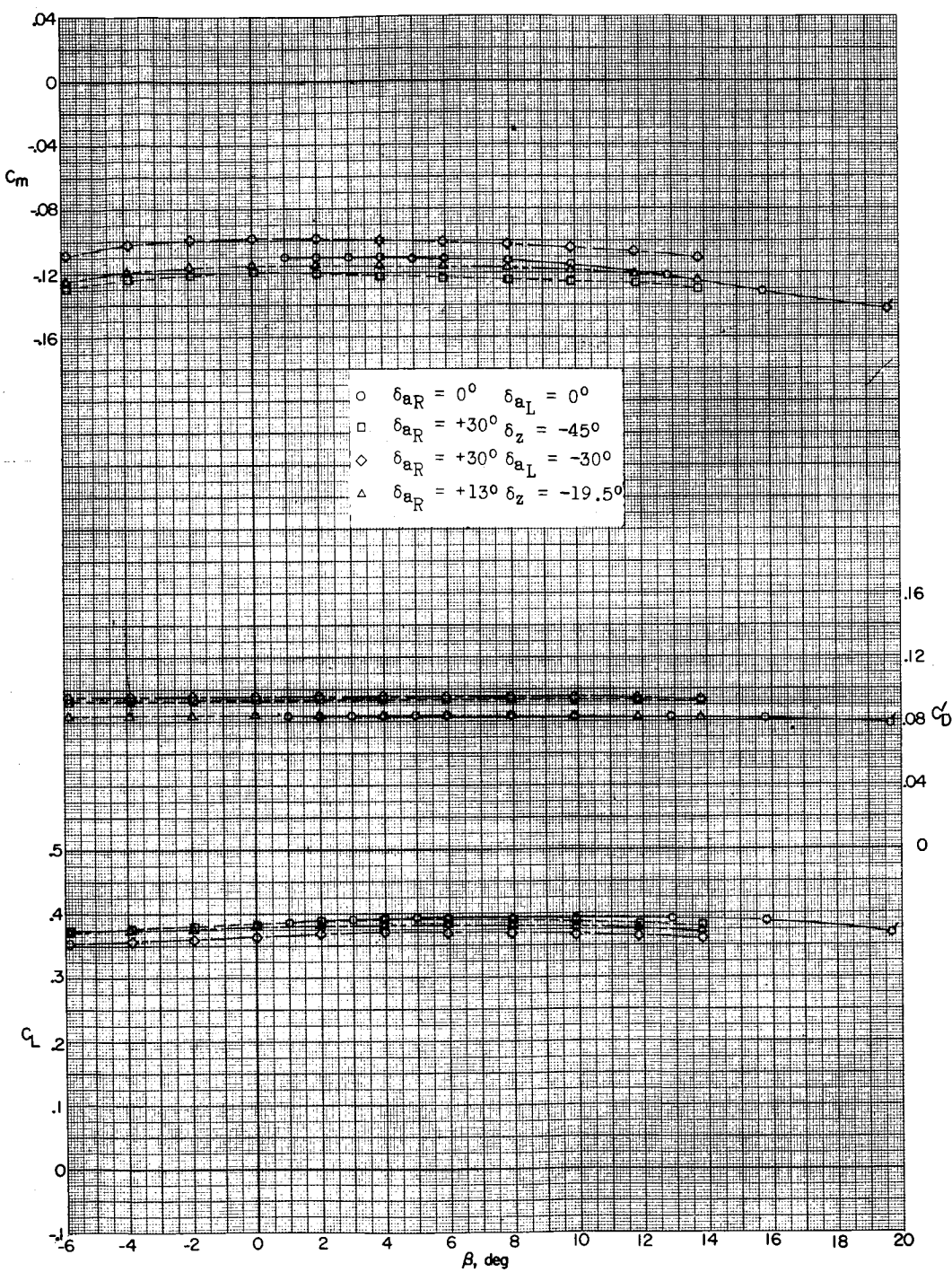
(b) $M = 1.57; \alpha = 6.7^\circ$.

Figure 16.- Continued.

031712261130

8

I-524



(b) Concluded.

Figure 16.- Continued.

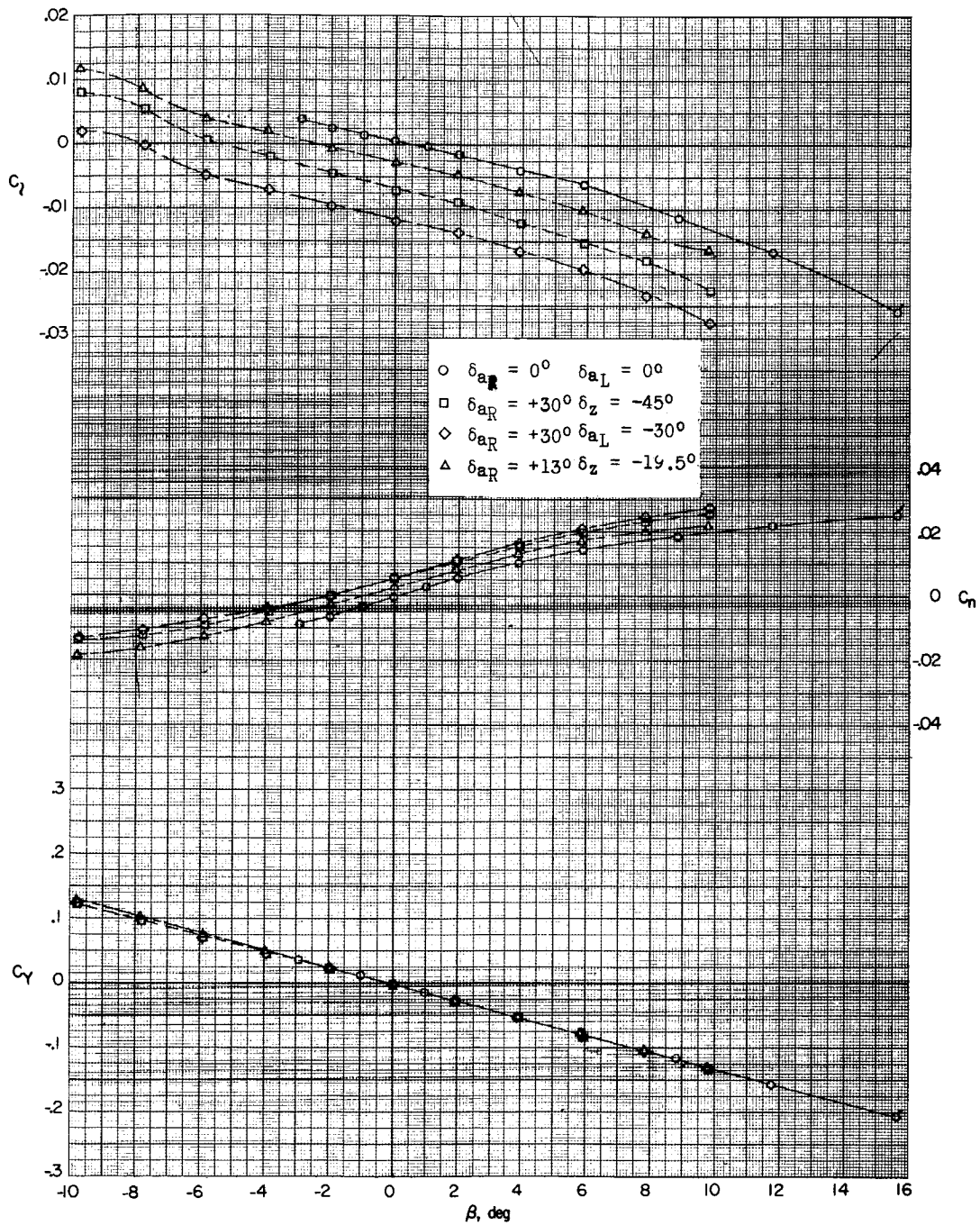
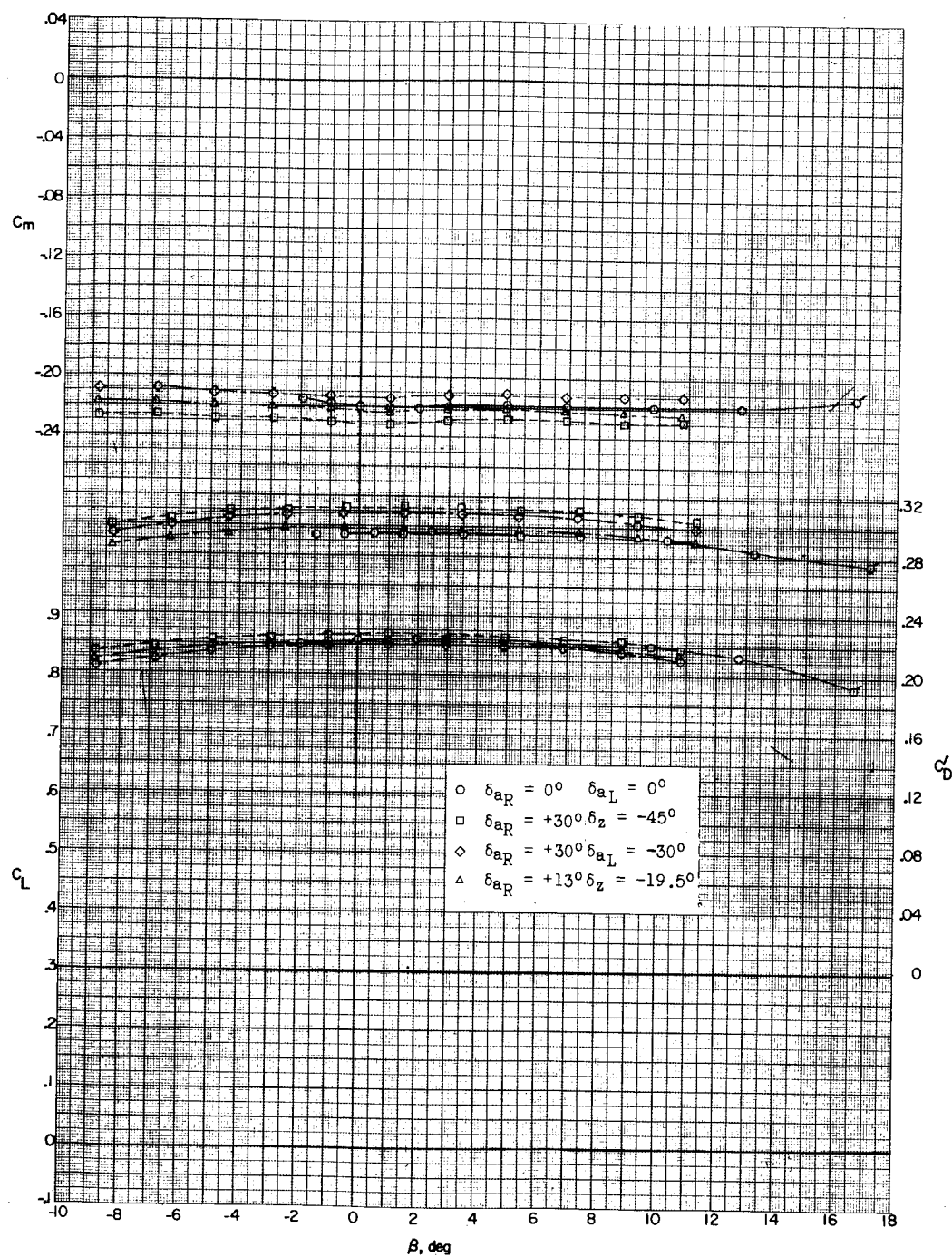
(c) $M = 1.57; \alpha = 17.4^\circ$.

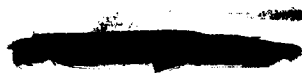
Figure 16.- Continued.

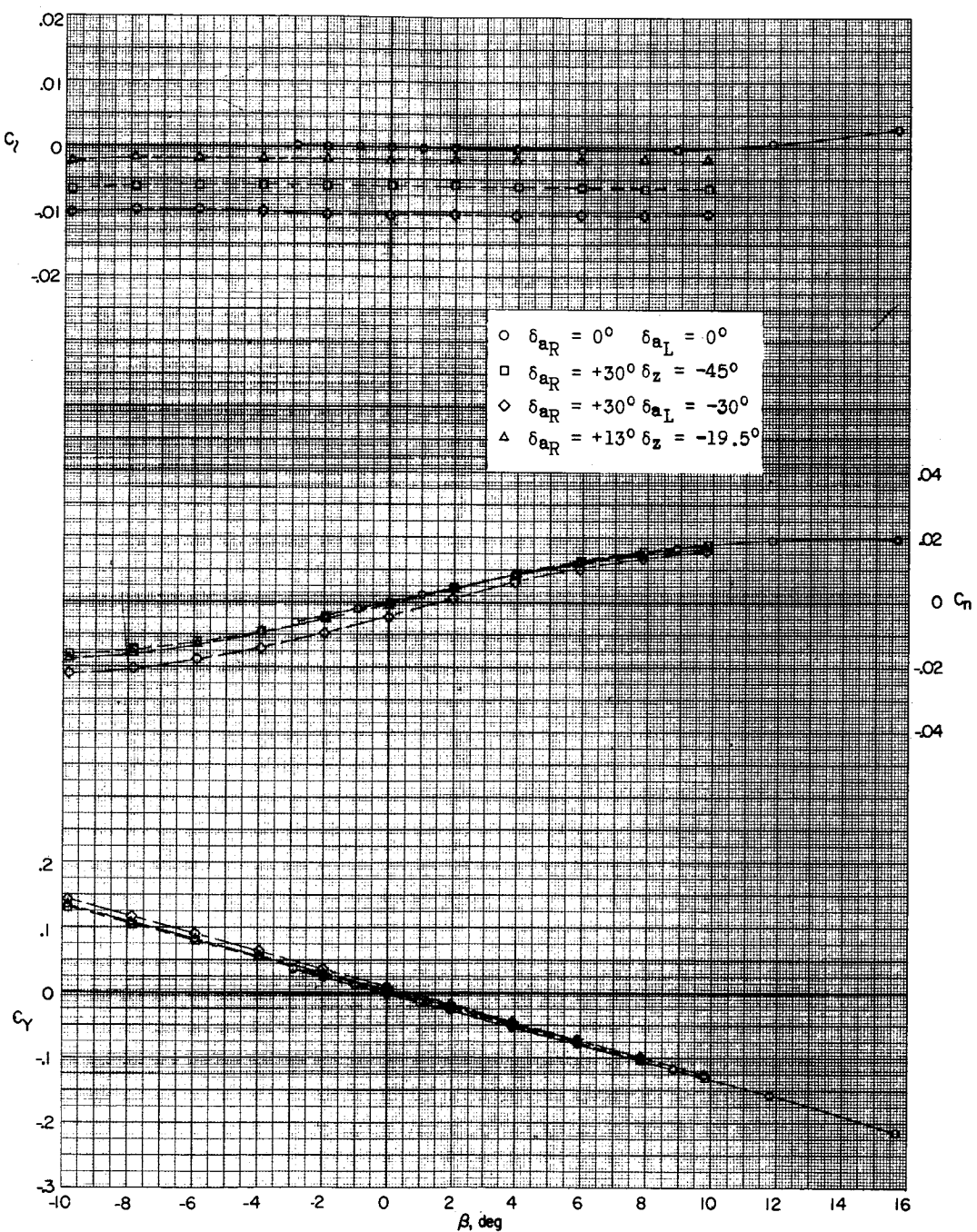
0313122 1130



(c) Concluded.

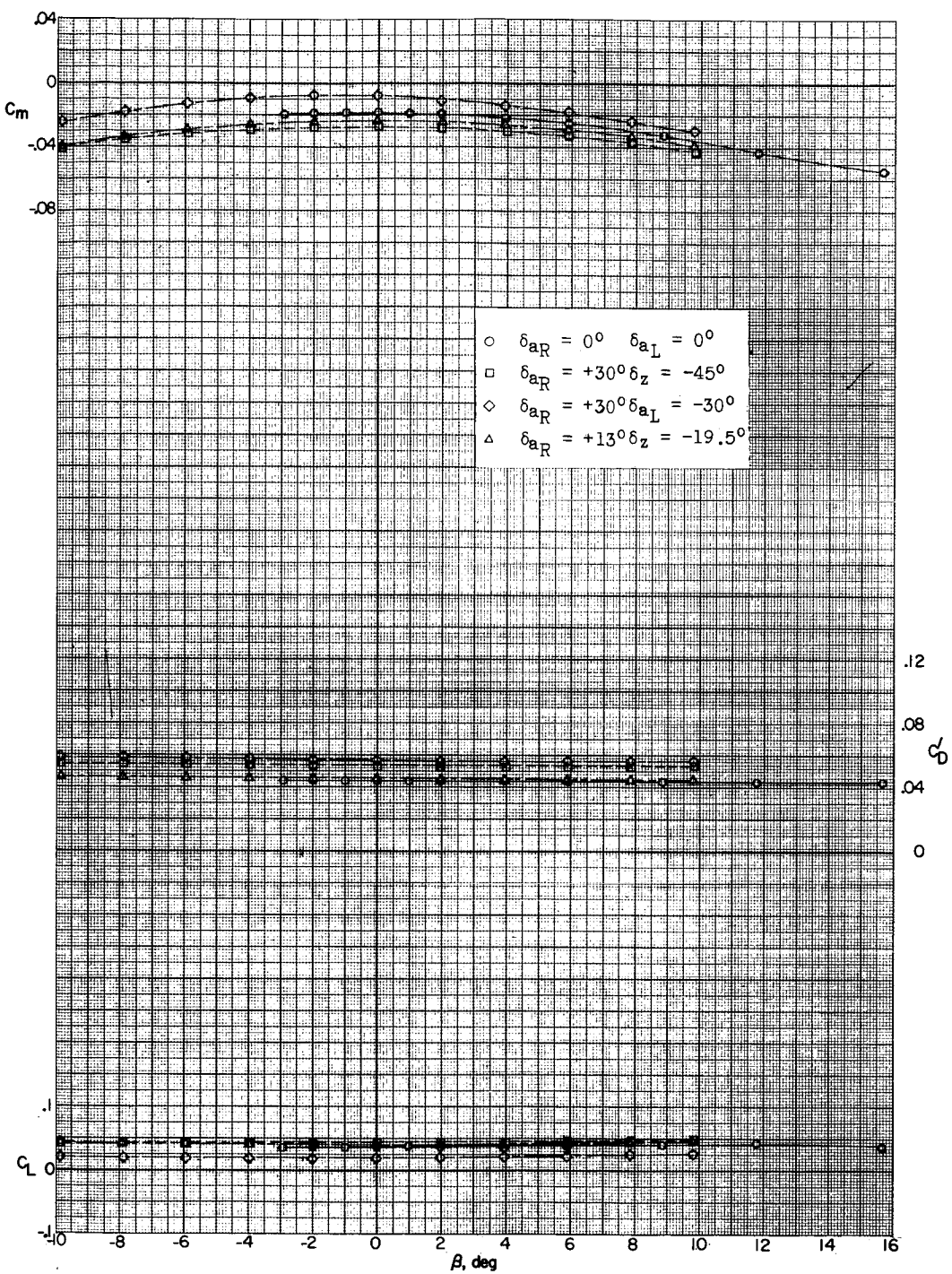
Figure 16.- Continued.





(d) $M = 1.87; \alpha = 0.4^\circ$.

Figure 16.- Continued.



(d) Concluded.

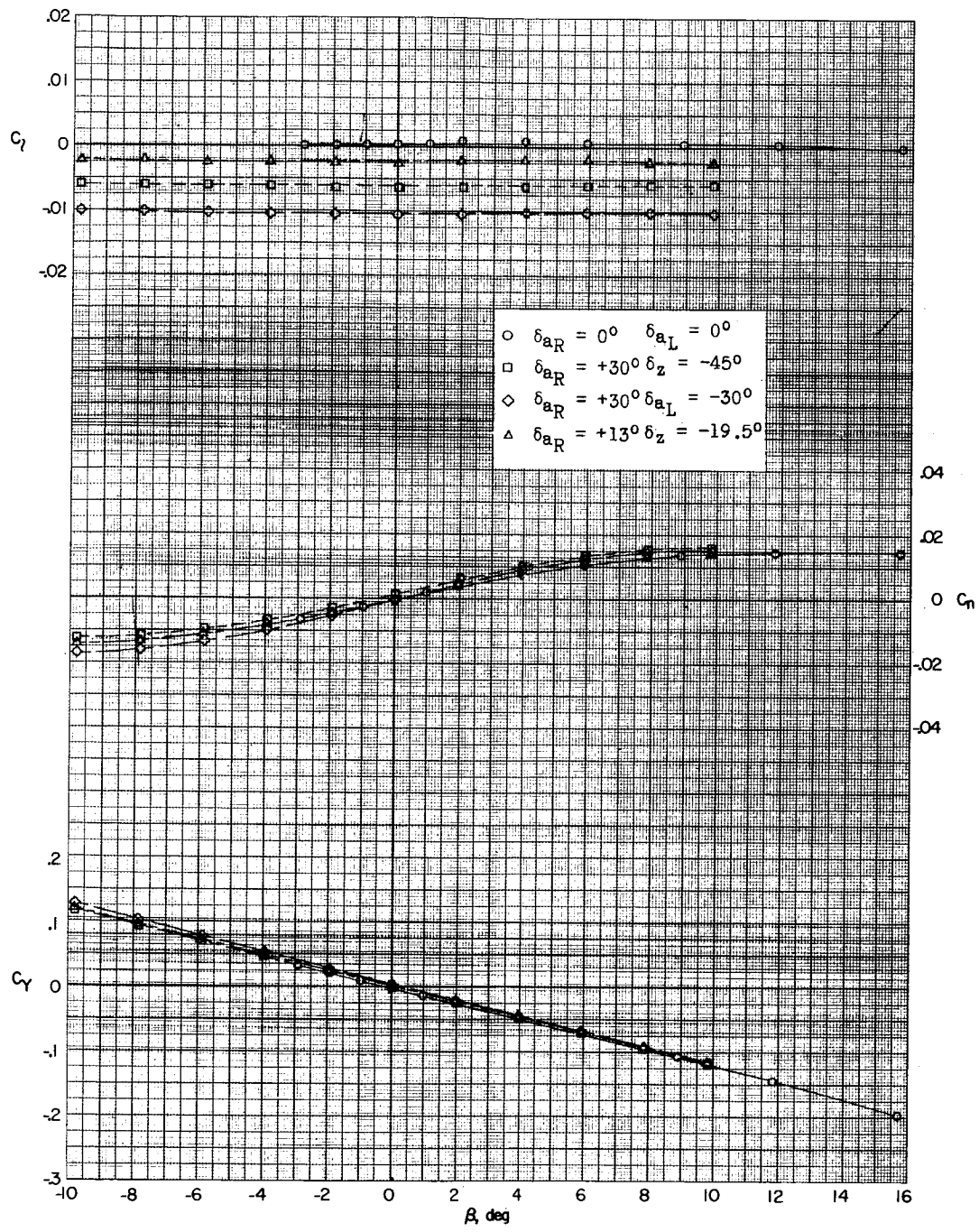
Figure 16.- Continued.

A 3x3 grid of nine black dots arranged in three rows and three columns.

REF ID: A6522

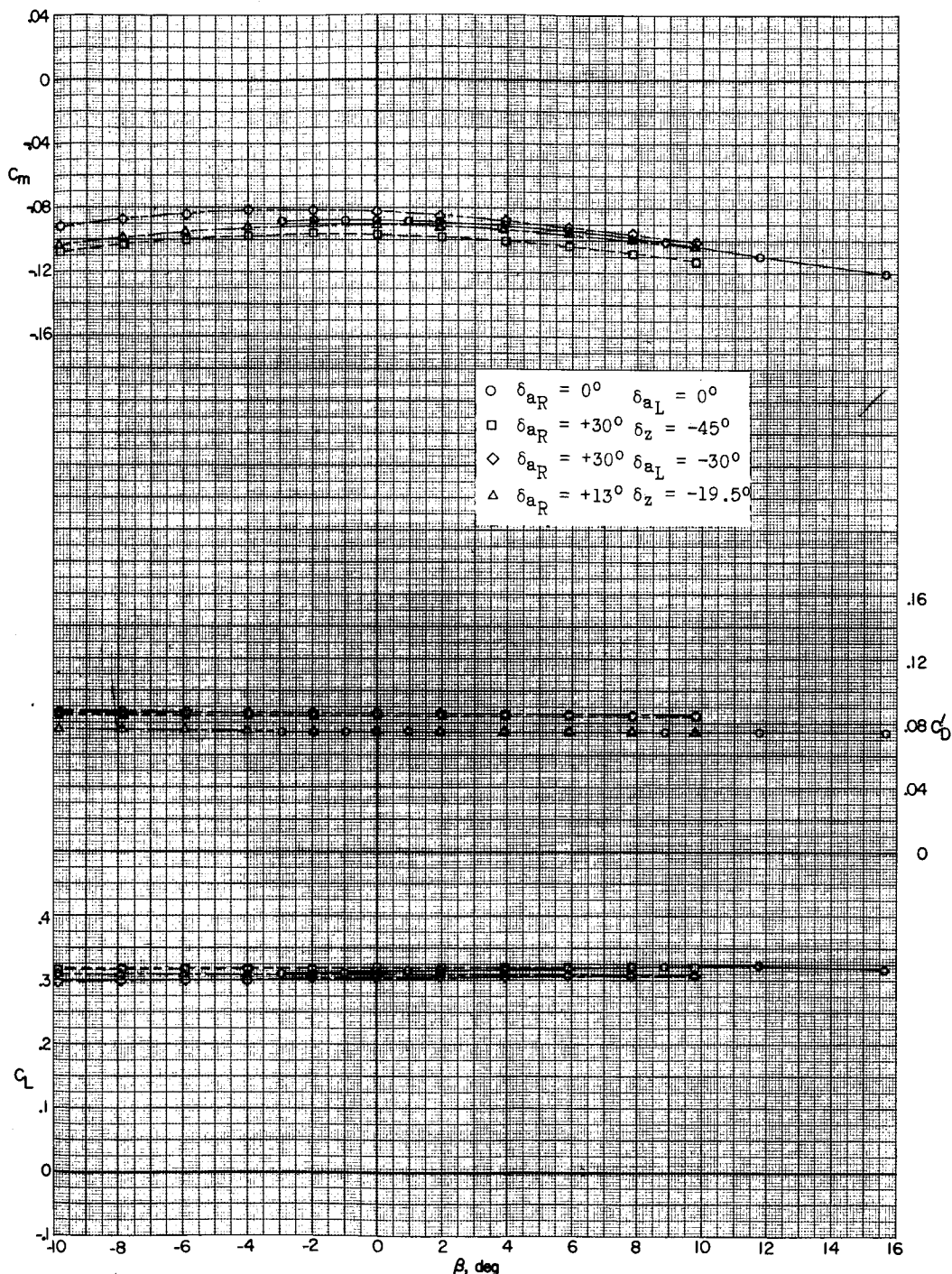
77

L-524



$$(e) \quad M = 1.87; \quad \alpha = 6.6^\circ.$$

Figure 16.- Continued.



(e) Concluded.

Figure 16.- Continued.

REF ID: A6572

REF ID: A6572
CLASSIFIED

79

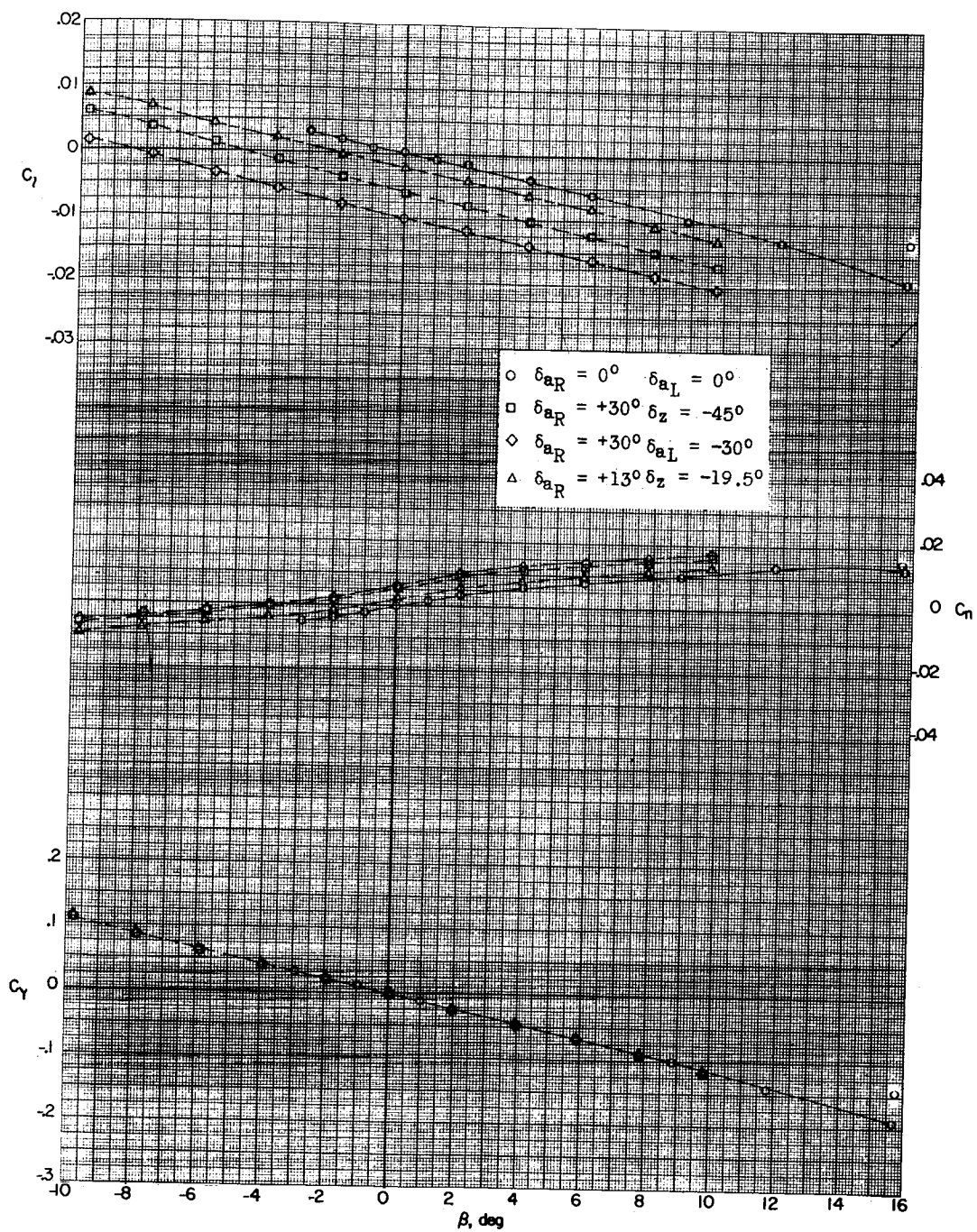
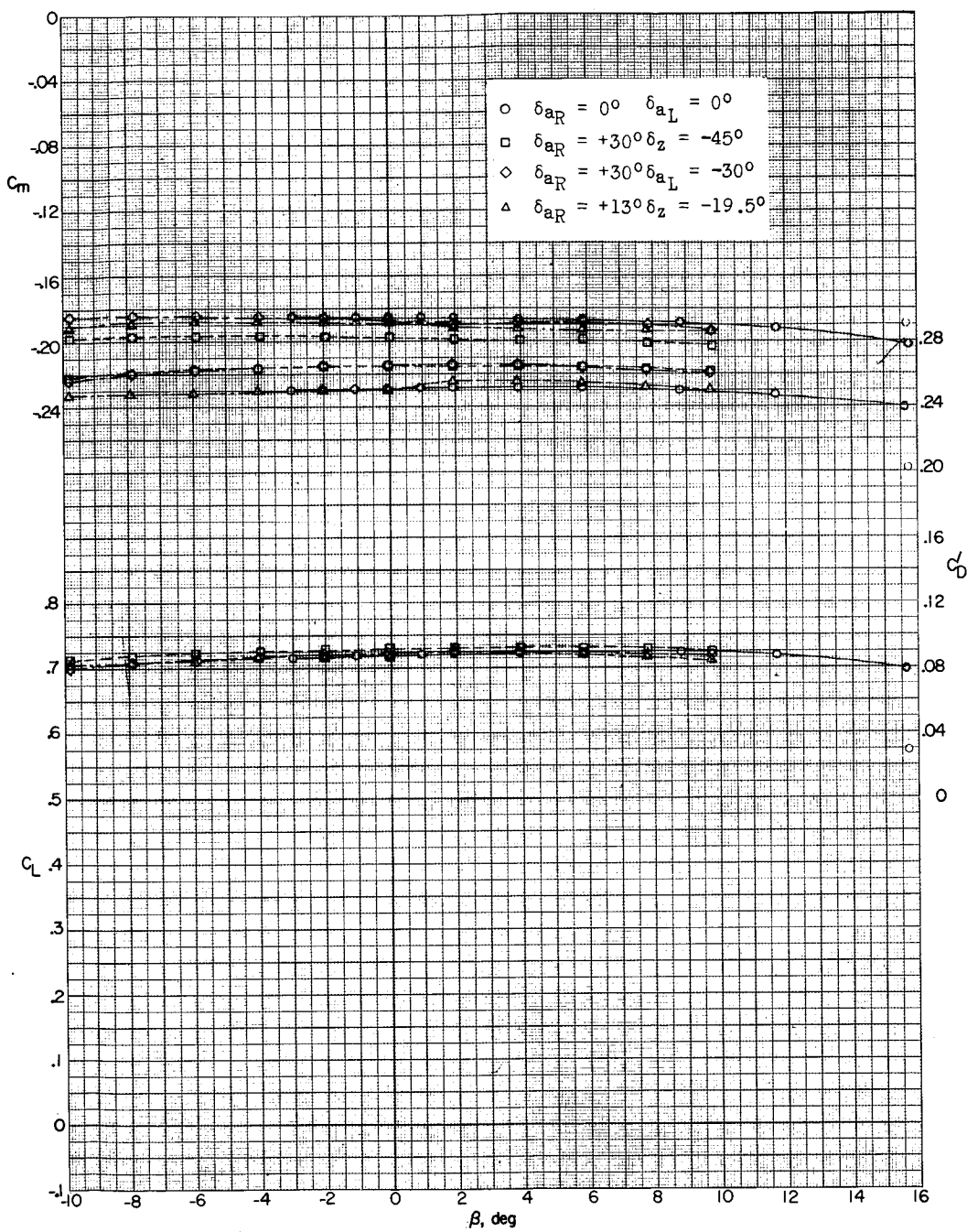
(f) $M = 1.87; \alpha = 17.1^\circ$.

Figure 16.- Continued.



(f) Concluded.

Figure 16.- Continued.

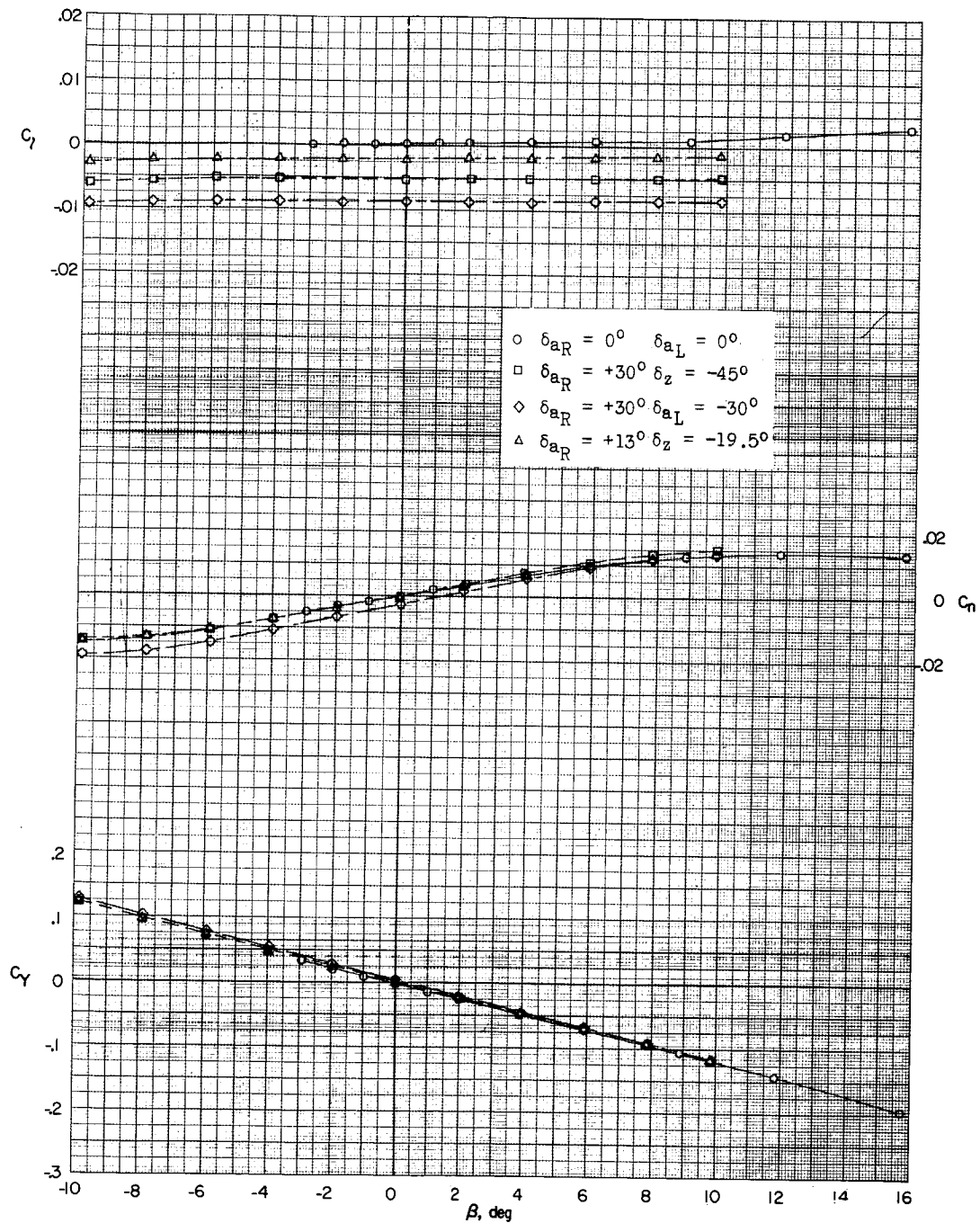
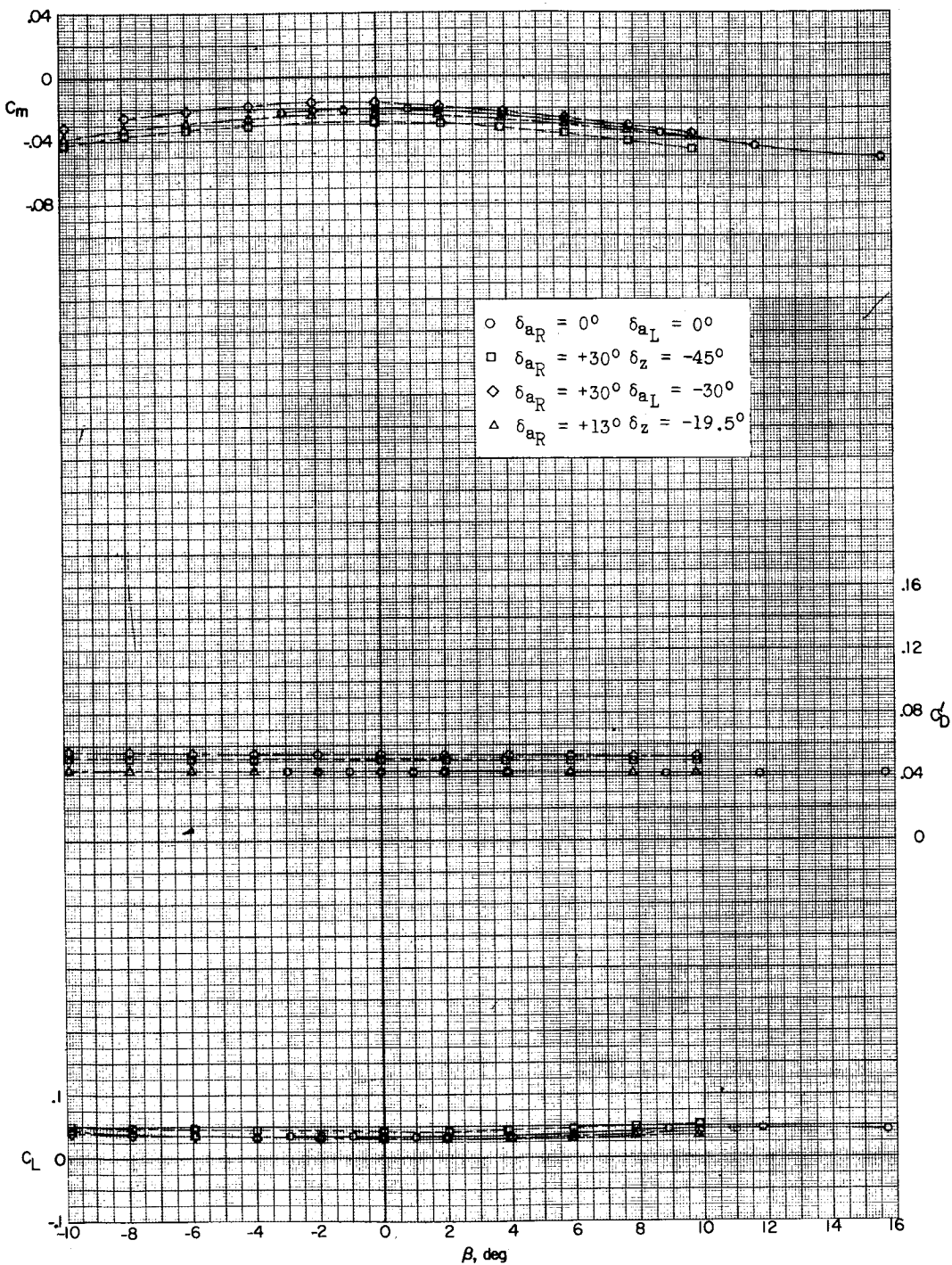
REF ID: A65422
DECLASSIFIED(g) $M = 2.16$. $\alpha = 0.4^\circ$.

Figure 16.- Continued.

031312 001000



(g) Concluded.

Figure 16.- Continued.

REF ID: A6512

REF ID: A6512
DECLASSIFIED

83

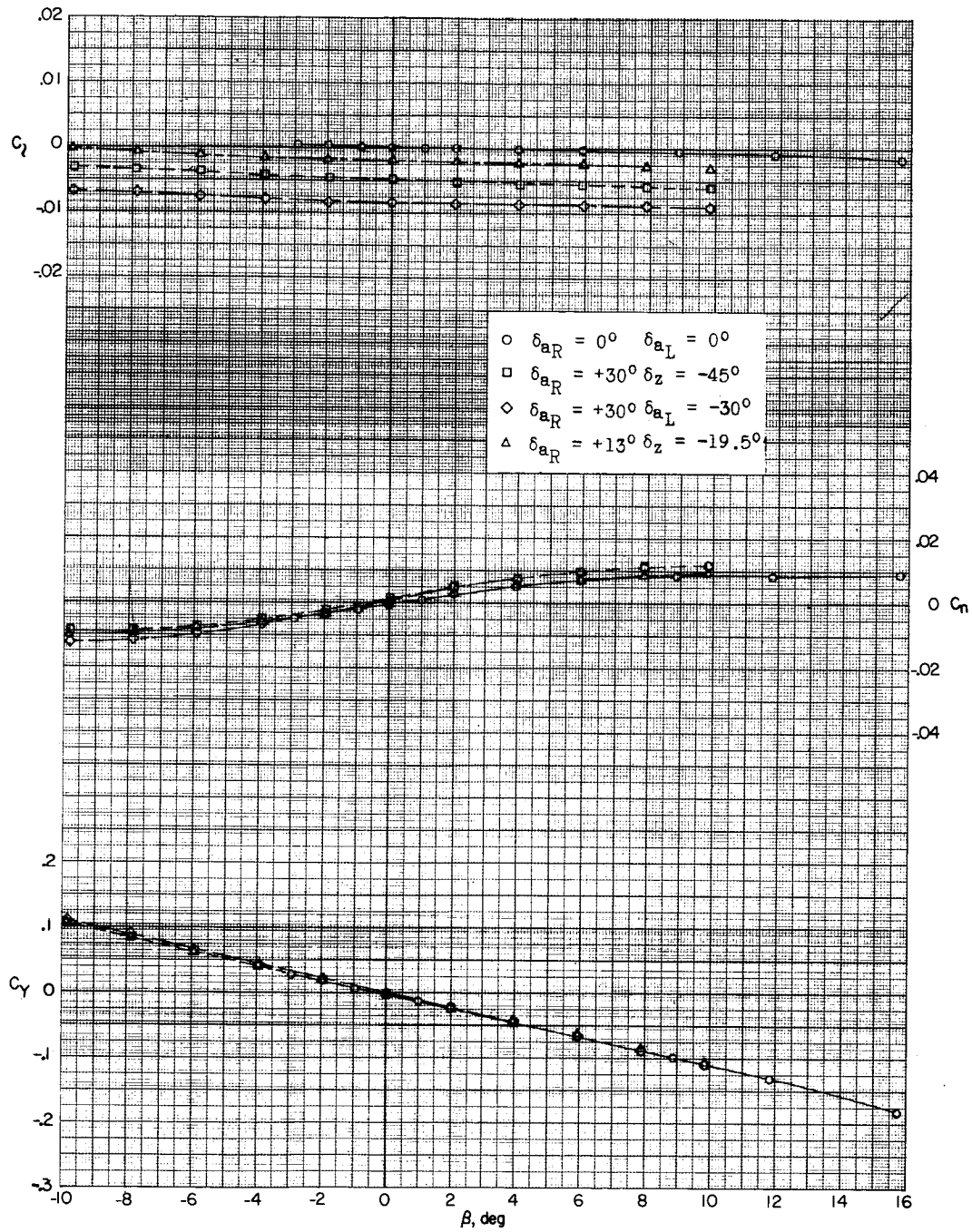
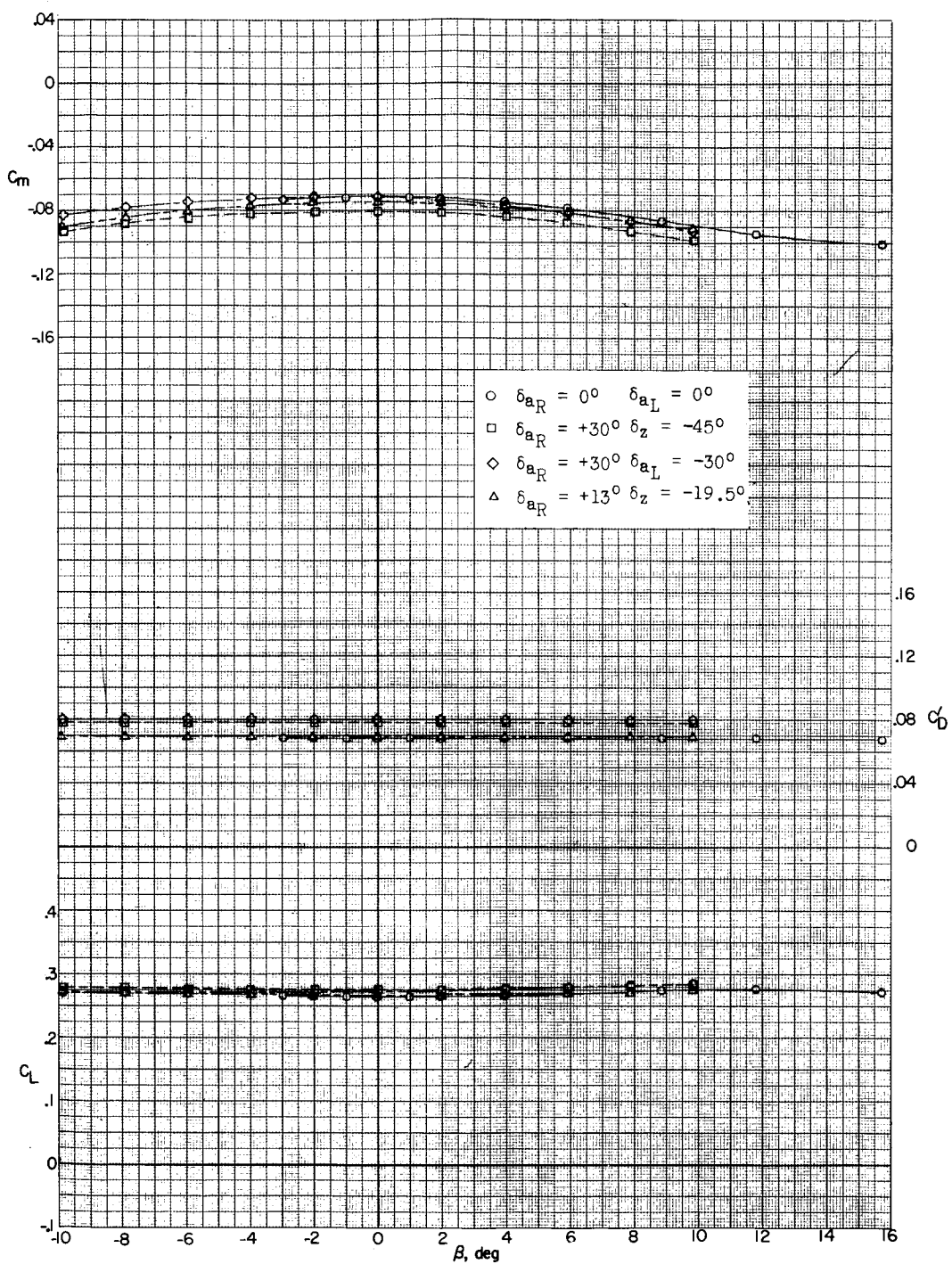
(h) $M = 2.16; \alpha = 6.5^\circ$.

Figure 16.- Continued.

031712 201100

84



(h) Concluded.

Figure 16.- Continued.

I-524

REF ID: A6512

REF ID: A6512
DECLASSIFIED

85

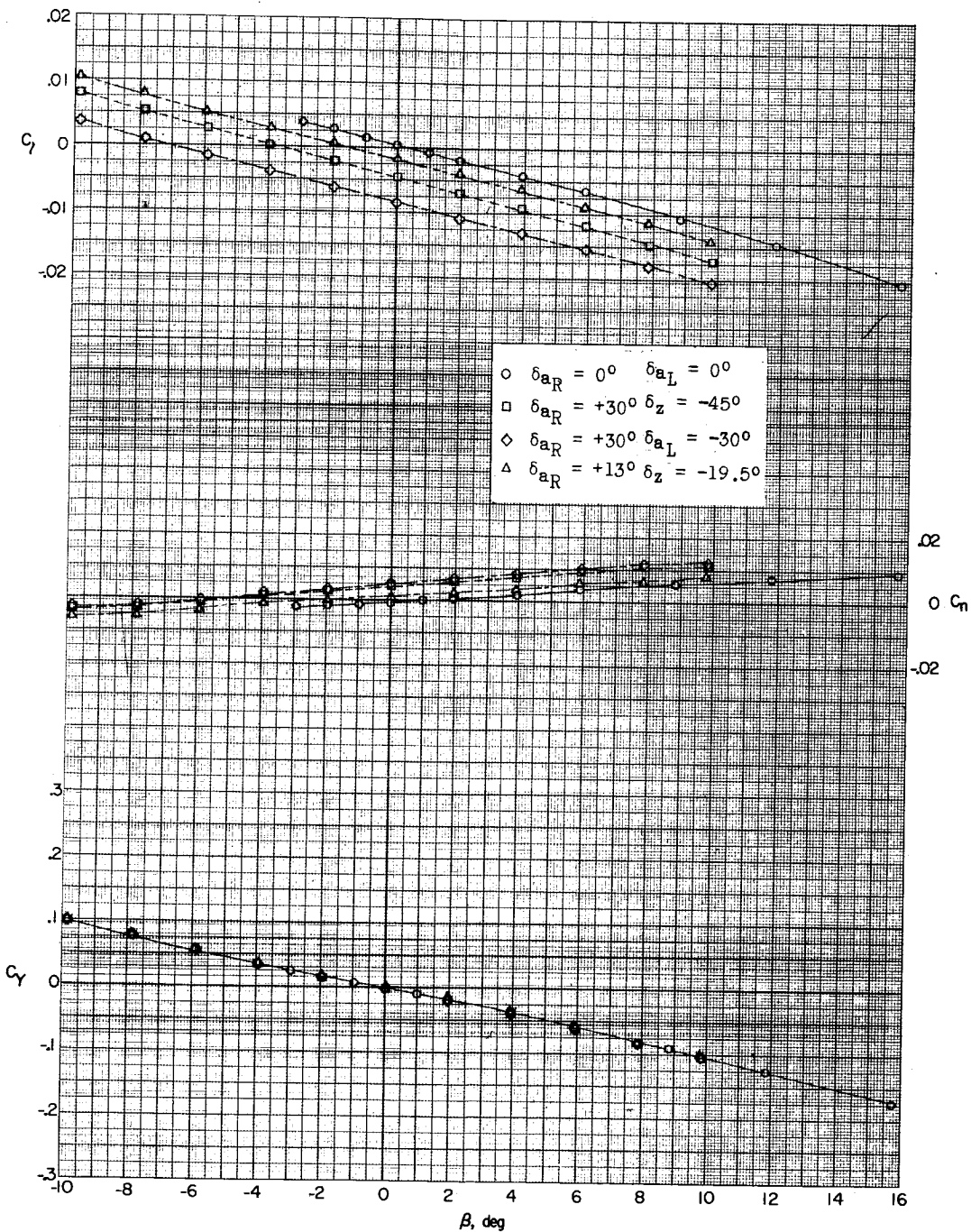
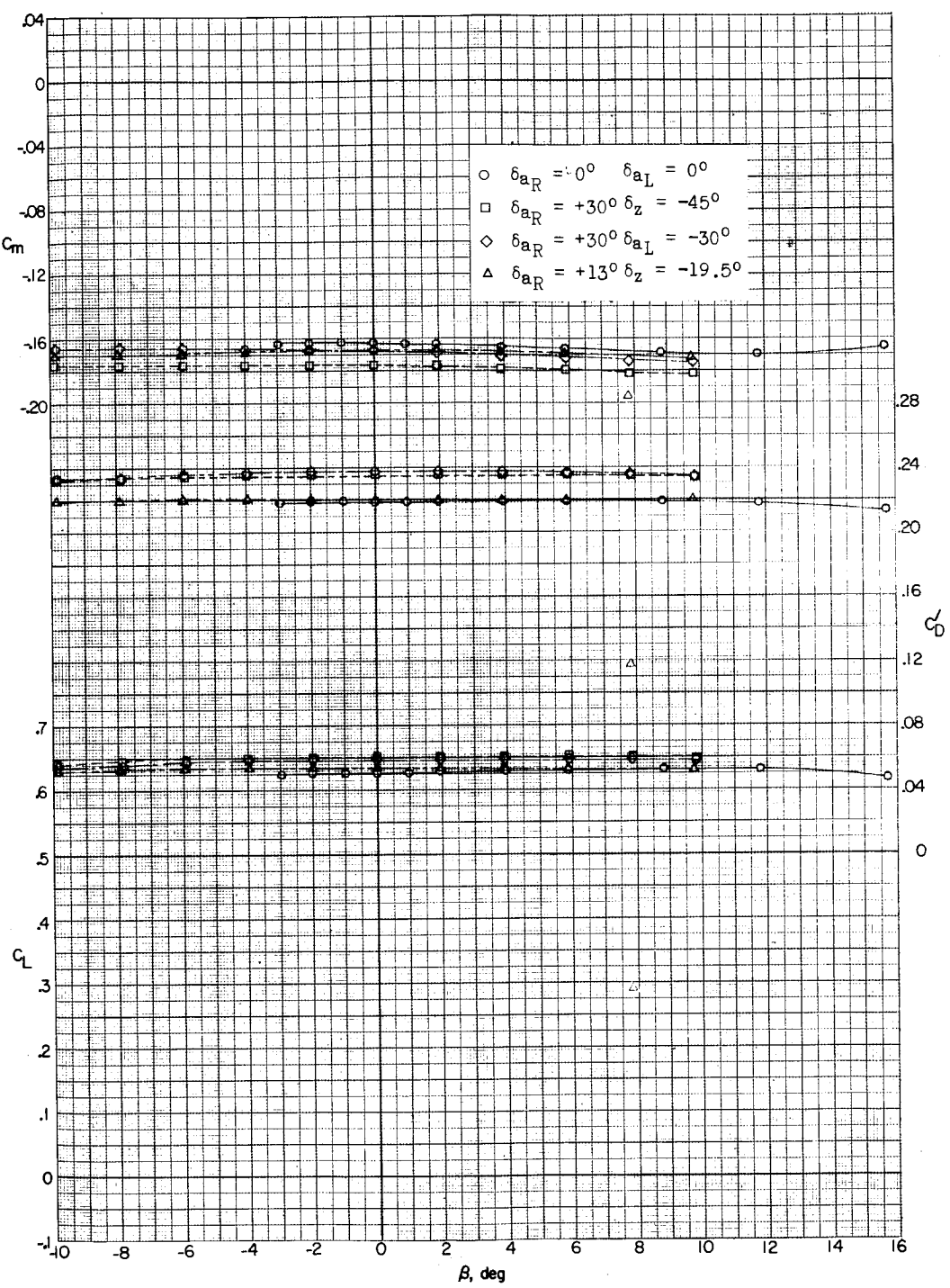
(i) $M = 2.16; \alpha = 16.9^\circ$.

Figure 16.- Continued.

031312201030

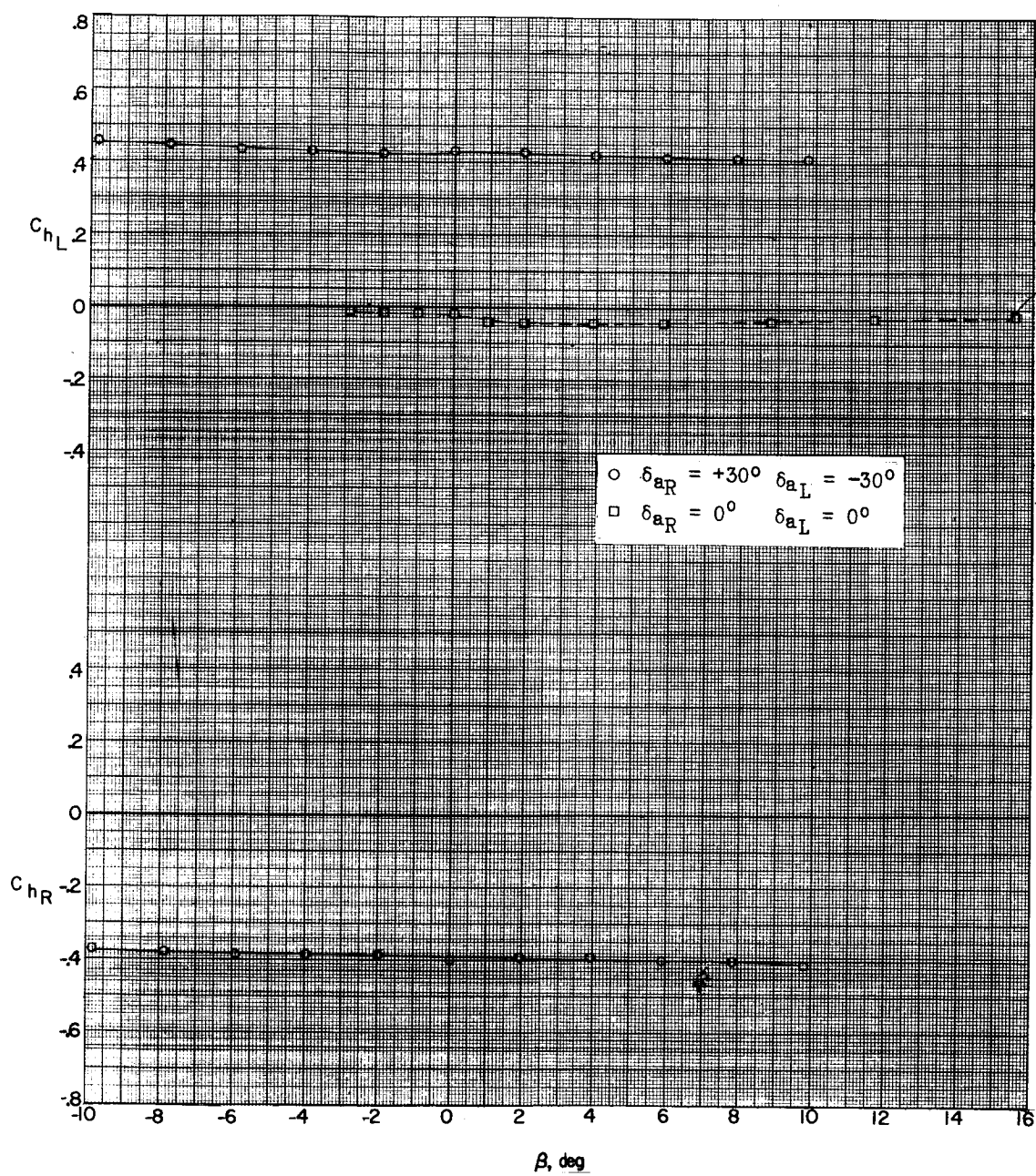


86



(i) Concluded.

Figure 16.- Concluded.

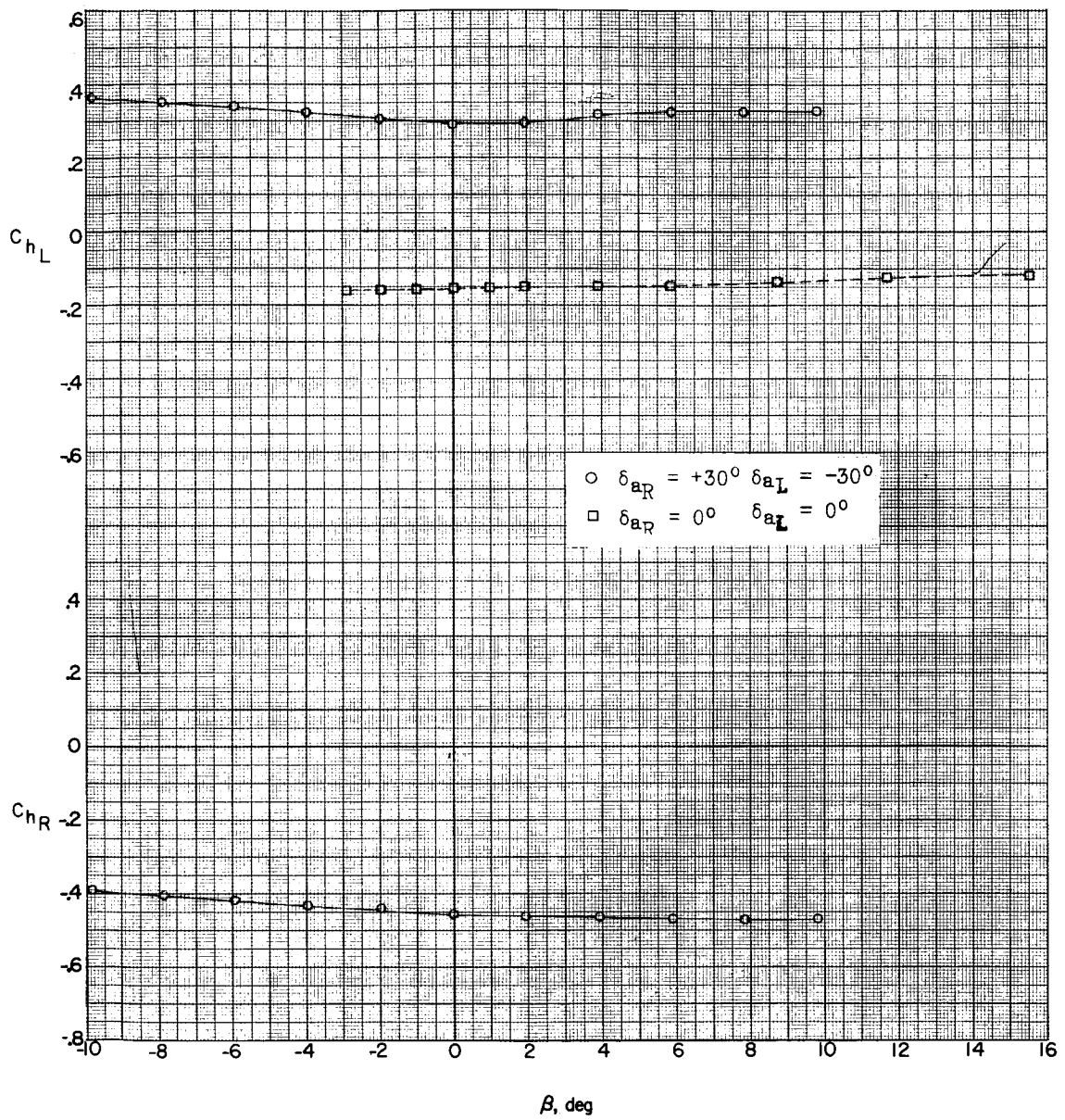


(a) $M = 1.57; \alpha = 0.4^\circ$.

Figure 17.-- Effect of aileron deflection on aileron hinge-moment coefficient in sideslip.

03191230 1030

88



(b) $M = 1.57; \alpha = 6.7^\circ$.

Figure 17.- Continued.

REF ID: A6512C

REF ID: A6512C
DECLASSIFIED

89

12C

L-524

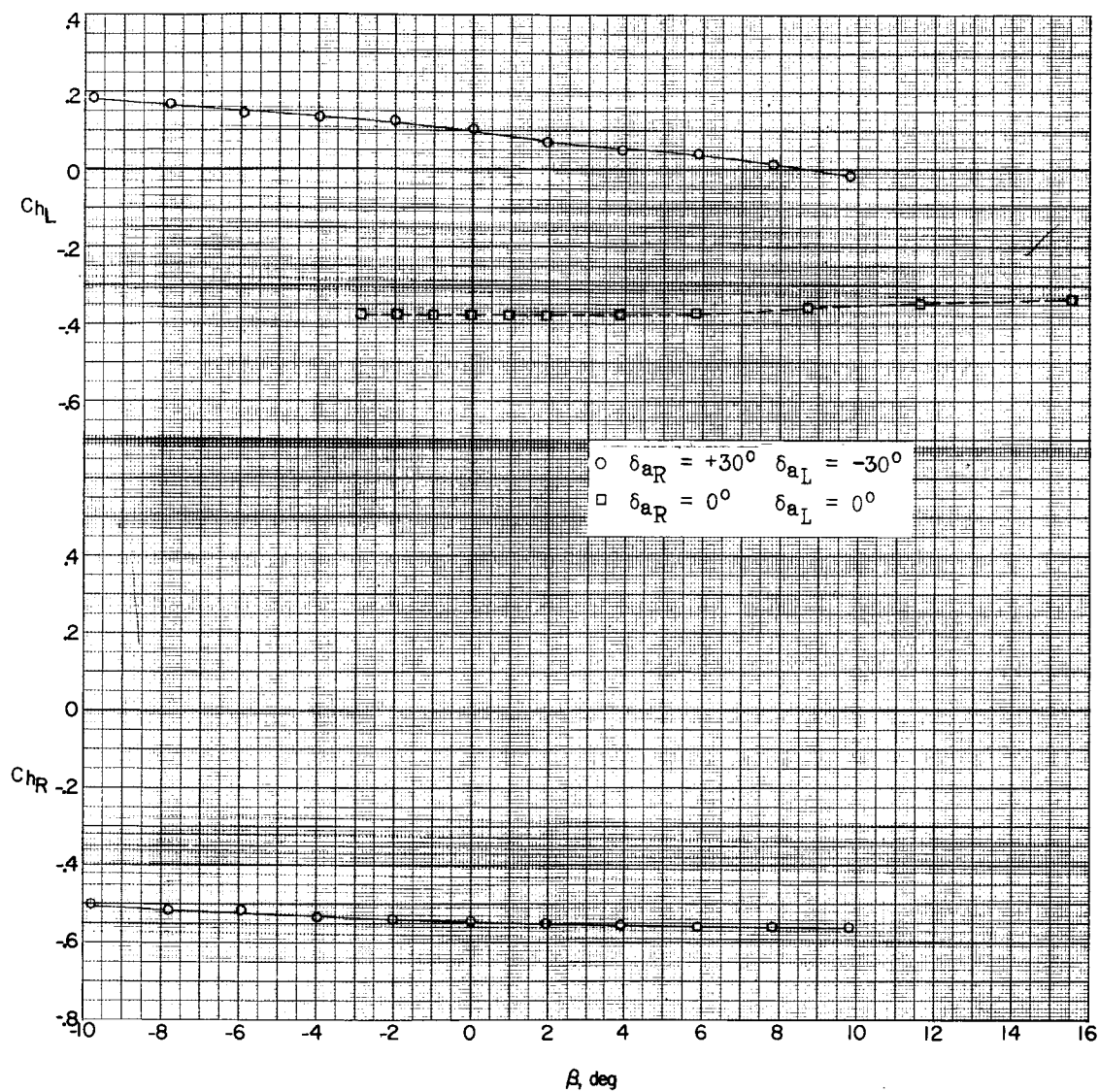
(c) $M = 1.57; \alpha = 17.4^\circ$.

Figure 17.- Continued.

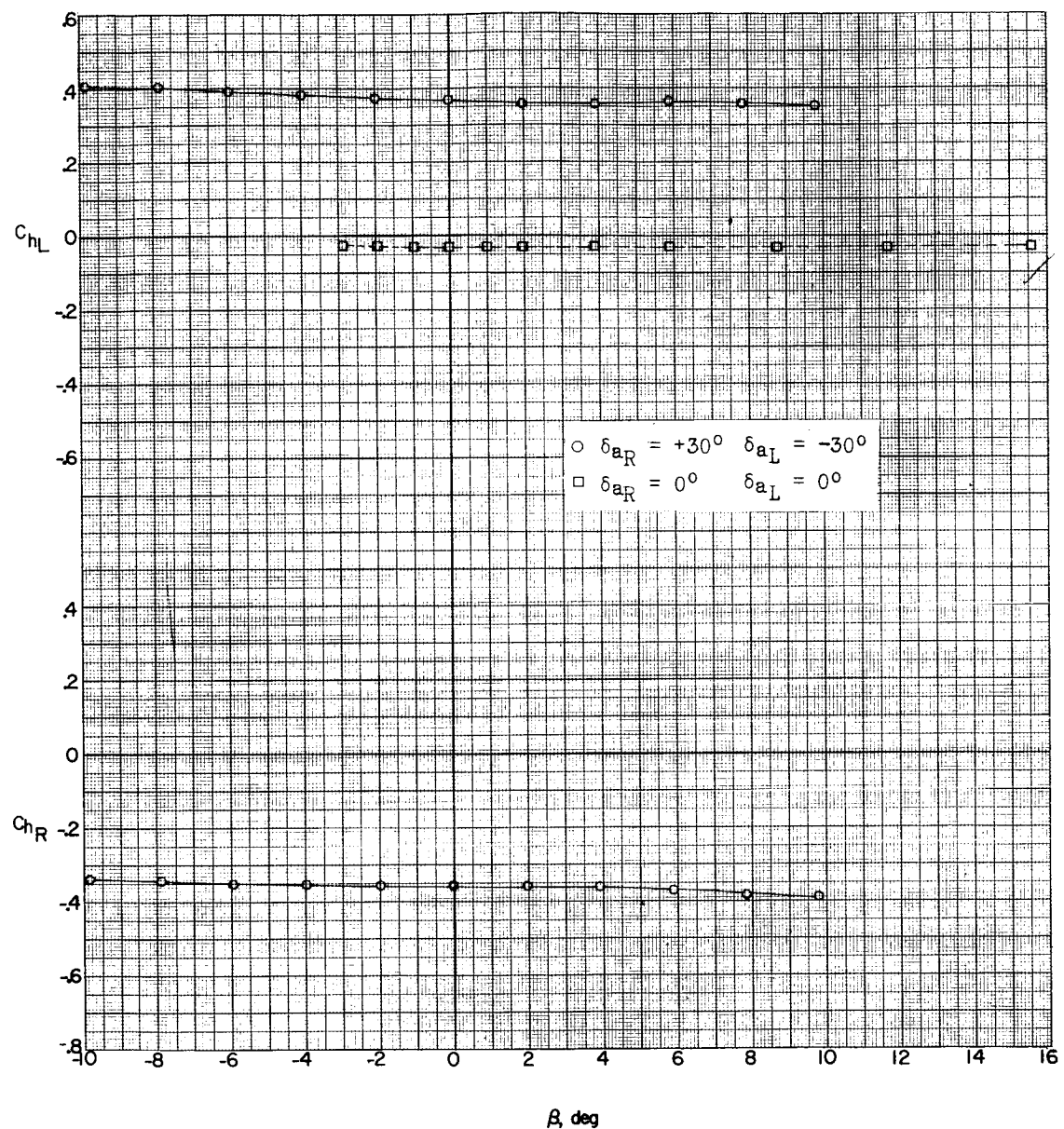
(d) $M = 1.87; \alpha = 0.4^\circ$.

Figure 17.- Continued.

REF ID: A6512

REF ID: A6512
DECLASSIFIED

91

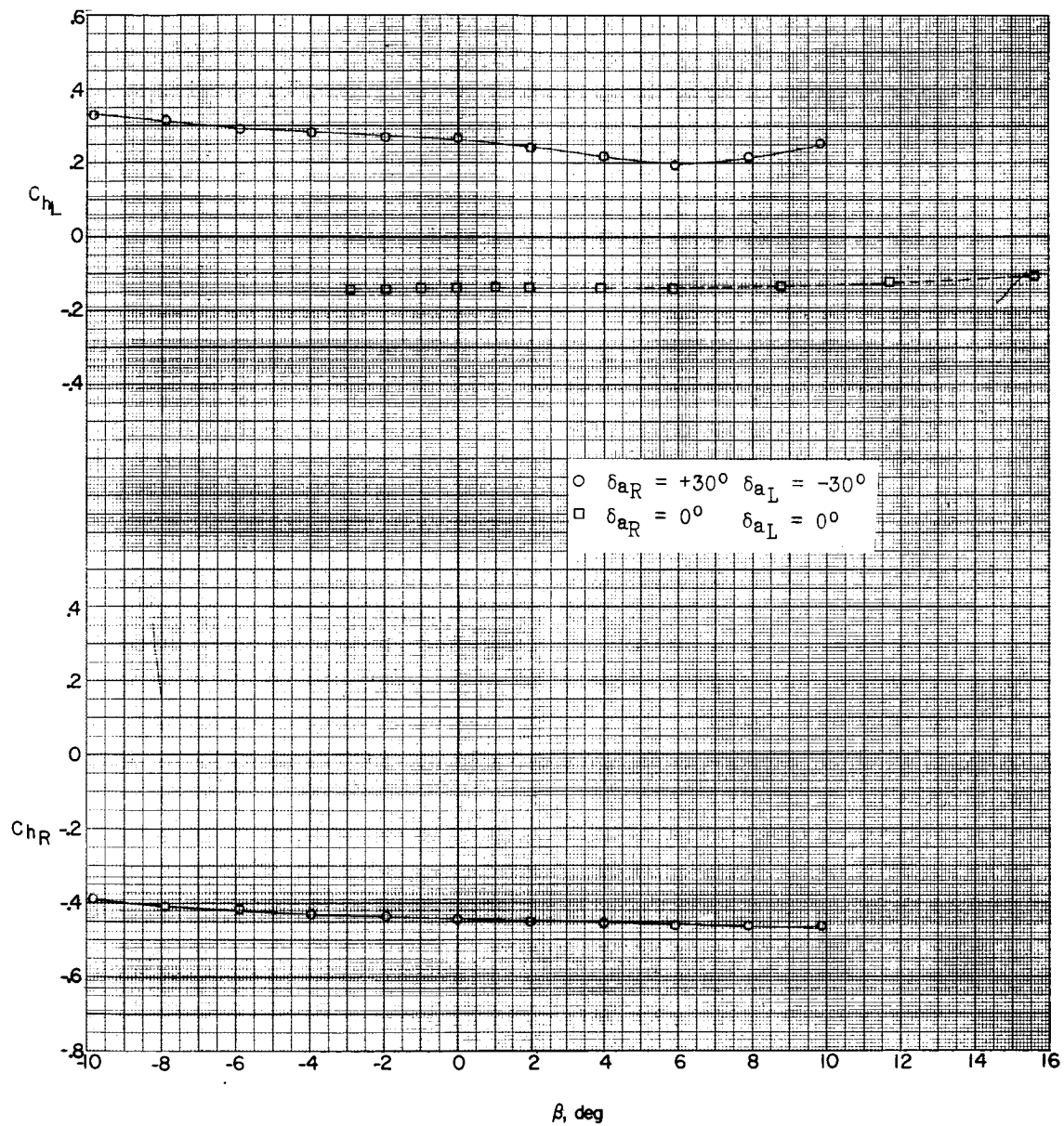
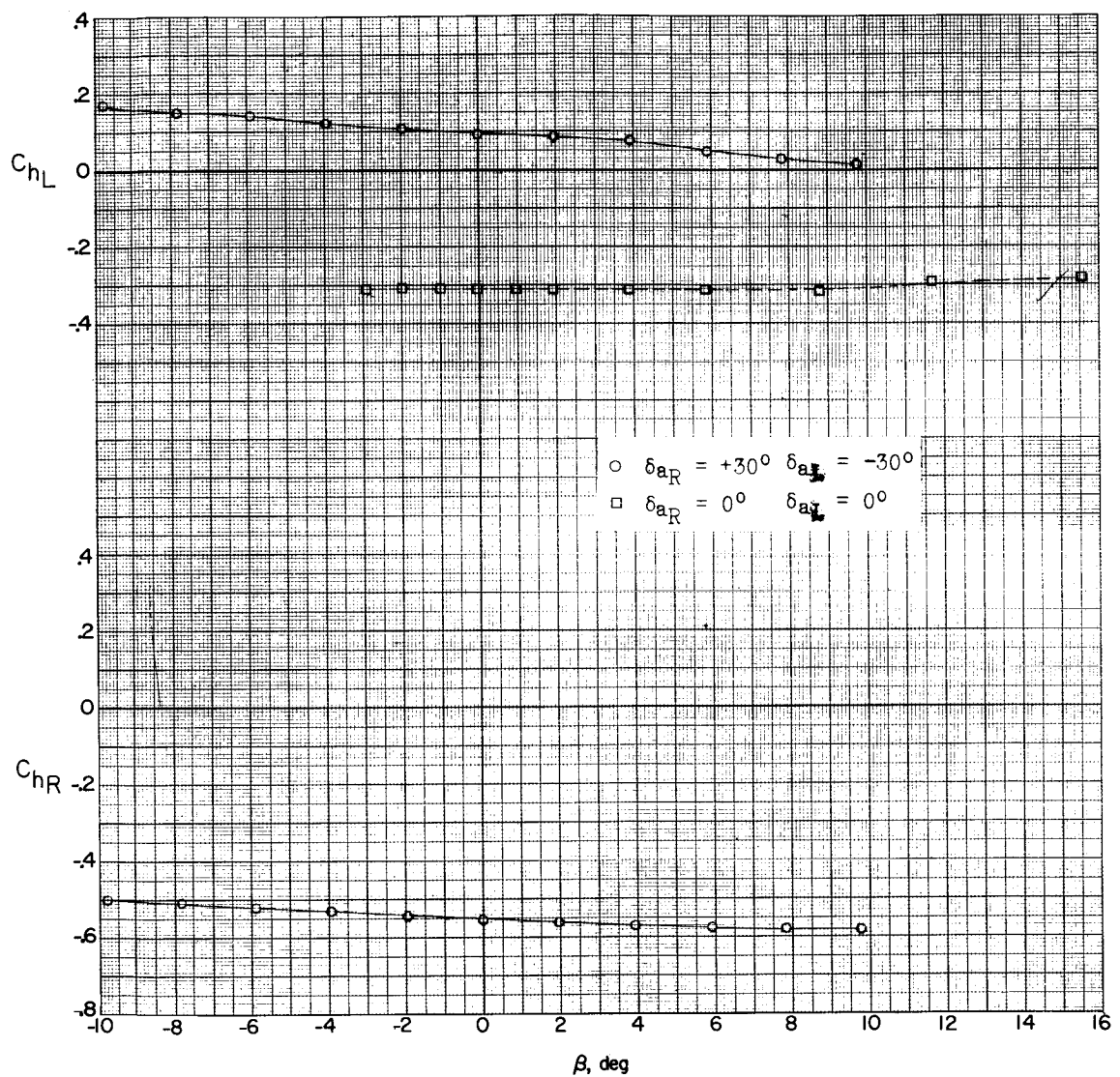
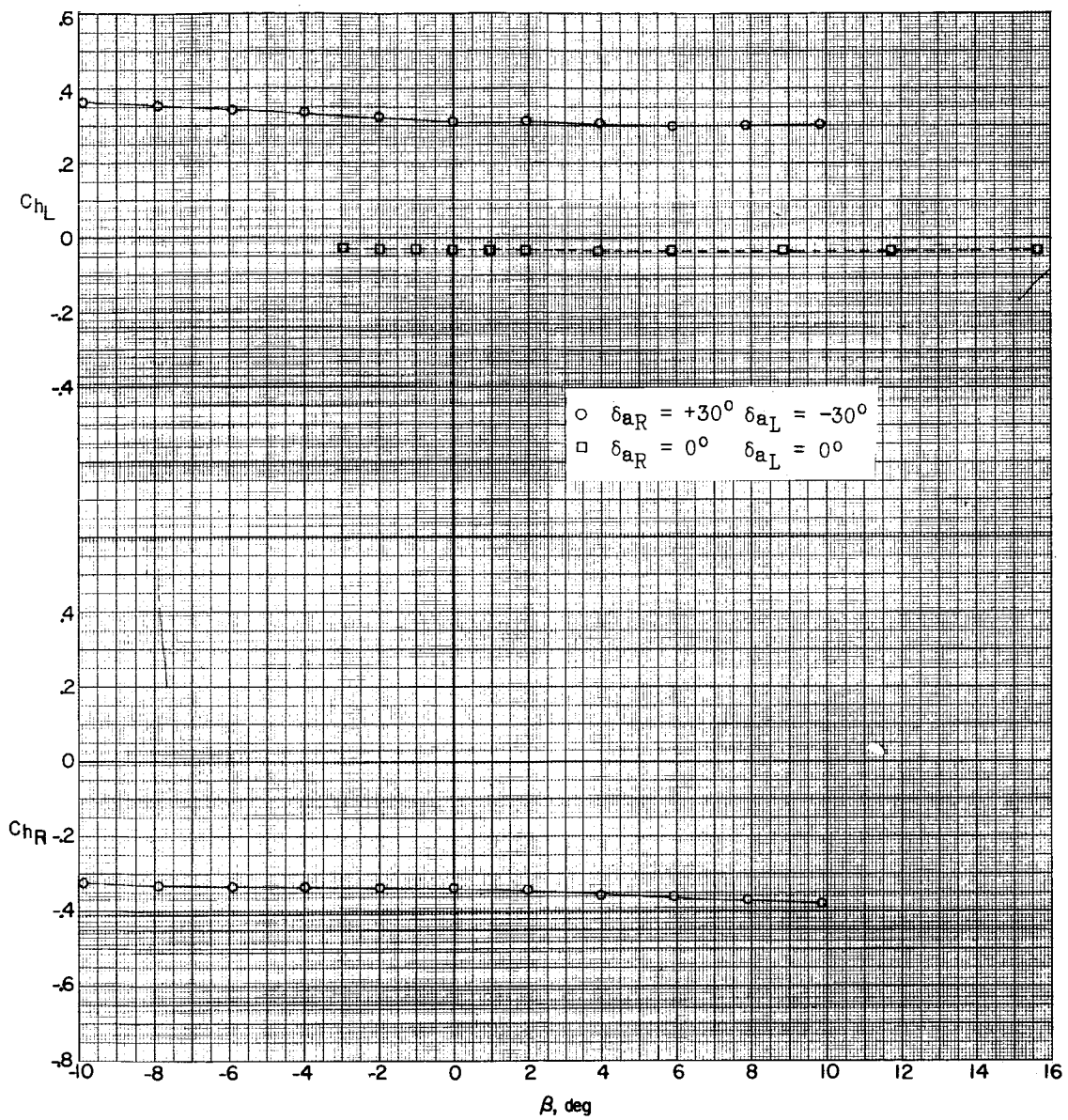
(e) $M = 1.87; \alpha = 6.6^\circ$.

Figure 17.- Continued.

031913291030

92



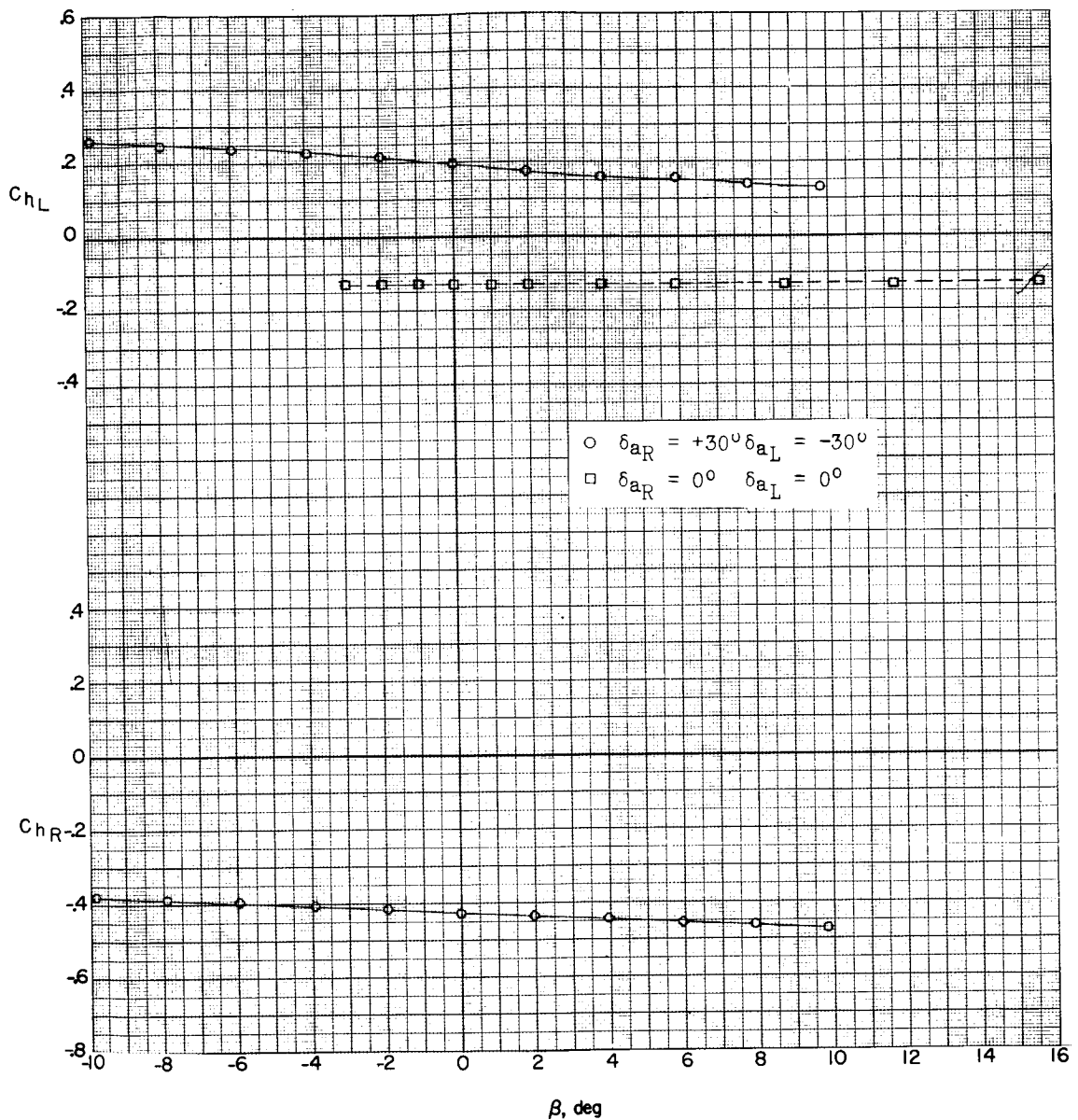


(g) $M = 2.16; \alpha = 0.4^\circ$.

Figure 17.- Continued.

DATA FOR L-300 8

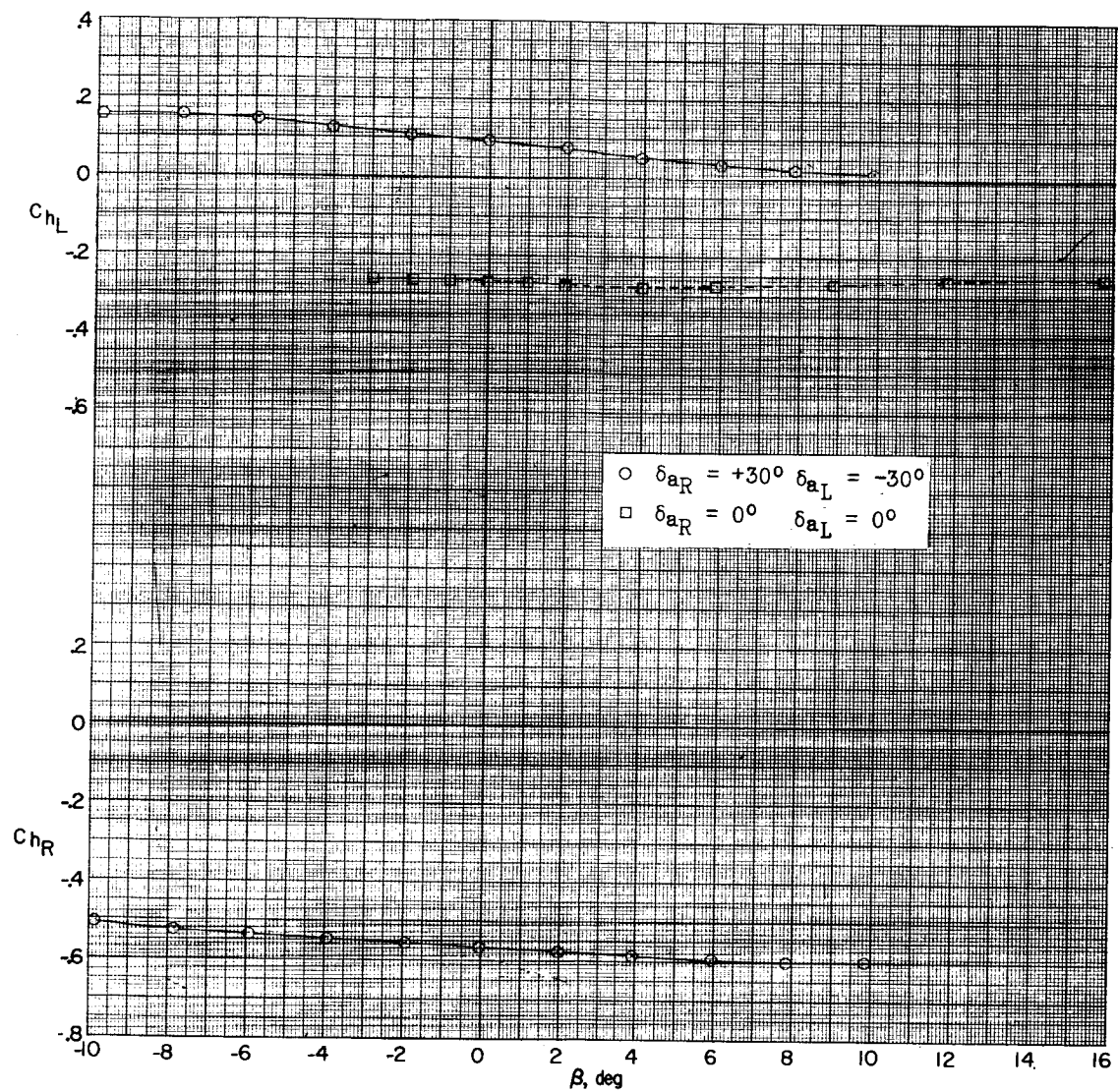
94



(n) $M = 2.16; \alpha = 6.5^\circ$.

Figure 17.- Continued.

REF ID: A6524
CLASSIFIED 95



(i) $M = 2.16; \alpha = 16.9^\circ$.

Figure 17.- Concluded.

0317022A1030

8

96

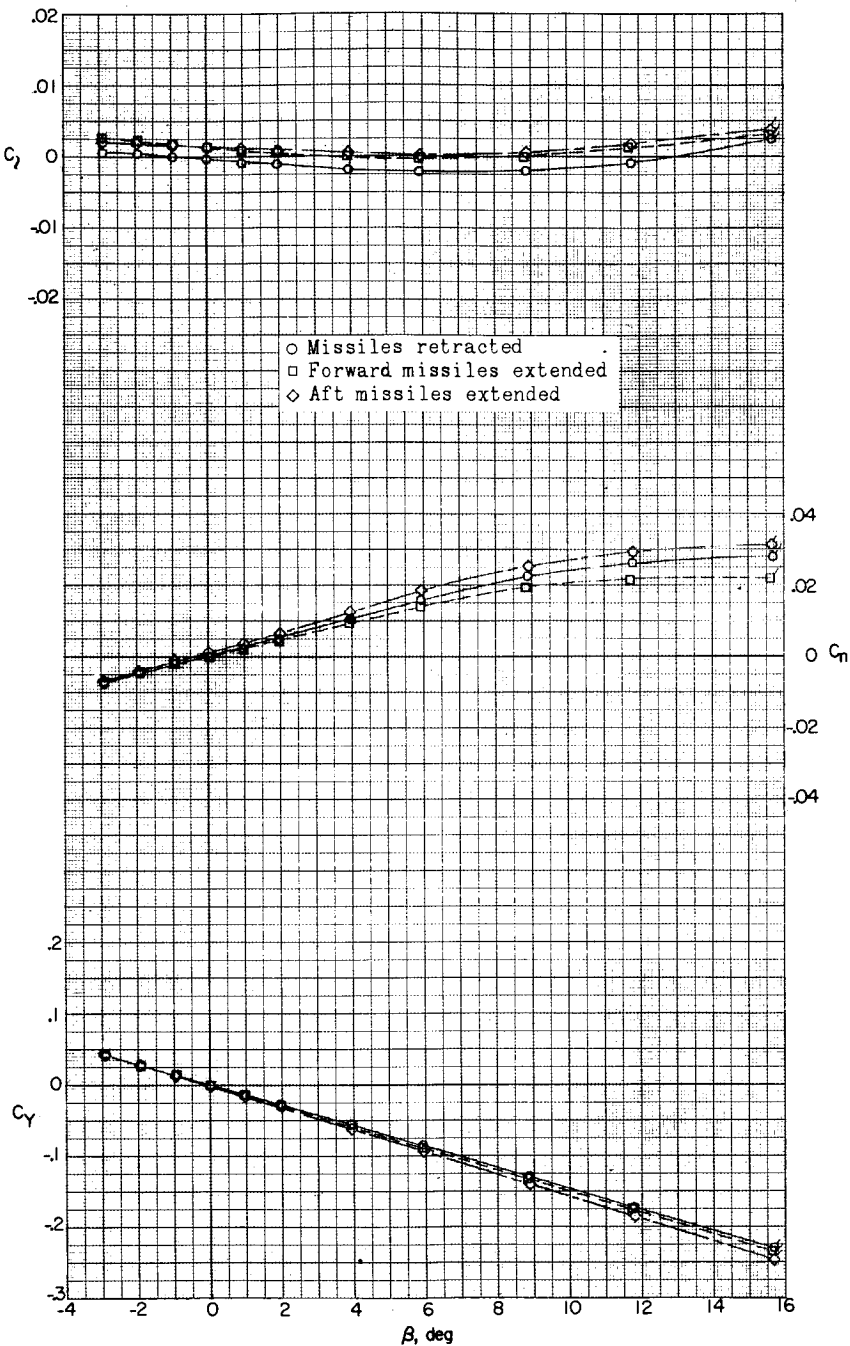
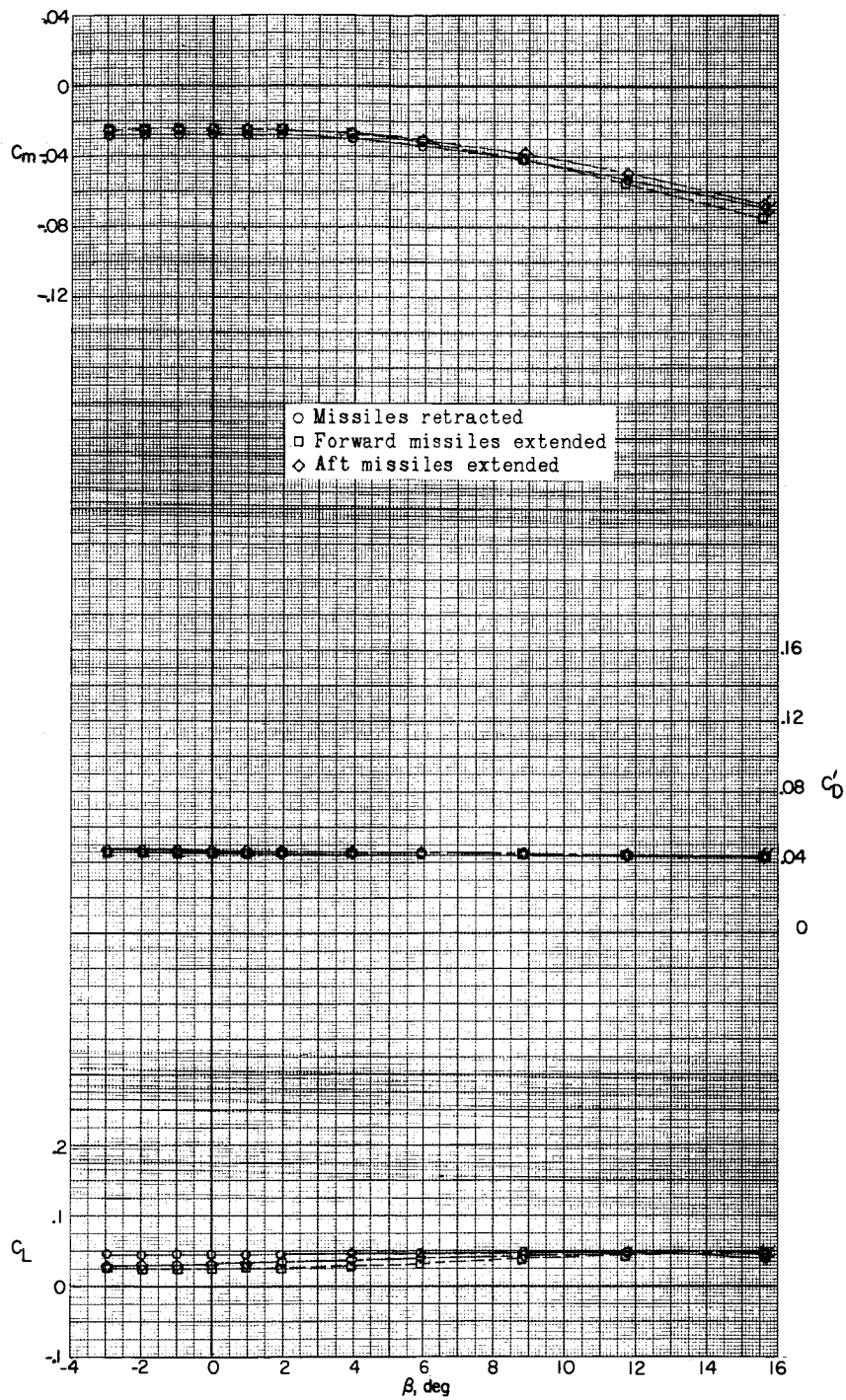
(a) $M = 1.57; \alpha = 0.4^\circ$.

Figure 18.- Effect of extended missiles on aerodynamic characteristics in sideslip. (Flagged symbols denote wall-reflected shock waves striking the tail.)



(a) Concluded.

Figure 18.- Continued.

03171820 1030

98

8

L-524

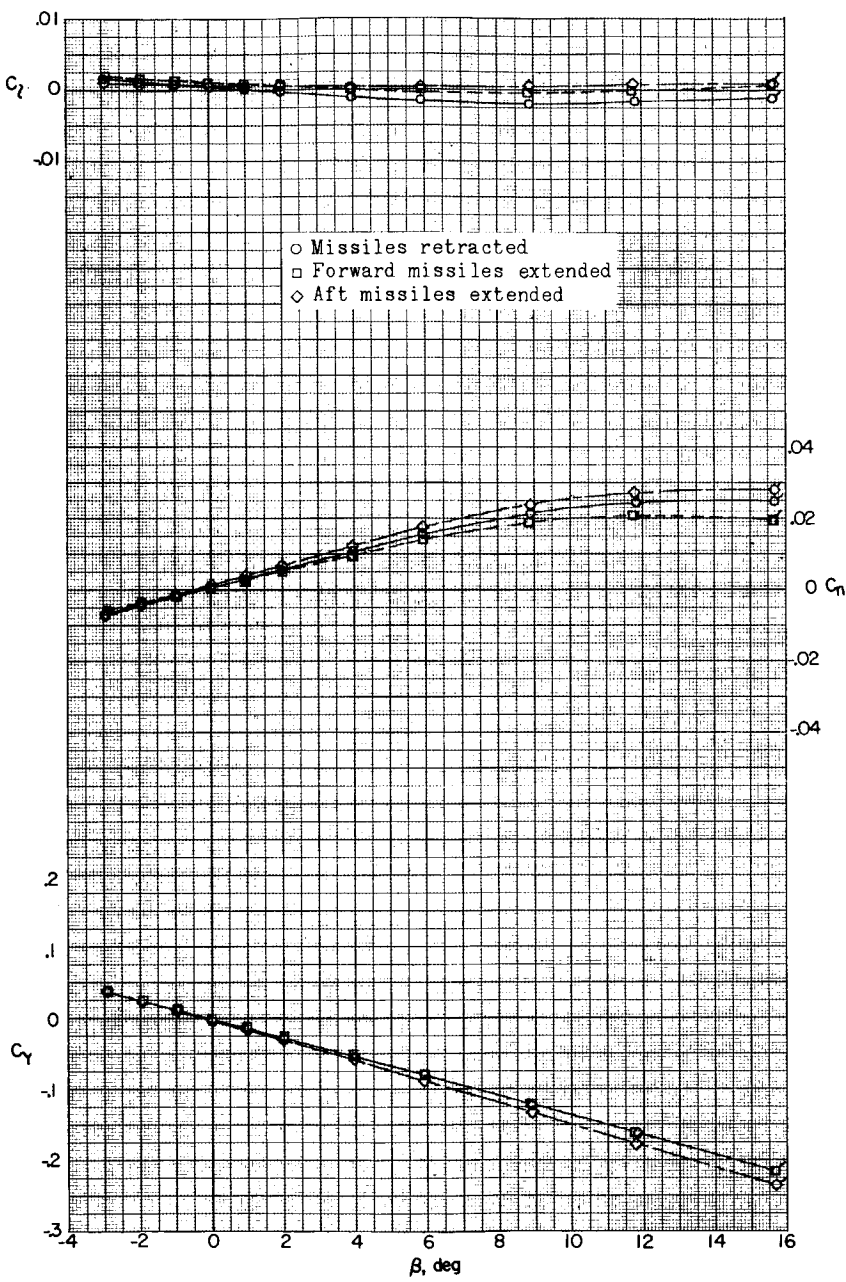
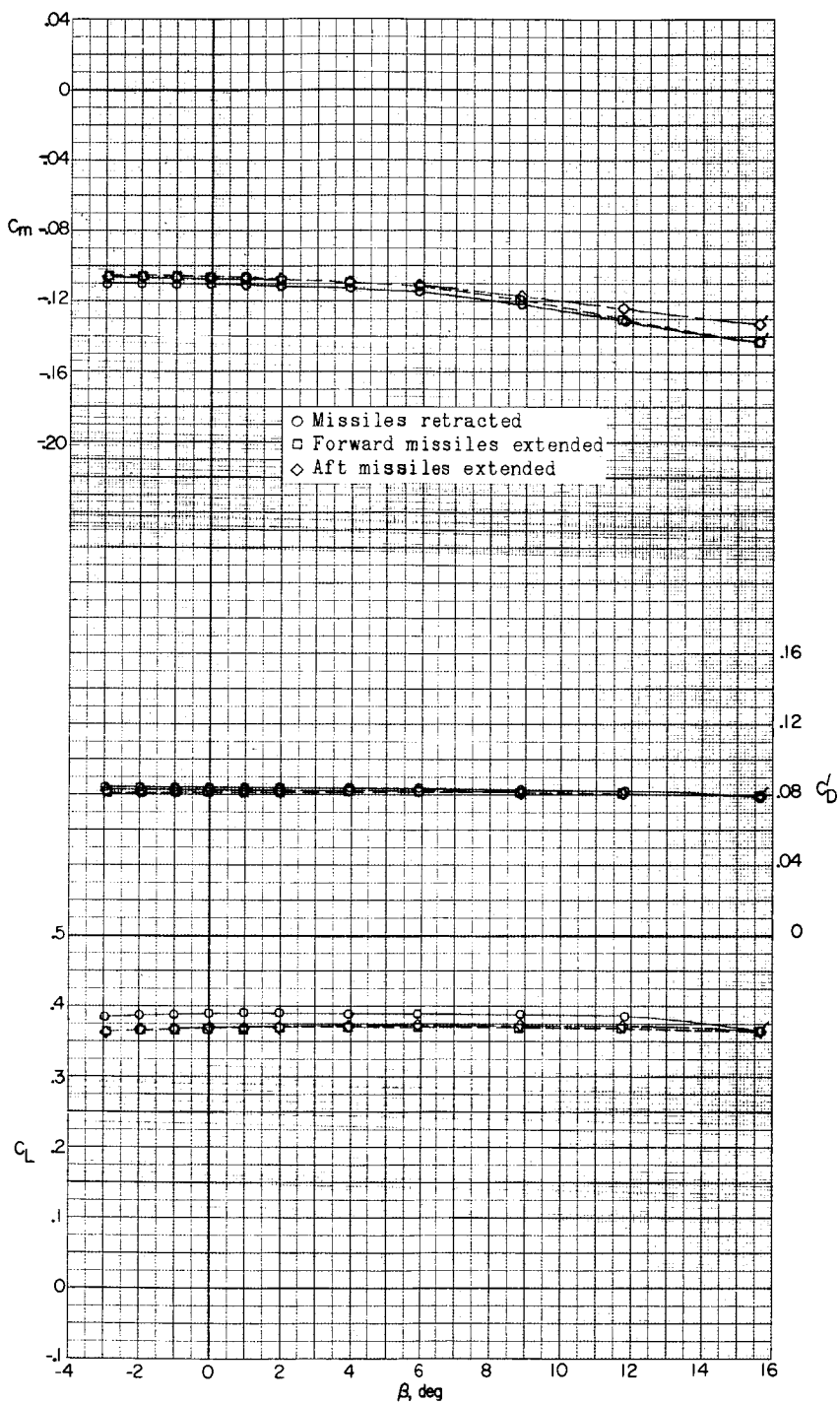
(b) $M = 1.57; \alpha = 6.7^\circ$.

Figure 18.- Continued.



(b) Concluded.

Figure 18.- Continued.

100

031712201530

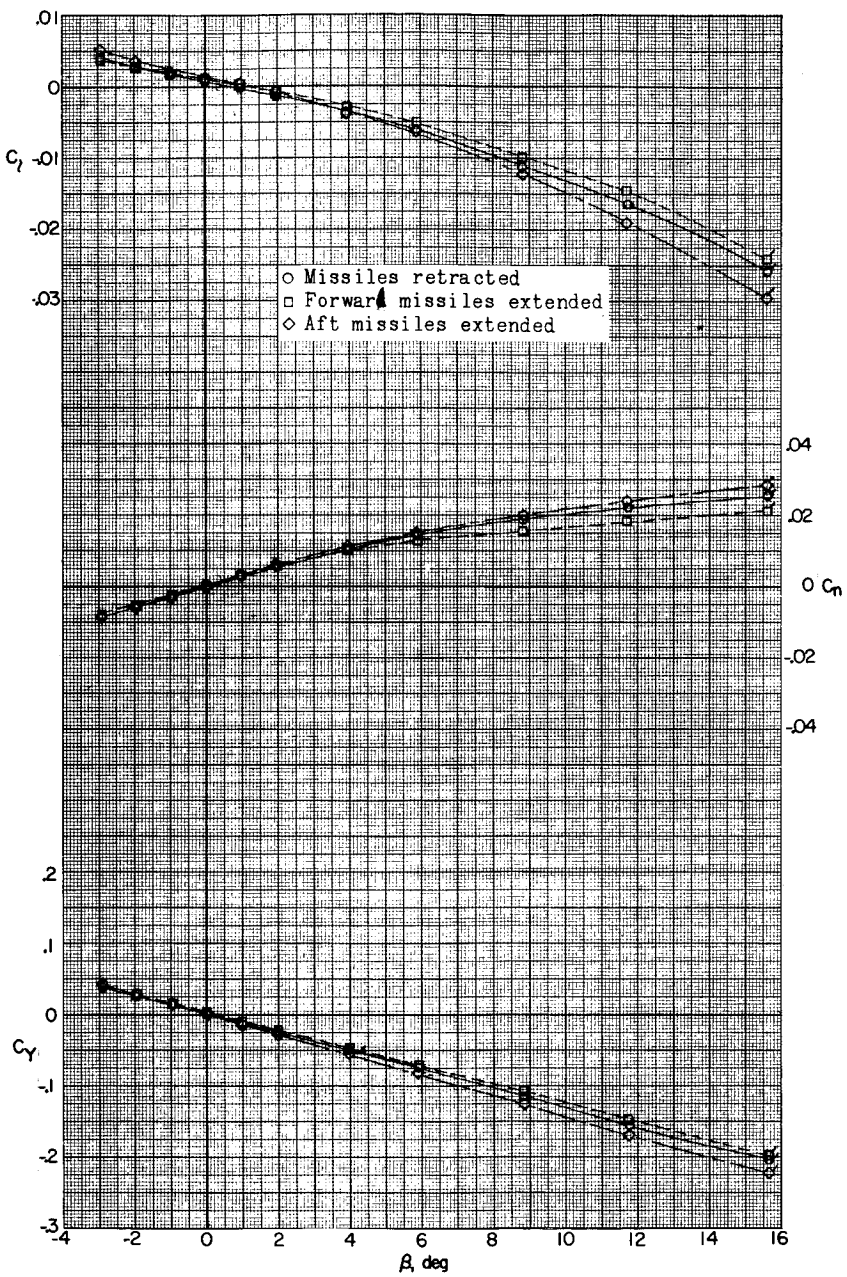
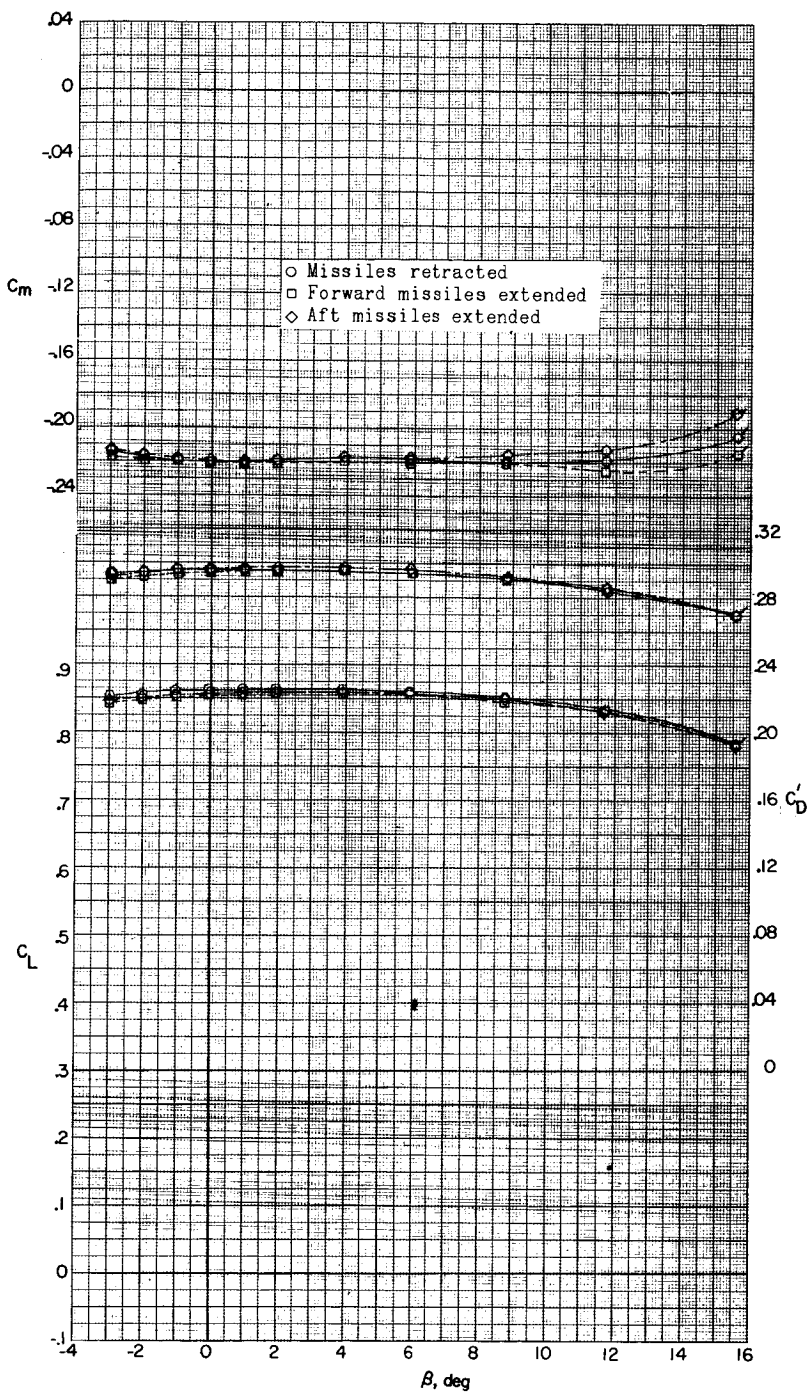
(c) $M = 1.57; \alpha = 17.4^\circ.$

Figure 18.- Continued.

L-524



(c) Concluded.

Figure 18.- Continued.

031712201530

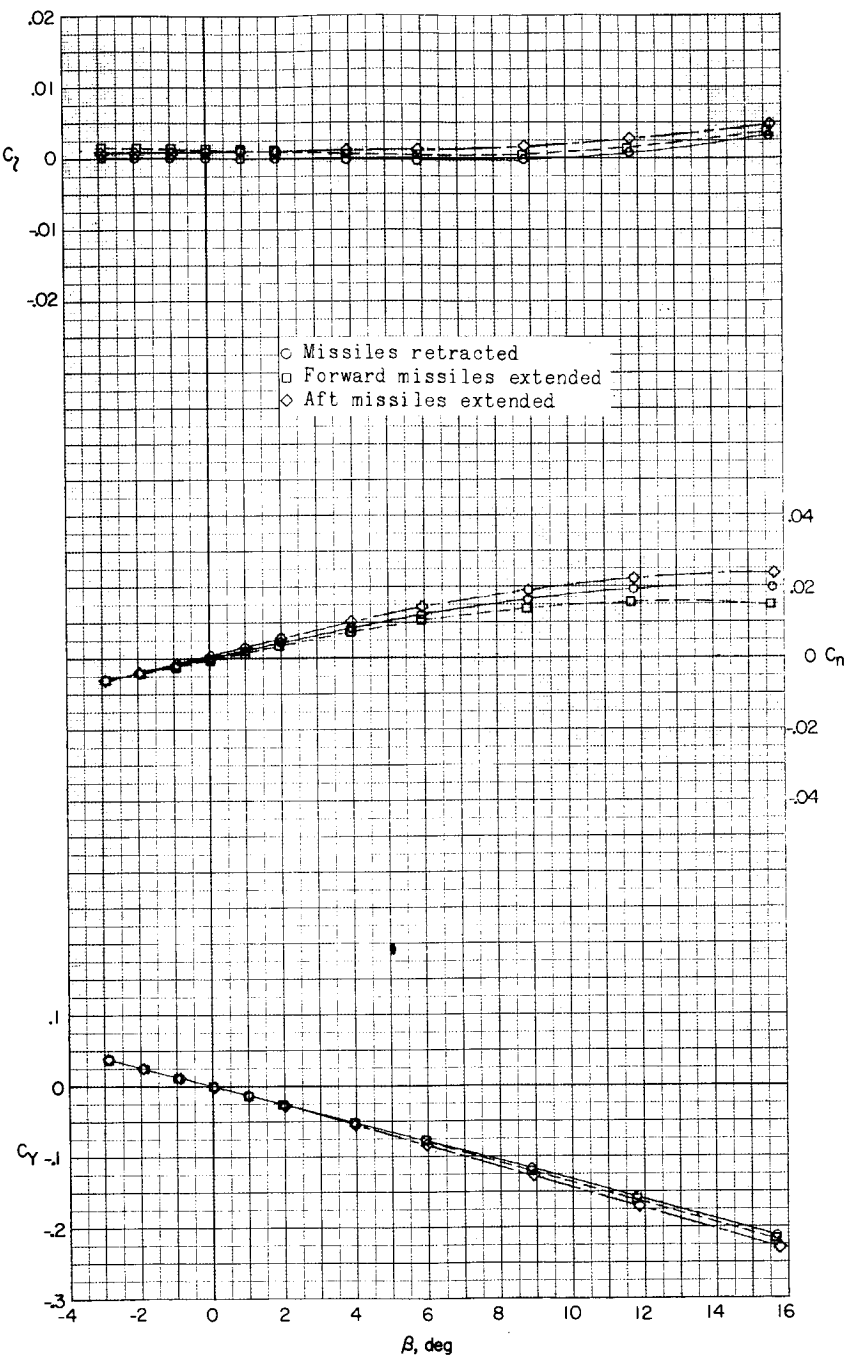
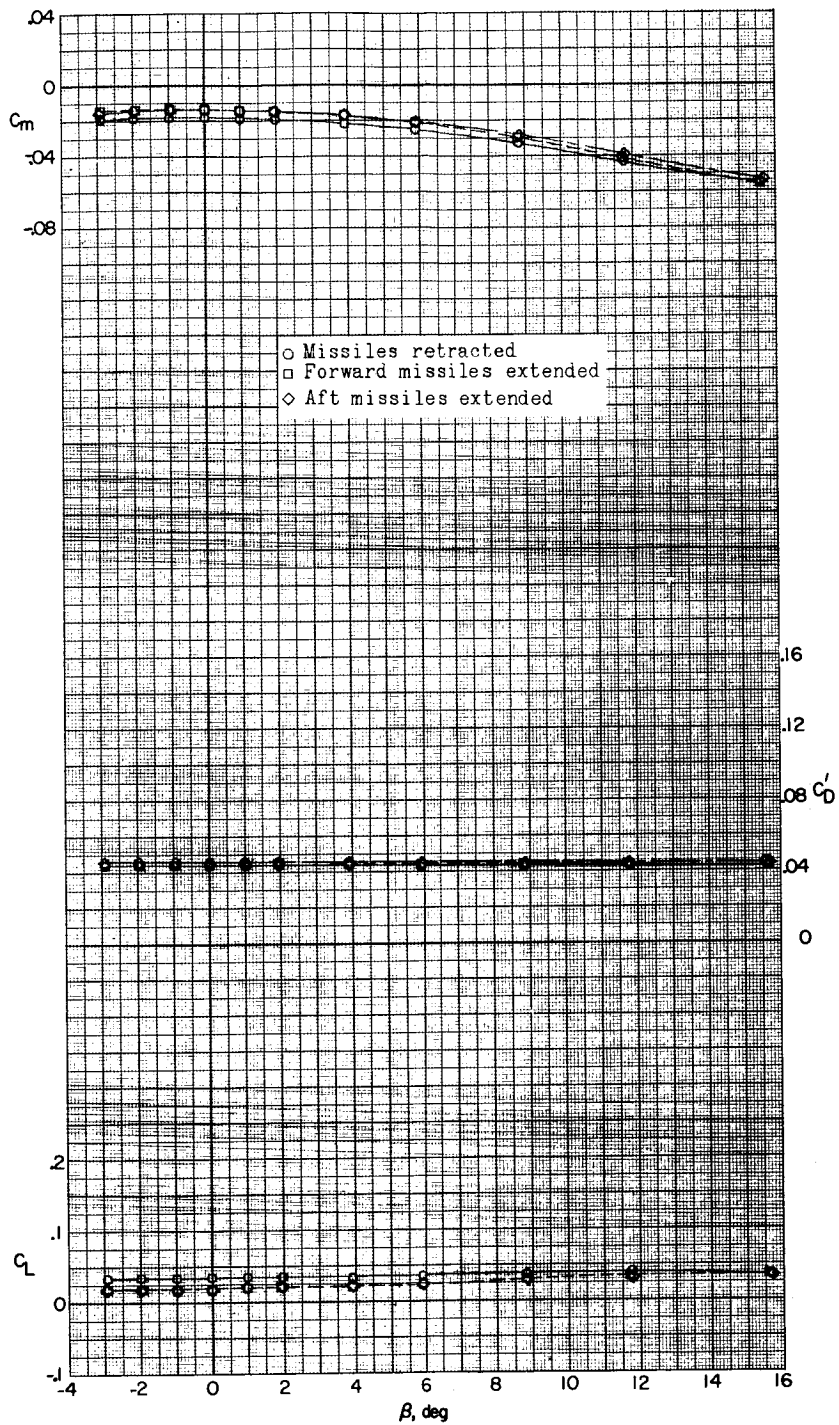
(d) $M = 1.87$; $\alpha = 0.4^\circ$.

Figure 18.- Continued.

SECRET//~~REF ID: A6512~~ 103



(d) Concluded.

Figure 18.- Continued.

03171020A 1930

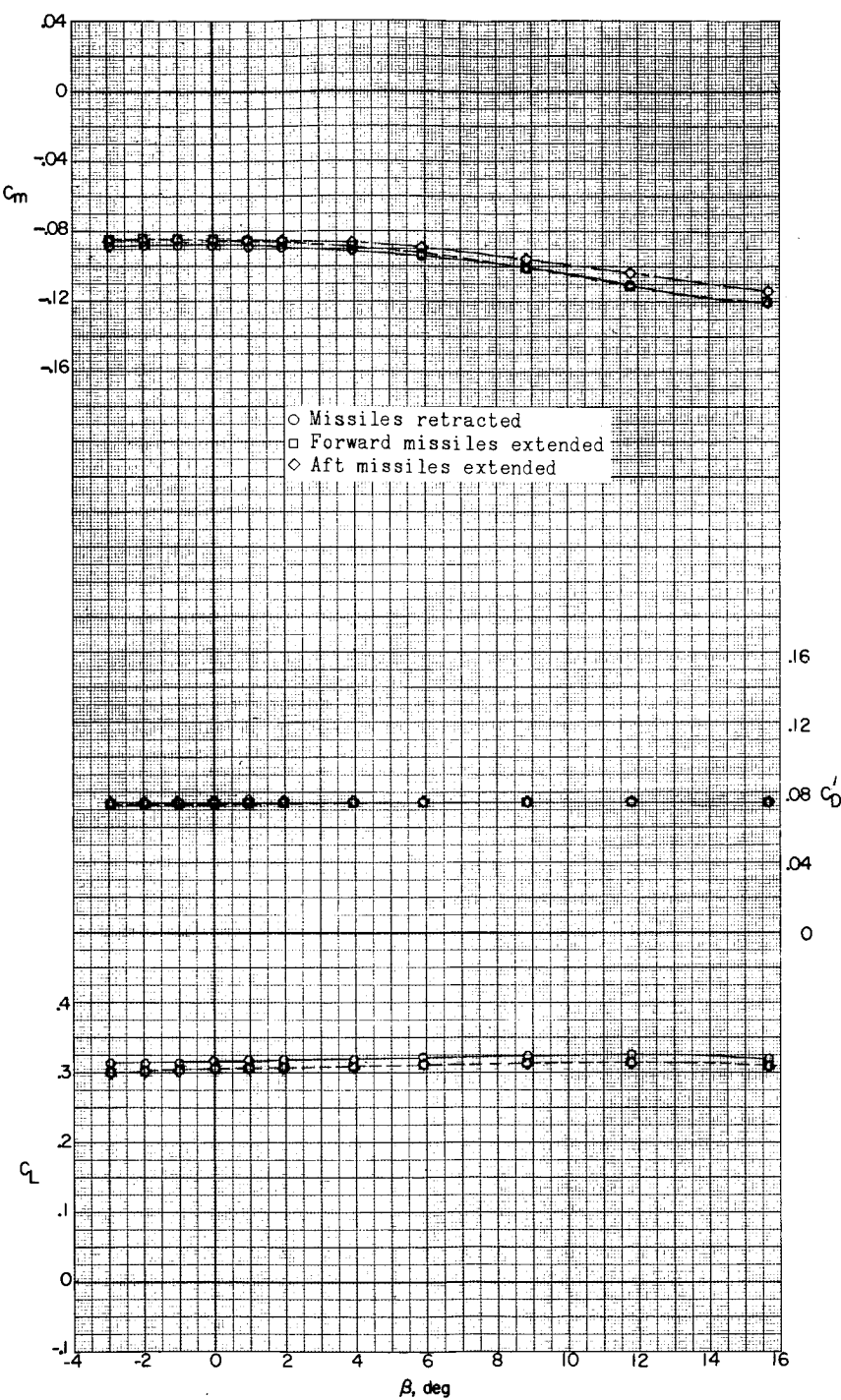
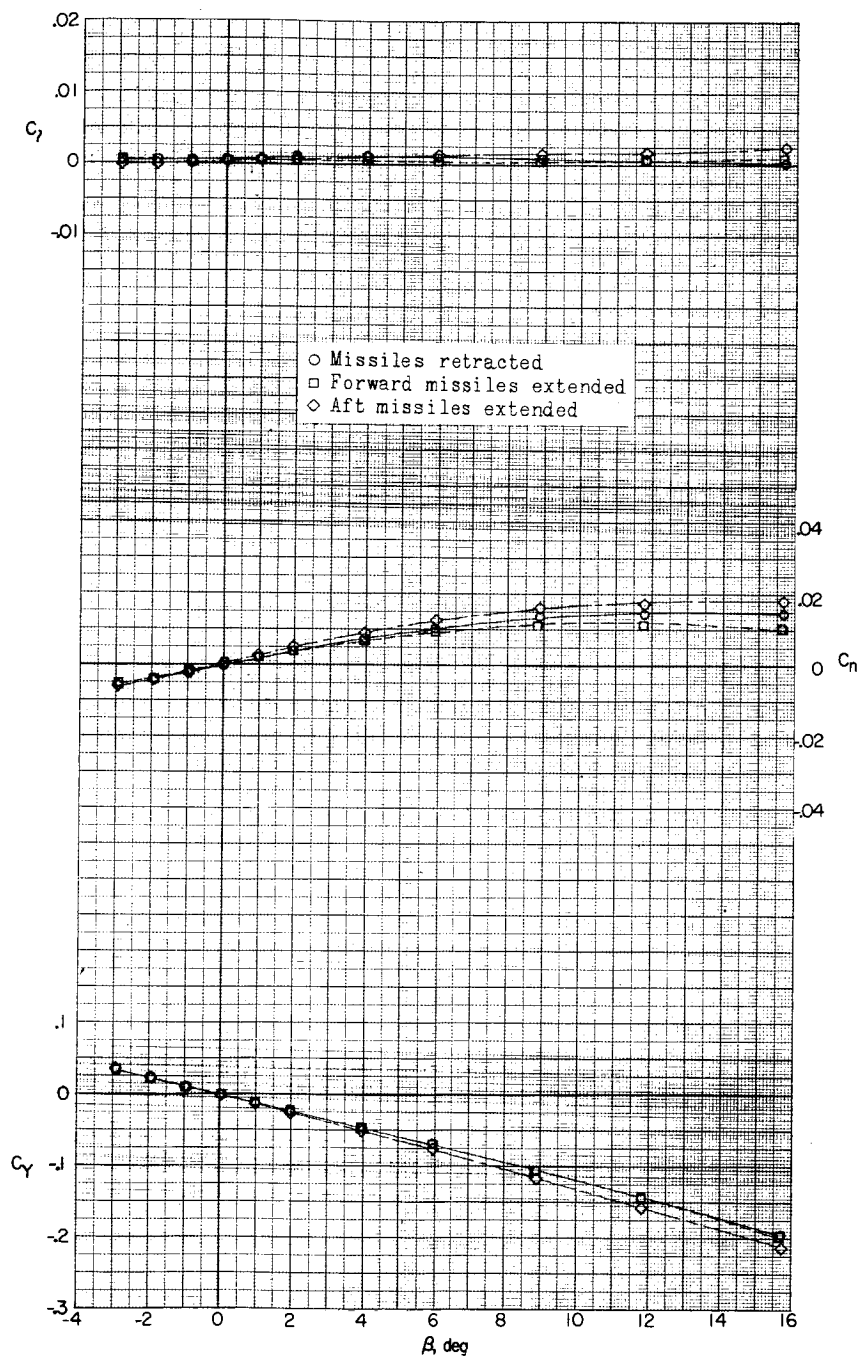
 10^4 (e) $M = 1.87$; $\alpha = 6.6^\circ$.

Figure 18.- Continued.



(e) Concluded.

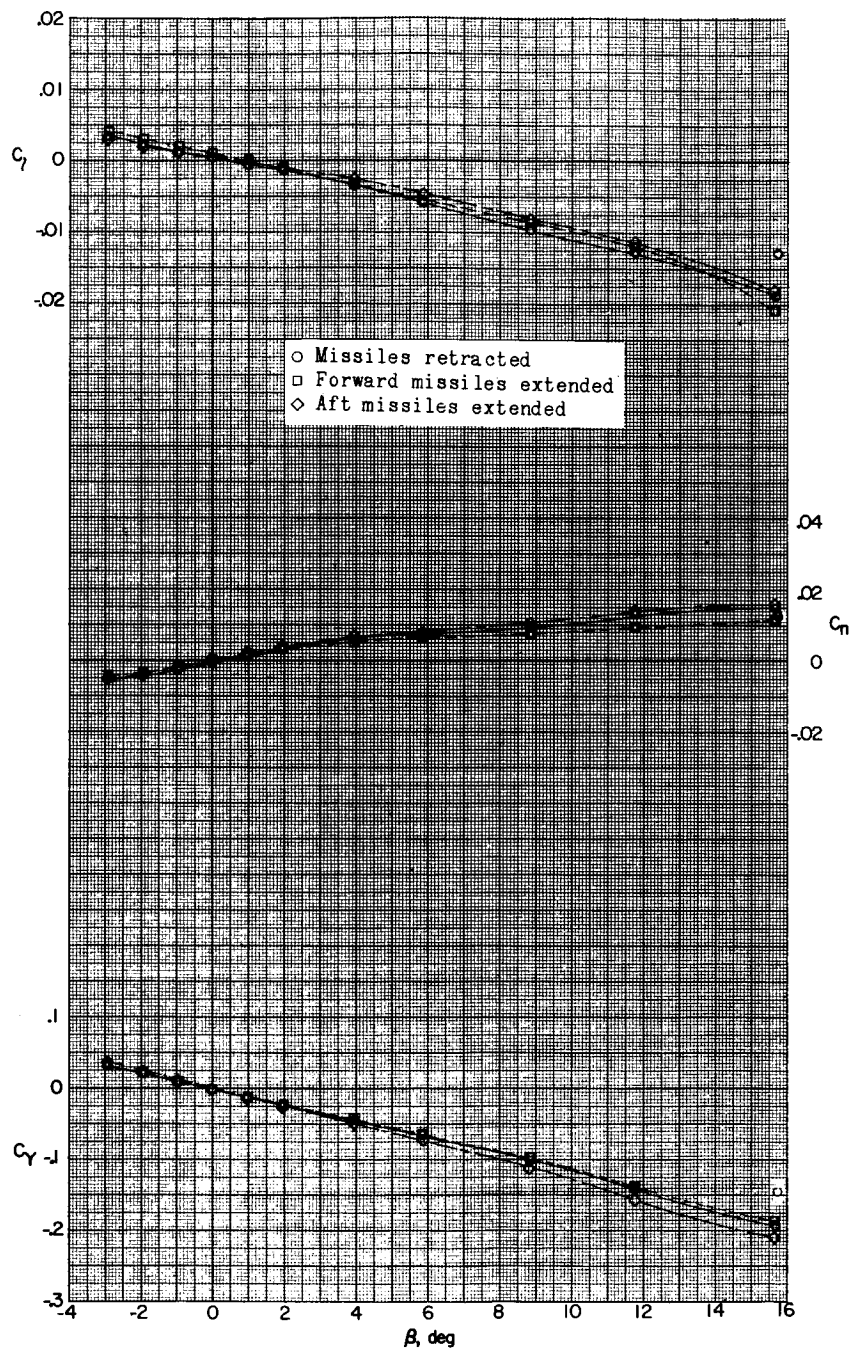
Figure 18.- Continued.

031702A.J030

106



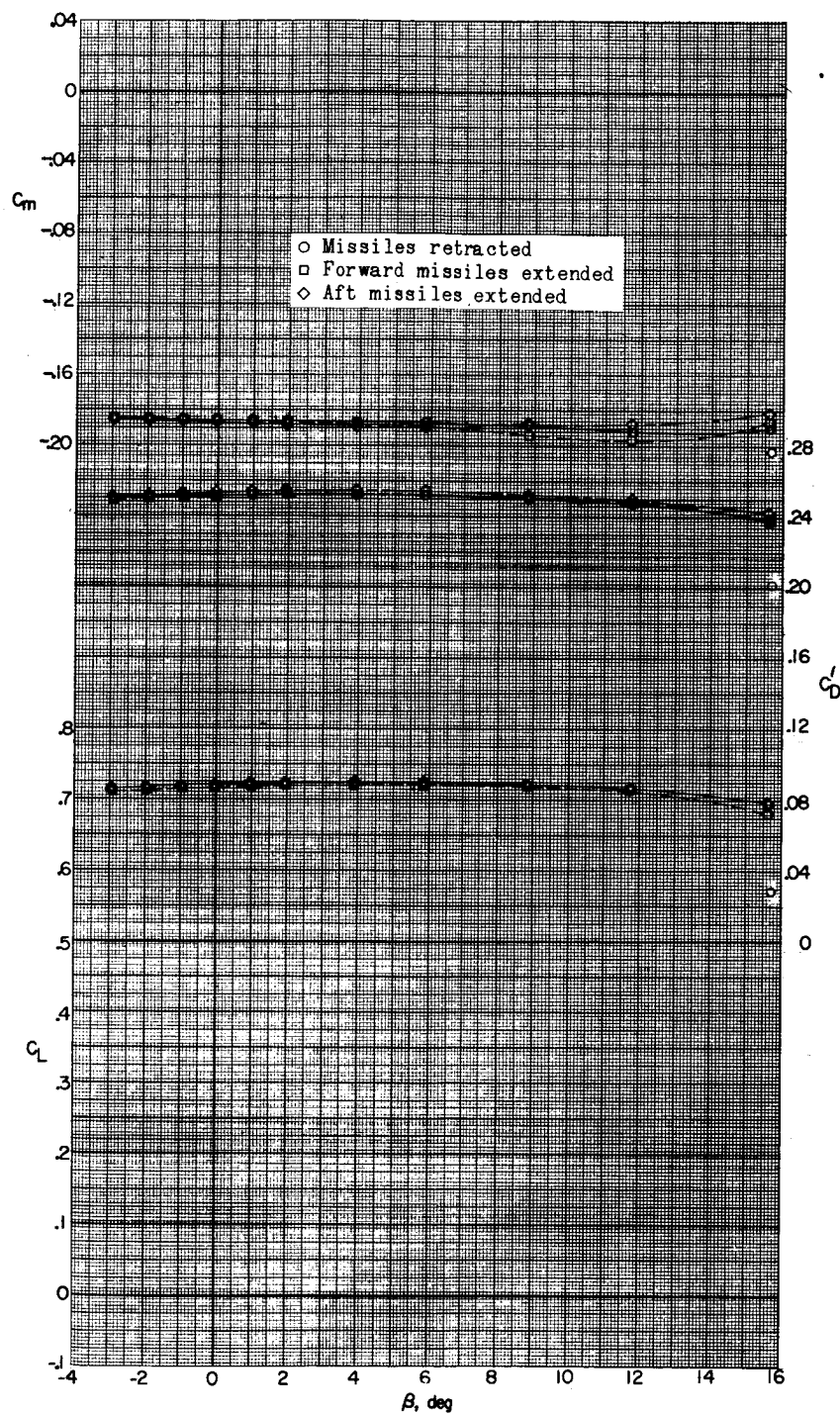
I-524



(f) $M = 1.87$; $\alpha = 17.1^\circ$.

Figure 18.- Continued.

DECLASSIFIED



(f) Concluded.

Figure 18.- Continued.

031710201030

8

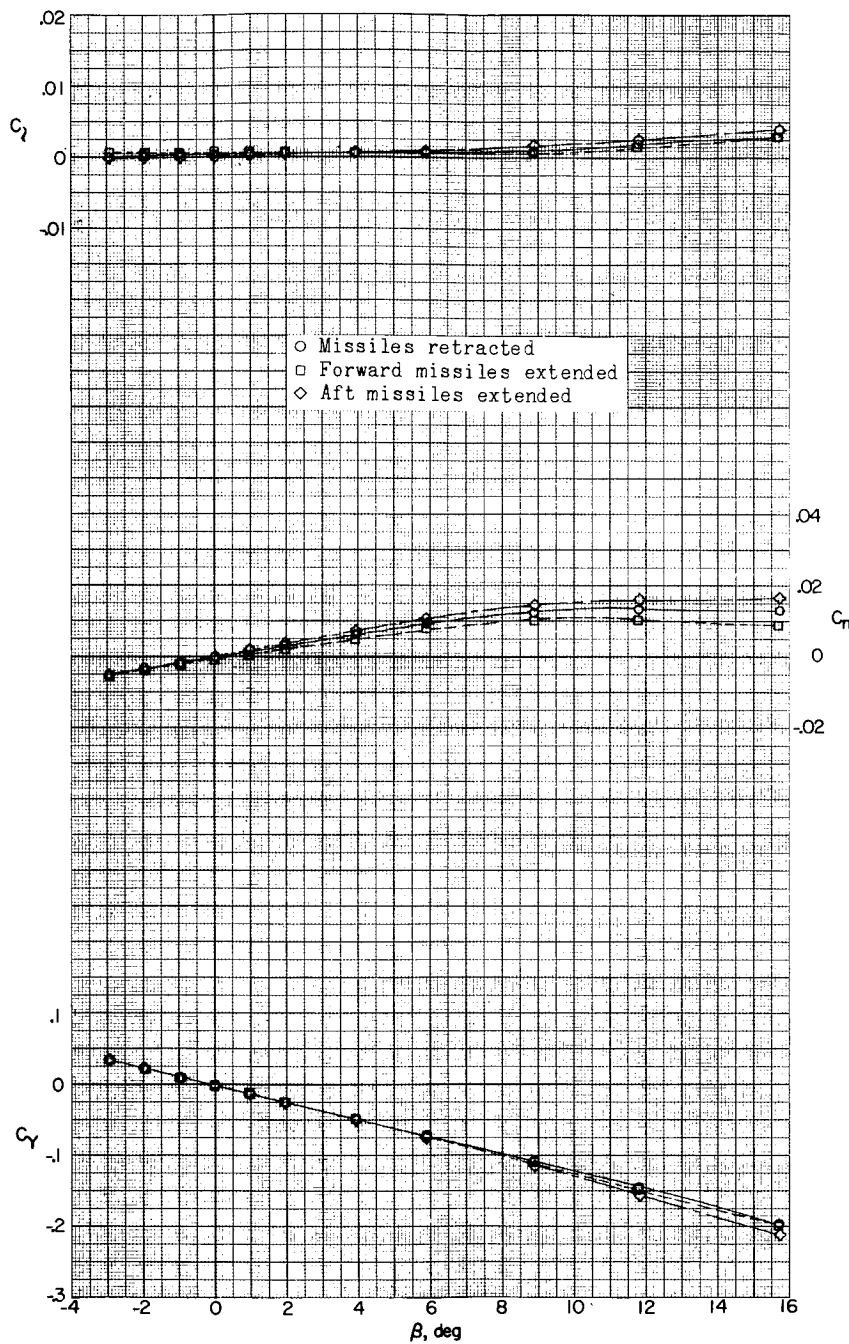
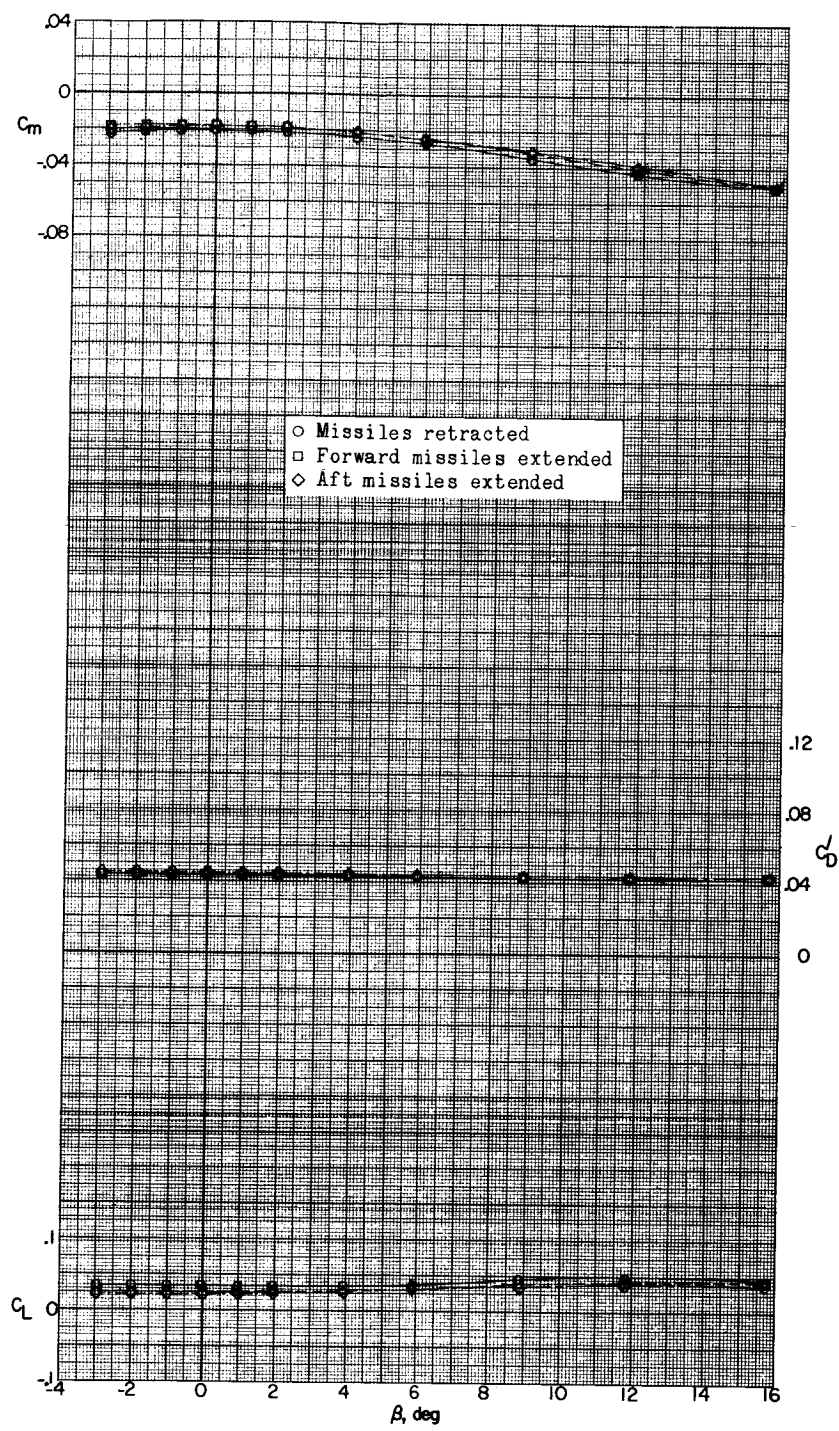
(g) $M = 2.16; \alpha = 0.4^\circ$.

Figure 18.- Continued.



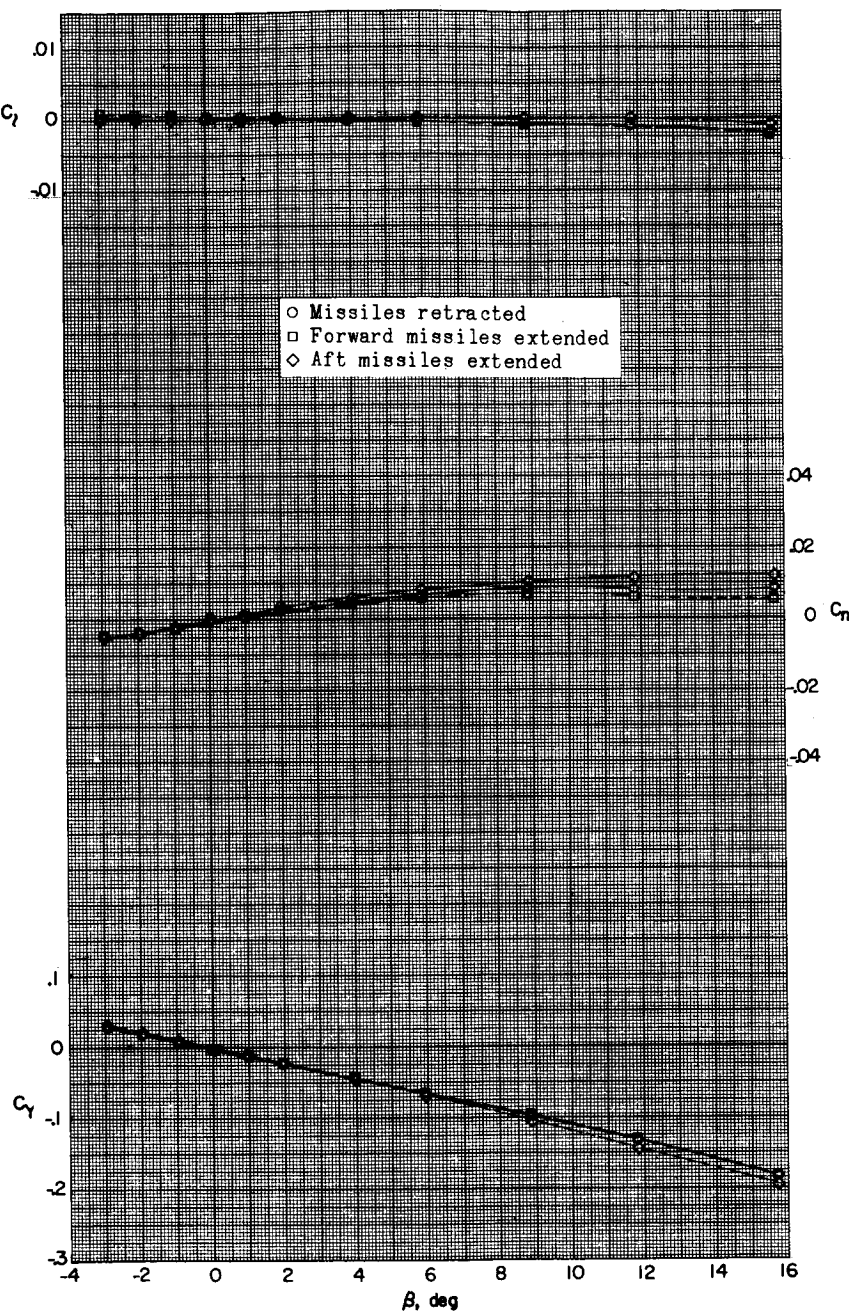
(g) Concluded.

Figure 18.- Continued.

110 03/7/82 0 1030

8

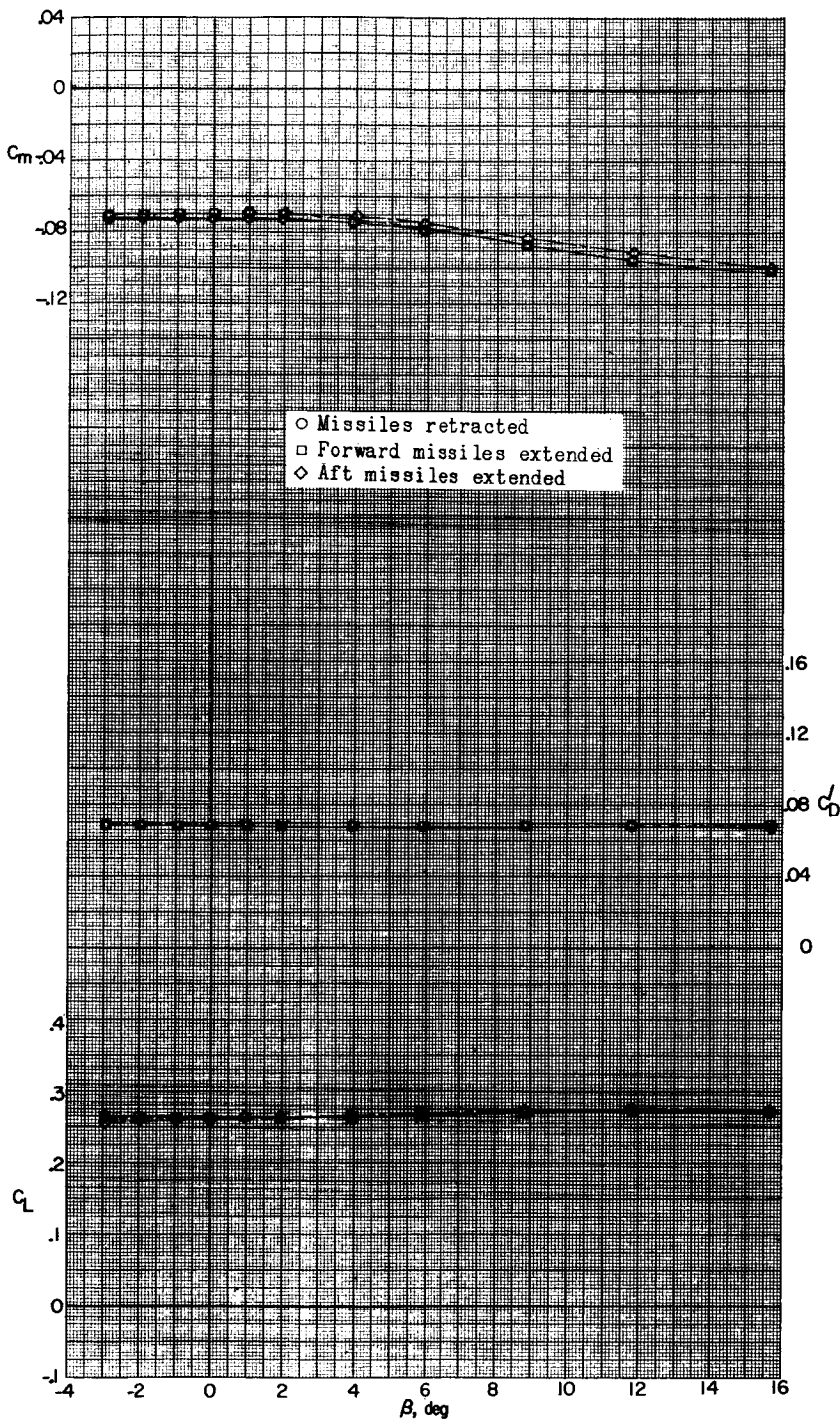
L-524



(h) $M = 2.16; \alpha = 6.5^\circ$.

Figure 18.- Continued.

SECRET//
CLASSIFIED: 111



(h) Concluded.

Figure 18.- Continued.

031710220 [REDACTED]

B

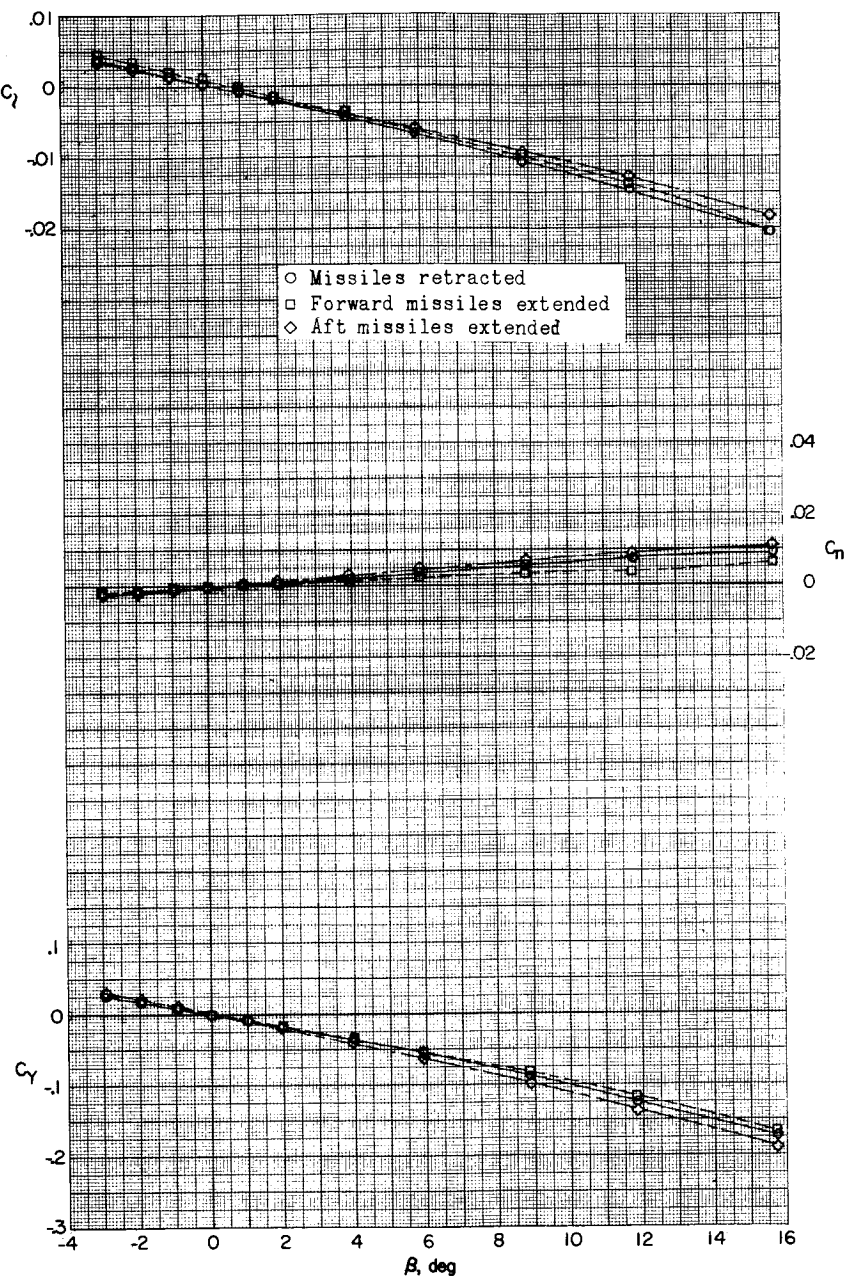
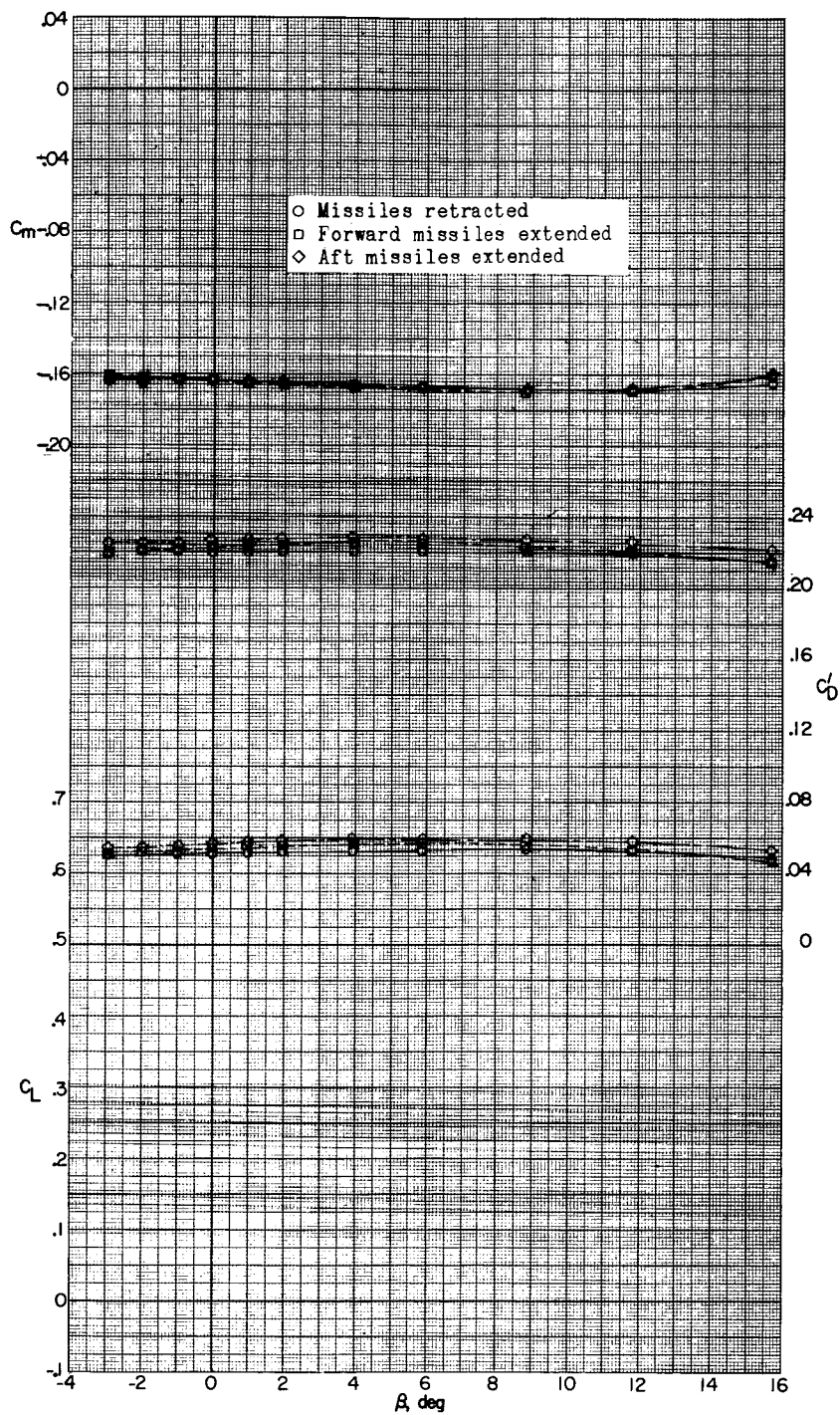
(i) $M = 2.16$; $\alpha = 16.9^\circ$.

Figure 18.- Continued.

REF ID: A65724
RECLASSIFIED 113

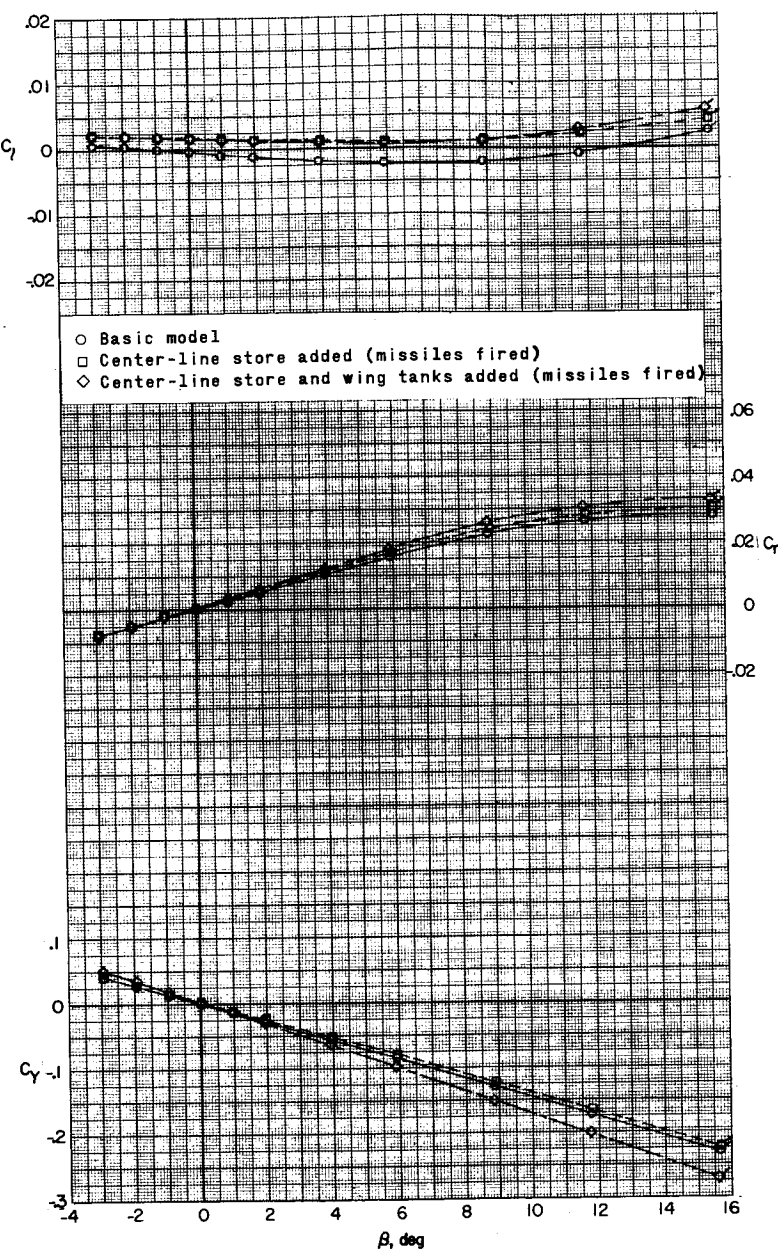


(i) Concluded.

Figure 18.- Concluded.

114 03171236110833

I-524

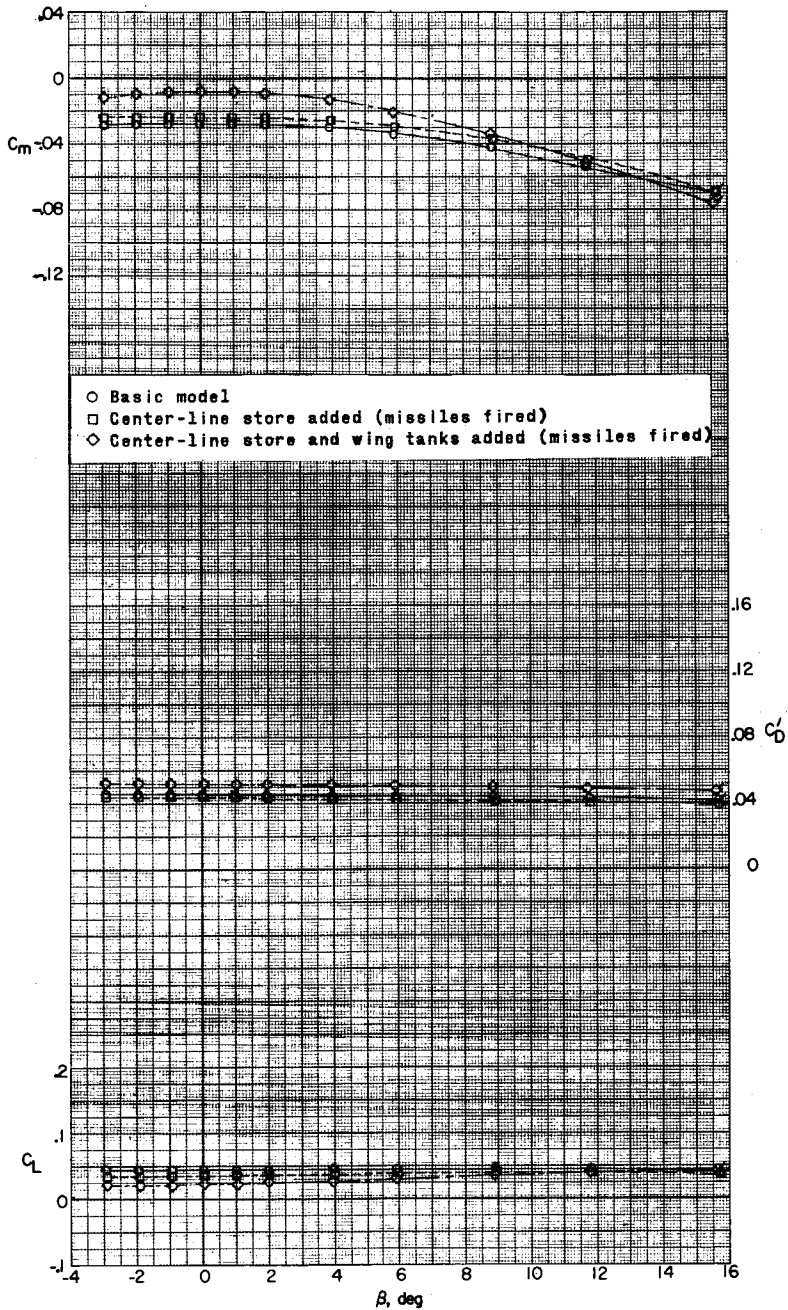


(a) $M = 1.57; \alpha = 0.4^\circ$.

Figure 19.- Effect of external stores on aerodynamic characteristics in sideslip. (Flagged symbols denote wall-reflected shock waves striking the tail.)

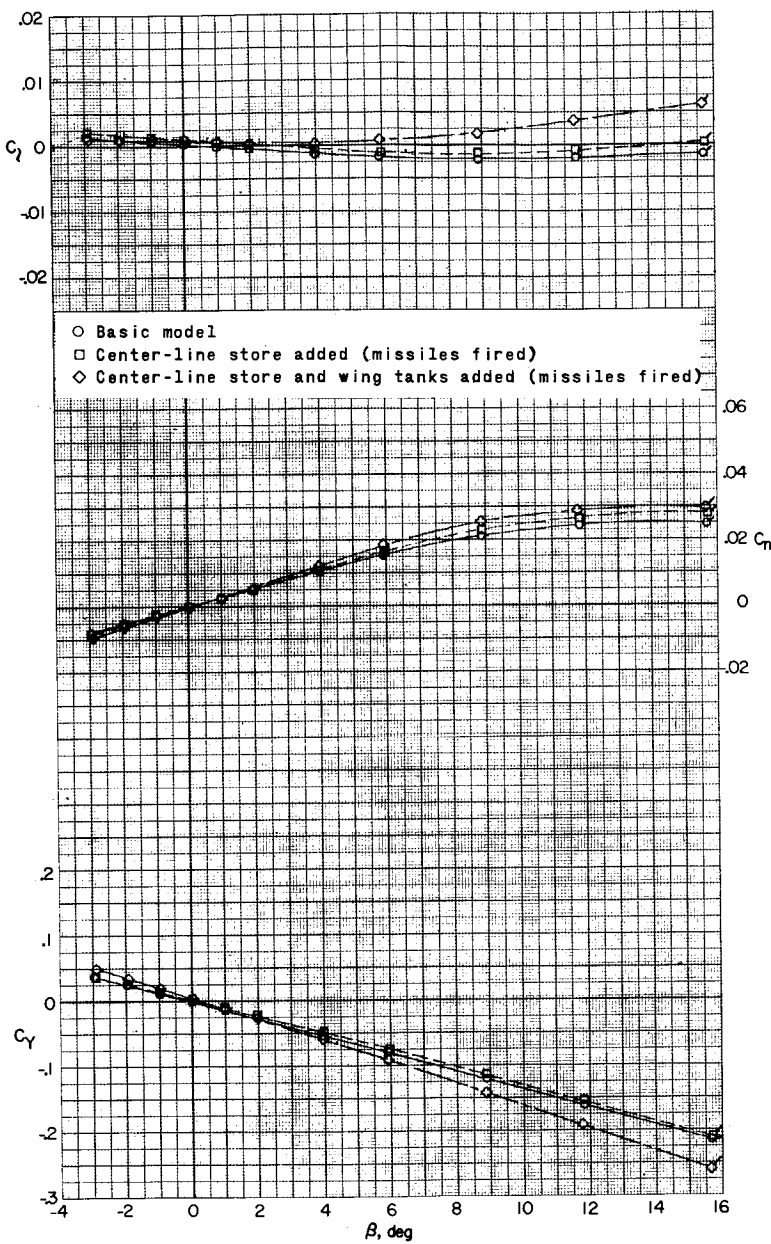
REF ID: A3115
CLASSIFIED

I-524



(a) Concluded.

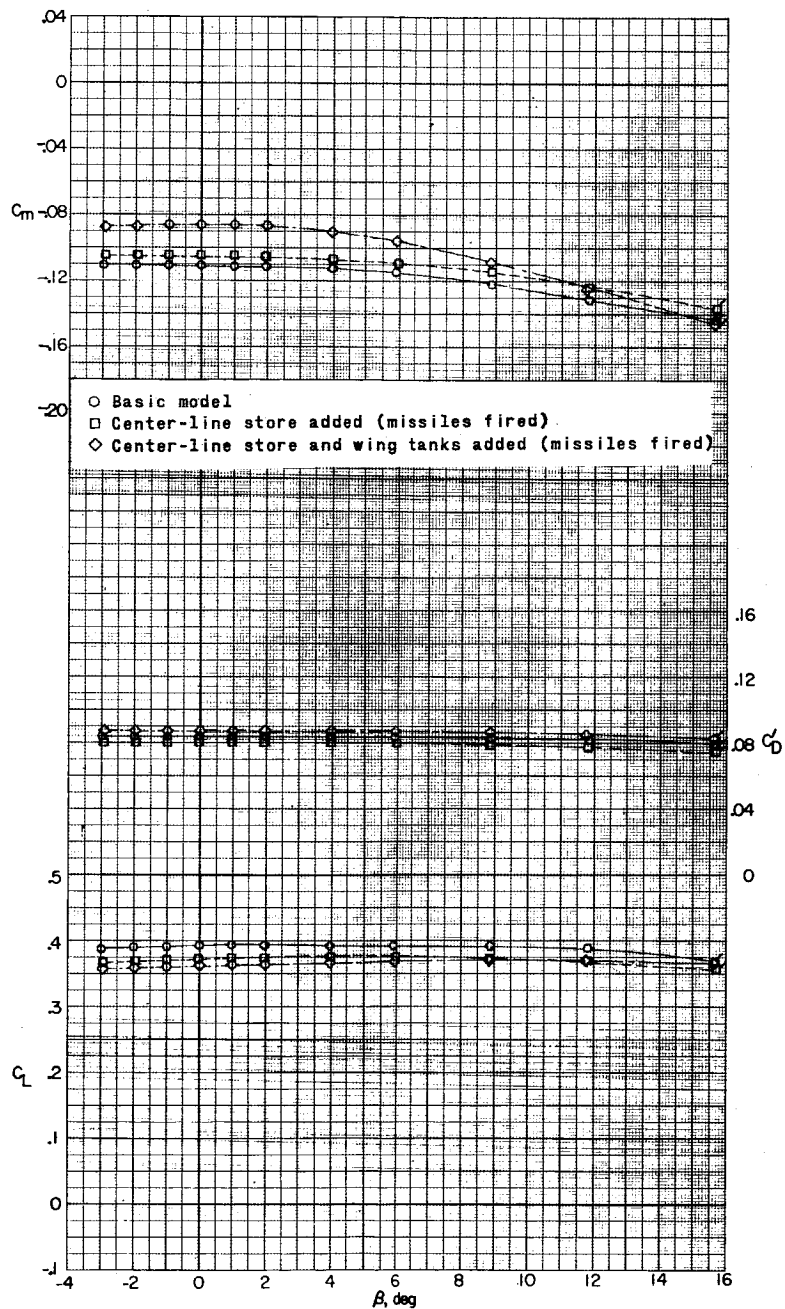
Figure 19.- Continued.



(b) $M = 1.57; \alpha = 6.7^\circ$.

Figure 19.- Continued.

CLASSIFIED 117



(b) Concluded.

Figure 19.- Continued.

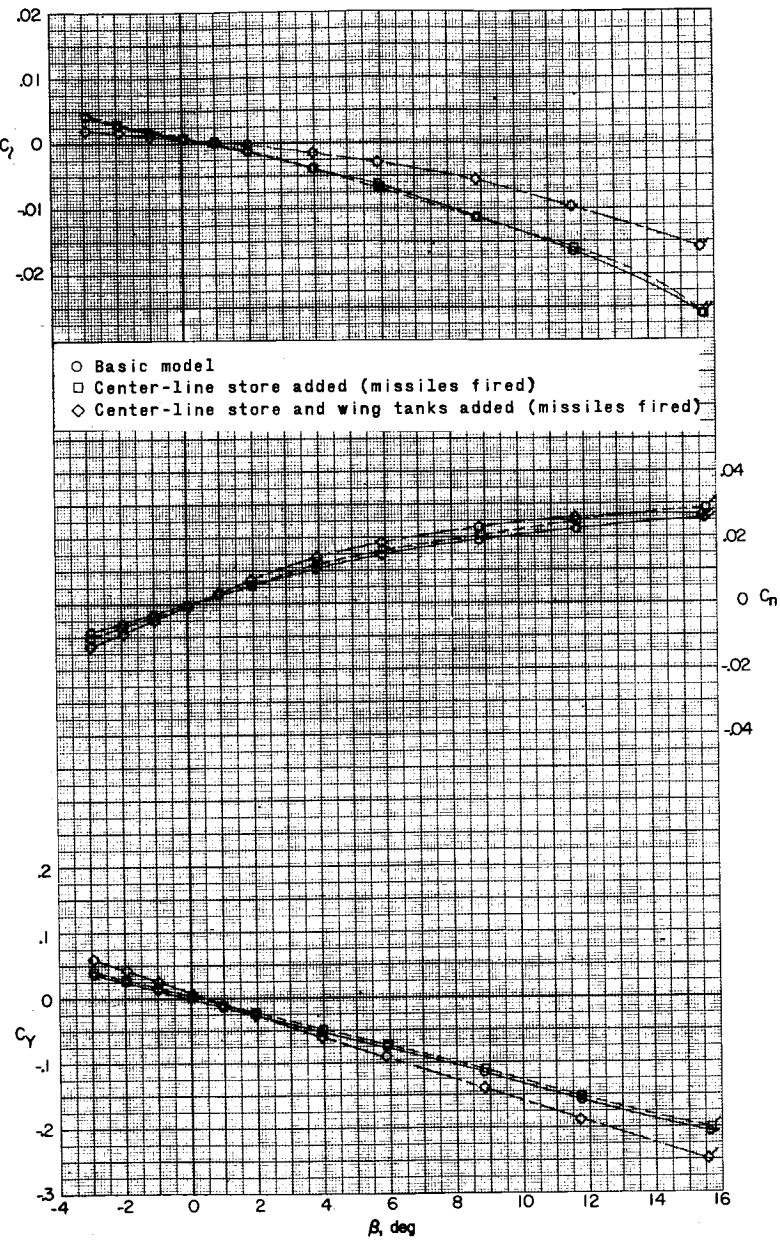
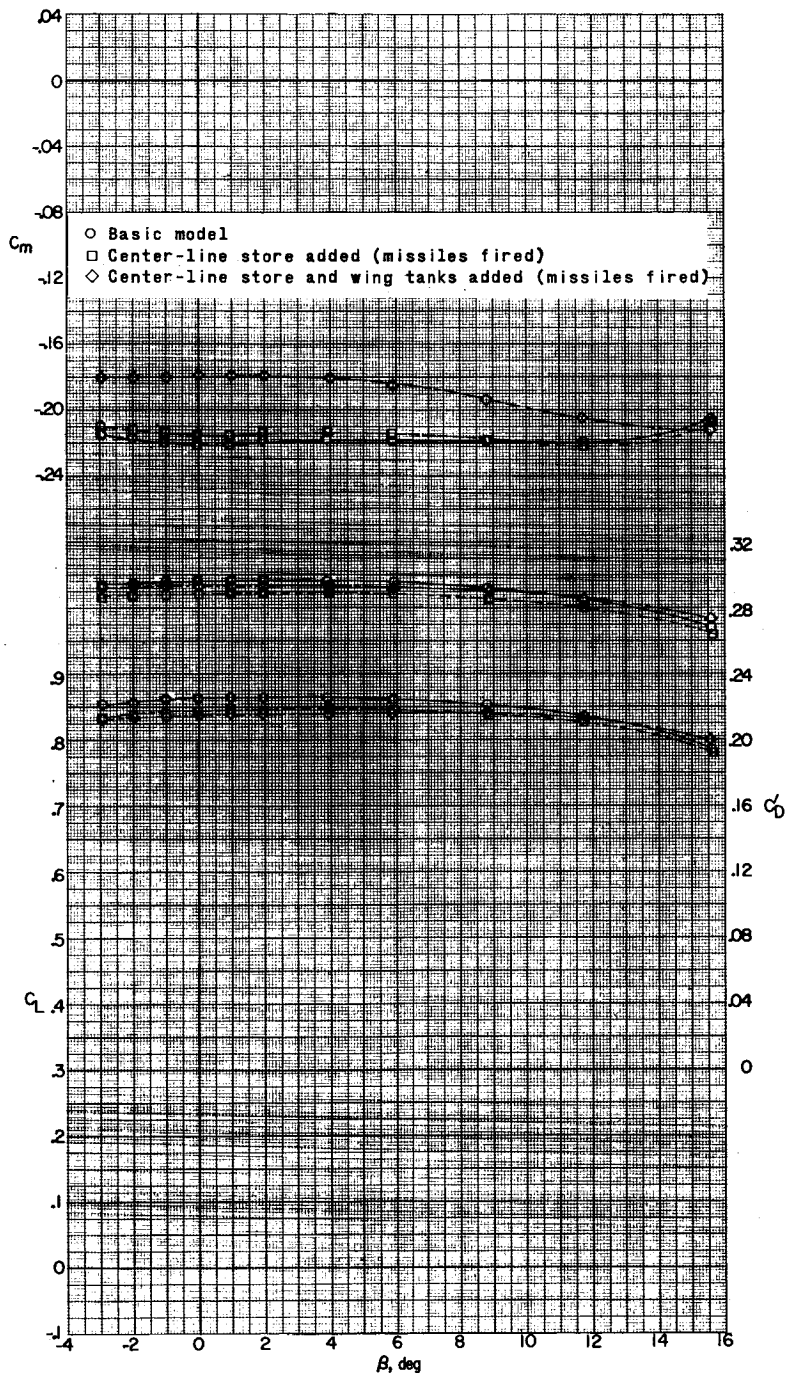
(c) $M = 1.57; \alpha = 17.4^\circ$.

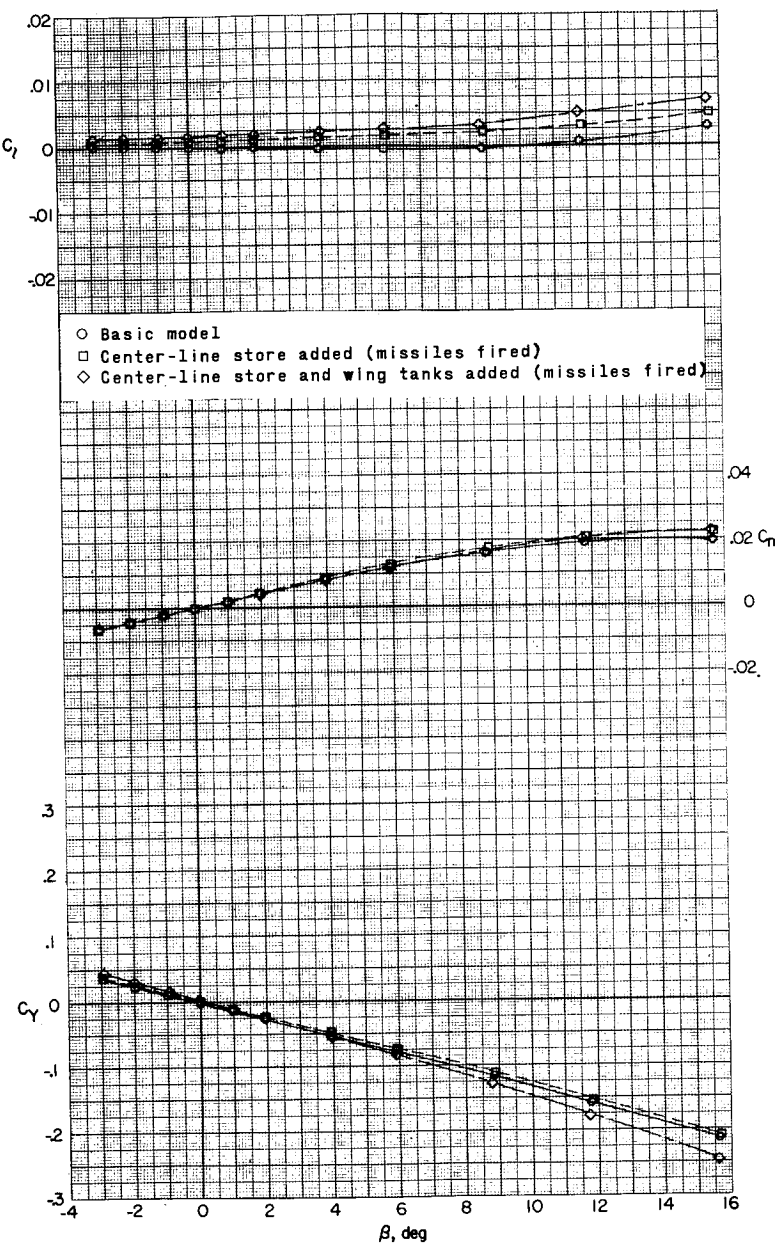
Figure 19.- Continued.

DECLASSIFIED



(c) Concluded.

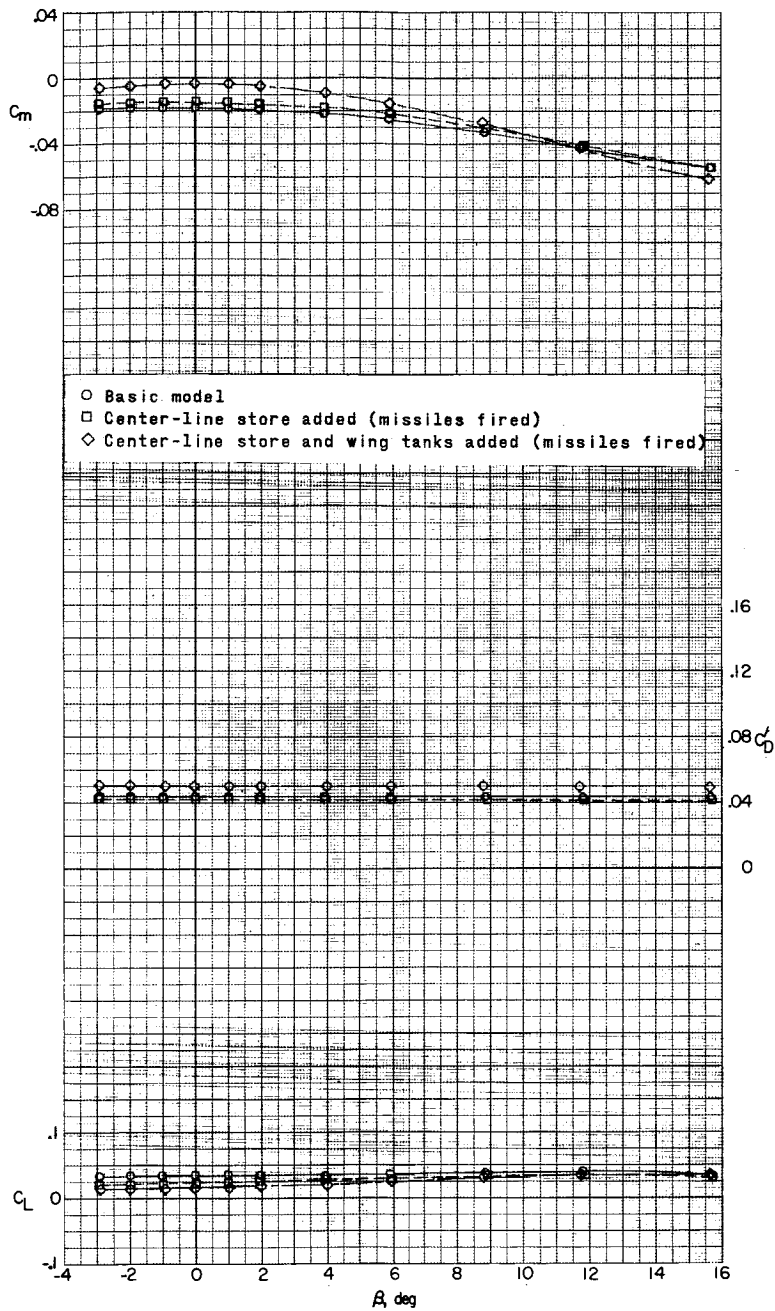
Figure 19.- Continued.



(d) $M = 1.87; \alpha = 0.4^\circ$.

Figure 19.- Continued.

THE CLASSIFIED

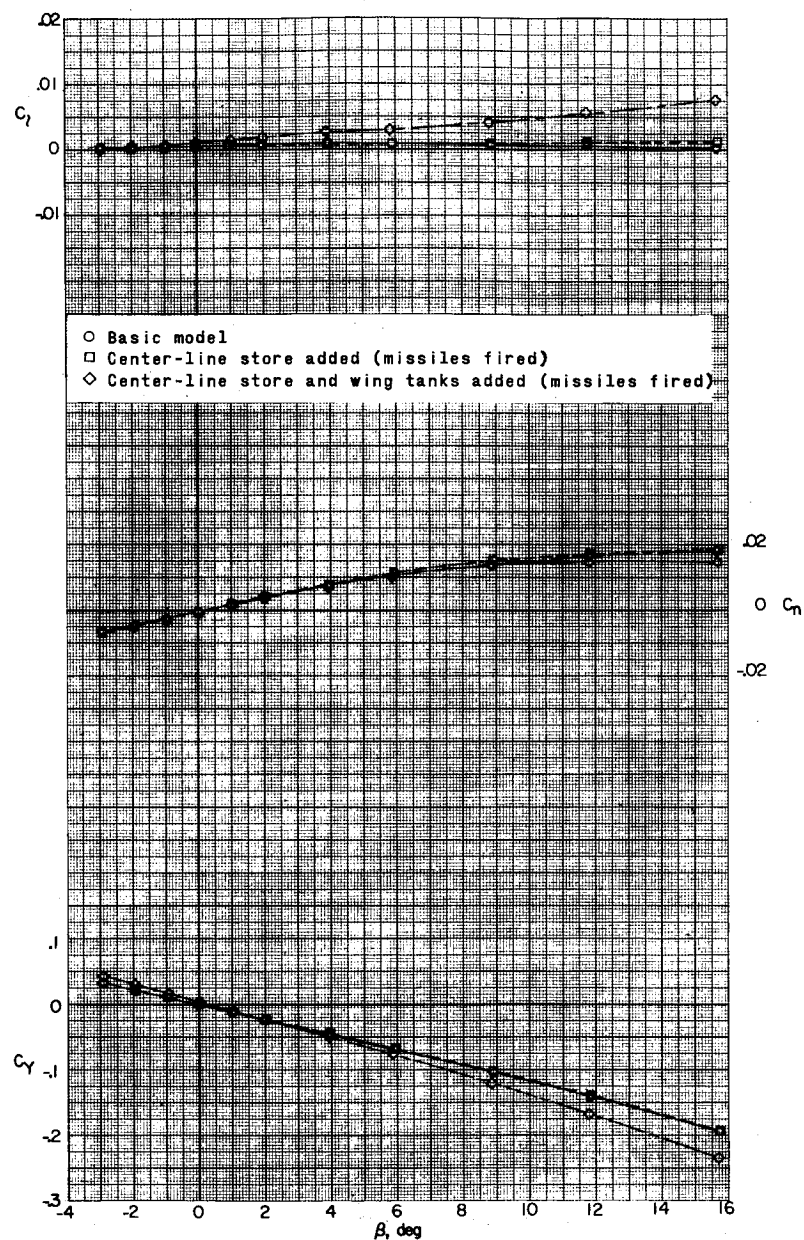


(d) Concluded.

Figure 19.- Continued.

122

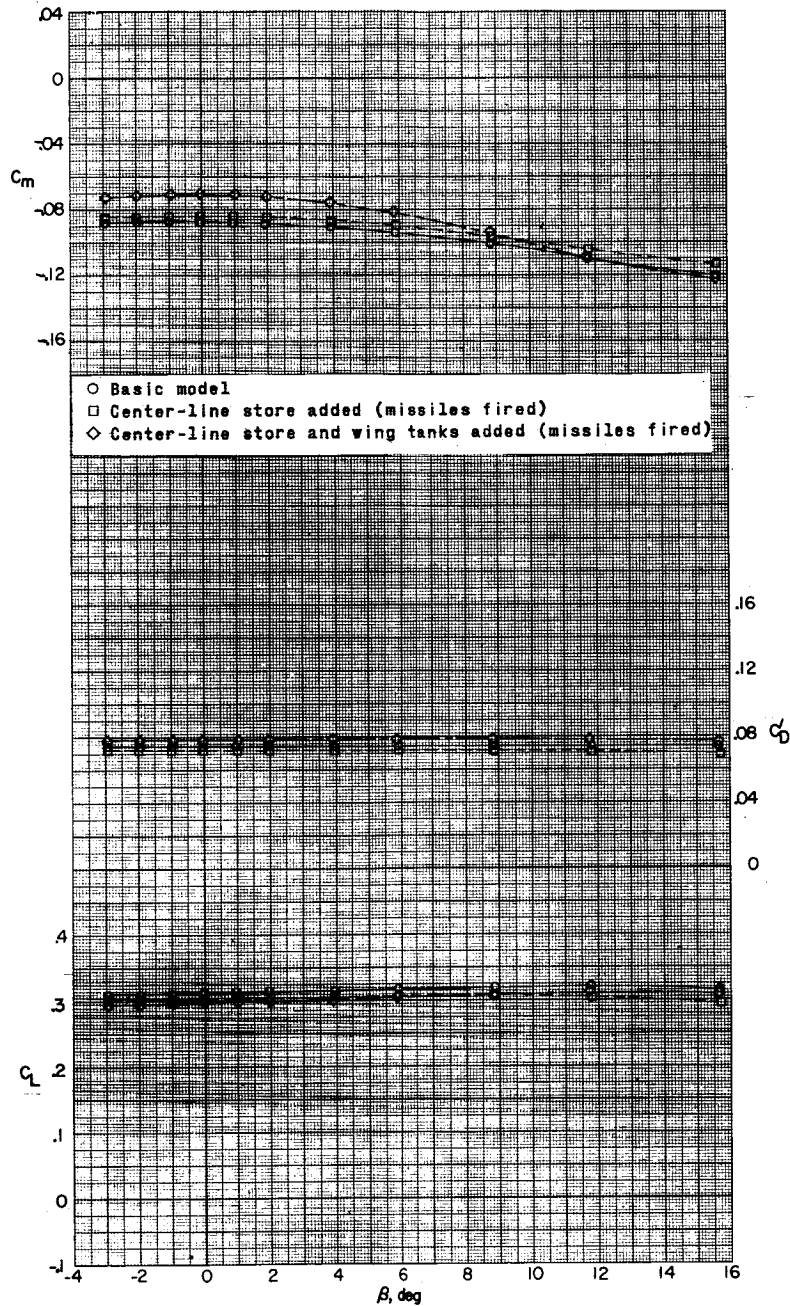
I-524



(e) $M = 1.87$; $\alpha = 6.6^\circ$.

Figure 19.- Continued.

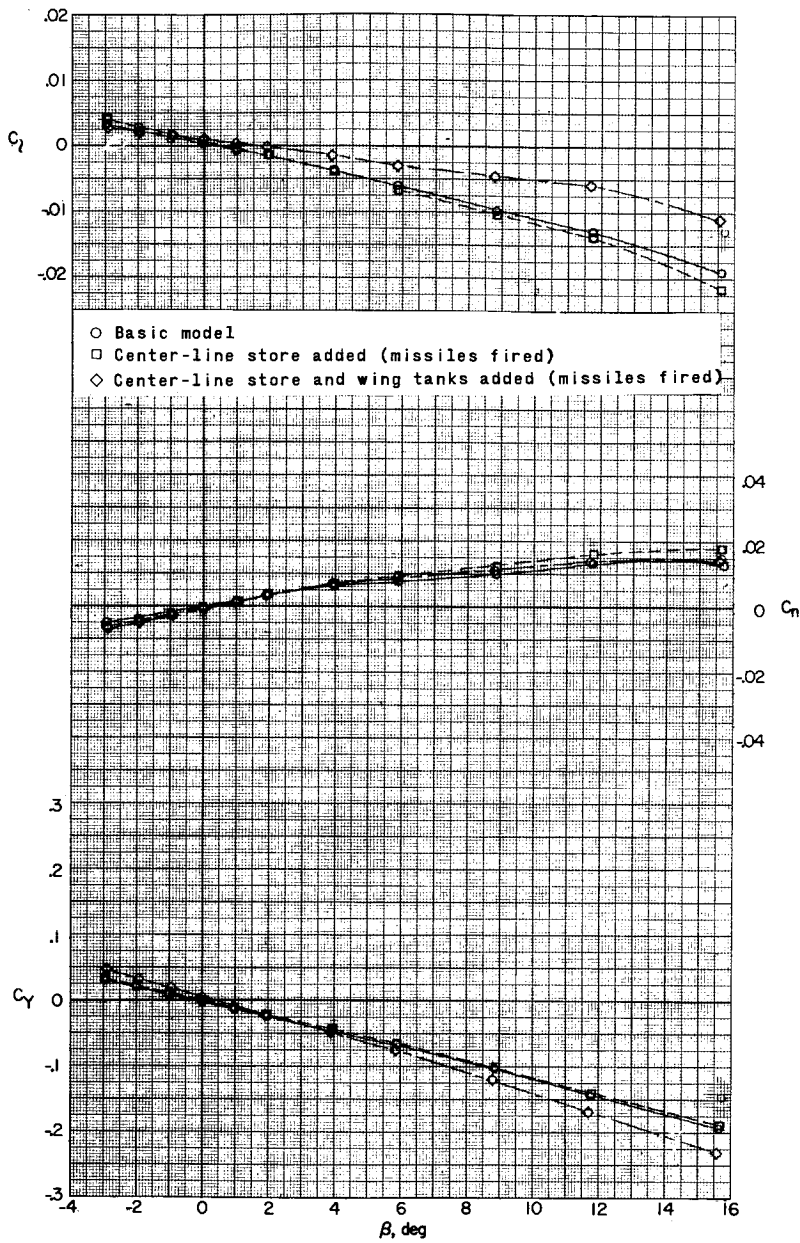
CLASSIFIED¹²³



(e) Concluded.

Figure 19.- Continued.

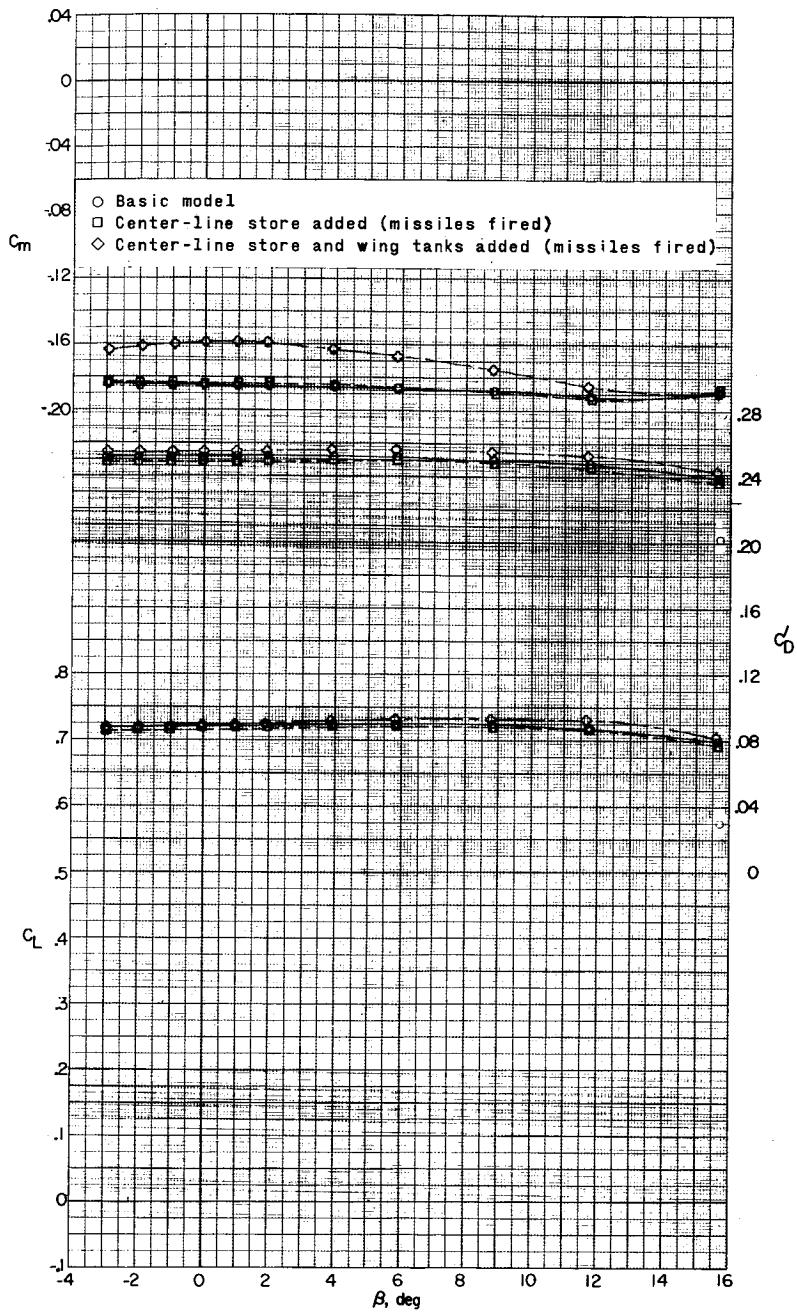
331712261630



(f) $M = 1.87$; $\alpha = 17.1^\circ$.

Figure 19.- Continued.

DECLASSIFIED

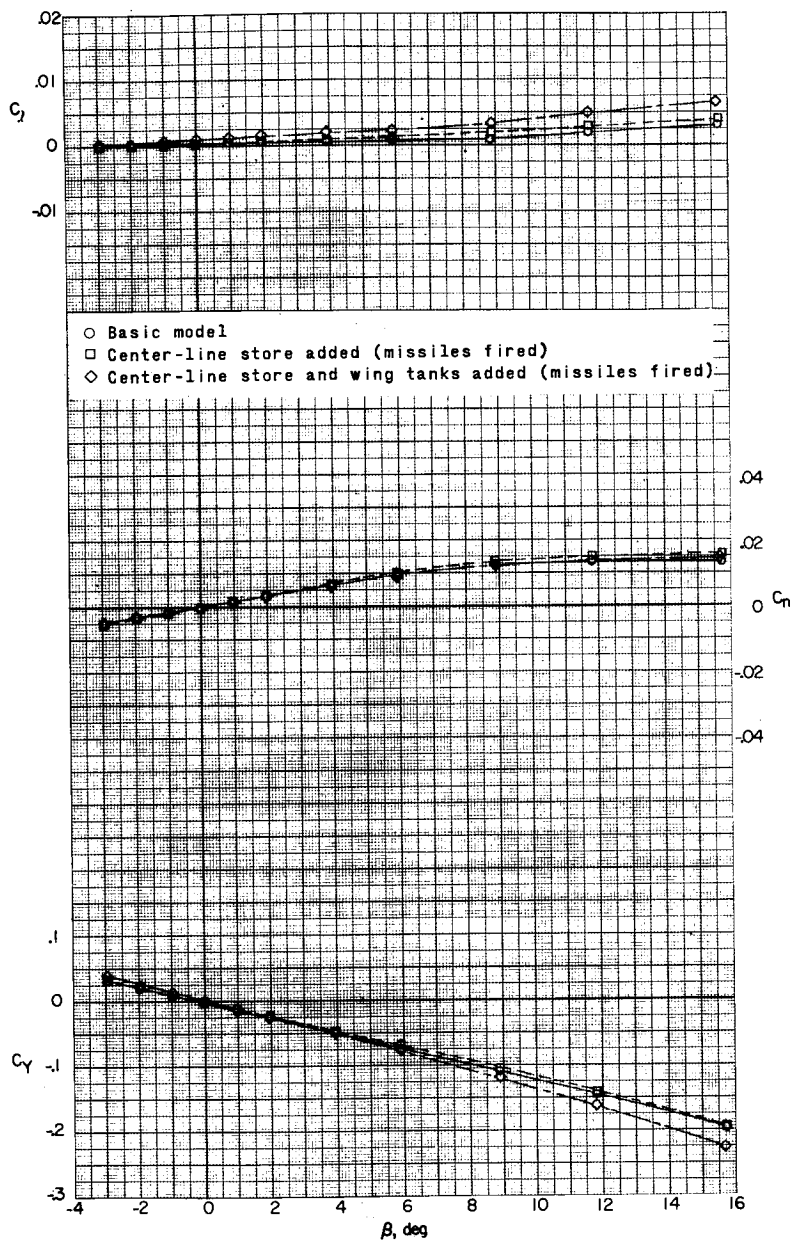


(f) Concluded.

Figure 19.- Continued.

031712241100

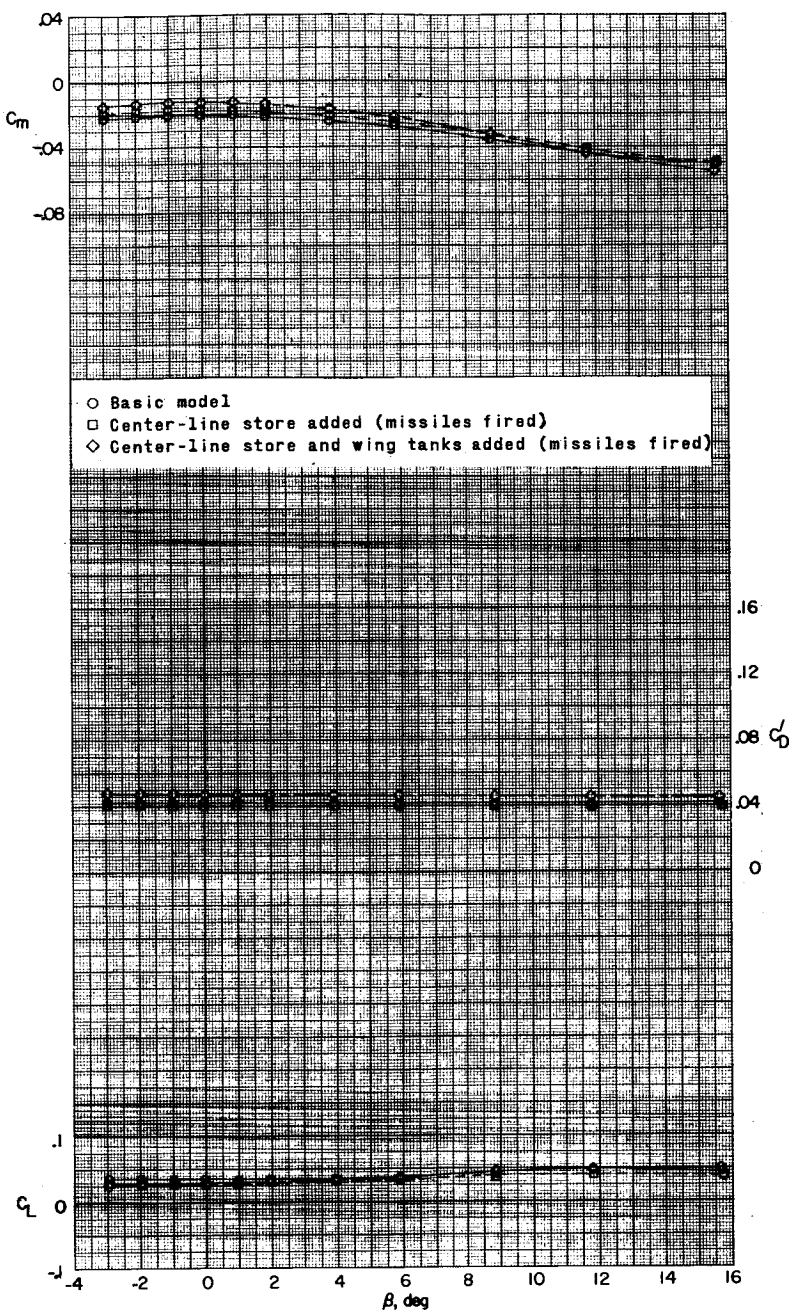
126



(g) $M = 2.16$; $\alpha = 0.4^\circ$.

Figure 19.- Continued.

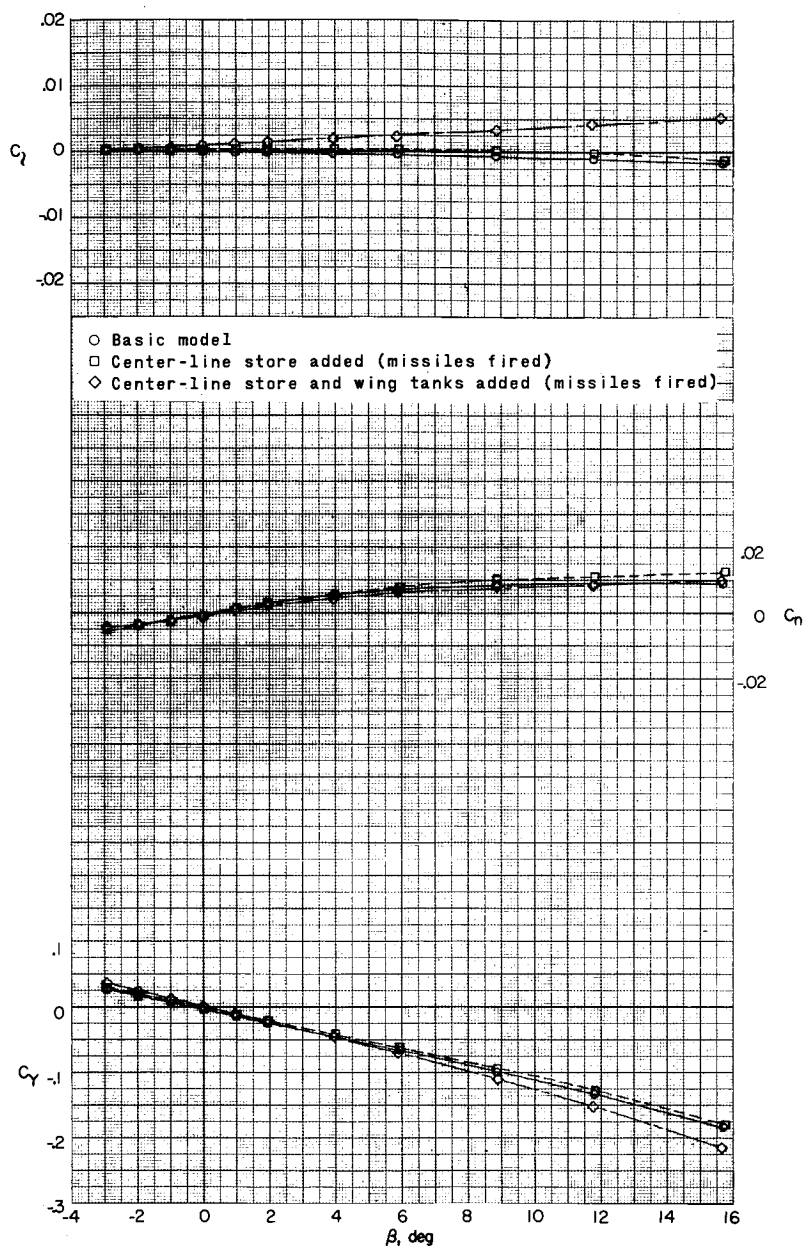
DECLASSIFIED



(g) Concluded.

Figure 19.- Continued.

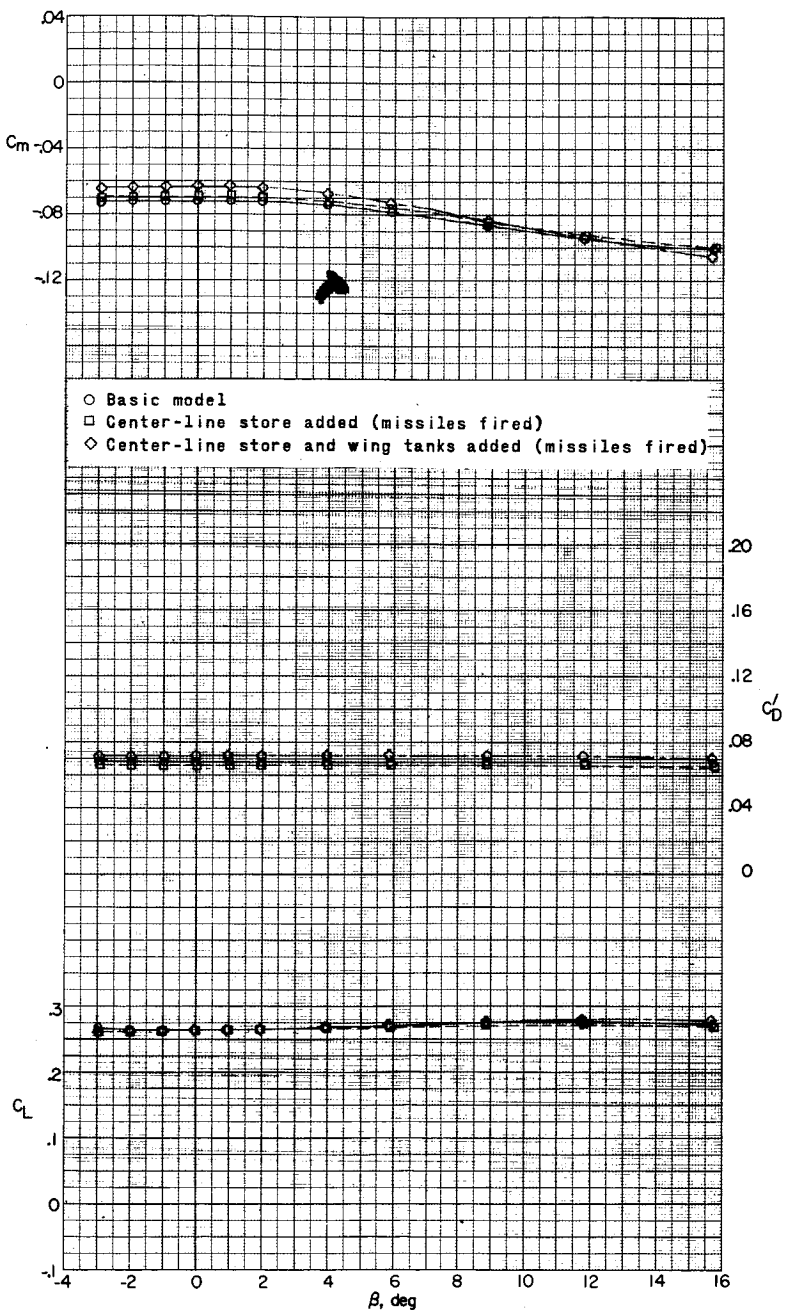
33171226 [REDACTED] 8



(h) $M = 2.16$; $\alpha = 6.5^\circ$.

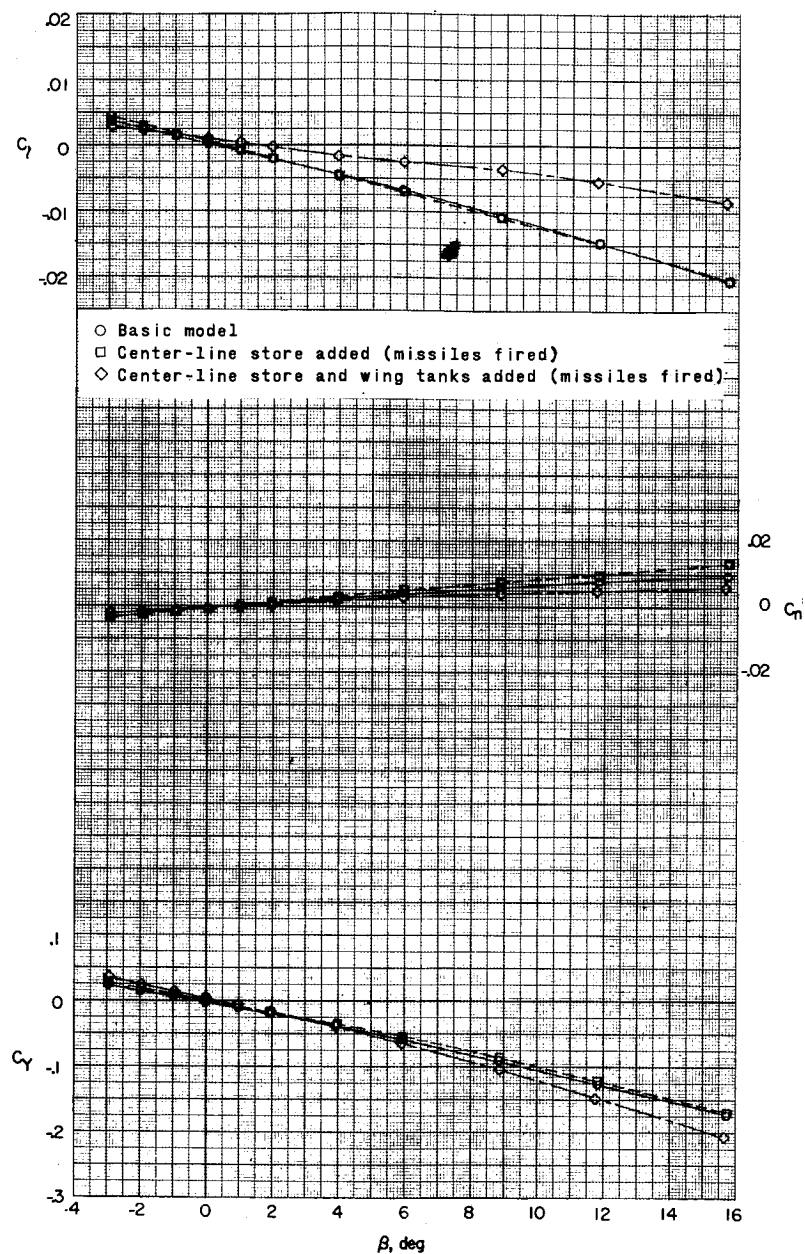
Figure 19.- Continued.

SECRET//CLASSIFIED



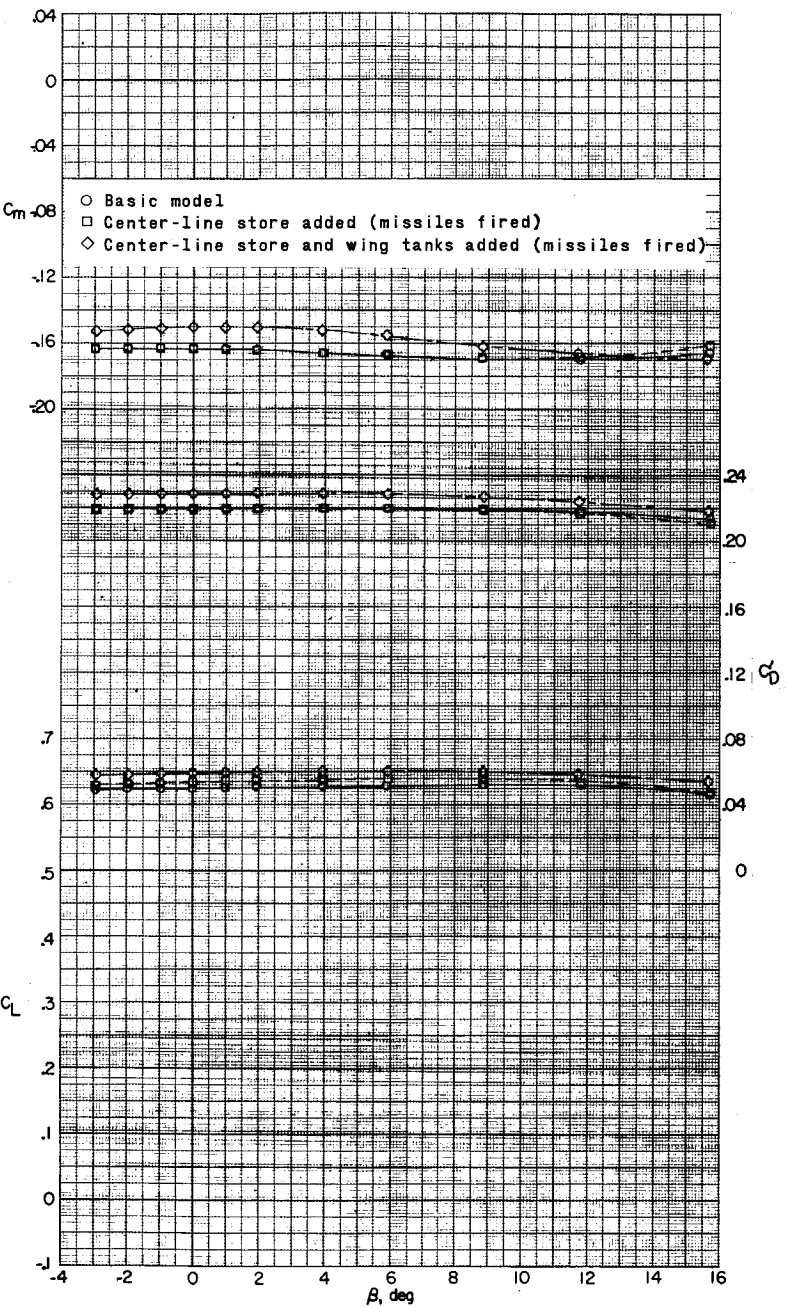
(h) Concluded.

Figure 19.- Continued.



(i) $M = 2.16$; $\alpha = 16.9^\circ$.

Figure 19.- Continued.



(i) Concluded.

Figure 19.- Concluded.

03171230 1030

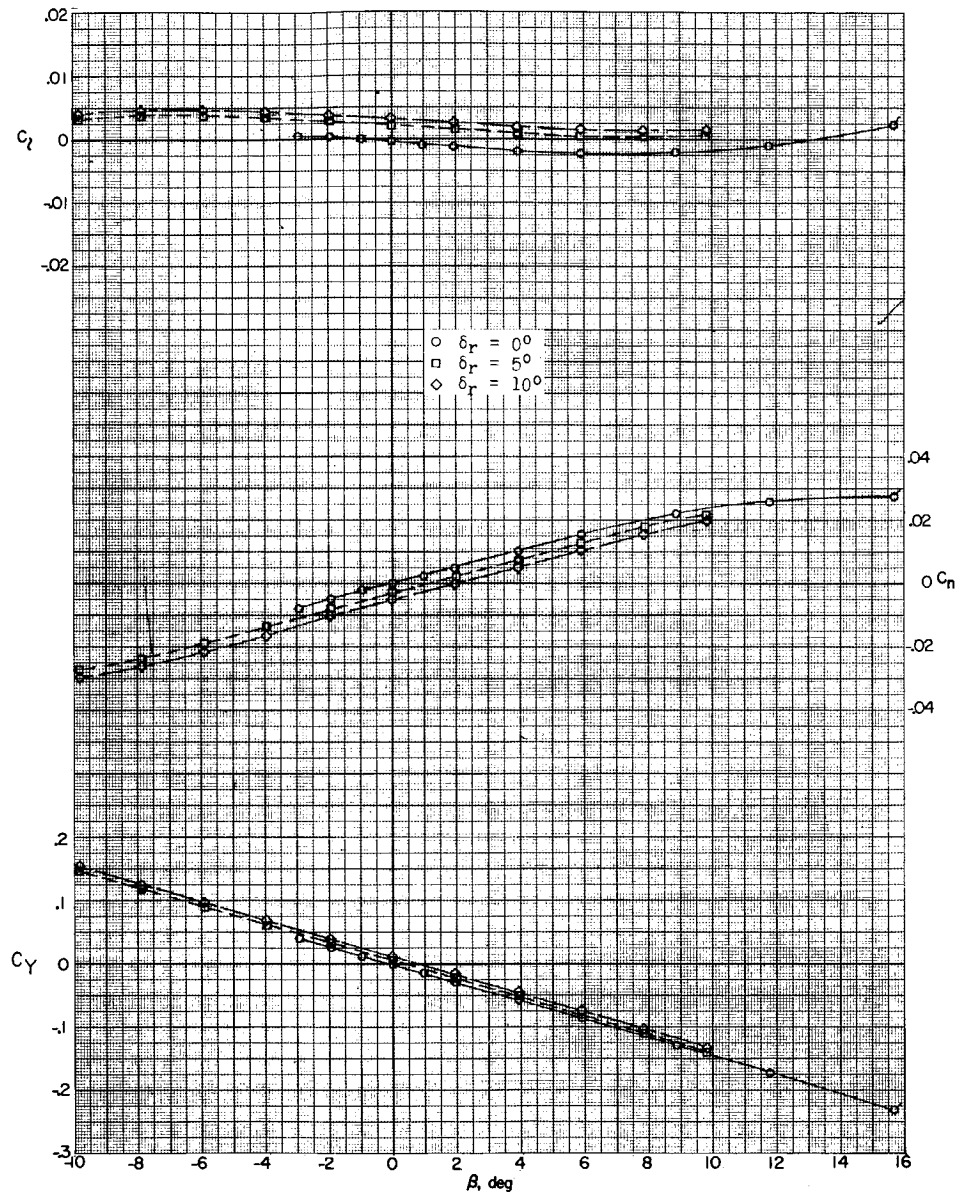
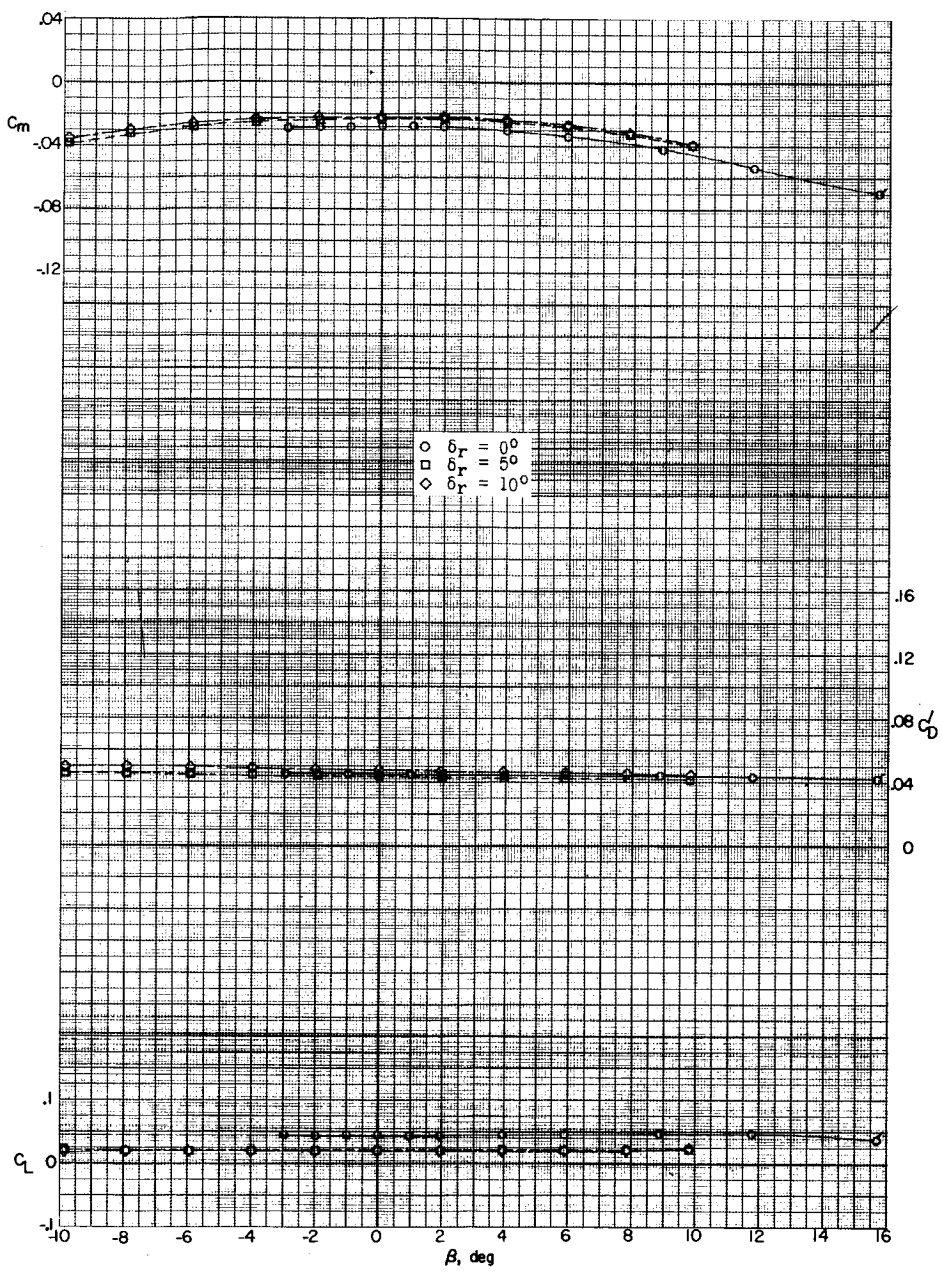
(a) $M = 1.57; \alpha = 0.4^\circ$.

Figure 20.- Effect of rudder deflection on aerodynamic characteristics in sideslip. (Flagged symbols denote wall-reflected shock waves striking the tail.)

[Redacted area at the bottom center]



(a) Concluded.

Figure 20.- Continued.

03171230 1130

8

134

1-224

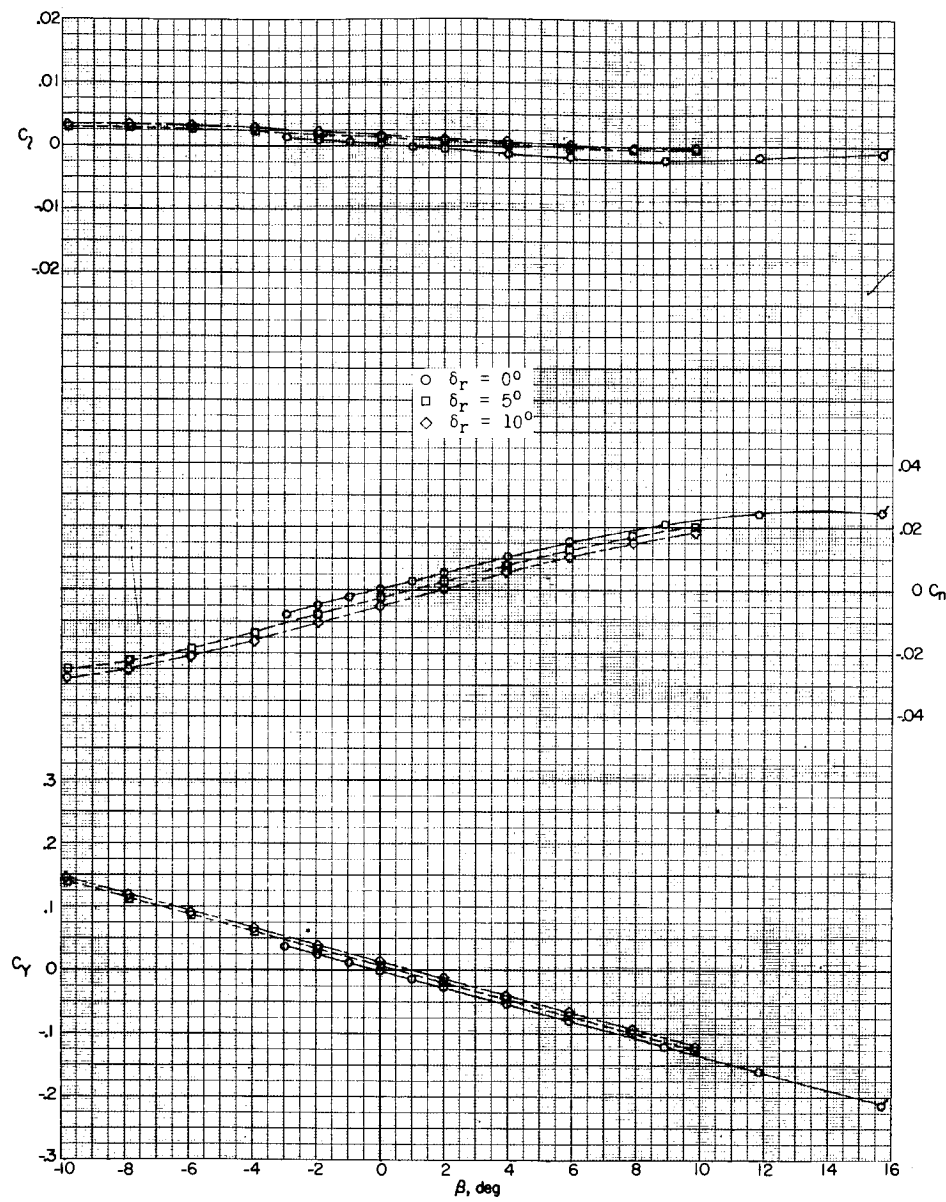
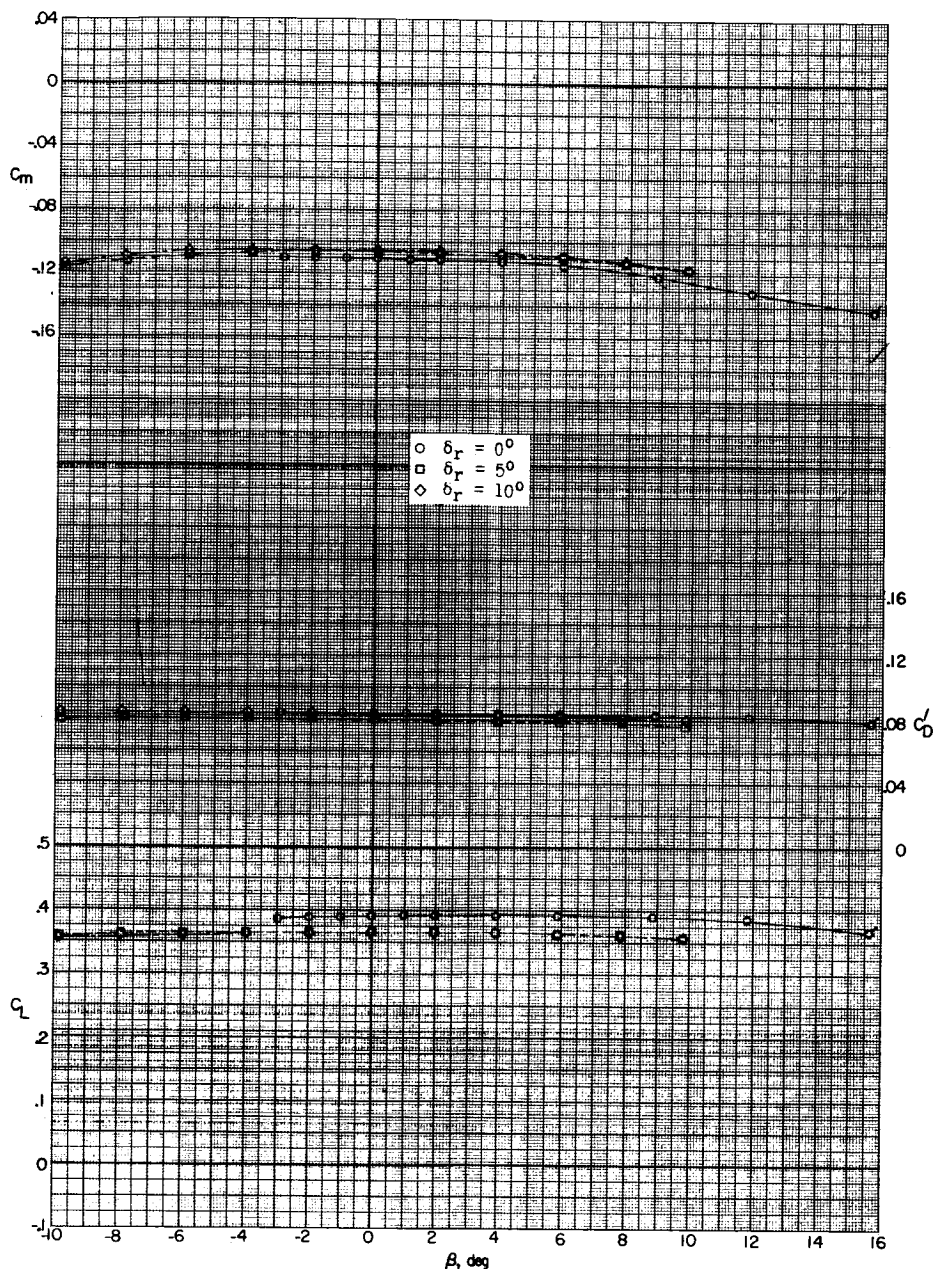
(b) $M = 1.57; \alpha = 6.7^\circ$.

Figure 20.- Continued.

CLASSIFIED

135



(b) Concluded.

Figure 20.- Continued.

03171230 1030

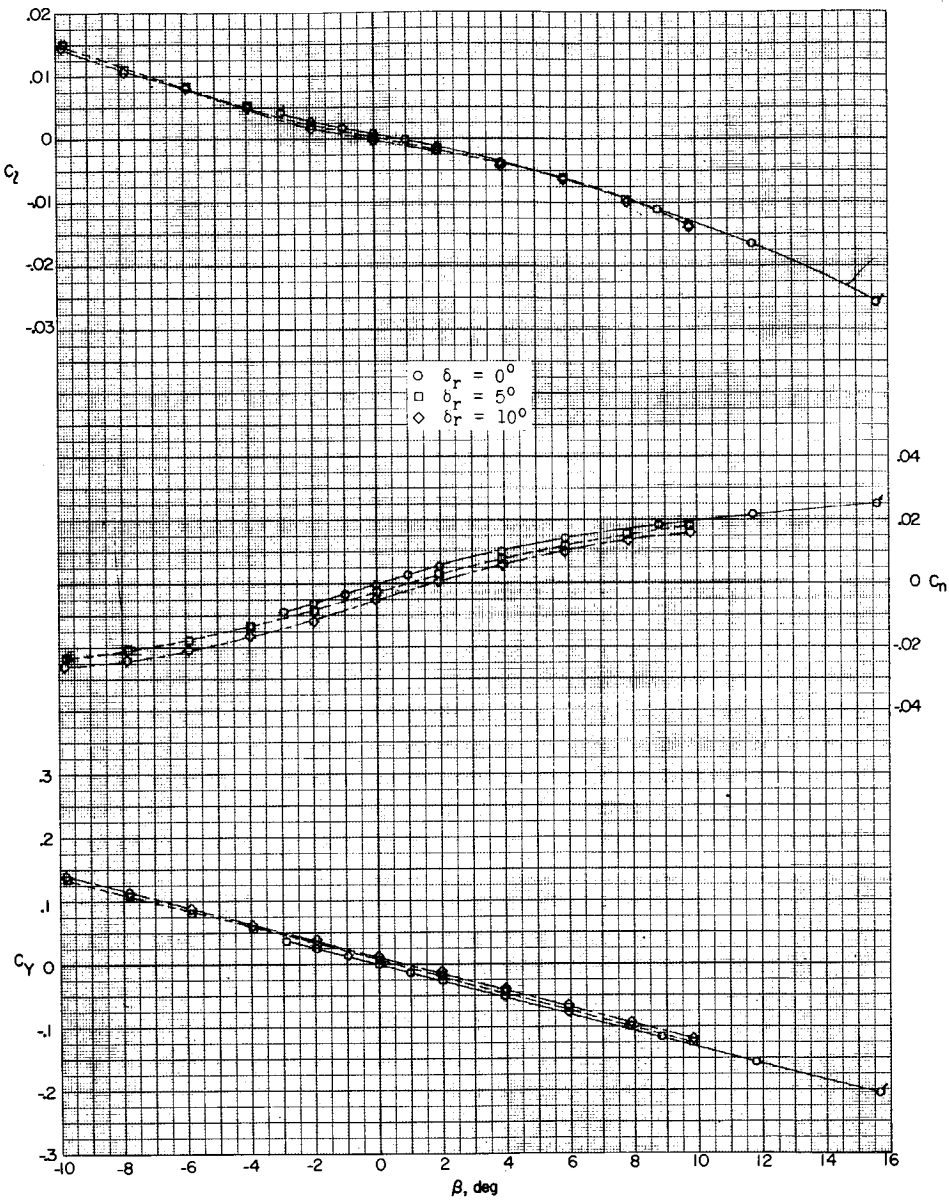
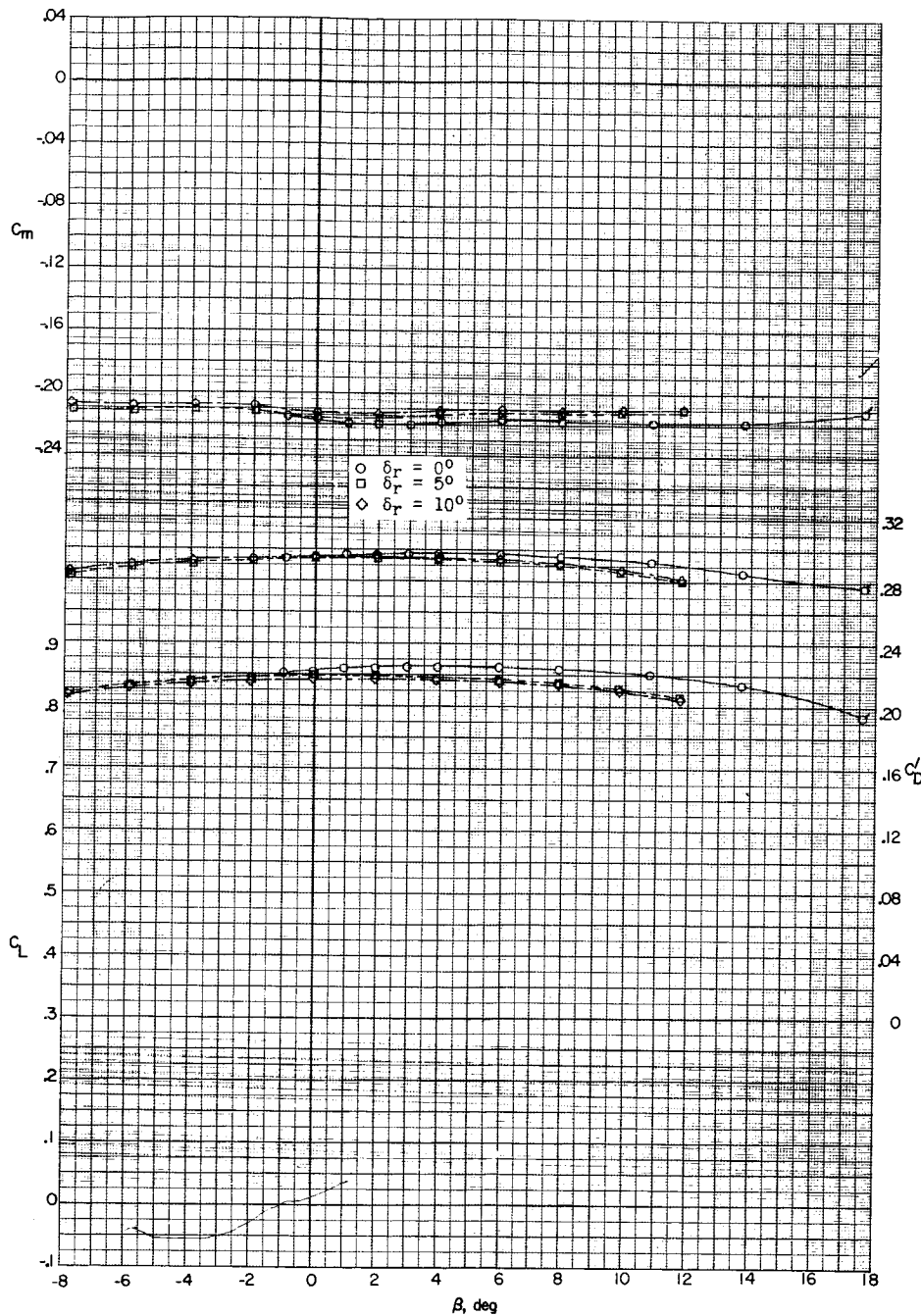
(c) $M = 1.57; \alpha = 17.4^\circ$.

Figure 20.- Continued.

DECLASSIFIED



(c) Concluded.

Figure 20.- Continued.

03171030010034

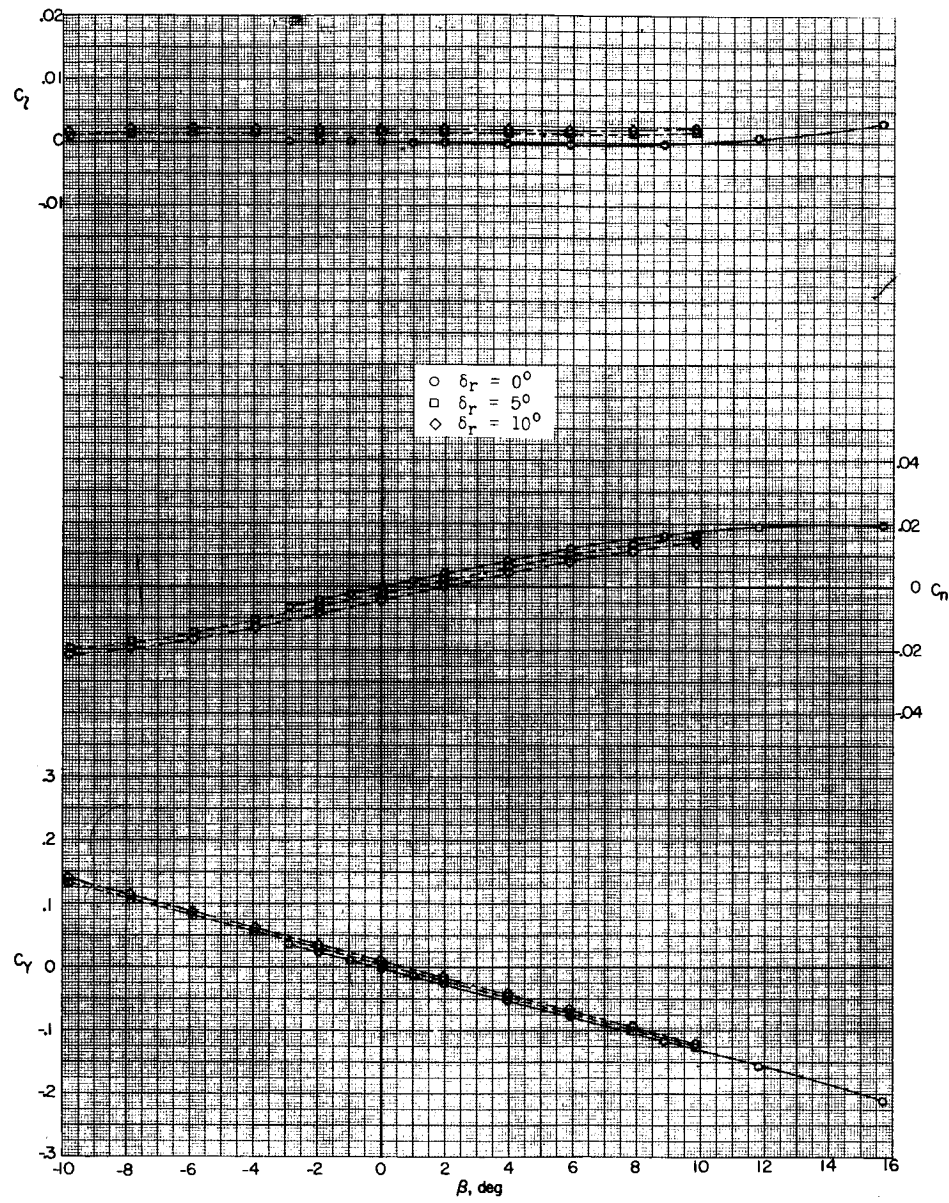
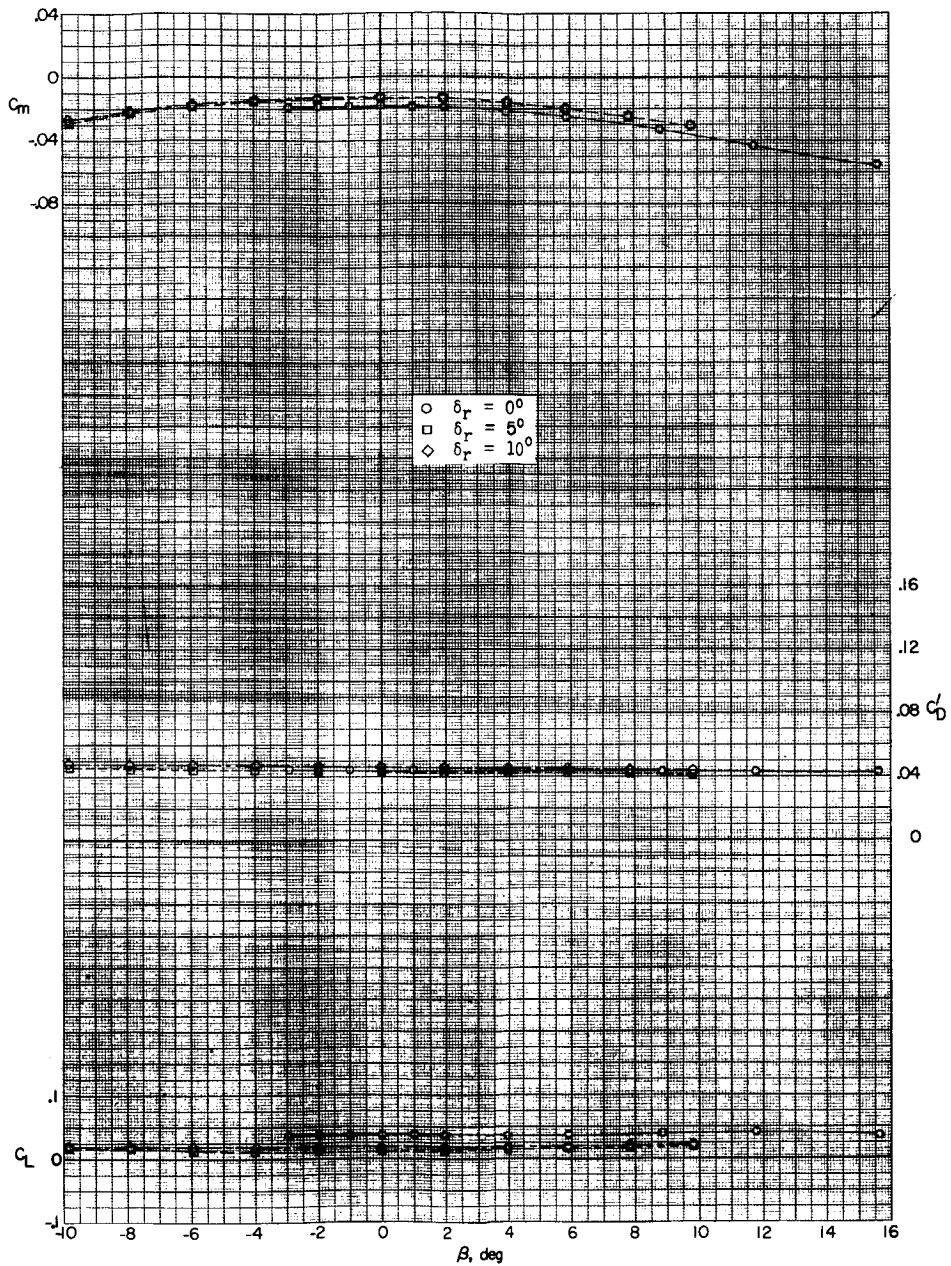
(d) $M = 1.87; \alpha = 0.4^\circ$.

Figure 20.- Continued.

CLASSIFIED 139



(d) Concluded.

Figure 20.- Continued.

03171220 11:30

140

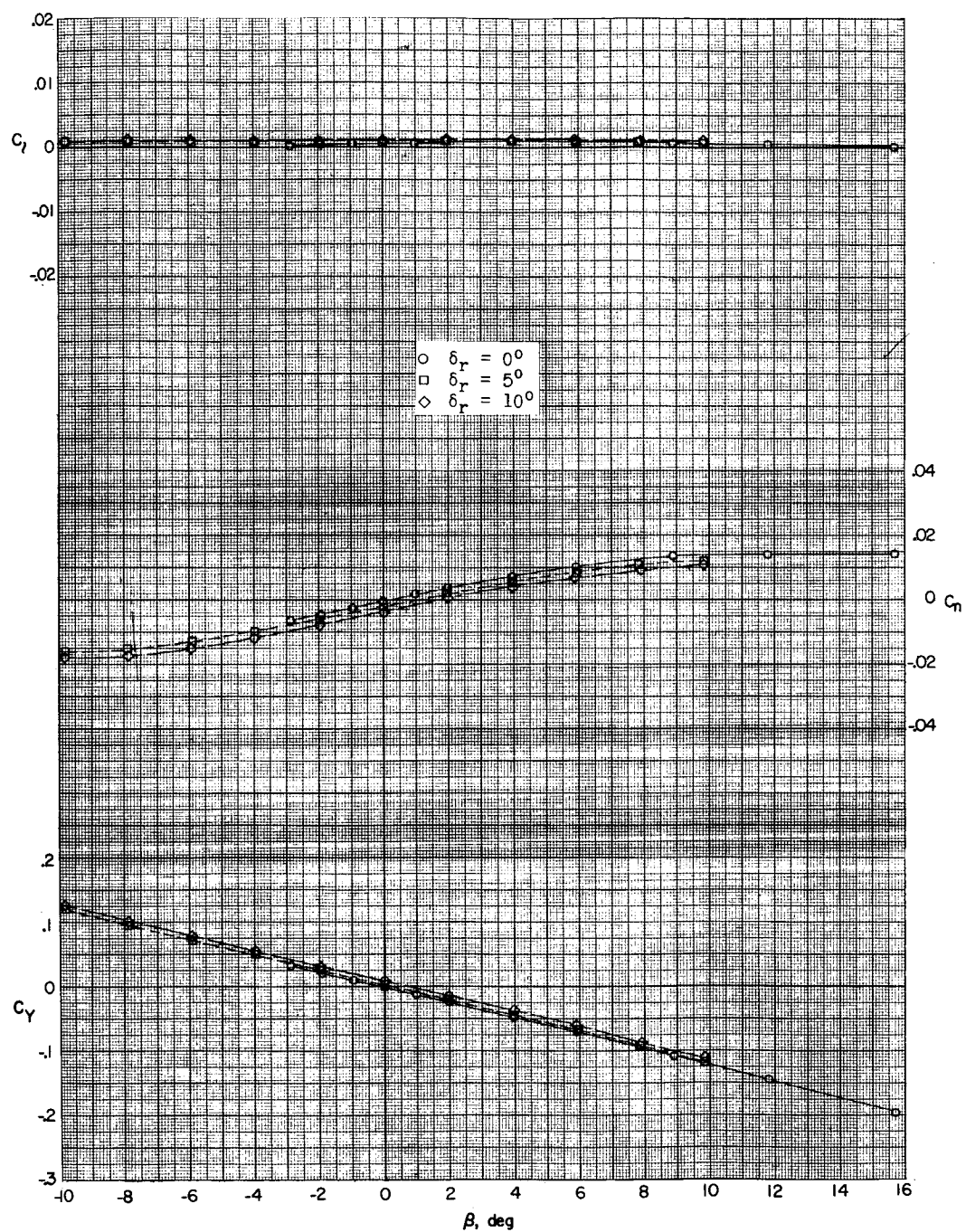
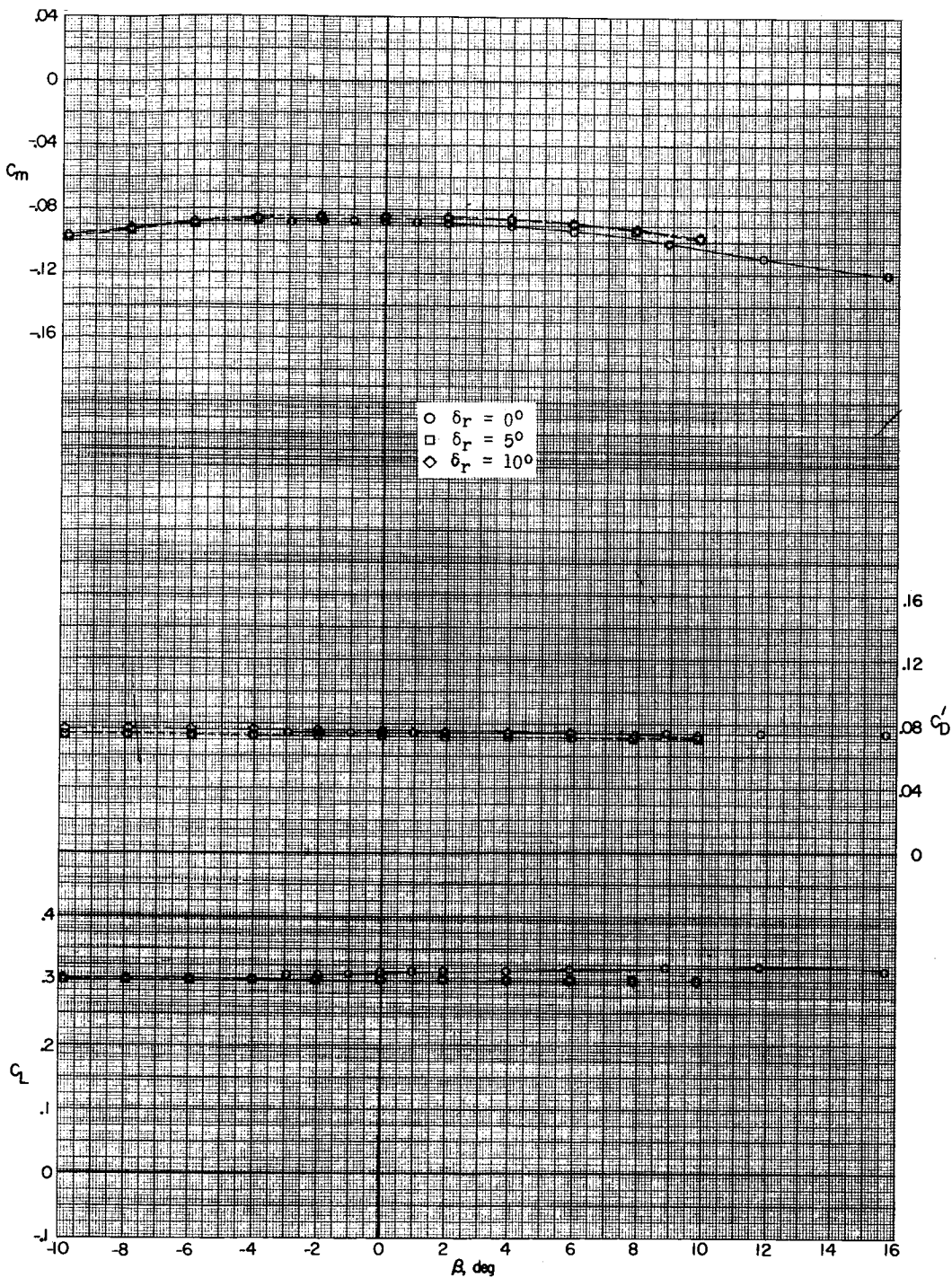
(e) $M = 1.87$; $\alpha = 6.6^\circ$.

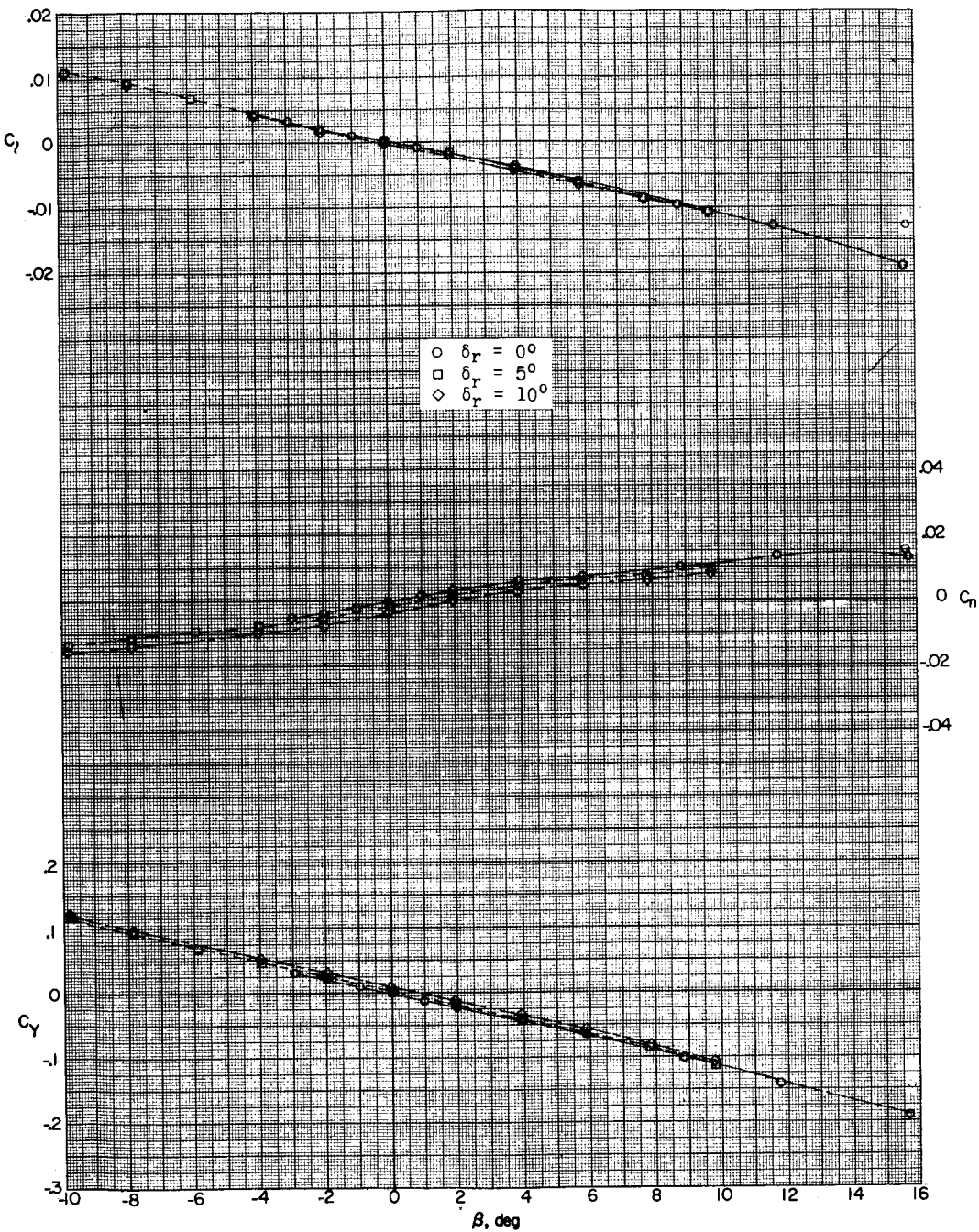
Figure 20.- Continued.

REF ID: A65141
CLASSIFIED



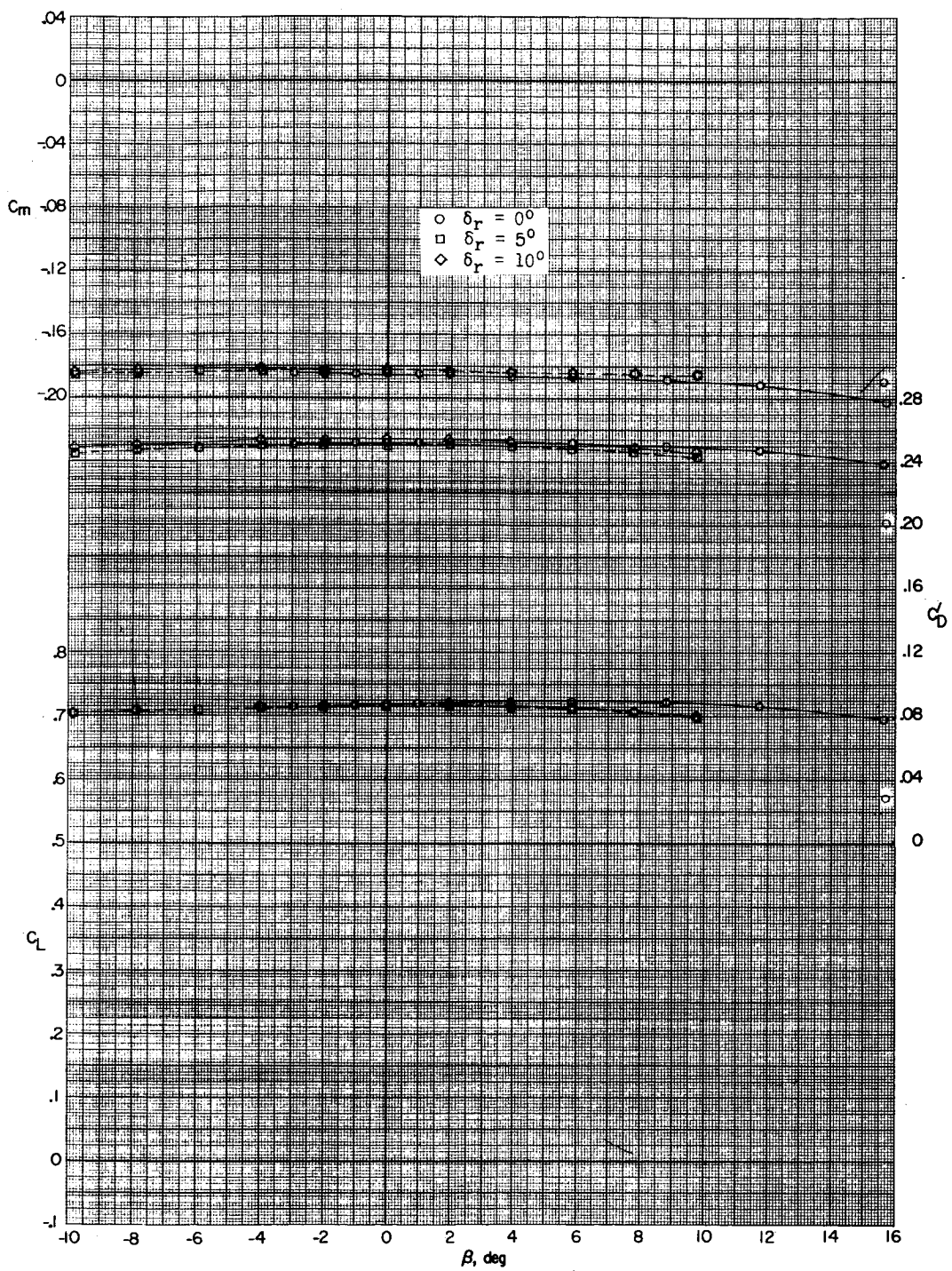
(e) Concluded.

Figure 20.- Continued.



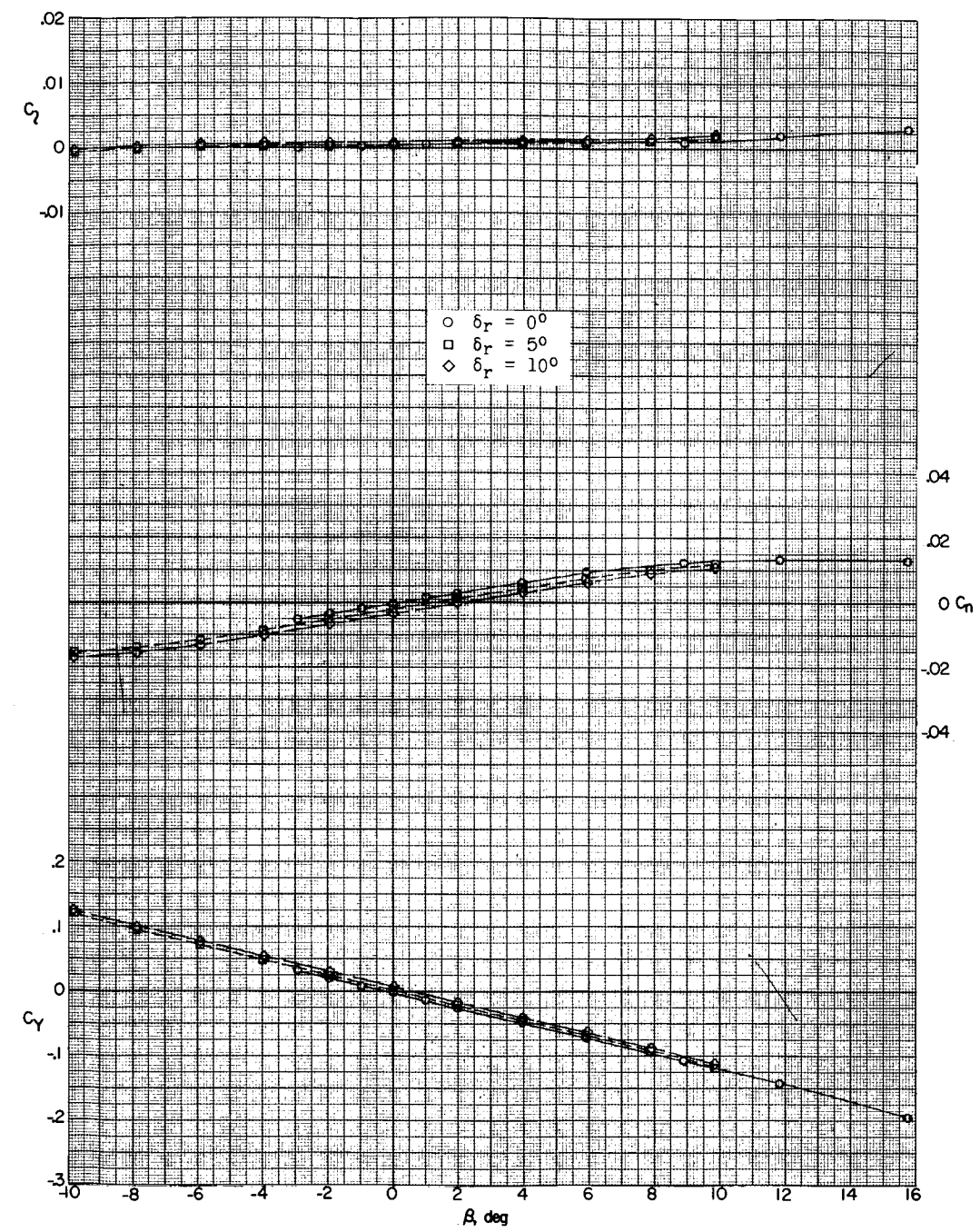
(f) $M = 1.87; \alpha = 17.1^\circ$.

Figure 20.- Continued.

REF ID: A6512
DECLASSIFIED

(f) Concluded.

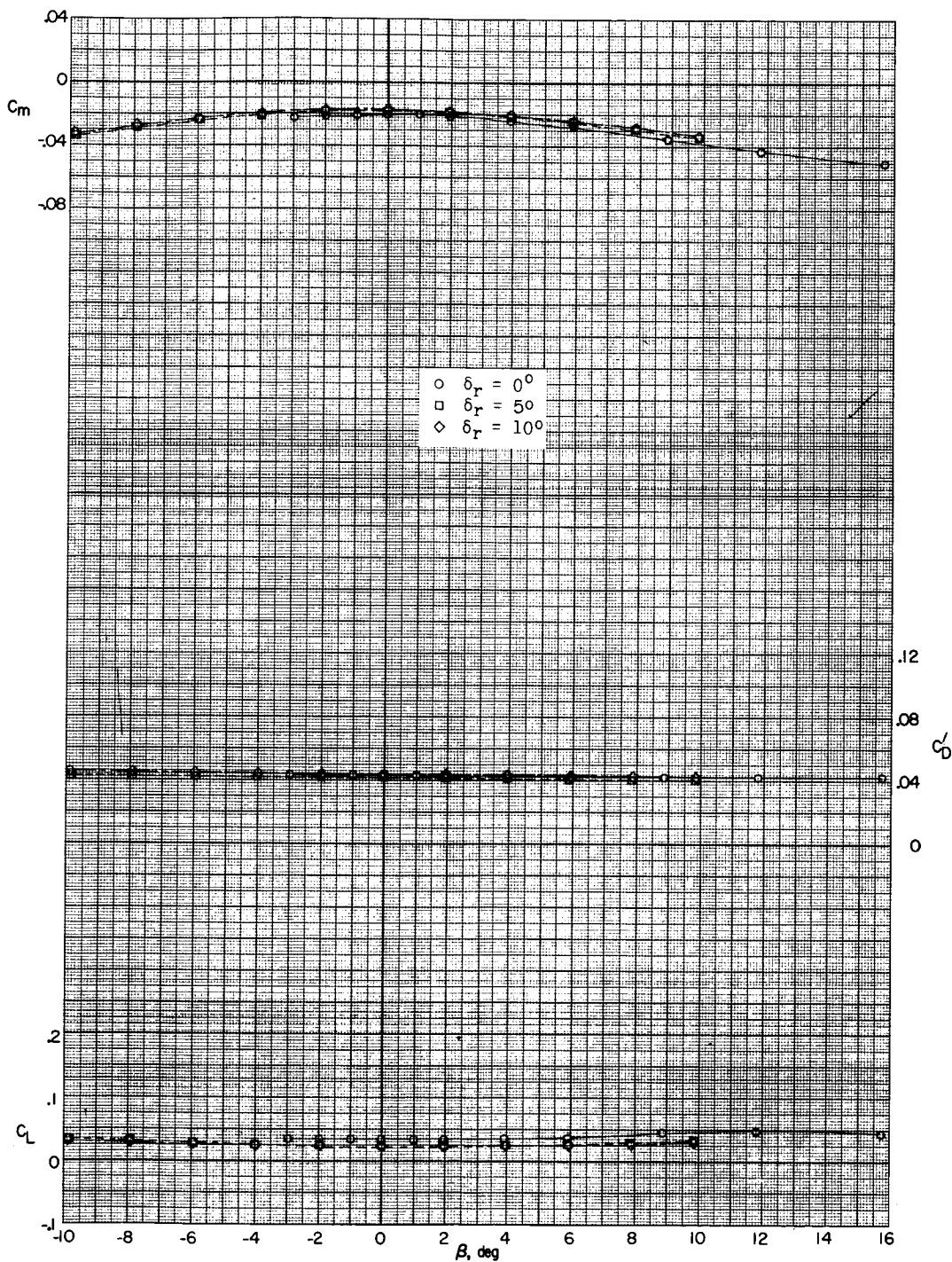
Figure 20.- Continued.



(g) $M = 2.16; \alpha = 0.4^\circ$.

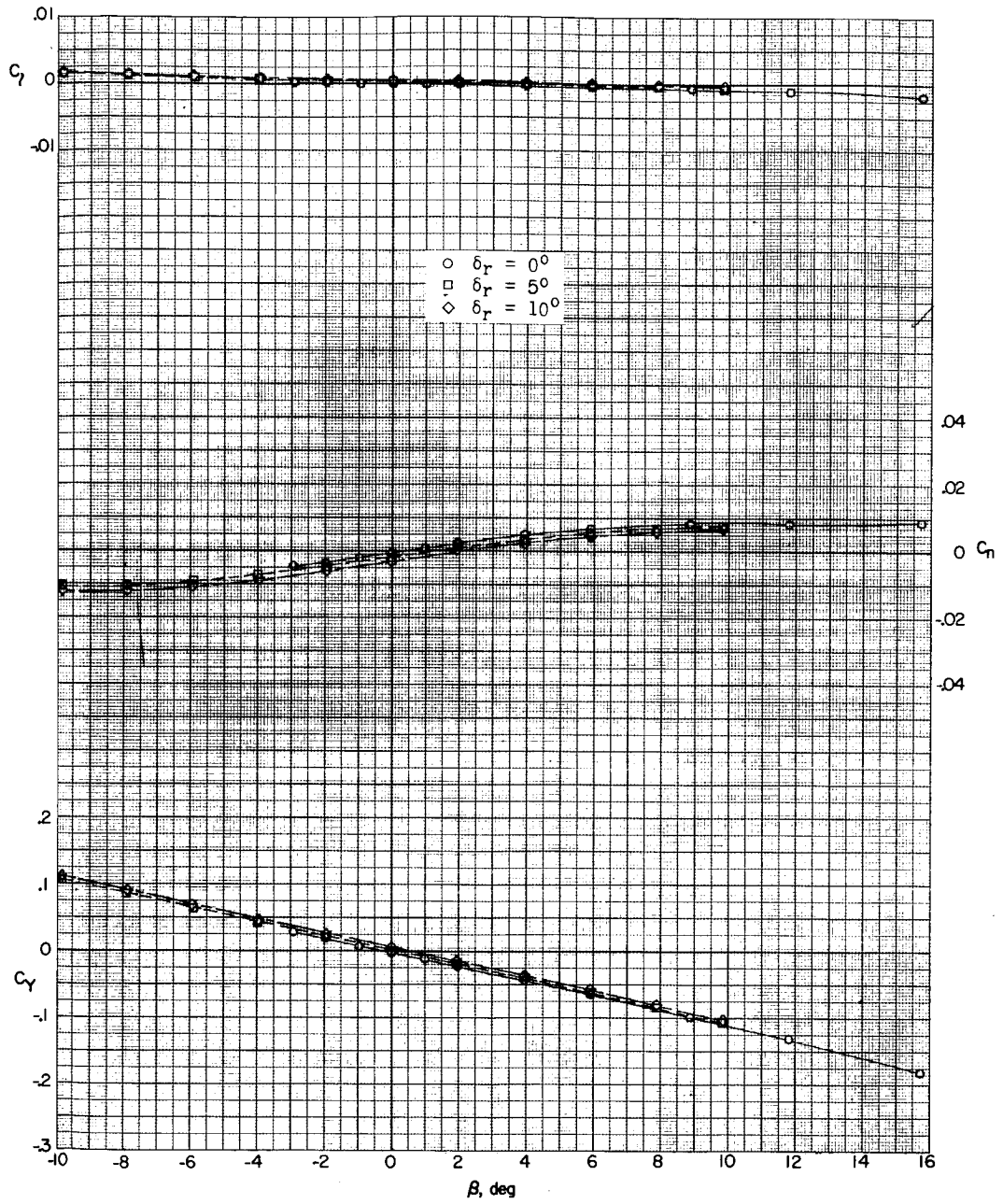
Figure 20.- Continued.

DECLASSIFIED



(g) Concluded.

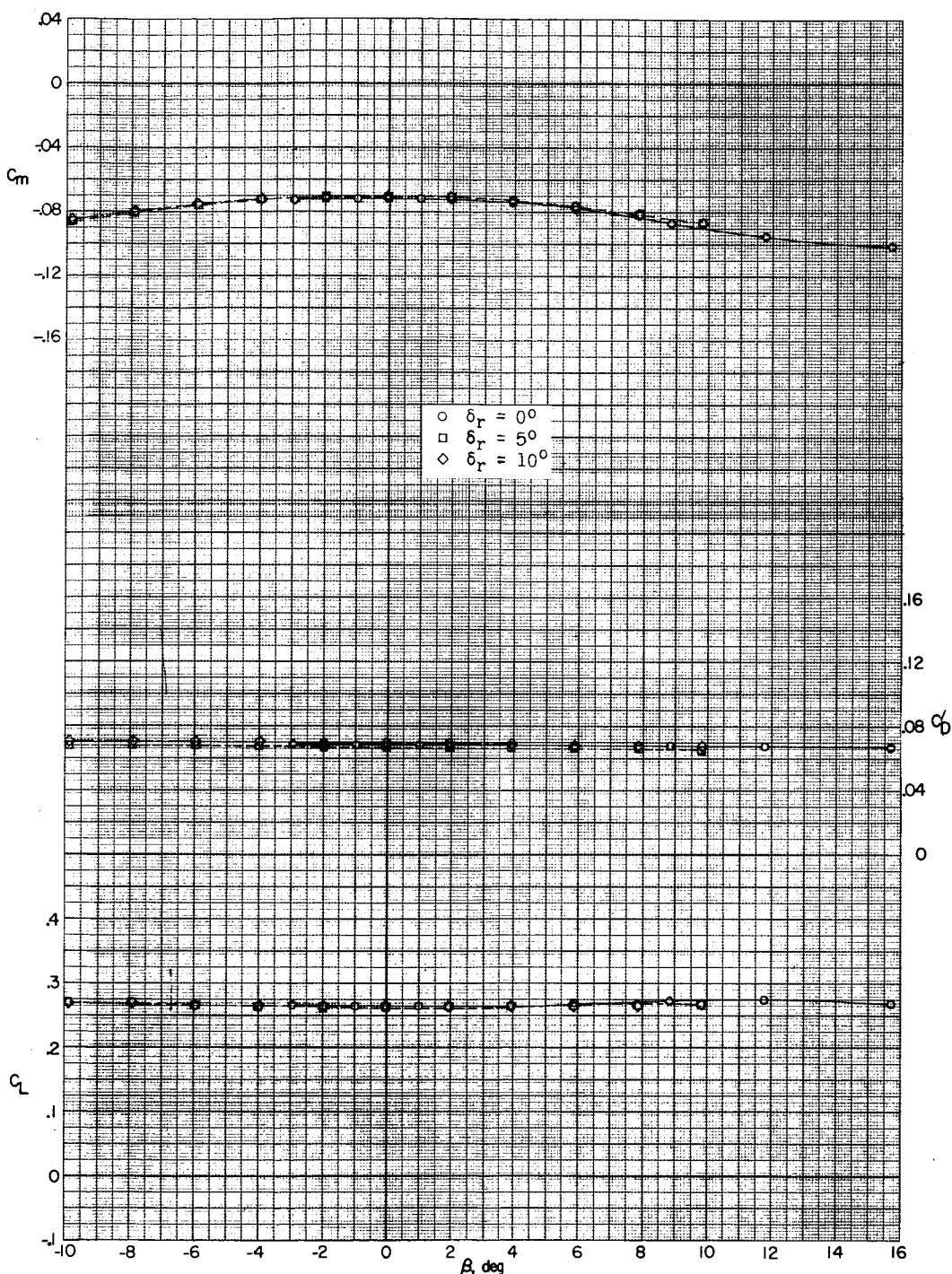
Figure 20.- Continued.



(h) $M = 2.16$; $\alpha = 6.5^\circ$.

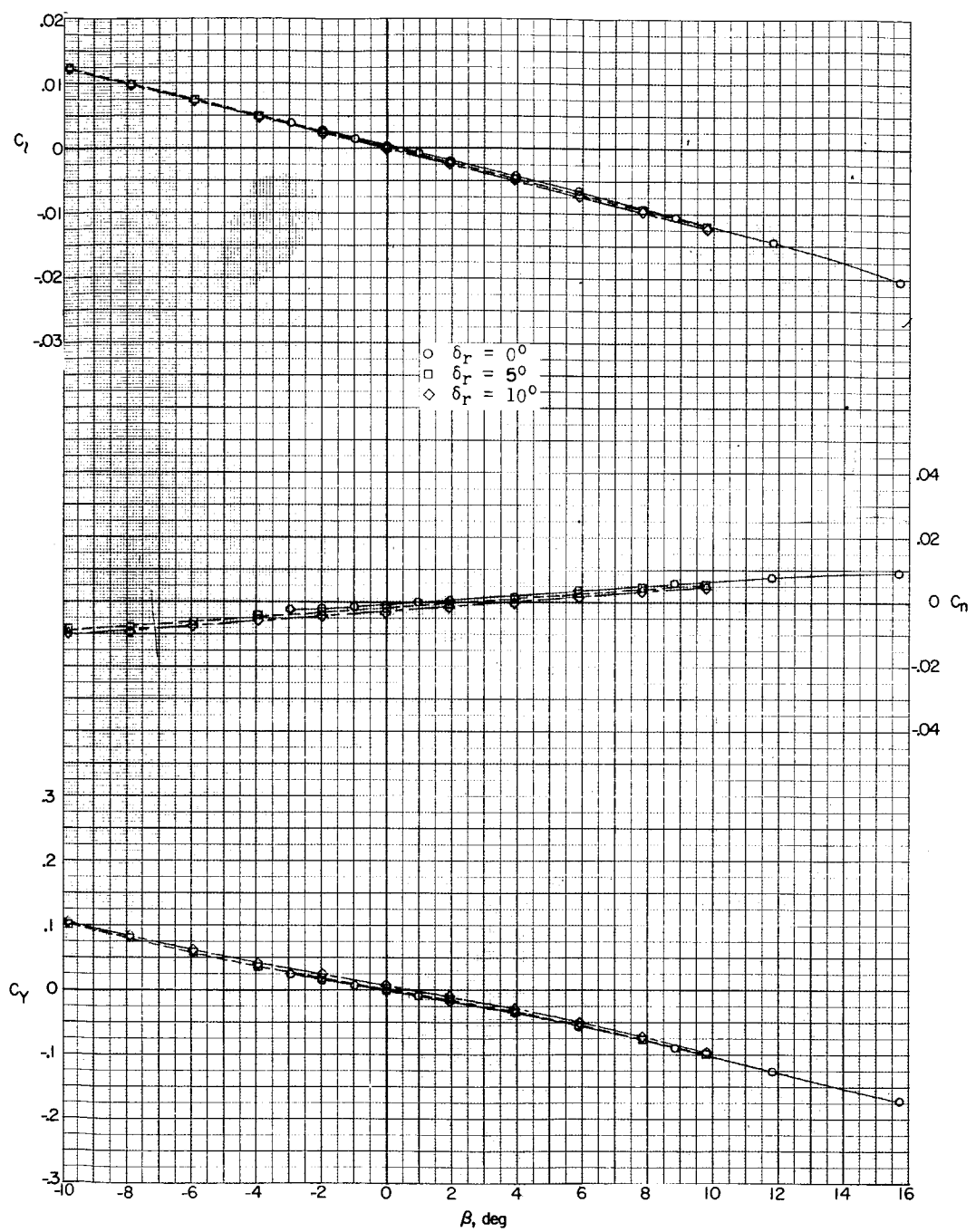
Figure 20.- Continued.

DECLASSIFIED



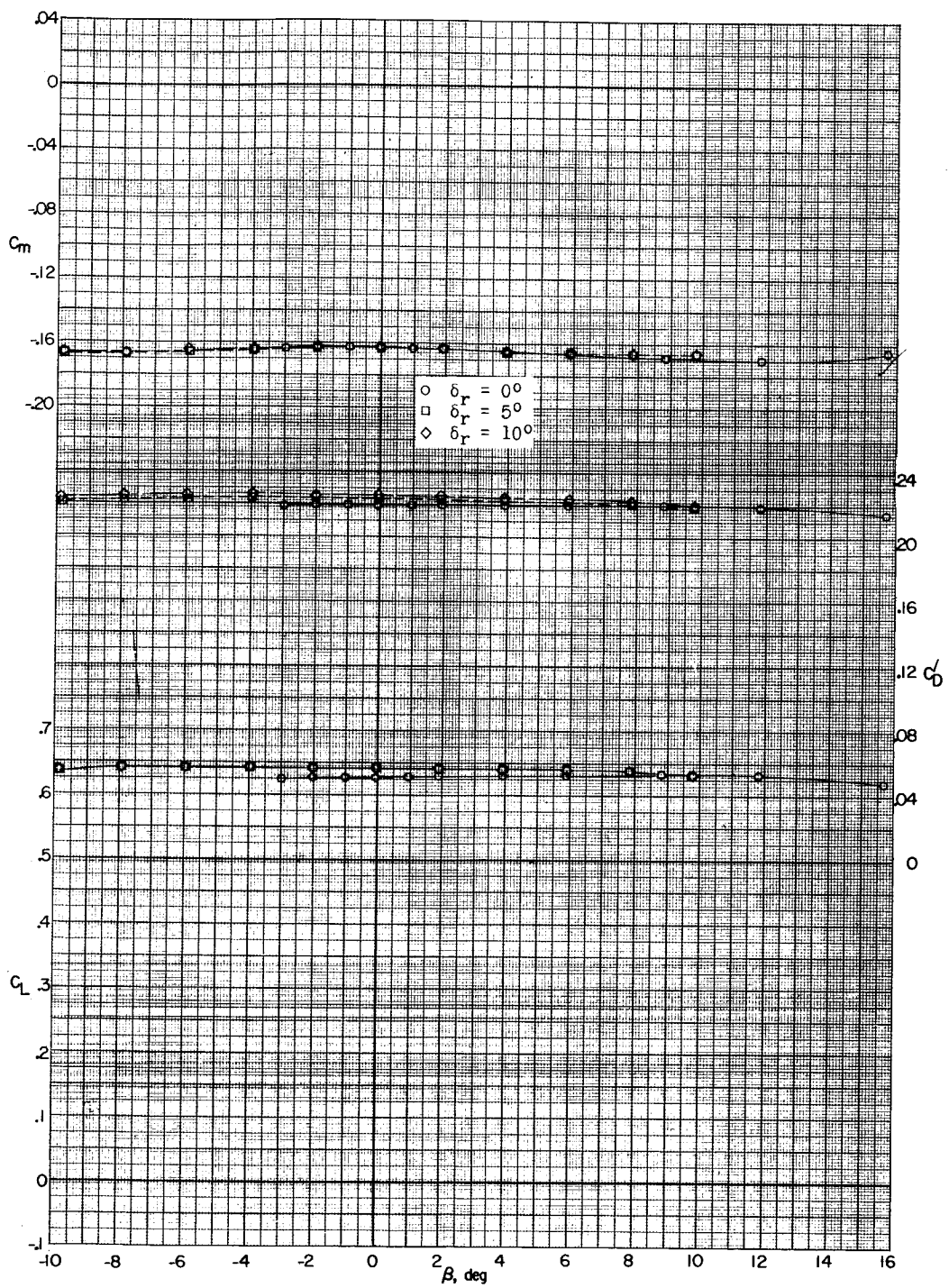
(h) Concluded.

Figure 20.- Continued.



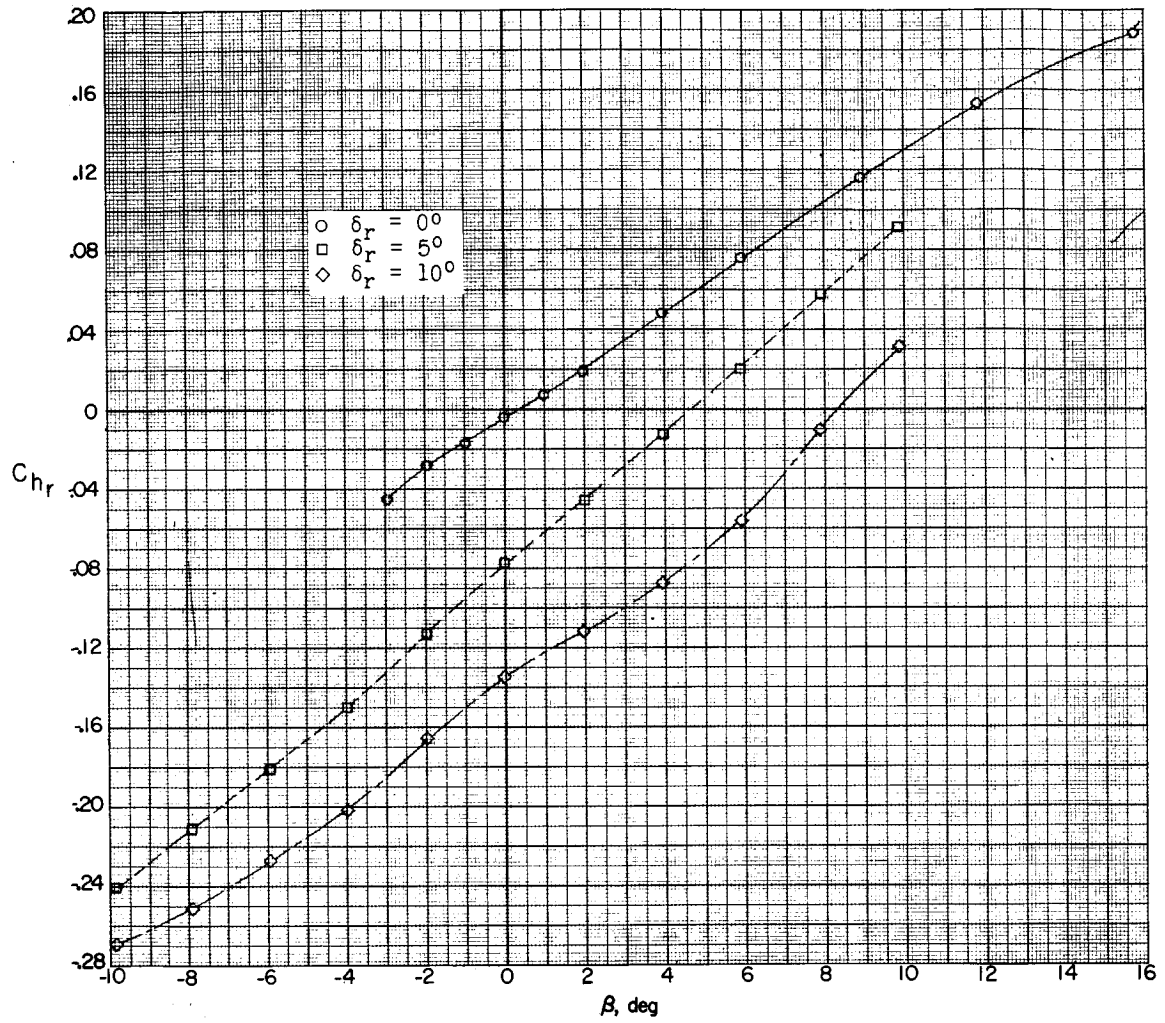
(i) $M = 2.16; \alpha = 16.9^\circ$.

Figure 20.- Continued.



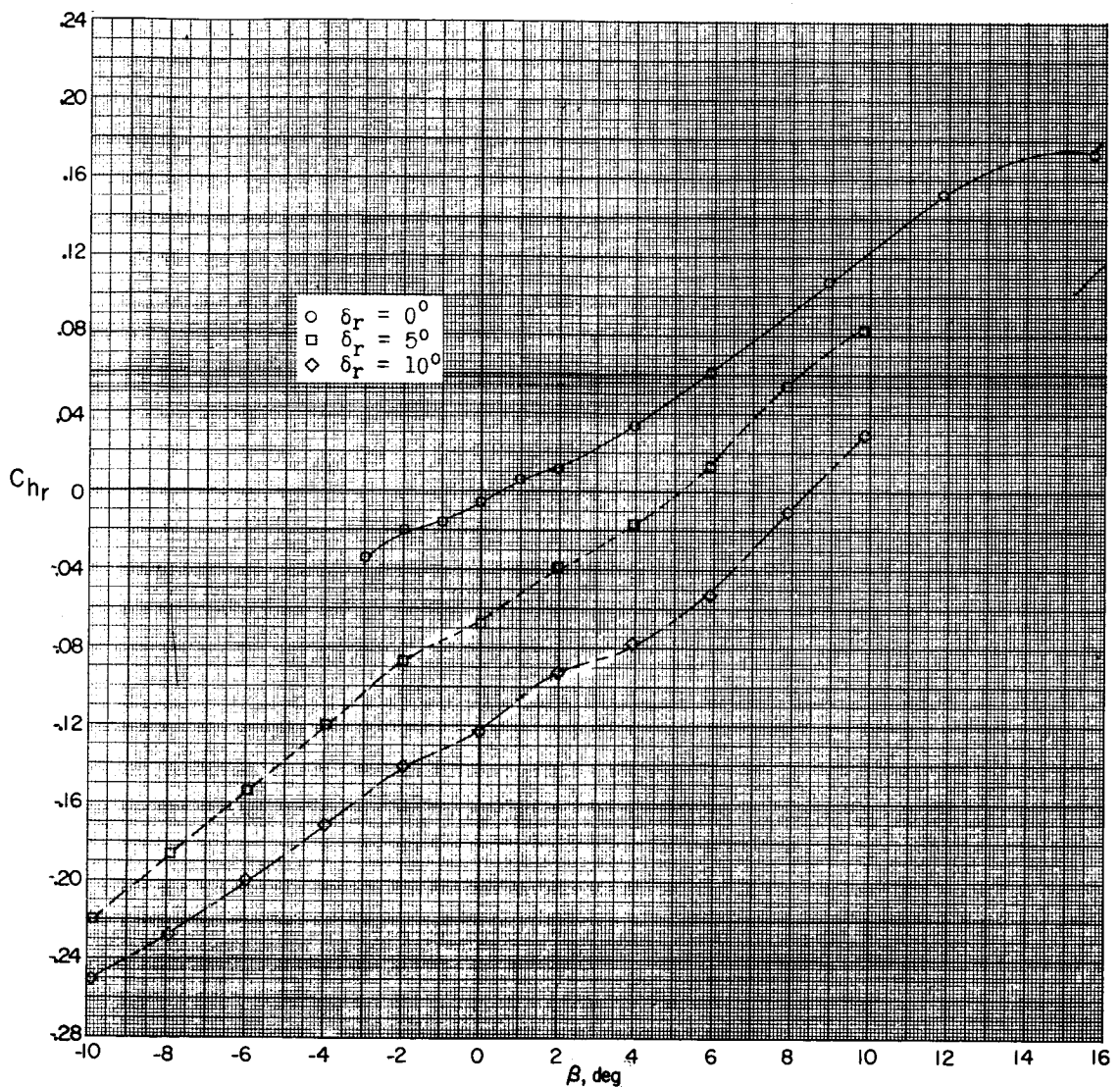
(i) Concluded.

Figure 20.- Concluded.



(a) $M = 1.57; \alpha = 0.4^\circ$.

Figure 21.- Effect of rudder deflection on rudder hinge-moment coefficient in sideslip. (Flagged symbols denote wall-reflected shock waves striking the tail.)



(b) $M = 1.57; \alpha = 6.7^\circ$.

Figure 21.- Continued.

152



I-524

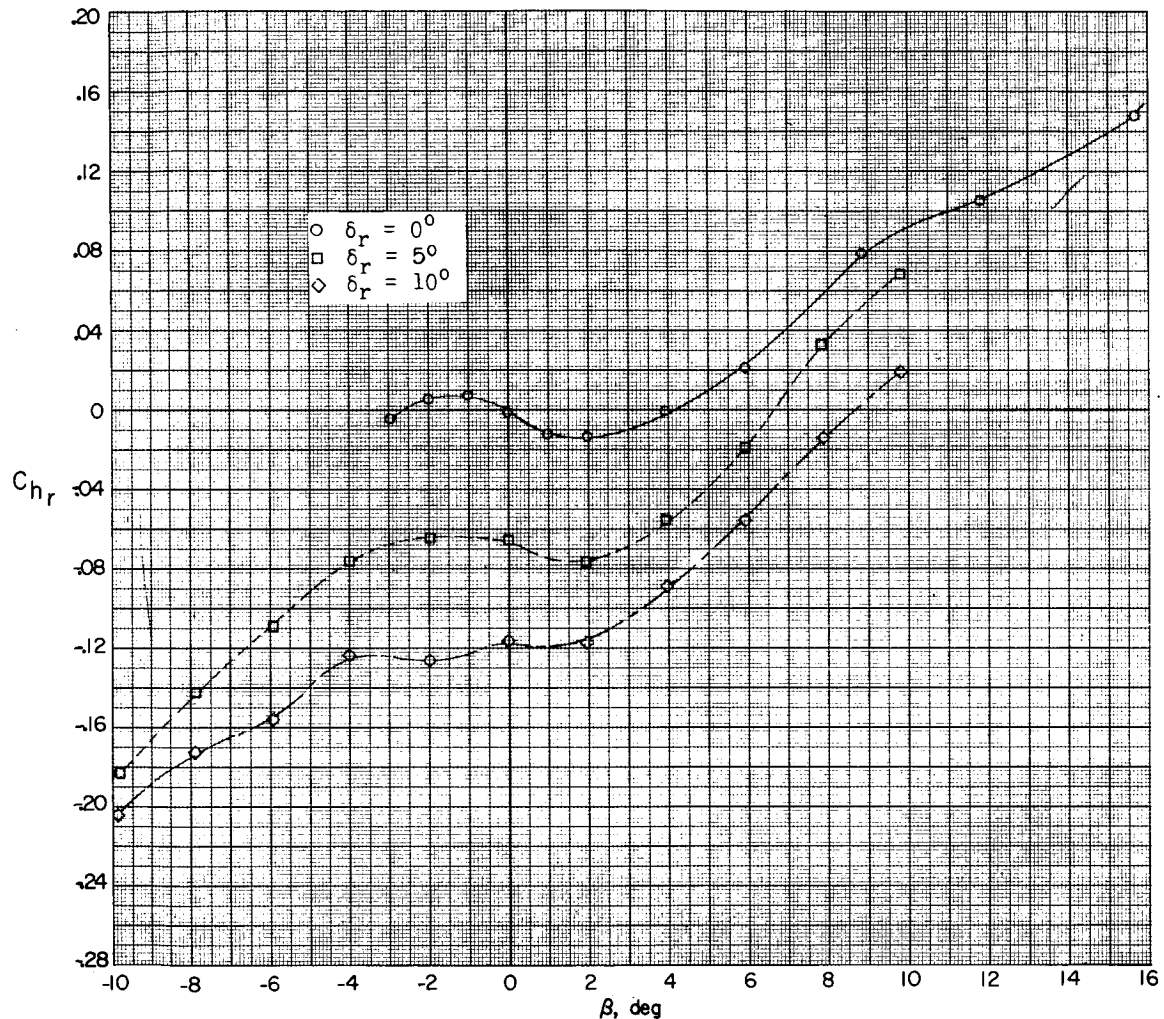
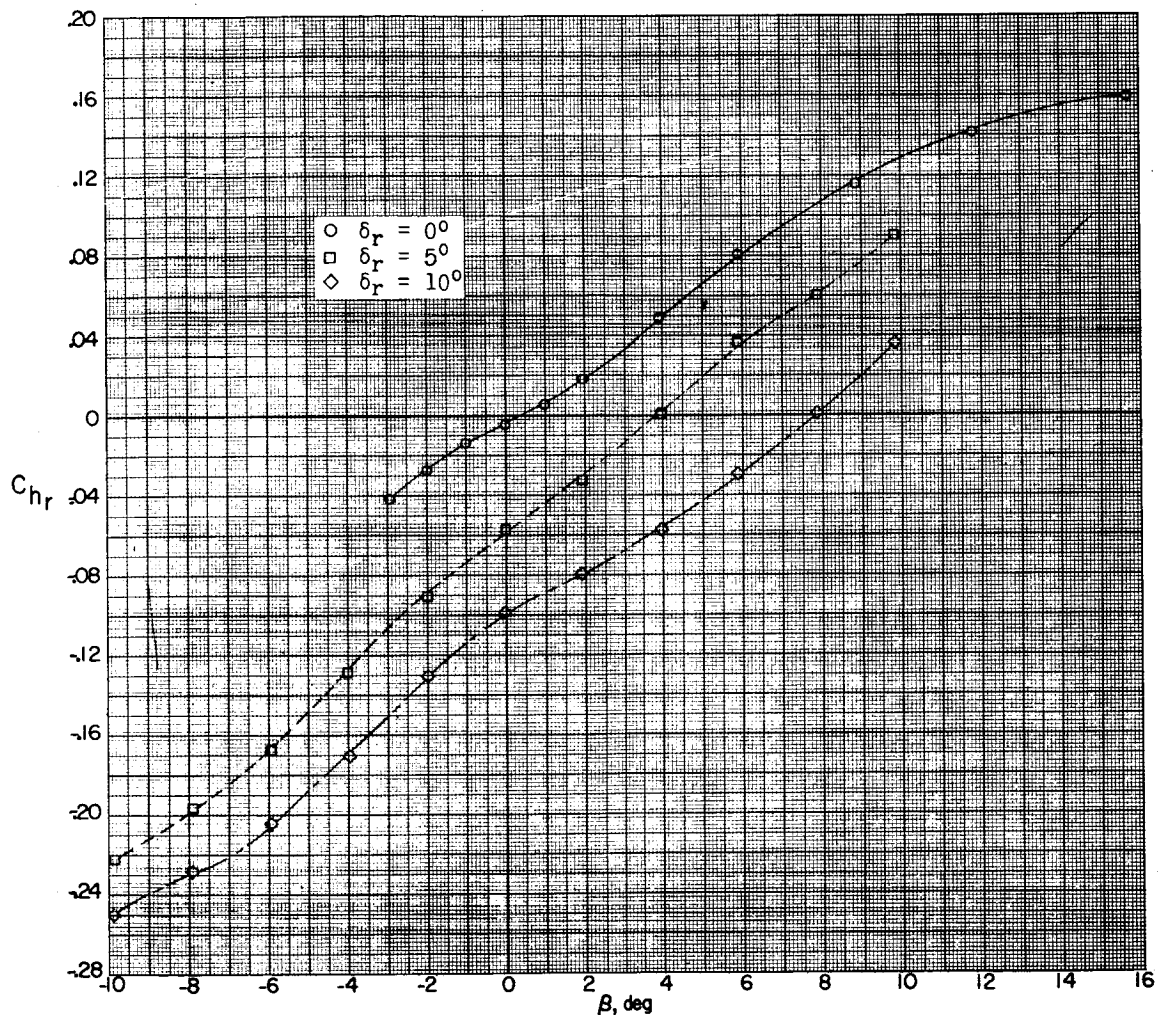
(c) $M = 1.57; \alpha = 17.4^\circ.$

Figure 21.- Continued.

REF ID: A6512
UNCLASSIFIED 153



(d) $M = 1.87; \alpha = 0.4^\circ$.

Figure 21.- Continued.

03191230 [REDACTED]

[REDACTED]

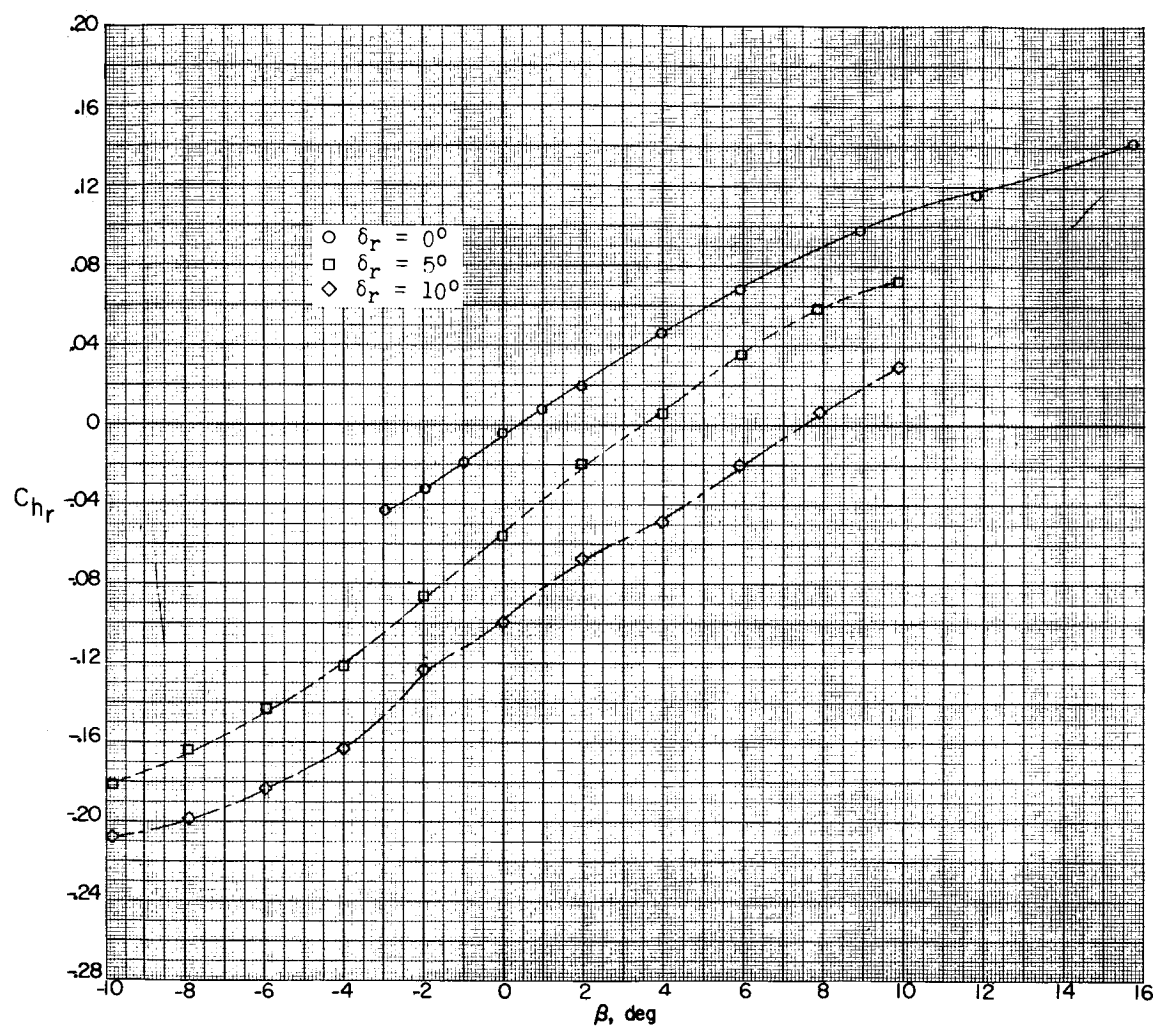
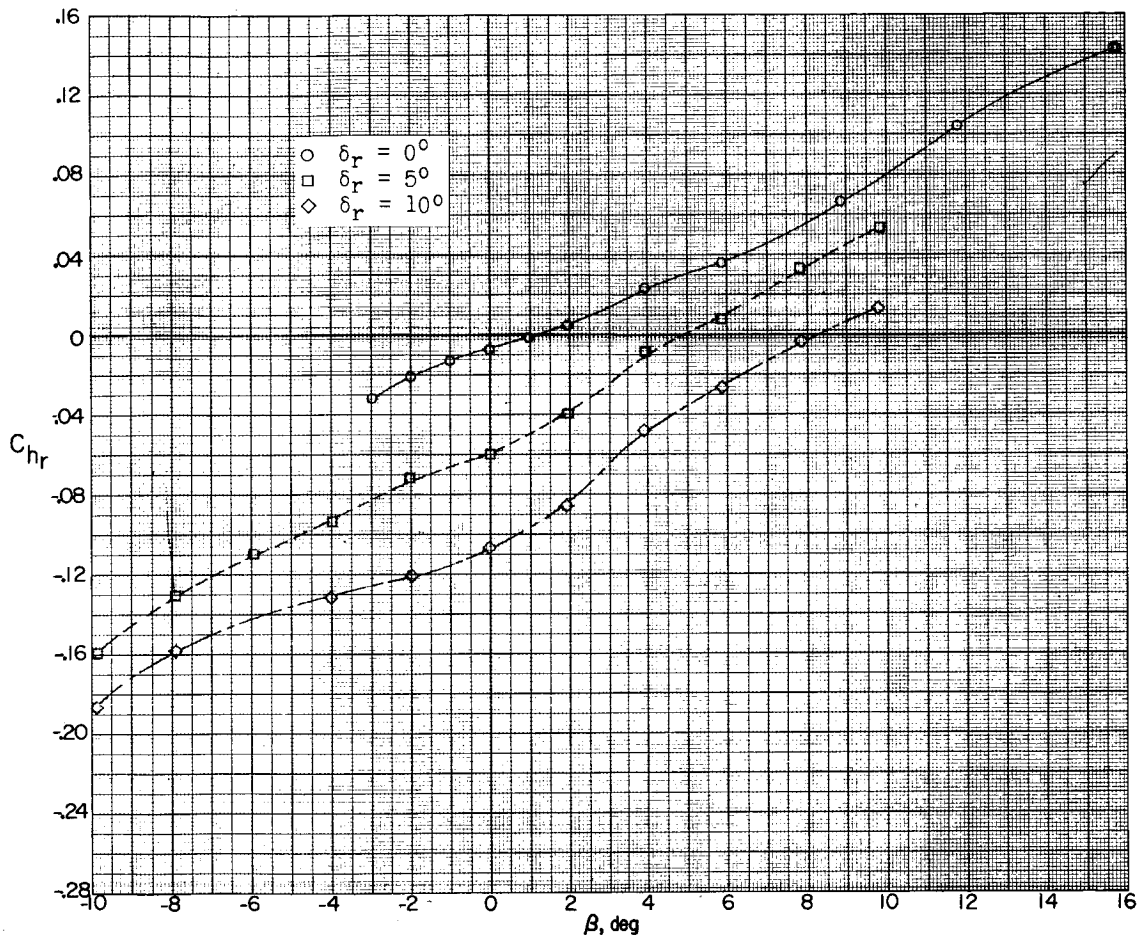
(e) $M = 1.87; \alpha = 6.6^\circ$.

Figure 21.- Continued.



(f) $M = 1.87; \alpha = 17.1^\circ$.

Figure 21.- Continued.

031712201030

8

156

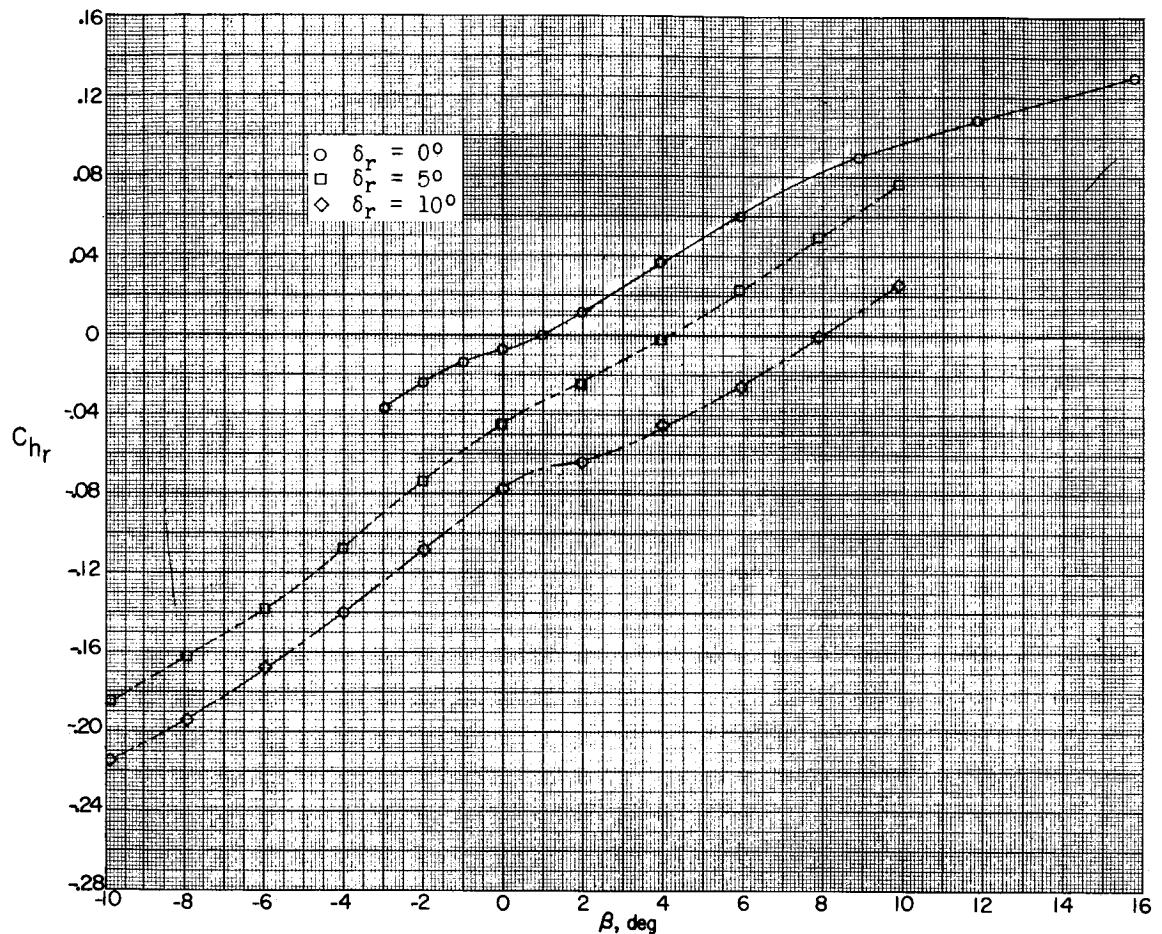
(g) $M = 2.16; \alpha = 0.4^\circ$.

Figure 21-- Continued.

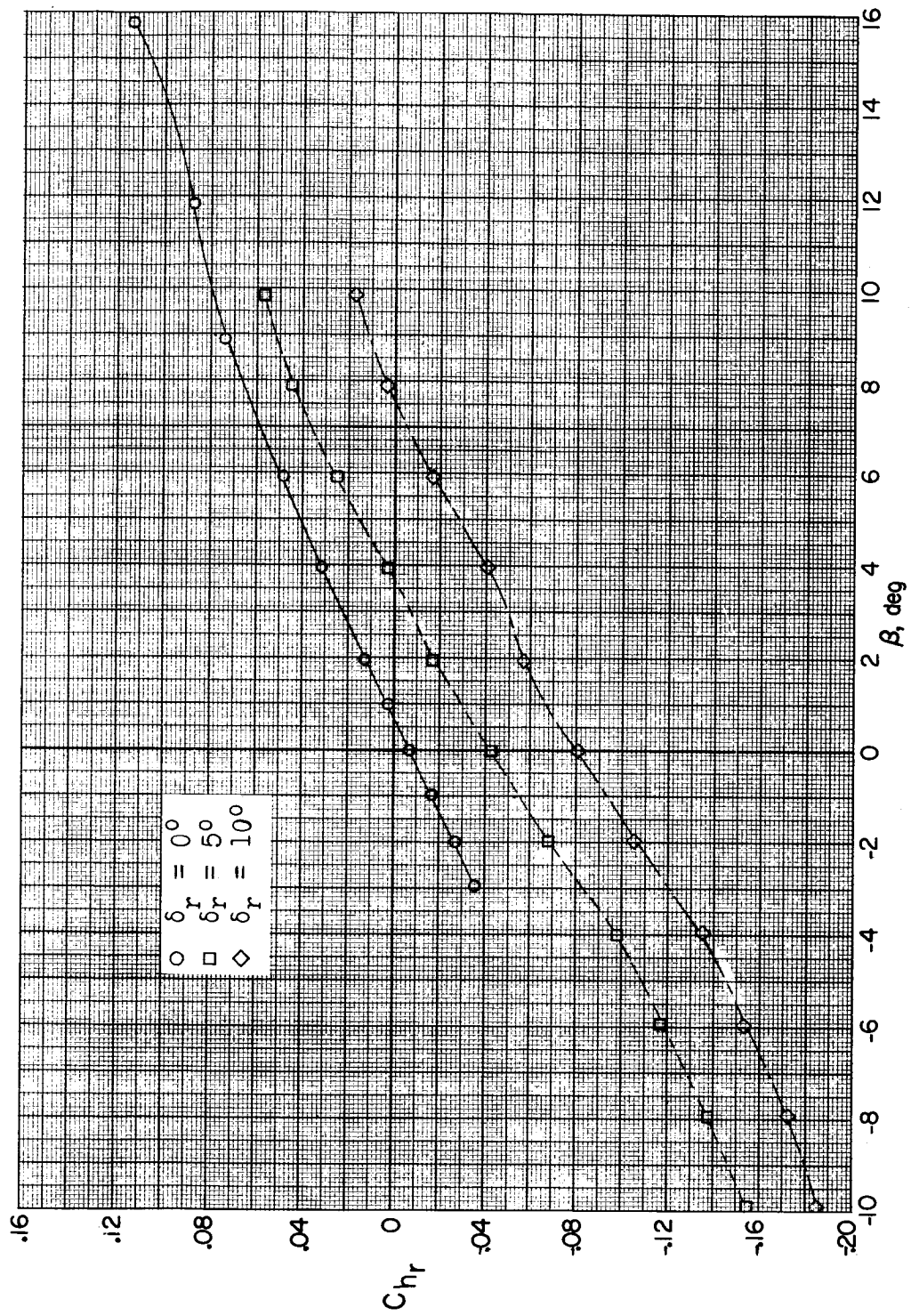
(h) $M = 2.16$; $\alpha = 6.5^\circ$.

Figure 21.- Continued.

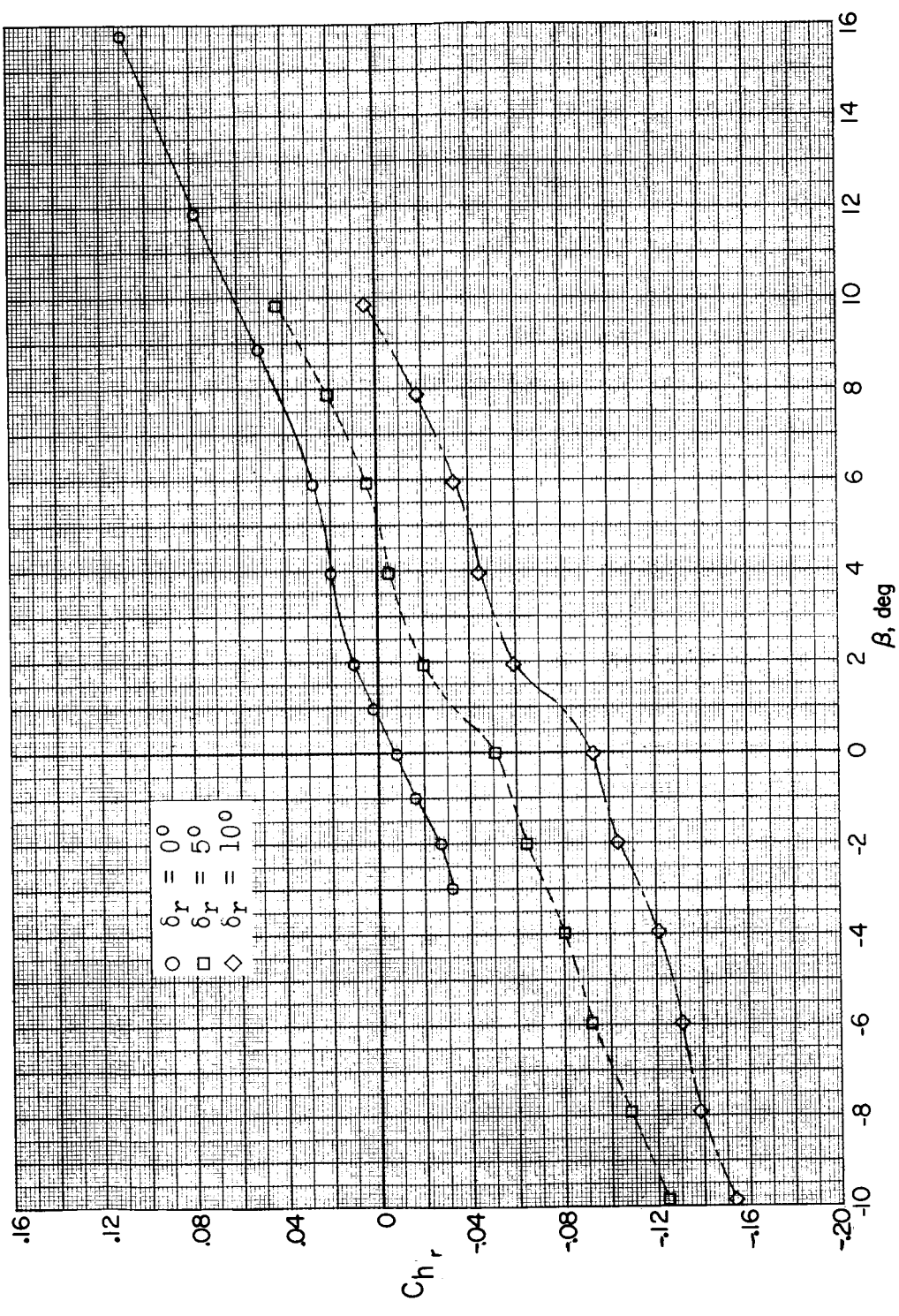
(i) $M = 2.16$; $\alpha = 16.9^\circ$.

Figure 21.- Concluded.

REF

CLASSIFIED

159

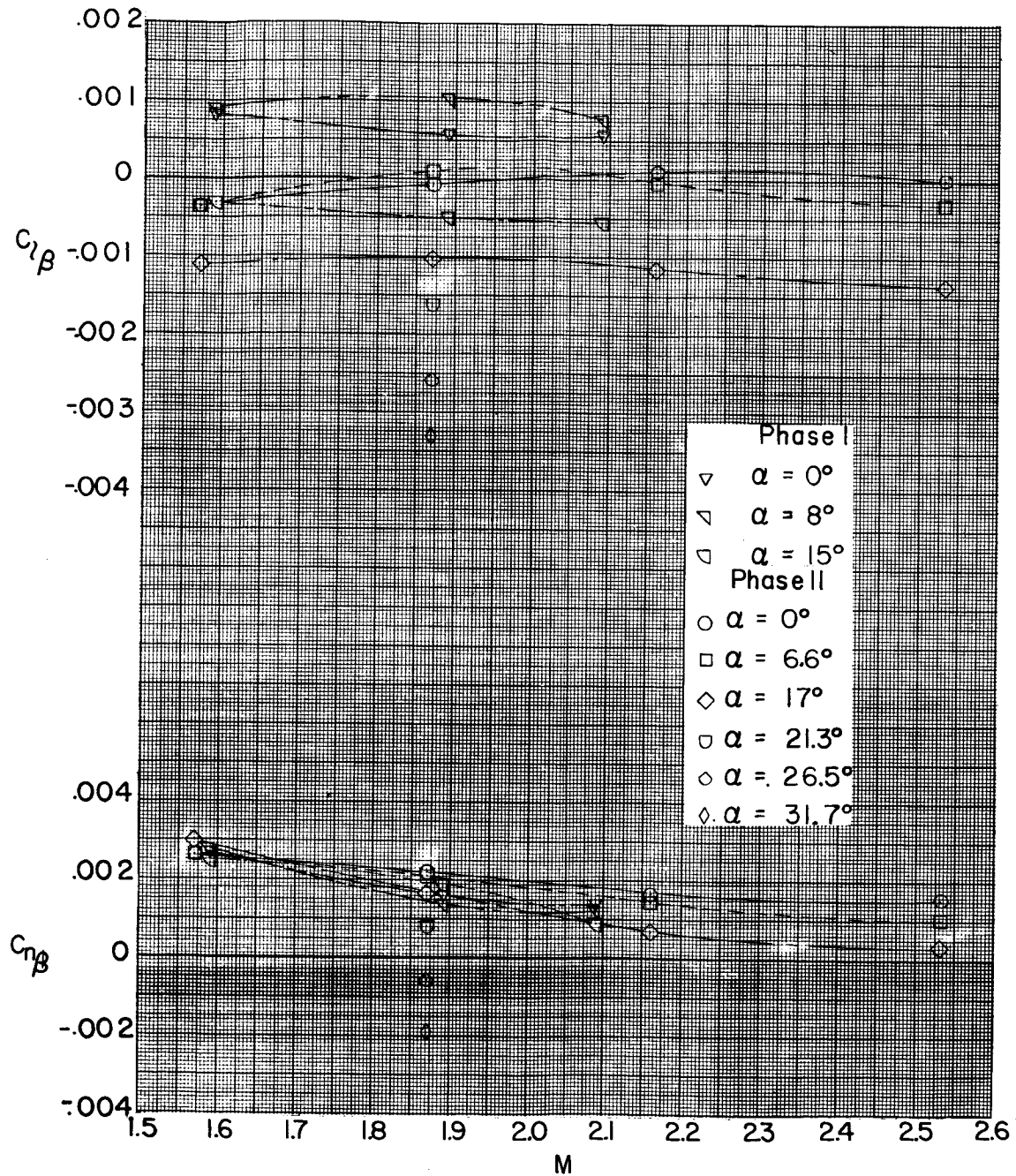


Figure 22.- Comparison of directional stability derivatives between results of phase I (ref. 1) and phase II tests.